698922

WSRC-TR-94-0468

The Effect of Regional-Scale Soil-Moisture Deficits on Mesoscale Atmospheric Dynamics that Influence Fire Severity

by

J. D. Fast

Westinghouse Savannah River Company
Savannah River Site
Aiken, South Carolina 29808

DOE Contract No. DE-AC09-89SR18035

DISCLAIMER

WSRC-TR-94-0468

THE EFFECT OF REGIONAL-SCALE SOIL-MOISTURE DEFICITS ON MESOSCALE ATMOSPHERIC DYNAMICS THAT INFLUENCE FIRE SEVERITY (U)

J. D. Fast

September 30, 1994

Westinghouse Savannah River Company
Savannah River Technology Center
Aiken, SC 29808

CONTENTS

LIST OF FIGURES

LIST OF TABLES

The Effect of Regional-Scale Soil-Moisture Deficits on Mesoscale Atmospheric Dynamics that Influence Fire Severity

Jerome D. Fast
Westinghouse Savannah River Company
Savannah River Technology Center
Aiken, SC 29080

ABSTRACT

This study employs a three-dimensional, nonhydrostatic mesoscale model to evaluate the effects of horizontally heterogeneous soil moisture and vegetation type on the atmosphere during two periods in which wildland fires occurred. Numerical sensitivity simulations demonstrate that evapotranspiration significantly affects the boundary-layer structure embedded in the synoptic-scale circulations. In regions with sufficiently moist soils, evapotranspiration increases the humidity and modifies the diurnally varying temperature near the surface. Occasionally, changes in the humidity and temperature fields can also be seen a significant distance downwind of the moist soil regions. The perturbations in the temperature fields ultimately affect the wind speed and direction over or at the boundaries of the moist-soil regions, but only at certain times during the simulation period. The higher humidity also increases the cloudiness and changes the precipitation amounts, indicating that soil moisture and vegetation may play an important role in modifying the spatial distribution and intensity of precipitation. A lower atmospheric stability index, that is an indicator of the potential for wildland fire, is also calculated from the model results. This index is also sensitive to the horizontal distribution of soil moisture and vegetation, especially in regions with relatively moist soils.

While only two periods are examined in this study, the impact of surface inhomogeneities in soil moisture and vegetation type on the atmosphere is expected to be highly dependent on the particular synoptic conditions and upon the distribution of soil moisture.

1. Introduction

Dry, unstable air is one factor that increases the probability that wildland fires will occur. Fire-weather forecasters have used various stability indices, based on observed profiles in the lower atmosphere, as indicators of the short-term potential of wildland fire severity. Observed meteorological conditions describe the current state of the atmosphere only at one particular time period; therefore, it is extremely useful to have tools that predict how the atmospheric conditions, including the humidity and stability, change with time. Fire-weather forecasters have also relied on output from the National Meteorological Center's (NMC) operational models to aid in predicting the likelihood of large wildland fires. These operational models may have significant forecast errors due to a combination of the limitations in the model's resolution and physics, deficiencies in the initial conditions, and inadequate treatment of various surface processes. Although there are plans to improve the surface processes, NMC's regional forecast models currently all use soil moisture fields based on a long-term vegetation index that is held constant and does not reflect observed rainfall patterns. Test simulations have shown that when these operational models incorporate realistic soil moisture

distributions due to rainfall patterns, the subsequent precipitation forecast is improved (Petersen et al. 1991). It is possible that the presence of soil moisture or vegetation may increase the humidity and stabilize the lower atmosphere; therefore, it is important to understand to what extent these effects have on the potential severity of wildland fires.

There has been an increasing recognition in the literature that inhomogeneities in land characteristics may play an important role in local and regional weather patterns. Horizontal variations in the sensible and latent heat fluxes associated with inhomogeneous distributions of soil moisture or vegetation can result in modifications of the boundary layer structure, secondary circulations, and the transport of heat and moisture from one location to another. Near-surface soil moisture can change rapidly in time due to evapotranspiration, runoff, and conduction into deeper soil layers; thus, its affect on the atmosphere can be transient and difficult to detect. Satellite infrared imagery has detected daytime surface temperatures that are several degrees cooler over irrigated agricultural areas in Colorado than in adjacent short-grass prairie regions (Segal et al. 1988; Segal et al. 1989). Observations and numerical simulations have also shown that the mixed-layer depth can be affected by the distribution of soil moisture (Zhong and Doran 1994). It has been hypothesized that thermally-induced circulations, similar in structure and magnitude to sea-breezes, may be established near strong horizontal gradients in soil moisture or vegetation (Segal and Arritt 1992).

There have been many numerical studies that have focused on the potential impact of simple discontinuities in soil type, soil moisture, or vegetation, while neglecting synoptic forcing and three-dimensional effects (Mahfouf et al., 1987; Ookouchi et al. 1984; Yan and Anthes, 1988; to name a few). Since these studies neglect synoptic forcing, the impact of surface inhomgeneities on the boundary layer could be over-predicted in many situations. Synoptic forcing may be large enough to mask or suppress these effects in numerical simulations as suggested by Segal et al. (1989); however, it is possible that they interact with larger-scale circulations under the proper circumstances. For instance, mesoscale models have been used to examine the influence of soil moisture variation in the southern Great Plains and the effect of the Mexican plateau on the evolution and structure of the dryline, elevated mixed layer, and the boundary layer (Lanicci et al. 1987; Ziegler et al. 1994). Variable soil moisture in the southern Great Plains was found to be important in determining differential heating and generation of low-level instability in the prestorm environment. Numerical simulations by Fast and McCorcle (1991) have also shown that variable soil moisture may alter the divergence fields associated with frontal systems in the central Great Plains.

In this study, a mesoscale model is used to evaluate the intensity and horizontal and vertical extent of the effects of inhomogeneous soil moisture and vegetation distributions on the atmospheric boundary layer and on typical synoptic-scale weather systems in the United States. Hypothetical, but realistic, soil-moisture distributions are used because of the lack of soil-moisture measurements. By comparing simulations with and without horizontally inhomogeneous land properties, an estimate of

their effect on the thermal and moisture structure within the boundary layer can be obtained. Inhomogeneous land properties may alter the structure of large-scale weather phenomena, such as fronts, as well. The presence of soil moisture may also alter the moisture-divergence fields and, ultimately, the spatial distribution and intensity of convective precipitation.

The configuration and the assumptions employed by the model in this study is described in section 2. The particular weather conditions during two wildland fire episodes, including some of the surface and upper-level characteristics, is described in section 3. The role of soil-moisture and soil-type parameterizations on boundary-layer and mesoscale circulations are examined by performing control and sensitivity experiments for each case. The details of the numerical experiments are described in section 4 and the results are presented in section 5. Difference fields are calculated for several variables by subtracting the results of the control simulations from the sensitivity simulations. Section 6 presents the conclusions of this study as well as possible implications for the prediction of wildland fires.

2. Model Description

The atmospheric model used in this study is the Regional Atmospheric Modeling System (RAMS - version 3a) developed at Colorado State University (Pielke et al. 1992). RAMS is a three-dimensional primitive equation model designed to simulate atmospheric phenomena from the synoptic scale down to large-eddy simulations of the planetary boundary layer. An overview of the model can be found in Pielke et al. (1992) and a detailed description of the model equations and numerical solution scheme is given by Tripoli and Cotton (1982). Some of the basic features and options of the model employed for the current application include:

- Nonhydrostatic, quasi-compressible primitive equations
- Terrain-following coordinate system with variable vertical resolution
- Two-way interactive nested grid structure
- Rigid-lid top boundary condition
- Radiative and zero gradient boundary conditions; with relaxation towards large-scale fields
- Prognostic soil-layer moisture and temperature model
- Vegetation parameterization
- Surface layer fluxes calculated from similarity equations
- Shortwave and longwave radiation that includes effects from cloud layers
- Modified Kuo cumulus parameterization
- Second-order turbulence parameterization

The turbulence parameterization consists of a simplified second-order closure method that employs a level-2 diagnostic scheme or a level-2.5 scheme with a prognostic turbulence kinetic energy equation as proposed by Mellor and Yamada (1982) and modified for the case of growing turbulence according to Helfand and Labraga (1988). By including a cumulus parameterization, the convective cloudiness affects low-level circulations by modifying the shortwave, longwave, temperature, and humidity distribution.

The model domain for this study encompasses the conterminous United States with a horizontal grid spacing of 60 km on a stereographic grid. The size of this domain was chosen because the atmospheric boundary-layer may be impacted by abnormally dry or moist soil conditions a significant distance upwind of a region where forest fires are occurring. A 60 km grid spacing is sufficient to resolve realistic mid-latitude synoptic systems (Giorgi 1994) while maintaining a feasible time frame for the simulation of fire-weather episodes that can last several days to weeks. In addition, the lateral boundaries of the model domain should be as far from the region of interest as possible. The model domain and the topography resolved by the 60 km horizontal grid spacing is shown in Fig. 1. The model employs a variable vertical grid spacing which increases from 52.7 m at the surface to 1000 m near the model top 15.5 km above ground level (AGL). The lowest model vertical coordinate, 52.7 m AGL, is located above the vegetation displacement height, which can be as high as 20 m. With this vertical resolution, 11 model grid points are positioned within 1000 m of the ground. A time step of 60 s is used for all of the simulations in this study.

A copy of one of the input files for RAMS used in this study is included in the appendix.

a. Initial and Lateral Boundary Conditions

The initial conditions for RAMS in this study are based on (1) the large-scale analyses from the National Meteorological Center (NMC) Limited Fine Model (LFM) and (2) surface and upper-air data from the National Weather Service (NWS). The fields from the LFM include horizontal wind components, geopotential heights, temperature, and humidity on a stereographic grid with a horizontal grid spacing of 180 km. Five vertical levels (1000, 850, 700, 500, and 400 mb) valid at 00 and 12 UTC are available from this particular LFM analyses archive. To obtain information in the upper-troposphere, the analyses were extrapolated to the 100 mb level using the hydrostatic relationship and using a constant temperature lapse rate above 400 mb. The isentropic analysis package within RAMS combines the large-scale LFM model output and the NWS observations to obtain the three-dimensional fields used to initialize and also provide the time-dependent lateral boundary conditions for RAMS.

b. Bottom Boundary Conditions

A soil layer is used to predict the sensible and latent heat fluxes at the soil-atmospheric interface. Eleven soil levels are used down to a depth of 50 cm below the surface with a constant grid spacing of 5 cm. The initial soil temperature is set equal to the atmospheric temperature at the lowest model grid point. Time-independent soil temperature and moisture values are employed at the lowest soil level. The soil type is specified as sandy clay loam (one of the eleven U. S. Department of Agricultural (USDA) soil texture classes) over the entire domain. While inhomogeneous distributions of soil type may force horizontal variations of sensible and latent heat fluxes at the surface, their effect is not examined in this study.

Soil moisture is an important quantity because latent heat effects can significantly affect the surface temperature, that in turn, can potentially modify low-level atmospheric circulations. This effect can be especially pronounced when horizontal soil moisture variations exist (Segal and Arritt 1992). Since soil moisture is not routinely measured over the entire U. S., the initial soil moisture is either set equal to a low (dry), but non-zero value or it is derived from the Palmer Drought Index as discussed in section 4.

The sea-surface temperature data for the ocean areas in Fig. 1 are specified by the mean monthly climatological value with a horizontal resolution of 1°. These temperatures are interpolated to the ocean grid points in the model domain and are held constant for the duration of a simulation.

A vegetation parameterization, in which the vegetation type is based on the Biosphere-Atmosphere Transfer Scheme (BATS) classification (Dickinson et al. 1986), is used in RAMS to more accurately represent the fluxes of heat and momentum at the surface. Albedo, emissivity, leaf-area index, fractional coverage, roughness, displacement height, and root fraction all depend upon the type of vegetation. The initial temperature of the vegetation is set equal to the surface air temperature for each simulation. The vegetation type for the model domain is shown in Fig. 2. It is derived from the USGS Advanced Very High Resolution Radiometer (AVHRR) imagery, available at 1 km horizontal resolution, that is reclassified and interpolated to the model grid (Lee 1992).

3. Case Description

a. Case 1: May 5 - 17, 1989

This particular time period in the spring was chosen because of the wildland fires that occurred in northwestern Minnesota and in central and southern Florida. The wildland fires in Minnesota took place between May 7 - 12, but Florida experienced a wildland fire almost every day of the month. The occurrence of wildland fires in these regions was probably due to the dry soil and vegetation conditions as well as a lack of significant precipitation during this period. As shown in Fig. 3., the Palmer Drought Index (PDI) for April and May of 1989 indicated extremely dry soil conditions for many parts of the midwest including Minnesota, North Dakota, Nebraska, Kansas, Iowa and Illinois. Moderate to

severe drought conditions were observed in central and southern Florida as well. The PDI is a measure of long-term departures from normal precipitation; therefore, the dry soil conditions depicted in Fig. 3 are an indication that there was little rainfall when and where the wildland fires occurred. In fact, precipitation records from NWS stations show that there were only a few days in which light rainfall occurred during this period in both Minnesota and in Florida. Except in the western U. S., heavier precipitation amounts were observed in other areas of the country.

The 500 mb geopotential height fields and the surface analyses are shown in Figs. 4 and 5, respectively, for four periods selected to depict the movement of synoptic systems during this case. On 12 UTC, May 6, a deep trough of low pressure was observed over the Great Lakes and Mississippi basin and a ridge of high pressure was observed over the Rocky Mountains (Fig. 4a). This trough weakened as it advected to the east over New England by 12 UTC, May 9 (Fig 4b). The high pressure ridge remained relatively stationary during this period as another trough of low pressure developed just off the west coast. Between May 9 and 13, the trough of low pressure over New England began to deepen and advect towards the west. During the same time period, the trough of low pressure in the Pacific moved into the western states by 12 UTC, May 13, forcing the high pressure ridge to weaken and move into the Great Plains (Fig. 4c). The two troughs both developed into cut-off lows that remained nearly stationary until 12 UTC, May 17 (Fig. 4d). Throughout the May 5 - 17 period, the upper-air patterns forced the surface low-pressure systems (Fig. 5) to develop only over the western and southern plains and the eastern U. S. With one exception, low-pressure systems in the west did not move into the midwest because they were blocked by the surface and upper-air ridge of high pressure in the middle of the country. No significant precipitation occurred in Minnesota because of these synoptic patterns. Although some of the cold fronts did push through Florida (Fig. 5), they were accompanied by little precipitation because most the energy of the synoptic systems was located in the northeastern U. S.

b. Case 2: October 25 - November 16, 1987

This particular time period in the fall was examined because of the wildland fires that occurred almost every day in West Virginia. The wildland fires in West Virginia took place almost every day during this period, except between November 10 - 14. As in the May 5 - 17, 1989 case, the occurrence of wildland fires in West Virginia was probably due to the dry soil and vegetation conditions as well as a lack of significant precipitation during this period. As shown in Fig. 6., the PDI for October and November of 1987 indicated moderately to extremely dry soil conditions for most of the Ohio River basin as well as the southeastern states and Minnesota and Wisconsin. There were also many areas that had unusually wet soil conditions including the central and southern Great Plains and the lower Great Lakes basin. The dry soil conditions depicted in Fig. 6 are an indication that there was little rainfall when and where the wildland fires occurred. In fact, precipitation records from NWS stations show that there were only a few days in which rainfall occurred during this period in West Virginia.

Significant rainfall did occur between November 10 - 11 when a particularly strong front moved through the eastern U. S., which is when the occurrence of wildland fires in West Virginia was temporarily eliminated. Most of the heavier precipitation events moved to the north of West Virginia during this period.

The 500 mb geopotential height fields and the surface analyses are shown in Figs. 7 and 8, respectively, for four periods selected to depict the movement of synoptic systems during this case. Since this period is in the fall, stronger midlatitude synoptic systems occurred than in the May 5 - 17, 1989 case. Several upper-air troughs of low pressure moved over the U. S. resulting in strong frontal systems being advected from Canada to the Gulf of Mexico. On 12 UTC, October 26, a trough of low pressure began developing over the central U. S. (Fig. 7a) that deepened as it advected to the east until it reached Labrador on 12 UTC, November 3 (Fig. 7b). As the trough moved past the east coast, a ridge of high pressure developed over the southeastern U. S. A surface high-pressure system also dominated the southeastern U. S. during this period (Fig. 8b) which resulted in the surface lows and most of the precipitation to pass to the north of West Virginia. The cut-off low over California on 12 UTC, November 3 (Fig. 7b) slowly advected to the east as it became a strong trough over the eastern U. S. by 12 UTC November 10 (Fig. 7c). This trough was strong enough so that the surface front pushed the high pressure system into the Atlantic so that precipitation occurred in must of the eastern U. S. including West Virginia. As this synoptic system moved out into the Atlantic, the upper-air winds became more zonal (Fig. 7d) and surface high pressure again settled into the southeastern U. S. (Fig. 8d).

4. Numerical Experiments

Table 1 lists the simulations performed to examine the effect of soil moisture and vegetation on the forecasts made by RAMS for the two case periods in which wildland fires occurred. The initial conditions for each of the simulations are based on the large-scale LFM analyses and the NWS upper-air and surface observations at 12 UTC May 5, 1989 or 12 UTC October 25, 1987. The initial conditions are created by an isentropic analysis package that combines the large-scale model results and the point observations using a Barnes objective analysis technique. These fields are also created for every 0 and 12 UTC period to provide the time-dependent lateral boundary conditions for RAMS. The forcing at the lateral boundaries is applied on the outermost five grid nodes and the magnitude of the forcing varies linearly in time between the 0 and 12 UTC periods.

As listed in Table 1, four simulations are performed for each case period. The two simulations denoted by ANAL indicate that FDDA is used to nudge the model's prognostic variables towards the large-scale analyses. The result of this simulation is a continuous set of mesoscale analyses (available at 3-h intervals) that are a combination the mesoscale circulations generated by RAMS and the observations. Since the large-scale analyses are only available every 12 h, the magnitude of the tendency terms in the FDDA technique decreases between the 0 and 12 UTC time periods. The

vegetation distribution given in Fig. 2 is employed in ANAL and the initial vegetation temperature is set equal to the atmospheric temperature of the lowest model level. The soil layer is initialized at 20% of saturation for sandy clay loam soil type throughout the domain and a temperature equal to the atmospheric temperature adjacent to the surface.

The two control simulations, denoted by CNTL, differ from ANAL only in the way FDDA is applied. In CNTL, only the horizontal wind components are nudged towards the large-scale analysis and the magnitude of the nudging is reduced within 1500 m of the ground so that the effect of FDDA on the wind field decreases to zero at the surface. FDDA is nearly removed in these simulations so that the mesoscale features produced by inhomogeneous surface characteristics are allowed to develop to the fullest extent; otherwise, these features may be smoothed out throughout the interior of the domain. In addition, by comparing the results from CNTL and ANAL, the forecast error in RAMS for the two case periods can be determined.

The two simulations denoted by SOILM are identical to the control simulations except that they are initialized with an inhomogeneous soil moisture distribution. The initial soil moisture distributions for the May 5 - 17, 1989 case and the October 25 - November 16, 1987 case are shown in Figs. 9 and 10, respectively. These distributions are based on the PDI depicted in Figs. 3 and 4 that were manually interpolated to the grid of the model domain. Table 2 lists the soil moisture value assigned to each PDI category. The soil moisture values in Canada and Mexico are assigned arbitrarily and are extrapolated from the values inside the U. S. boundary. The severe wetness category of the PDI is assigned a soil moisture value very near to the saturation value (95% of saturation) and the extreme drought category is assigned a very low soil moisture value (10% of saturation). The soil moisture distributions in Figs. 9 and 10 are also smoothed horizontally before they are used to initialize the model. The entire vertical profile of soil moisture is set equal to the surface value. By comparing the CNTL and the SOILM simulations, the effect of soil moisture on the synoptic and mesoscale circulations can be isolated.

Two additional simulations, denoted by BARE, are identical to SOILM except that bare-soil conditions (desert category of the BATS vegetation type) are used throughout the model domain. By comparing the SOILM and BARE simulations, the effect of vegetation on the synoptic and mesoscale circulations can be isolated.

Unfortunately, FDDA could not be removed entirely from the CNTL, SOILM, and BARE simulations during the extended forecast periods. Test simulations without FDDA indicated that after five simulation days forecast error growth adversely affected the position and strength of at least one upper-level synoptic system. These errors resulted in large forecast errors in the surface circulations as well. Although some investigators have used RAMS in a mode similar to this study (Copeland 1994), the behavior of the model during extended forecast periods has not been fully documented yet. RAMS is normally run to produce mesoscale forecasts from several hours to one or two days so that the error

growth in the upper-level large-scale systems is usually not significant. Hypothetically, forecast error growth should be limited even during extended simulation periods when the model is forced by analyses at the lateral boundaries; nevertheless, data from the boundaries is not being communicated properly into the interior of the domain in these simulations. Clearly, it would be incorrect to perform model sensitivity studies and draw conclusions from synoptic situations that did not actually occur. A compromise was achieved by nudging the wind fields above 1500 m so that the error-growth in the upper-air wind field was minimized. In this way, the sensitivity simulations would still affect the temperature and moisture fields throughout the domain and the winds fields within the boundary layer.

The total simulation length for the May 5 - 17, 1989 case is 10 days. Assuming a 60 s time step and the grid configuration discussed in section 2, a 12-day simulation requires 85.4 h of CPU time on a IBM RS/6000 model 580 workstation. A 22-day simulation for the October 25 - November 16, 1987 simulation requires about 158.4 h to complete on the same workstation. Some of the runs performed for this study were done on a model 590 workstation which reduced the CPU time by 30%. The total computational time used for all of the simulations listed in Table 1 was approximately 35 days. However, the total computational time was actually higher because of additional test simulations performed during the course of this study. Output files from RAMS are saved at three-hour intervals during the simulation period. Each output file is approximately 4.56 mb; therefore, the total storage required for the May 5 - 17, 1989 case is 1.8 gb and the October - November 16, 1987 case is 3.3 gb.

5. Numerical Results

a. May 5 - 17, 1989

1) Instantaneous Quantities

The near-surface wind field, temperature, relative humidity, and vertically-summed cloud mixing ratio from simulation ANAL-89 is shown in Figs. 11 - 14, respectively, to demonstrate the ability of RAMS to reproduce the observed weather conditions during this case. For comparison purposes, the same four time periods as the observations in Fig. 5 are shown. As expected, the results from ANAL-89 are very similar to the observations since FDDA is employed. The wind fields in Fig. 11 clearly depict the large-scale synoptic circulations that agree qualitatively with the position of the highs, lows, and frontal systems shown in Fig. 5. Nevertheless, the model wind field is smoother than the winds from the NWS surface observations and there may be errors when both the model and observed wind speed is low. This occurs because the lowest model level is 53 m AGL and the horizontal resolution is 60 km; therefore, the model cannot represent local phenomena that might affect the surface wind field. The large, cold air mass in the northern U. S. produced in Fig. 12a corresponds to the high-pressure system in Figs. 5a. Warmer temperatures occur throughout the Great Plains in Fig. 12d because of the southerly winds that advect warm air from the Gulf of Mexico into Canada (Figs. 5d and

12d) at that time. As with the surface wind field, there are some differences in the model temperature in Fig. 13 when compared to the observations in Fig. 5 because the lowest model level is 53 m AGL. These differences can be attributed to large temperature gradients near the ground, or to the differences between the model topography and the elevation of the surface observation that are as large as a few hundred meters in mountainous areas of the domain. The near-surface relative humidities are quite high in Fig. 13 because these periods are at 12 UTC (early morning hours in the U. S). Still, the humidity is too high at times, especially in the large regions of 100% relative humidity in Figs. 13b and 13c. The observed relative humidity in these regions is actually between 80 and 95%. The cloud water mixing ratio is summed over a vertical column of grid points and is shown in Fig. 14 so that the horizontal extent of the three-dimensional cloud distribution can be depicted in two-dimensions. The positions of the clouds produced by the model closely follow the centers of the strongest synoptic systems shown in Fig. 5.

The results from CNTL-89 are shown in Figs. 15 - 18 for the same time periods as in Figs. 11 - 14. While the overall wind direction is similar to those from ANAL-89, the wind speeds are not. For instance, the wind speeds in CNTL-89 are generally much stronger over the ocean. When FDDA is removed, the full effect of the low roughness lengths over the ocean (z_o = 2.4 cm) in the model is evident. Also, the model predicts the circulation around in the low-pressure system in the Great Lakes in Fig. 15a to be much stronger and the flow behind the cold front in Fig. 15b to be slightly weaker than in ANAL-89. While the near-surface temperature patterns in Fig. 16 are qualitatively similar to those from ANAL-89 in Fig. 12, the magnitudes are significantly different and additional mesoscale features are produced by CNTL-89. The largest differences between CNTL-89 and ANAL-89 occur in the relative humidity fields (Figs. 17 and 13). Since FDDA is also applied to the specific humidity in ANAL-89, it acts as an artificial source term for moisture. This artificial source is eliminated in CNTL-89, and other physical processes (such as evaporation and advection through the lateral boundaries) do not make up for this loss in moisture; therefore, the relative humidities in CNTL-89 are much lower. Despite the fact that there is less moisture at the surface, the amount of cloud water and the spatial distribution of clouds in CNTL-89 has increased dramatically (Fig.18) when compared to the clouds from ANAL-89 (Fig. 14). FDDA in ANAL-89 probably reduces the horizontal and vertical gradients in wind, temperature, and moisture that also reduce the strength of convection. For instance, the stronger circulation around the low in the Great Lakes in Fig. 15a forces larger secondary circulations that increase the amount of cloud water in the northeastern U. S. at that time. The deepest cloud layers in Fig. 18 occur near the center of the 500 mb low-pressure systems (Figs. 18c and Fig. 4c).

Figure 19 shows the differences in temperature and relative humidities 36 and 96 h into the simulation period, the results from ANAL-89 having been subtracted from those in CNTL-89 (CNTL-89 - ANAL-89). These fields are created to demonstrate and quantify the differences between the simulations. By 00 UTC May 7, the surface temperatures are as much as 12° C warmer in CNTL-89

around the Great Lakes and 8° C cooler in the southwest. The warmer temperatures around the Great Lakes are probably due, in part, to the increased cloud amounts in CNTL-89 that reduce the radiational cooling near the surface the previous evening. This effect can also be seen by comparing the clouds that extend from the Rocky Mountains and central Great Plains into the southeastern U. S. in Fig. 18b with the positive temperature differences in Fig. 19b. The negative temperature differences in Figs. 19a and 19b occur because the cooler air behind the two cold fronts is advected further south in CNTL-89. There appears to be no overall bias in the temperature fields from CNTL-89, since both positive and negative temperature differences occur during the entire simulation period (not shown). On the other hand, the relative humidities in CNTL-89 are almost always lower than those in ANAL-89. As stated previously, when the FDDA source term is removed, the model does not produce enough moisture. Since the soil moisture in this simulation is set to a dry value, there is little, if any, evaporation from the soil and transpiration from the vegetation.

When soil moisture is added to the domain, the temperature and moisture fields are modified considerably throughout the simulation period. An example of how soil moisture affects the near-surface temperature and relative humidity fields is shown in Fig. 20 where the results from CNTL-89 have been subtracted from those in SOILM-89 (SOILM-89 - CNTL-89). During an afternoon period at 00 UTC May 7, the surface temperature is lower (Fig. 20a) and the relative humidity (Fig. 20c) is higher in regions where there is sufficient soil moisture. Note that the contours of the difference fields in Figs. 20a and 20c are closely correlated to the soil moisture distribution given in Fig. 9. In these regions, the latent heat flux due to evaporation from the soil and transpiration from the vegetation cools and moistens the air adjacent to the ground. This suggests that the effects of soil moisture on the boundary layer are primarily local during the daytime. However, there are times in which the air mass that is modified by soil moisture is advected a significant distance downwind. The temperature and relative humidity differences for an early morning period at 12 UTC May 9 (Figs. 20b and 20d) indicate that the air over Kentucky and Tennessee (high soil moisture region) was advected to the south into Mississippi, Louisiana, and Texas (moderate soil moisture region), reducing the temperature by as much as 5° C and increasing the relative humidity by as much as 55%. While the soil along the Gulf coast is not completely dry, it is significantly drier than the soil in Kentucky and Tennessee.

The effects of vegetation alone on the atmospheric boundary layer are not as straightforward as those from soil moisture. The effects of vegetation on the near-surface temperature and relative humidity fields are shown in Fig. 21 where the results from SOILM-89 have been subtracted from those in BARE-89 (BARE-89 - SOILM-89). By comparing Figs. 21a and 21c with Figs. 20a and 20c, the near-surface temperature is higher and the relative humidity is lower in BARE-89 than in SOILM-89 36 h into the simulation. When the vegetation layer is removed, the latent heat flux is reduced at this time. In SOILM-89, the latent heat flux is partitioned between the evaporation from the soil and the transpiration from the vegetation. Removing the vegetation layer eliminates transpiration, but

evaporation from the soil should increase somewhat because the shading from the vegetation is also eliminated. The amount of moisture evaporated from the soil in BARE-89 does exceed that in SOILM-89 later in the period as seen in the temperature and relative humidity differences 96 h into the simulation. The temperature along the Gulf coast is 1 - 2° C cooler (Fig. 21b) and the relative humidity is 5 - 15 % higher (Fig. 21d) than in SOILM-89.

To demonstrate how the model behaves in time when inhomogeneous soil moisture and vegetation distributions are employed, several parameters have been extracted from the results at three locations. Two of the locations are at grid points in the vicinity of the observed wildland fires in Minnesota and Florida. The third location is in western Kentucky where the soil is nearly saturated. A summary of the differences in near-surface temperature between the simulations during the entire simulation period at the three locations in the domain is shown in Fig. 22. As expected, the largest differences in temperature occur in western Kentucky, where the soil is dry in CNTL-89 and is nearly saturated in SOILM-89 and BARE-89. Both of the moist-soil simulations reduce the temperature in that area; the largest differences occur during the late afternoon when the evaporation rates are the highest. The differences in temperature between the control simulation and the moist-soil simulations are not as large during the nighttime hours. However, at the two locations where wildland fires occurred in Minnesota and Florida, the temperature differences are usually less than 2° C. Since these two locations have relatively low soil-moisture content, the evaporation rate is small. The reduction in temperatures that do occur in Minnesota may be due to air masses that are modified by soil moisture at other locations. As seen in Fig. 23, the differences in relative humidity between the simulations at these locations can be quite large at times. In western Kentucky, the control simulation consistently underpredicts the relatively humidity, although the daytime values are closer to those in ANAL-89. Adding soil moisture increases the relative humidity by as much as 60%; the increases in relative humidity are most apparent during the daytime which corresponds to the largest cooling in Fig. 22. Interestingly, more moisture is added to the atmosphere in the first three days of the simulation by SOILM-89; however, the relative humidity becomes similar to CNTL-89 after 144 h. This occurs because the soil moisture is drying out later in the simulation period. Although the soil is nearly dry in Minnesota, the soil moisture incorporated in other parts of the domain increases the relative humidity in Minnesota by as much as 30% and the largest increases usually occur during the evening or early morning hours. If this moisture is evaporated from the soil somewhere upwind of western Minnesota during the previous day, the transport time can only be several hours. Therefore, the increase in relative humidity is probably due to the moist soils in northeastern Minnesota, northern Wisconsin, and Michigan. In Florida, the BARE-89 simulation actually decreases the relative humidity by as much as 30% when compared to the control simulation. This indicates that there is some feedback process in the atmosphere that diverts moist air out of Florida.

The effect of soil moisture on the near-surface wind field is considerably less than on the temperature or moisture variables. During most of this case, the differences in wind speed between SOILM-89 and CNTL-89 are less than 1 m s^{-1}; however, the are few periods in which horizontal soil moisture gradients may be affecting the circulations near the surface. For instance, at 36 and 228 h into the simulation period in Figs. 24 a and 24b, the winds speeds are reduced by as much as 3 m s^{-1} over or at the boundaries of the moist-soil regions. Secondary circulations (if they exist) due to horizontal soil moisture gradients (Segal and Arritt 1992) are difficult to find in SOILM-89, probably because the grid spacing cannot resolve these circulations adequately. On the other hand, the effect of vegetation alone on the surface wind speeds can be quite large as seen in Figs. 24 c and 24d. In general, the near-surface wind speeds from BARE-89 are larger than those from SOILM-89. Without a vegetation layer, the model domain has one value of the roughness length (10 cm) for the land portion of the domain. The vegetation parameterization has various roughness lengths depending upon the type of vegetation and can be as high as 1 m for evergreen and deciduous needleleaf trees (vegetation types 3 and 4 in RAMS). The larger roughness lengths employed in SOILM-89 increase the surface friction and reduce the near-surface wind speeds. This effect can also be seen in Fig. 25, in which BARE-89 consistently predicts higher wind speeds at the three select locations than the other simulations that incorporate vegetation. The effect of soil moisture alone on the wind speed at these locations is negligible at most times by comparing the winds speeds from CNTL-89 and SOILM-89. Since the wind speeds from CNTL-89 and SOILM-89 are closer to those in ANAL-89, the inclusion of vegetation is probably very important in producing the best surface wind speed.

The soil moisture and vegetation not only affect the model variables near the surface, but they can affect the entire boundary-layer structure. For instance, the modification of the surface quantities also affects the development of clouds and precipitation as seen in Figs. 26 and 27.

The accumulated precipitation during the May 5 - 17, 1989 case for the four simulations is given in Fig. 26. The control simulation produces the largest precipitation in western Texas, with lesser amounts in the Rocky Mountains and along the East coast. CNTL-89 produces significantly more precipitation in the southeast with additional amounts in the midwest. Although the control simulation produces a precipitation maximum in western Texas, the magnitude is smaller than in ANAL-89. The soil moisture and vegetation does not affect the overall precipitation pattern, as seen by comparing the results from SOILM-89 and BARE-89 to CNTL-89. Still, there are relatively large differences in the amount and spatial distribution of precipitation. For instance, precipitation amounts over the Rocky Mountains are smaller in BARE-89 than in SOILM-89. On the other hand, most of the changes in the precipitation amounts due to soil moisture alone are highly localized in SOILM-89. The main reason for the overall increase in precipitation coverage in CNTL-89, SOILM-89, and BARE-89 over ANAL-89 is due to the increase in cloud water amounts when FDDA is removed (Fig. 18). This can be seen in the time-dependent cloud water content for the three select locations shown in Fig. 27. The simulations without

FDDA all predict mostly cloudy conditions in Kentucky during the entire period, but higher cloud water contents are produced when soil moisture is incorporated in SOILM-89 and BARE-89. Intermittent cloudiness with low cloud water contents is predicted for Minnesota and Florida for the SOILM-89 and BARE-89 simulations. The cloudiness is changed somewhat due to the modified air masses upwind of these locations. None of the simulations produced significant precipitation in Minnesota where wildland fires were observed to occur. Precipitation was produced in central Florida (Fig. 26), but most of it occurred towards the end of the simulation period when mostly cloudy conditions occurred (Fig. 27).

While surface temperatures and relative humidities affect the development of wildland fires, fire-weather specialists have also identified lower atmospheric parameters that may be indicators of the potential for severe fires. A summary of some of those efforts is reported in Haines (1988). Haines proposed a Lower Atmospheric Severity Index (LASI) that is based on temperature lapse rate and dew point temperatures in the lower atmosphere. He found that the index is a good predictor of the probability of large wildland fires when it was compared and correlated to the occurrence of wildland fires. While the LASI in Haines' study is based on observed weather conditions from rawinsonde data, the LASI in this study is computed from model data to determine (1) if it is correlated to the wildland fires for this case and (2) to determine the sensitivity of the LASI to soil moisture and vegetation variations. Since the LASI uses temperature and moisture quantities in the lower atmosphere, any change in the LASI from SOILM-89 and BARE-89 when compared to CNTL-89 will indicate that soil moisture or vegetation affected not only the surface, but the entire lower atmosphere.

The LASI is computed for each of the simulations and is based on the method given in Table 3 (Haines 1988). Since RAMS has a terrain-following vertical coordinate system, the temperatures and dew-point temperatures in Table 3 are obtained by interpolating the RAMS results to the appropriate pressure surface. The LASI computed by RAMS during the entire period for the three select locations is shown in Fig. 28. At all three locations in CNTL-89, the magnitude of the LASI increases and decreases diurnally, with the highest values usually during the afternoon. In western Kentucky, the addition of soil moisture in SOILM-89 and BARE-89 reduced the LASI by a value of 1 or 2 during much of the simulation period; however, the LASI is modified only during short periods in Minnesota and Florida where wildland fires occurred. In central Florida, BARE-89 has higher values of LASI at times than CNTL-89 which corresponds to the lower relative humidity in BARE-89 (Fig. 23). Therefore, soil moisture and vegetation can affect the entire boundary layer structure as well as surface atmospheric quantities, but usually only in regions with high soil moisture content.

2) Time-Averaged Quantities

Many of the atmospheric quantities described in the previous section have also been averaged over the entire simulation period so that long-term effects from the soil moisture and vegetation distributions can be ascertained. If there are significant differences in the averaged quantities between

the simulations, it may indicate that inhomogenous distributions of soil moisture or vegetation play an important role in the deviations from normal climatic patterns. Anomalous distributions of soil moisture during one month or season might also affect the subsequent climate. For instance, the heavy rainfall in the midwest during the spring and summer of 1993 that saturated the soils and lead to flooding over large areas in the upper Mississippi Basin (Kunkel et al. 1994) may have influenced the normal climatic patterns not only in that area, but in other parts of the country as well.

The average near-surface temperature over the entire simulation period for ANAL-89, CNTL-89, SOILM-89, and BARE-89 is shown in Figs. 29, 30, 32, and 34, respectively. In each figure, the average temperature over the simulation at 00, 06, 12, and 18 UTC is shown. This is done to determine whether there are any diurnal effects due to the soil moisture and vegetation distributions. In Fig. 29, the diurnal temperature variation from ANAL-89 is shown. As expected, the warmest temperatures occur at the 00 UTC period (local time is the late afternoon or early evening) and the coolest temperatures occur at the 12 UTC period (local time is the early morning). The effect of elevation on the surface temperature is evident over the Rocky Mountains and the Appalachians. The Great Lakes also reduce the surface temperatures a few degrees as seen in Figs. 29a and 29d. In Fig. 30, the same qualitative average temperature pattern is reproduced with the model without FDDA in CNTL-89. The differences in the average temperature when the results from ANAL-89 are subtracted from CNTL-89 are shown in Fig. 31 (CNTL-89 - ANAL-89). Without FDDA, the model tends to overpredict the near-surface temperature in the eastern and western U. S. by as much as 6° C and underpredicts the near-surface temperature in the northern plains and southern Rocky Mountains and Texas by as much as 4° C.

The effect of soil moisture alone on the average temperatures from SOILM-89 is shown in Figs. 32 and 33. While the average temperature patterns (Fig. 32) are similar to the control simulation (Fig. 30), there are some minor differences (Fig. 33). The temperature differences in Fig. 33 are obtained by subtracting the values in CNTL-89 from those in SOILM-89 (SOILM-89 - CNTL-89). By incorporating soil moisture, the average surface temperature is reduced, but usually in regions where the soil is relatively moist. The temperature difference fields resemble the soil-moisture distributions in Fig. 9 and the instantaneous results shown in Fig. 20a. The strongest cooling occurs during the 00 and 18 UTC periods where the average temperatures are 2.5° C lower than those in CNTL-89. As stated previously, the evaporation and transpiration rates are higher during the daylight hours. The cooler temperatures at night are probably due, in part, to the reduced temperatures from the daytime. There were a few periods during this case in which the air mass cooled by the evapotranspiration was advected downwind of the moist soil regions (Fig. 20b); however, this did not happen often enough to significantly influence the average temperature distribution.

The effect of vegetation alone on the average surface temperature is quite pronounced. The temperature patterns in Fig. 34 are similar to those of the control simulation in Fig. 30 in the dry soil regions, but cool temperature anomalies are located in the moist soil regions. The temperature

differences in Fig. 35 are obtained by subtracting the values in SOILM-89 from those in BARE-89 (BARE-89 - SOILM-89). The average temperatures over the moist soil regions in the lower Ohio River and mid-Mississippi basins from BARE-89 are 2° C cooler than those in SOILM-89 during the daytime hours, indicating that the vegetation layer is acting as a moderating influence on the surface temperatures. The rate of evapotranspiration from the vegetation and soil is evidently much less than evaporation from the bare soil alone. Interestingly, the average surface temperatures in BARE-89 are a few degrees warmer than SOILM-89 in regions that have relatively dry soil. In SOILM-89, the vegetation has varying albedo and emissivity properties, while in BARE-89, these properties are constant throughout the domain. The inhomogeneity in these properties no doubt have some effect on the sensible heat flux as well. Nevertheless, the largest effect of the vegetation occurs in modifying the latent heat flux in the moist soil regions.

The average near-surface relative humidity over the entire simulation period for ANAL-89, CNTL-89, SOILM-89, and BARE-89 is shown in Figs. 36, 37, 39, and 41, respectively. As with the surface temperature, the relative humidity has been averaged over the simulation at 00, 06, 12, and 18 UTC. The diurnal fluctuation in relative humidity is clearly evident in the ANAL-89 results in Fig. 36 where low values of occur during the daytime and high values occur during the night. Another climatological feature is the higher relative humidities in the eastern U. S. and drier conditions in the southwest, as expected. The air over the ocean is very humid at all times and the air over the Great Lakes has higher relative humidities during the daytime. The general patterns and diurnal fluctuations in the humidities from CNTL-89 in Fig. 37 are similar to those in Fig. 36, except that the magnitudes have been reduced and there are more terrain-induced effects during the nighttime hours. The differences in the average relative humidity shown in Fig. 38 are obtained by subtracting the values in ANAL-89 from those in CNTL-89 (CNTL-89 - ANAL-89). Without FDDA, the model tends to underpredict the relative humidity at all times of the day, but it is particularly low at night where the average humidity is as much as 30% lower. This indicates that the control simulation does not have the correct moisture sources.

The pattern of the average relative humidity fields from SOILM-89 (Fig. 39) is similar to the control simulation, except that maximas in the relative humidity fields can clearly be seen during the daytime hours at 00 and 18 UTC over the moist soil regions. Evaporation from the soil and vegetation increases the average relative humidity by as much as 25%, as shown in the relative humidity difference fields in Fig. 40 (SOILM-89 - CNTL-89). During the daytime hours the increase in moisture occurs only in areas immediately adjacent to the moist soil regions. However, at night, the moisture becomes advected somewhat further away from these sources as seen by the weaker gradients in the contours in Figs. 40b and 40c. SOILM-89 is adding moisture into the model domain so that the surface relative humidities are now closer to those in ANAL-89, indicating that soil moisture is a necessary component in predicting the correct atmospheric moisture in the boundary layer.

Anomalies in the average relative humidity from BARE-89 (Fig. 41) are even more pronounced than those in SOILM-89. While it is important to examine the response of the model when the vegetation layer is removed, the relative humidity fields produced in BARE-89 are unrealistic. It is unlikely to see patterns such as those in Figs. 41a and 41d in a surface weather analysis. By subtracting the results of SOILM-89 from those in BARE-89 (BARE-89 - SOILM-89), the magnitude of the changes can be seen in Fig. 42. Without vegetation, the relative humidity is 15 - 20 % higher during the daytime over the moist soil regions. Unlike SOILM-89, the additional moisture does not advect downwind at night. In fact, the relative humidities are 10 - 20% lower than SOILM-89 over the dry soil regions of the domain. It is possible that evapotranspiration from the vegetation played an important role in adding more moisture into the atmosphere in the regions with drier soils. In those areas, even though evaporation from the bare-soil surface is small, vegetation can extract moisture from the deeper layers of the soil through its roots.

To determine whether the lower atmosphere is sensitive to soil moisture and vegetation distributions over a long period of time, the average LASI throughout the period is also computed for the simulations in this study. As stated previously, differences in the LASI between simulations are due to changes in the temperature lapse rate and dew-point depression in the lower atmosphere (see Table 3). In Figs. 43, 44, 46, and 48, the average LASI from ANAL-89, CNTL-89, SOILM-89, and BARE-89, respectively, are shown. The average LASI during the daytime periods from ANAL-89 in Fig. 43 show that there is a moderate to high risk for wildland fire severity in most of the central and southeastern U. S. This includes Minnesota and Florida were wildland fires were observed. During the night, the values of LASI decrease because of the decrease in the dew point depression in the lower atmosphere. Values of the LASI fall to less than 4.0 at night in most parts of the country, indicating a low risk for wildland fire. Note that there are large gradients in the LASI in mountainous regions and caution should be used in interpreting the LASI in these areas. These gradients occur because the LASI is calculated using lapse rates and dew point depressions up to the 700 mb level over high-elevation regions (instead of the 850 mb in the eastern U. S.) as indicated in Table 3.

The average LASI computed from CNTL-89 are higher nearly everywhere in the domain during both the daytime and nighttime hours than those in ANAL-89. In contrast to ANAL-89, LASI values in the central and southeastern U . S. also indicate moderate to severe risk of wildand fire, even at night. This occurs because CNTL-89 has lower relative humidities which increases the dew-point depression and, thus, increases the LASI. It also indicates that the temperature and moisture structure is modified, not only at the surface, but in the lower atmosphere as well. By subtracting the results of ANAL-89 from those in CNTL-89 (CNTL-89 - ANAL-89), the specific differences in the LASI are shown in Fig. 45. The LASI is generally 1.0 - 1.5 higher than ANAL-89.

The LASI values from SOILM-89 shown in Fig. 46 are very similar to those from CNTL-89. By subtracting the results of CNTL-89 from those of SOILM-89, the differences in Fig. 47 indicate that the

values of the LASI are decreased in SOILM-89 by as much as 1.0 over the moist-soil regions. The pattern of these differences closely corresponds to the temperature and humidity difference fields in Figs. 33 and 40. Most of the changes in the LASI are due to the dew-point depression term (part B from Table 3), although the reduction in surface temperature will also reduce the temperature lapse rate near the surface during the daytime and, therefore, reduce the LASI. In this case, a change of 1.0 in the LASI might mean a change of wildland fire severity risk from severe to moderate, but only in the moist-soil regions. Minor differences in the LASI occur over the dry-soil regions.

The effect of vegetation alone on the LASI in BARE-89 is larger than the effect of soil moisture alone in SOILM-89. The LASI values from BARE-89 shown in Fig. 48 are also similar to those from CNTL-89 and SOILM-89, but there are distinct reductions in the LASI over the moist-soil regions during the daytime. By subtracting the results of SOILM-89 from those of BARE-89 (BARE-89 - SOILM-89), the differences in Fig. 49 show that the increased humidity in BARE-89 over the moist-soil regions is enough to decrease the value of the LASI by as much as 0.75 over the moist soil area during the daytime. Therefore, the value of the LASI is as much as 1.75 lower in BARE-89 than in CNTL-89.

b. October 25 - November 16, 1987

1) Instantaneous Quantities

The near-surface wind field, temperature, relative humidity, and vertically-summed cloud mixing ratio from simulation ANAL-87 are shown in Figs. 50 - 53, respectively, to demonstrate the ability of RAMS to reproduce the observed weather conditions during this case. For comparison purposes, the same four time periods as the observations in Fig. 8 are shown. As in the previous case, the results from ANAL-87 are very similar to the observations in Fig. 8 since FDDA is employed. The wind fields in Fig. 50 clearly depict the large-scale synoptic circulations that agree qualitatively with the position of the highs, lows, and frontal systems shown in Fig. 8. The temperatures are below freezing in many parts of the country during this period. For instance, the large high-pressure system over the midwest in Fig. 8c brought below-freezing temperatures as far south as Texas, as seen in Fig. 51c. Temperatures in the southcentral and southeastern U. S. are several degrees C too cold at times (Fig. 51b and 51d) because the model fails to produce the southerly warm-air advection at the surface associated with low-pressure systems moving through the midwest. At these times the model produces easterly or southeasterly winds in the southern plains (Figs. 50b and 50d) when the observations show southerly winds in that area. As in the previous case, the near-surface relative humidities are quite high in Fig. 52 because these periods are at 12 UTC (early morning hours in the U. S). Still, the humidity is too high at times, especially in the large regions of 100% relative humidity in Fig. 52a and 52b. The observed relative humidity in these regions is actually between 70 and 100%. The positions of the clouds produced by the model, as indicated by the vertically-summed cloud water mixing ratio in Fig. 53, closely follow the centers of the strongest synoptic systems in Fig. 5.

The results from CNTL-87 are shown in Figs. 54-57 for the same time periods as in Figs. 50-53. While the overall wind directions are similar to those from ANAL-87, the wind speeds are generally higher in the vicinity of strong synoptic systems. For instance, stronger southerly winds are produced ahead of the cold front in the central plains (Fig. 54c) and stronger northerly winds are produced behind the cold front that passes through the southern plains (Fig. 54d). The winds speeds over the ocean in ANAL-87 and CNTL-87 are about the same. While the near-surface temperature distributions in Fig. 55 are qualitatively similar to those from ANAL-87 in Fig. 51, the temperatures are too cold in the middle of the simulation period. The temperatures are about 5° C colder in the southern states (Fig. 55b) and in the central Rocky Mountains (Fig. 55c); however, the temperatures are a few degrees warmer than ANAL-87 in many parts of the domain (Fig. 55d). The artificial source of moisture through FDDA is eliminated in CNTL-87 and other physical processes do not make up for this loss in moisture; therefore, the relative humidities in CNTL-87 (Fig. 56) are significantly lower in most parts of the domain as in the May 5 - 17, 1989 case. The amount of cloud water (but not the spatial distribution of clouds) in CNTL-87 has increased somewhat (Fig. 57) when compared to the clouds from ANAL-87 (Fig. 53), despite the fact that there is less moisture at the surface. Stronger circulations at the surface force larger secondary circulations that increase the amount of cloud water near the frontal boundaries. Also, slope flows in the mountains result in higher vertical velocities and increased cloud water in the northwestern U. S. as seen in Fig. 57d.

Figure 58 shows the differences in temperature and relative humidities 36 and 480 h into the simulation period where the results from ANAL-87 have been subtracted from those in CNTL-87 (CNTL-87 - ANAL-87). By 00 UTC October 28, the surface temperatures are as much as 9° C warmer in CNTL-87 in the northeastern U. S. and 3° C cooler in the Rocky Mountains. The warmer temperatures in the northeast are probably due to the increased cloud amounts in CNTL-87 that reduced the radiational cooling near the surface the previous evening. The locations of the positive temperature differences around the Great Lakes and in the central Great Plains and the negative temperature differences in the southern plains and the Ohio River basin indicate that the temperature gradient across the warm front at 12 UTC November 14 (Fig. 8d) in CNTL-87 is not as strong as in ANAL-87. There appears to be no overall bias in the temperature fields from CNTL-87, since both positive and negative temperature differences occur during the entire simulation period (not shown). Contrary to the May 5- 17, 1989 case, the relative humidities in CNTL-87 are usually, but not always, lower than those in ANAL-87. There are times and places for which the relative humidity in CNTL-87 is as much as 30% higher.

Even though this case is in the fall when surface temperatures are cooler than the previous case, the temperature and moisture fields are modified considerably throughout the simulation period when soil moisture is added to the domain. An example of how soil moisture affects the near-surface temperature and relative humidity fields is shown in Fig. 59 where the results from CNTL-87 are subtracted from those in SOILM-87 (SOILM-87 - CNTL-87). During an afternoon period at 00 UTC

October 28, the surface temperature is lower (Fig. 59a) and the relative humidity (Fig. 59c) is higher in regions where there is sufficient soil moisture. Note that the contours of the difference fields in Figs. 59a and 59c are closely correlated to the soil moisture distribution given in Fig. 10. In these regions, the latent heat flux due to evaporation from the soil and transpiration from the vegetation cools and moistens the air adjacent to the ground. Because this case is in the fall, the surface temperatures are significantly lower in the northern U. S. than the May 5 - 17; therefore, the latent heat flux in that region is smaller. During most of the simulation period the effects of soil moisture on the boundary layer are primarily local during the daytime. However, as in the May 5 - 17, 1989 case, there are times at which the air mass that is modified by soil moisture is advected a significant distance downwind. The temperature and relative humidity differences for an early morning period at 12 UTC November 14 (Figs. 59b and 59d) indicate that the air that was over the south-central U. S. (high soil moisture region) was advected into the Ohio River valley (moderate soil moisture region), increasing the relative humidity by as much as 45% south of the warm front (Fig. 8d). North of the warm front in Iowa, Minnesota and Wisconsin, the temperatures are as much as 7.5° C warmer and the relative humidity is 30% less than CNTL-89.

The effects of vegetation alone on the near surface temperature and relative humidity fields is shown in Fig. 60 where the results from CNTL-87 are subtracted from those in BARE-87 (BARE-87 - SOILM-87). Comparing Figs. 60a and 60c with Figs. 59a and 59c shows that the near-surface temperature and relative humidity in BARE-87 is not much different than SOILM-87 36 h into the simulation. When the vegetation layer is removed, the latent heat flux has not been changed significantly at this time. However, the differences in temperature and relative humidity increase in time so that the difference fields become quite complicated by 480 h into the simulation period as shown in Figs. 60b and 60d. The relatively drier regions in Fig. 60d (negative differences) correspond to the relatively warmer regions in Fig. 60b (positive differences).

As in the previous case, several parameters have been extracted from the model results at three locations. One of the locations is at grid point in central West Virginia in the vicinity of the observed wildland fires during this case. The other two locations are in northwestern Texas and western New York where the soil is nearly saturated. A summary of the differences in near-surface temperature between the simulations during the entire simulation period at three select locations in the domain is shown in Fig. 61. As expected, the largest differences in temperature occur in northwestern Texas, where the soil is dry in CNTL-87 and is nearly saturated in SOILM-87 and BARE-87. Both of the moist-soil simulations reduce the temperature during the late afternoon when the evaporation rates are the highest, but the temperatures are higher than CNTL-87 during the night. The effect of soil moisture on temperature is much smaller in western New York than in Texas because the temperatures in the north are much colder so that evaporation rates are much less. In West Virginia where wildland fires occurred, the temperature differences due to soil moisture or vegetation are also very small throughout

the simulation period. As seen in Fig. 62, the differences in relative humidity between the simulations at these locations can be quite large at times. In northwestern Texas, the control simulation consistently underpredicts the relatively humidity by 10 - 20%, although the daytime values are closer to those in ANAL-89. Adding soil moisture in SOILM-87 increases the relative humidity by as much as 60%; these increases are most apparent during the daytime which corresponds to the largest cooling in Fig. 61. In contrast to the May 5 - 17, 1989 case, the soil in Texas does not appear to be drying out later in the simulation period. There are also significant relative humidity changes due to soil moisture and vegetation in western New York, although the magnitude is smaller than in Texas. In West Virginia, the relative humidity in SOILM-87 and BARE-87 is usually 10 - 20% higher than the control simulation, but there are periods in which there is no difference. Since the soil in West Virginia and most of the Ohio River basin is dry, this additional moisture must be advected from other portions of the domain.

As in the May 5 - 17, 1989 case, the effect of soil moisture on the wind field is considerably less than on the temperature or moisture variables. During most of this case, the differences in wind speed between SOILM-87 and CNTL-87 are usually less than 1 m s^{-1}; however, there are a few periods in which horizontal soil moisture gradients may be affecting the circulations near the surface. For instance, at 24 and 240 h into the simulation in Figs. 63a and 63b, the winds speeds are modified by as much as 4 m s^{-1} over or at the boundary of moist-soil regions. The horizontal soil moisture gradients cause large enough horizontal gradients in temperature for the synoptic period in this case to force secondary circulations (Segal and Arritt 1992) in the central plains (Fig. 63b). Nevertheless, the relatively large grid spacing cannot resolve these circulations most of the time (if they exist). On the other hand, the effect of vegetation on the surface wind speeds can be large as seen in the positive differences throughout the domain in Figs. 63c and 63d. As in the May 5 - 17, 1989 case, the near-surface wind speeds from BARE-87 are larger than those from SOILM-87 because the model domain has one value of the roughness length (10 cm) for the land portion of the domain without a vegetation layer. This effect can also be seen in Fig. 64, in which BARE-87 consistently predicts higher wind speeds at the three select locations than the other simulations that incorporate vegetation. The effect of soil moisture alone on the wind speed at these locations is seen to be less by comparing the winds speeds from CNTL-87 and SOILM-87. Where there are differences, the wind speeds are generally higher in SOILM-87 than CNTL-87. As found in the previous case, the inclusion of vegetation is necessary for producing the best surface wind fields since the wind speeds from CNTL-87 and SOILM-87 are closer to those in ANAL-87.

The modification of the surface quantities will also affect the development of clouds and precipitation as seen in Figs. 65 and 66. The accumulated precipitation during the October 25 - November 16, 1987 case for the four simulations is given in Fig. 65. ANAL-87 produces the largest precipitation in central Texas and in Florida, with trace amounts in the southwest. CNTL-87 produces

significantly more precipitation in Texas and in the western U. S. The soil moisture and vegetation does not affect the overall precipitation pattern, as seen by comparing the results from SOILM-87 and BARE-87 to CNTL-87. In contrast to the May 5 - 17, 1989 case, there are relatively few differences in the amount and spatial distribution of precipitation due to soil moisture or vegetation. The exception to this is in Arizona where SOILM-87 produces more precipitation in that area than CNTL-87. The main reason for the overall increase in precipitation coverage in CNTL-87, SOILM-87, and BARE-87 over ANAL-87 is due to the increase in cloud water amounts when FDDA is removed (Fig. 57). The time-dependent cloud amounts for three locations is shown in Fig. 66. The simulations with soil moisture both predict mostly cloudy conditions in northwest Texas during most of the simulation period, but higher cloud water contents are produced for BARE-89. While intermittent cloudiness with low cloud water contents is predicted for western New York in both ANAL-87 and CNTL-87, the soil moisture in the other two simulations increases the cloud water amounts. The increase in frequency of clouds and the increase in cloud amounts in West Virginia are due to the modified air masses upwind of this location. None of the simulations produced significant precipitation in West Virginia where wildland fires were observed to occur.

The LASI computed by RAMS during the entire period for three locations are shown in Fig. 67. At all three locations in CNTL-87, the magnitude of the LASI increases and decreases diurnally, with the highest values usually during the afternoon. There are periods in which synoptic systems disrupt this oscillation so that the LASI may remain constant for a few days. During most of this case, the LASI for West Virginia was 4.0 or lower indicating a low probability of large wildland fires; however, there are a few periods in which the model does predict a moderate probability of wildland fire when the LASI reaches a value of 5.0. Despite the fact the surface temperature and relative humidities in West Virginia are modified slightly by soil moisture or vegetation, the LASI is reduced by 1.0 or 2.0 during the first half of the simulation period. In northwestern Texas and western New York, the addition of soil moisture in SOILM-87 and BARE-87 reduced the LASI by a value of 1.0 or 2.0 during much of the simulation period and as much as 3.0 at times.

2) Time-Averaged Quantities

As in the May 5 - 17 case, many of the atmospheric quantities described in the previous section have also been averaged over the entire simulation period so that long-term effects from the soil moisture and vegetation distributions can be ascertained. Since the simulation period for this case is 22 days, the differences in the averaged quantities between the simulations may indicate that an inhomogeneous distribution of soil moisture or vegetation can modify the climate patterns over a month-long period.

Near-surface temperatures at selected times averaged over the entire simulation period are shown in Figs. 68, 69, 71, and 73 for ANAL-87, CNTL-87, SOILM-87, and BARE-87, respectively. The

temperatures for 00, 06, 12 and 18 UTC were averaged to determine whether there are any diurnal effects due to the soil moisture and vegetation distributions. The diurnal temperature variation is evident in the results from ANAL-87 where the warmest temperatures occur at the 00 UTC period (Fig. 68a) and the coolest temperatures occur at the 12 UTC period (Fig. 68c). Since this period is in the fall, many parts of the northern U. S. have average temperatures below freezing in the morning (Fig. 68c). The effect of elevation on the surface temperature is evident over the Rocky Mountains and the Appalachians. The Great Lakes also warm the surface temperatures a few degrees during the night and morning periods as seen in Figs. 68b and 68c. During this time of the year the lake temperatures are warmer than the ambient air above it. In Fig. 69, the same qualitative average temperature pattern is reproduced with the model without FDDA in CNTL-87. The differences in the average temperature when the results from ANAL-87 are subtracted from CNTL-87 (CNTL-87 - ANAL-87) are shown in Fig. 70. Without FDDA, the model tends to underpredict the near-surface temperature in most parts of the domain (by as much as 5° C in New Mexico and Texas). The near-surface temperatures in the northeast and northwest are overpredicted by only 1 - 2° C.

The effect of soil moisture alone on the average temperatures from SOILM-87 is shown in Figs. 71 and 72. While the average temperature patterns (Fig. 71) are similar to the control simulation (Fig. 69), there are some minor differences (Fig. 72). The temperature differences in Fig. 72 are obtained by subtracting the values in CNTL-87 from those in SOILM-87 (SOILM-87 - CNTL-87). By incorporating soil moisture, the average surface temperature is reduced during the daytime by as much as 3° C, but usually in regions where the soil is relatively moist. The temperature difference fields resemble the soil moisture distributions in Fig. 10 and the results shown in Fig. 59a since the evaporation and transpiration rates are higher during the daytime hours. In contrast to the results from the May 5 - 17, 1989 case, the surface temperatures at night are generally warmer than the control simulation (by as much as 3° C in New Mexico and Texas). This occurs because the higher humidity reduces the amount of longwave radiational cooling at night for days that have little cloudiness. There were a few periods during this case in which the air mass cooled by the evapotranspiration was advected downwind of the moist soil regions; however, this did not happen often enough to significantly alter the average temperature distribution.

The effect of vegetation alone on the average surface temperature is not as pronounced as in the May 5 - 17, 1989 case. The temperature patterns in Fig. 73 are similar to those of the control simulation in Fig. 69. The temperature differences between SOILM-87 and BARE-87 (BARE-87 - SOILM-87) show that the average temperatures over the moist soil regions in the southwest are as much as 1.5° C lower than SOILM-87 during the late afternoon (Fig. 74a). Otherwise, the temperature differences are much smaller and usually less than 0.5° C the rest of the day. The vegetation layer is acts as a moderating influence in this case only during the daytime in the southern part of the domain, where temperatures are at their highest because vegetation is not as active in the fall. The average surface temperatures in

BARE-87 are slightly warmer than SOILM-87 in regions that have relatively dry soil, indicating that the vegetation layer also significantly affects the sensible heat flux, probably through the varying albedo and emissivity properties. Nevertheless, the largest effect of the vegetation is due to the modification of the latent heat flux in the moist soil regions.

The average near-surface relative humidity over the entire simulation period for ANAL-87, CNTL-87, SOILM-87, and BARE-87 is shown in Figs. 75, 76, 78, and 80, respectively. As with the surface temperature, the relative humidity has been averaged over either the 00, 06, 12, or 18 UTC periods. The diurnal fluctuation in relative humidity is clearly evident in the ANAL-87 results in Fig. 75, where low values occur during the daytime and high values occur during the night. The air over the ocean is very humid at all times and the air over the Great Lakes has some impact on the locally higher relative humidities in the morning. The general patterns and diurnal fluctuations in the humidities from CNTL-87 in Fig. 76 are similar to those in Fig. 75, except that the magnitudes have been reduced and there are more terrain-induced effects during the nighttime hours. Note that large gradients of relative humidity occur on the northern boundary of the model domain in Fig. 76a. This occurs because the model is being nudged to the values from the analysis and the model is not predicting high humidity values in this portion of the domain. The differences in average relative humidity shown in Fig. 77 are obtained by subtracting the values in ANAL-87 from those in CNTL-87 (CNTL-87 - ANAL-87). Without FDDA, the model tends to underpredict the relative humidity at all times of the day, but it is particularly low at night where the average humidity is as much as 20 - 25% lower in the central and southern Great Plains. As in the May 5 - 17, 1989 case, it is apparent that the control simulation does not have the correct moisture sources.

The pattern of the average relative humidity fields from SOILM-87 (Fig. 78) is similar to the control simulation, except that maximas in the relative humidity fields can clearly be seen during the entire day over the moist soil regions. By subtracting the results of CNTL-87 from those of SOILM-87 (SOILM-87 - CNTL-87), these differences can seen more clearly in Fig. 79. Evaporation from the soil and vegetation increases the average relative humidity by 25% over the Great Plains and by as much as 50% over New Mexico. There are also increases in relative humidity over the southern Great Lakes by as much as 25% during the 00 and 18 UTC periods. During the entire day, the increase in moisture occurs only in areas immediately adjacent to the moist soil regions. At night, increases in the humidity are still evident over the large areas of soil moisture in the Great Plains, but the humidity in the southern Great Lakes regions becomes diffuse (Figs. 79b and 79c) so that there is little difference in that region between CNTL-87 and SOILM-87. It does not appear that moisture becomes advected very far from the sources of moisture. SOILM-87 is adding moisture into the model domain so that the surface relative humidities are now closer to those in ANAL-87, indicating that soil moisture may be a necessary factor in predicting the correct moisture in the lower atmosphere.

Anomalies in the average relative humidity from BARE-87 (Fig. 80) are even more pronounced than those in SOILM-87. While it is important to examine the response of the model when the vegetation layer is removed, the relative humidity fields produced in BARE-87 are unrealistic as in BARE-89. It is unlikely that patterns and the strong horizontal gradients such as those in Figs. 80a and 80d are seen in a surface weather analysis. By subtracting the results of SOILM-87 from those in BARE-87 (BARE-87 - SOILM-87), the magnitude of the changes can be seen in Fig. 81. Without vegetation, the relative humidity is 15 - 20 % higher during the daytime over the moist-soil regions; but, the relative humidities are as much as 25% lower along the Gulf coast. It is possible that evapotranspiration from the vegetation played an important role in adding more moisture into the atmosphere in the regions with drier soils in this area. In these regions, even though evaporation from the bare-soil surface is small, vegetation can extract moisture from the deeper layers of the soil through its roots.

The average LASI throughout the period is also computed for this case to determine whether the lower atmosphere is sensitive to the particular soil moisture and vegetation distributions chosen for this study. As stated previously, differences in the LASI between simulations are due to changes in the temperature lapse rate and dew point depression in the lower atmosphere (see Table 3). In Figs. 82, 83, 85, and 87, the average LASI from ANAL-87, CNTL-87, SOILM-87, and BARE-87, respectively, are shown. The average LASI during the daytime periods from ANAL-87 in Fig. 82 show that there is a moderate to high risk for wildland fire in only portions of the southwestern U. S. Values of 3.5 - 4.0 (low risk of wildland fire) occurred in West Virginia were wildland fires were observed throughout the period. During the night, the values of LASI decrease because of the decrease in the dew-point depression in the lower atmosphere. The LASI falls to 2.5 - 3.0 at night in most parts of the country, indicating a very low risk for wildland fire. As in the May 5 - 17, 1989 case, there are large gradients in the LASI in mountainous regions due to the way it is calculated (Table 3) and caution should be used in interpreting the LASI in these areas.

The average LASI computed from CNTL-87 is higher nearly everywhere in the domain during both the daytime and nighttime hours than those in ANAL-87 (Fig. 83). In contrast to ANAL-87, LASI values in the central and southeastern U. S. also indicate moderate risk of wildland fire during the day. This occurs because CNTL-87 has lower relative humidities which increase the dew-point depression and, thus, increases the LASI. It also indicates that the temperature and moisture structure is modified, not only at the surface, but in the lower atmosphere. By subtracting the results of ANAL-87 from those in CNTL-87, the specific differences in the LASI are shown in Fig. 84. The LASI are generally 0.5 - 1.0 higher in CNTL-87 than in ANAL-87.

The LASI values from SOILM-87 shown in Fig. 85 are very similar to those from CNTL-87, except that the magnitudes are somewhat lower throughout much of the domain. By subtracting the results of CNTL-87 from those of SOILM-87, the differences in Fig. 86 indicate that the values of the LASI are lower in SOILM-87 by as much as 2.0 over the moist-soil regions. The pattern of these differences

closely corresponds to the temperature and humidity difference fields in Figs. 72 and 79. Most of the changes in the LASI are due to the dew-point depression term (part B from Table 3), although the reduction in surface temperature also reduces the temperature lapse rate near the surface during the daytime and, therefore, reduces the LASI. In this case, a change of 2.0 in the LASI might mean a change of a moderate to very low risk of wildland fire, but only in the moist soil regions. Minor differences in the LASI occur over the dry soil regions. For instance, the LASI are slightly reduced in West Virginia, probably due to the increases in moisture from the southern Great Lakes.

Contrary to the May 5 - 17, 1989 case, the effect of vegetation alone on the LASI in BARE-87 is smaller than the effect of soil moisture alone in SOILM-87. The LASI values from BARE-87 shown in Fig. 86 are also similar to those from CNTL-87 and SOILM-87, but only during the late afternoon are there minor reductions in the LASI. By subtracting the results of SOILM-87 from those of BARE-87, the differences in Fig. 88 show that the increased humidity in BARE-87 over the moist soil regions is enough to decrease the value of the LASI by as much as 0.5 over the moist-soil region in Texas during the daytime. Therefore, the value of the LASI are as much as 2.5 lower in BARE-87 than in CNTL-87 in that area.

6. Conclusion

Atmospheric processes are inherently connected to energy exchanges at the ocean and earth surface. The presence of inhomogeneous distributions of soil moisture and vegetation is expected to modify the surface thermal fluxes when compared to a bare-soil surface under the same environmental conditions. Numerical studies have simulated secondary circulations due to these distributions that may play an important role in local meteorology and climatology, cumulus convection, and air quality.

Meteorological conditions for the May 5 - 17, 1989 and October 25 - November 16, 1987 periods have been simulated in this study by a mesoscale model so that the impact of surface characteristics could be examined. These cases were chosen because of wildland fires and the abnormally dry and wet soil conditions present during both of these periods. Four simulations are performed for each case period. In the first simulation, the model is run with a vegetation layer and dry soil while FDDA nudges the model parameters towards the large-scale analyses. The result from this simulation is series of mesoscale analysis fields. The second simulation is identical to the first, except that FDDA was removed. In this control simulation, the model is allowed to fully prognose the thermodynamics in the boundary layer. The third similation is identical to the control simulation, except that a realistic soil moisture distribution is employed so that its effects on the boundary layer could be ascertained. The fourth simulation is identical to the third simulation, except that the vegetation layer is removed so that the effects of vegetation could be determined. The results from this modeling study are summarized as follows:

- the addition of soil moisture significantly affects the near-surface temperature and relative humidity fields, and affects the cloud cover, precipitation, and wind speeds to a lesser extent
- largest effects due to soil moisture usually occur only where the soil is sufficiently moist; but, there are situations in which these effects are advected downwind
- soil moisture plays an important role in bringing the near-surface humidity in the model closer to the observed values
- for the May 5 - 17, 1989 case, the addition of soil moisture reduces the surface temperature and increases the surface humidity during the entire day, although the largest changes occur during the daytime
- for the October 25 - November 16, 1987 case, the addition of soil moisture reduces the surface temperature and increases the surface humidity during the day, and increases both the surface temperature and humidity at night
- the effects of soil moisture diminish with cooler temperatures in the fall season for the October 25 - November 16, 1987 case because the latent heat flux is reduced
- the model is very sensitive to the particular horizontal soil moisture distribution; however, it is difficult to obtain this quantity in real-time since it is not routinely measured in most parts of the country
- the model does not produce realistic conditions within the boundary layer when vegetation is neglected and a soil-moisture distribution is employed
- vegetation moderates the transfer of water from the soil into the atmosphere; vegetation reduces the amount of water evaporated into the atmosphere where the soil is wet and increases the amount evaporated where the soil is relatively dry
- vegetation reduces the surface wind field predominately through the inhomogeneous roughness lengths that increase the surface friction
- the mesoscale model can produce indices, similar to the LASI in this study, that are indicators of the potential for wildland fires
- the LASI is affected by soil-moisture and vegetation distributions, although it is affected mostly through evapotranspiration which reduces the dew-point depression within the boundary layer
- the LASI is usually reduced over the moist-soil regions, so that the potential for wildland fire can change from a moderate-to-severe risk to a low risk
- the mesoscale model could be used in a prognostic mode to produce parameters useful in predicting the likelihood of wildland fires
- the mesoscale model is able to produce realistic regional climate patterns so that the effects of surface characteristics on the climate patterns can be simulated

- inhomogeneous soil moisture and vegetation distributions not only affect the boundary layer characteristics, but they also affect the temperature and humidity fields averaged over the entire simulation period

An operational atmospheric numerical model could be used to produce forecasts of the LASI which could be used as a forecast tool to aid forest service personnel to determine likely locations where wildland fires could occur. While forest service personnel already use the NMC's operational meteorological models, it would be useful to employ a mesoscale model so that regional-scale circulations, not resolved by NMC models, can be represented. In this way circulations affected by local terrain, soil, and vegetation characteristics can be simulated more accurately. These atmospheric forecasts could be used to derive quantities useful to forest service personnel in predicting likely wildland fire occurrences.

7. Acknowledgments

This research was performed at Savannah River Technology Center and was supported by the U. S. Department of Agriculture (USDA), Forest Service under an interagency agreement (NC-93-2). The Savannah River Technology Center is operated for the U. S. Department of Energy by Westinghouse Savannah River Company. Dan P. Griggs performed many of the numerical simulations and analyses during the course of this project.

8. References

Copeland, J. H., 1994: The use of RAMS to downscale general circulation model results. Preprints, *Second RAMS Users' Workshop*, Fort Collins, CO, 3- 7.

Dickinson, R. E., A. Henderson-Sellers, P. J. Kennedy, and M. F. Wilson, 1986: Biosphere-Atmosphere Transfer Scheme (BATS) for the NCAR Community Climate Model. National Center for Atmospheric Research, Boulder, CO, Tech. Note NCAR/TN-275+ST.

Fast, J. D., and M. D. McCorcle, 1991: The effect of heterogeneous soil moisture on a summer baroclinic circulation in the central United States. *Mon. Wea. Rev.*, **119**, 2140-2167.

Hefland, H. M., and J. C. Labraga, 1988: Design of a nonsingular level 2.5 second-order closure model for the prediction of atmospheric turbulence. *J. Atmos. Sci.*, **45**, 113-132.

Haines, D. A., 1988: A lower atmospheric severity index for wildland fires. *Nat. Wea. Digest*, **13**, 23-27.

Giorgi, F., C. S. Brodeur, and G. T. Bates, 1994: Regional climate change scenarios over the United States produced with a nested regional climate model. *J. Climate.*, 7, 375-399.

Lanicci, J. M., T.N. Carlson, and T. T. Warner, 1987: Sensitivity of the Great Plains severe-storm environment to soil-moisture distribution. *Mon. Wea. Rev.*, **115**, 2660-2673.

Lee, T., 1992: The impact of vegetation on the atmospheric boundary layer and convective storms. M. S. Thesis, Atmos. Sci. Paper No. 509, Department of Atmospheric Science, Colorado State University, Fort Collins, CO 80523, 137 pp.

Kunkel, K. E., S. A. Changnon, and J. A. Angel, 1994: Climatic aspects of the 1993 upper Mississippi River basin flood. *Bull. Amer. Meteor. Soc.*, **75**, 811-822.

Mahfouf, J., E. Richard, and R. Mascart, 1987; The influence of soil and vegetation on the development of mesoscale circulations. *J. of Climate and Appl. Meteor.*, **26**, 1483-1495.

Mellor, G. L., and T. Yamada, 1982: Development of a turbulent closure model for geophysical fluid problems. *Rev. Geophys. Space Phys.*, **20** (10), 851-875.

Ookouchi, Y., M. Segal, R. C. Kessler, and R. A. Pielke, 1984: Evaluation of soil moisture effects on the generation and modification of mesoscale circulations. *Mon. Wea. Rev.*, **112**, 2281-2292.

Petersen, R. A., K.E. Mitchell, G. J. DiMego, and N.W. Junker, 1991: Tests of soil moisture enhancements on regional and mesoscale precipitation forecasts. Preprints, Ninth Conference on Numerical Weather Prediction, Denver, CO, 248-249.

Pielke, R. A., W. R. Cotton, R. L. Walko, C. J. Tremback, W. A. Lyons, L. D. Grasso, M. E. Nicholls, M. D. Moran, D. A. Wesley, T. J .Lee, and J. H. Copeland, 1992: A comprehensive meteorological modeling system - RAMS. *Meteor. Atmos. Phys.*, **49**, 69-91.

Segal, M., and R. W. Arritt, 1992: Nonclassical mesoscale circulations caused by surface sensible heat-flux gradients. *Bull. Amer. Meteor. Soc.*, **73**, 1593-1604.

Segal, M., R. Avissar, M. C. McCumber, and R. A. Pielke, 1988; Evaluation of vegetation effects on the generation and modification of mesoscale circulations. *J. Atmos. Sci.*, **45**, 2268-2292.

Segal, M., W. E. Schreiber, G. Kallos, J. R. Garratt, A. Rodi, J. Weaver, and R. A. Pielke, 1989: The impact of crop areas in Northeast Colorado in midsummer mesoscale thermal circulations. *Mon. Wea. Rev.*, **117**, 809-825.

Tripoli, G. J, and W. R. Cotton, 1982: The Colorado State University three-dimensional cloud / mesoscale model - 1982, Part I: General theoretical framework and sensitivity experiments. *J. de Rech. Atmos.*, **16**, 185-219.

Yan, H., and R. A. Anthes, 1988: The effect of variations in surface moisture on mesoscale circulations. *Mon. Wea. Rev.*, **116**, 192-208.

Zhong, S., and J. C. Doran, 1994: An experimental and numerical study of the modifications of mixed-layer structure by inhomogenous surface fluxes and secondary circulations. Preprint, Sixth Conference on Mesoscale Processes, Portland, OR, 288-291.

Ziegler, C. L., T. J. Lee, and R. A. Pielke, 1994: Simulations of the dryline with a 3-D mesoscale model. Preprints, Sixth Conference on Mesoscale Processes, Portland, OR, 242-245.

APPENDIX

Example RAMSIN file used for model simulations:

```
$MODEL_GRIDS

! Simulation title (64 chars)
  EXPNME  =    'Version 3a' ,

  IOTYPE   = 0,                              ! -1=diagnostic, 0=normal run

  RUNTYPE ='INITIAL',    ! type of run: MAKESFC, INITIAL, HISTORY, or MAKEVFILE

  TIMEUNIT = 'h',                            ! 'h','m','s' - Time units of
                                             !   TIMMAX, TIMSTR, VTIME

  TIMMAX=   528.,                            ! Final time of simulation

  NGRIDS  =   1,                             ! Number of grids to run

  NNXP    =  85,                             ! Number of x gridpoints, US@60
  NNYP    =  55,                             ! Number of y gridpoints, US@60
  NNZP    =  30,                             ! Number of z gridpoints
  NNZG    =  11,                             ! Number of soil gridpoints
  NXTNEST =   1,                             ! Grid number which is the next
                                             !   coarser grid

     ! Coarse grid specifications

  IHTRAN  =      1,                          ! 0-Cartesian, 1-Polar stereo
  DELTAX  =  60000.,
  DELTAY  =  60000.,                         ! X and Y grid spacing

  DELTAZ  =      0.,                         ! Z grid spacing (set to 0. to use ZZ)
  DZRAT   =    1.15,                         ! vertical grid stretch ratio
  DZMAX   =    1000.,                        ! maximum delta Z for vertical stretch

  ZZ=    0.00,   90.00,  135.00,  186.30,  244.78,  311.45,  387.45,  474.09,
       572.86,  686.46,  813.82,  960.15, 1129.89, 1333.58, 1590.23, 1934.15,
      2429.39, 3142.54, 4169.48, 5196.42, 6223.36, 7250.30, 8277.24, 9304.18,
     10331.12,11358.06,12385.00,13411.94,14438.88,15465.82,
                                             ! Vertical levels if DELTAZ = 0

  DTLONG  =     60.,                         ! Coarse grid long timestep
  NRATIO  =      2,                          ! Small timestep ratio

  IMONTH1 =   10,                            ! Month
  IDATE1  =   25,                            ! Day
  IYEAR1  =   87,                            ! Year
  STRTIM  = 12.0,                            ! GMT of model TIME = 0.

                                             ! Nest ratios between this grid
                                             !  and the next coarser grid.
  NSTRATX =   1, 4,                          ! x-direction
  NSTRATY =   1, 4,                          ! y-direction
  NNDTRAT =   1, 1,                          ! time
```

```
  NESTZ = 0,                              ! contort coarser grids if negative
  NSTRATZ=4,4,3,3,3,3,2,2,2,2,1,1,1,1,


  POLELAT  =    40.0,                     ! Latitude of pole point
  POLELON  =   -98.0,                     ! Longitude of pole point

  CENTLAT=    40.0,
  CENTLON=   -98.0,

                                        ! Grid point on the next coarser
                                        ! nest where the lower southwest
                                        ! corner of this nest will start.
                                        ! IF NINEST or NJNEST = 0, use CENTLAT/LON
  NINEST  =   1,                        ! i-point
  NJNEST  =   1,                        ! j-point
  NKNEST  =   1,                        ! k-point

  NNSTTOP =   1,                        ! Flag (0-no or 1-yes) if this
  NNSTBOT =   1,                        ! nest goes the top or bottom of the
                                        ! coarsest nest.

  GRIDU   =  0., 0.,                    ! u-component for moving grids
  GRIDV   =  0., 0.,                    ! v-component for moving grids
                                        !  (still not working!)
$END

$MODEL_FILE_INFO

               ! History file input

 TIMSTR=           0.,  ! time of history start (see TIMEUNIT)
 HFILIN =    'ps.h0h',  ! input history file name

               ! History/analysis file output

 IOUTPUT=       1,                      ! 0-no files, 1-save/dispose
 HFILOUT='ps.h',                        ! history file prefix
 AFILOUT='ps.a',                        ! analysis file prefix
 HFUNITS='h',      AFUNITS='h',         ! history/anal file units (M,m,H,h,S,s)
 FRQHIS  =43200.,  FRQANL  =10800.,     ! history/anal file frequency

               ! Variable initialization input

 INITIAL =   2,             ! Initial fields - 1=horiz.homogeneous, 2=variable
 VTIME   =  0., 12., 24.,   ! model times for varfiles (See TIMEUNIT)
           36., 48., 60., 72., 84., 96.,108.,120.,132.,144.,156.,
          168.,180.,192.,204.,216.,228.,240.,252.,264.,276.,288.,
          300.,312.,324.,336.,348.,360.,372.,384.,396.,408.,420.,
          432.,444.,456.,468.,480.,492.,504.,516.,528.,
 VARFIL ='isan_obs_87/varfil_i/iv25-oct-87-12',
         'isan_obs_87/varfil_i/iv26-oct-87-00',
         'isan_obs_87/varfil_i/iv26-oct-87-12',
         'isan_obs_87/varfil_i/iv27-oct-87-00',
         'isan_obs_87/varfil_i/iv27-oct-87-12',
         'isan_obs_87/varfil_i/iv28-oct-87-00',
         'isan_obs_87/varfil_i/iv28-oct-87-12',
```

```
        'isan_obs_87/varfil_i/iv29-oct-87-00',
        'isan_obs_87/varfil_i/iv29-oct-87-12',
        'isan_obs_87/varfil_i/iv30-oct-87-00',
        'isan_obs_87/varfil_i/iv30-oct-87-12',
        'isan_obs_87/varfil_i/iv31-oct-87-00',
        'isan_obs_87/varfil_i/iv31-oct-87-12',
        'isan_obs_87/varfil_i/iv01-nov-87-00',
        'isan_obs_87/varfil_i/iv01-nov-87-12',
        'isan_obs_87/varfil_i/iv02-nov-87-00',
        'isan_obs_87/varfil_i/iv02-nov-87-12',
        'isan_obs_87/varfil_i/iv03-nov-87-00',
        'isan_obs_87/varfil_i/iv03-nov-87-12',
        'isan_obs_87/varfil_i/iv04-nov-87-00',
        'isan_obs_87/varfil_i/iv04-nov-87-12',
        'isan_obs_87/varfil_i/iv05-nov-87-00',
        'isan_obs_87/varfil_i/iv05-nov-87-12',
        'isan_obs_87/varfil_i/iv06-nov-87-00',
        'isan_obs_87/varfil_i/iv06-nov-87-12',
        'isan_obs_87/varfil_i/iv07-nov-87-00',
        'isan_obs_87/varfil_i/iv07-nov-87-12',
        'isan_obs_87/varfil_i/iv08-nov-87-00',
        'isan_obs_87/varfil_i/iv08-nov-87-12',
        'isan_obs_87/varfil_i/iv09-nov-87-00',
        'isan_obs_87/varfil_i/iv09-nov-87-12',
        'isan_obs_87/varfil_i/iv10-nov-87-00',
        'isan_obs_87/varfil_i/iv10-nov-87-12',
        'isan_obs_87/varfil_i/iv11-nov-87-00',
        'isan_obs_87/varfil_i/iv11-nov-87-12',
        'isan_obs_87/varfil_i/iv12-nov-87-00',
        'isan_obs_87/varfil_i/iv12-nov-87-12',
        'isan_obs_87/varfil_i/iv13-nov-87-00',
        'isan_obs_87/varfil_i/iv13-nov-87-12',
        'isan_obs_87/varfil_i/iv14-nov-87-00',
        'isan_obs_87/varfil_i/iv14-nov-87-12',
        'isan_obs_87/varfil_i/iv15-nov-87-00',
        'isan_obs_87/varfil_i/iv15-nov-87-12',
        'isan_obs_87/varfil_i/iv16-nov-87-00',
        'isan_obs_87/varfil_i/iv16-nov-87-12',
IVWIND =       0,       ! initial winds ( only 0 works)

NUDLAT   =     5,       ! number of points in the lateral bnd region
TNUDLAT  =     900.,    ! nudging time scale (s) at lateral boundary
TNUDCENT =     21600.,  ! nudging time scale (s) in center of domain
TNUDTOP  =      3600.,  ! nudging time scale (s) at top of domain
ZNUDTOP  =     11000.,  ! nudging at top of domain above this height (m)

              ! Printed output controls

 FRQPRT  =   10800.,     ! Printout frequency
 FRQIPR  =   86400.,     ! Integral print frequency
 FRQIST  =   86400.,     ! Integral store frequency

 ISTPFL  =         1,    ! Timestep message frequency flag
 INITFLD =         1,    ! Initial field print flag 0=no print, 1=print
 INPRTFL =         1,    ! Namelist print flag 0=no print, 1=print

             ! Input topography variables
```

```
   SFCFILES = 'NONE',      ! File path and prefix for surface characteristic
                           ! files.

   ITOPTFLG = 1,           ! 2 - Fill data in "ruser"
   IPCTLFLG = 1,           ! 1 - Interp data from latlon dataset
   ISSTFLG  = 1,           ! 0 - Interpolate from coarser grid
   IVEGTFLG = 2,
                           !
                           ! The following only apply for IxxxxFLG=1
                           !
   ITOPTFN = '/cms/topography/world/topo/U',
             '/cms/topography/world/topo/U',
                           ! Input topography file name
   IPCTLFN = '/cms/topography/world/pctland/L',
             '/cms/topography/world/pctland/L',
   ISSTFN  = '/cms/sst/climatology/november/sst',
             '/cms/sst/climatology/november/sst',
   IVEGTFN = '/erdas/u1/lee/usgs/DATA/V',



   SILAVWT  = 0.0,         ! Weighting of topo silhouette averaging
   TOPTWVL  = 4.0,         ! Topo wavelength cutoff in filter
   PCTLWVL  = 2.0,         ! Land pct wavelength cutoff in filter
   SSTWVL   = 2.0,         ! Land pct wavelength cutoff in filter

$END

$MODEL_OPTIONS

  NADDSC    =    0,     ! Number of additional "scalar" variables to add (<= 5)

  NTOPSMTH  =    0,     ! Number of passes for topography smoother
  IZFLAT    =    2,     ! Width of flat margin around domain (in grid points)

      ! Numerical schemes

  ITMDIFF =      2,     ! 1=forward, 2=leapfrog, 3=hybrid
  NONHYD  =      1,     ! nonhydrostatic=1, hydrostatic=0
  SSPCT   =     0.,     ! Sound speed fraction for the nonhydrostatic model
  IMPL    =      1,     ! Implicit flag for acoustic model  -  0=off, 1=on
  ICNTEQ  =      2,     ! Hyd - continuity equation - 1 -incomp, 2 -anelastic
  WTKD    =     0.,     ! Klemp/Durran - current timestep weighting

  ICORFLG =      1,     ! Coriolis flag/2D v-component  -  0=off, 1=on

  IBCTOP =       0,     ! top boundary condition
                        ! 0-wall on top(nonhyd)       2-prognostic sfc prs(hyd)
                        ! 1-Klemp-Durran(nonhyd/hyd) 3-material surface(hyd)

  IBND    =      1,     ! Lateral boundary condition flags
  JBND    =      1,     ! 1-Klemp/Wilhelmson, 2-Klemp/Lilly, 3-Orlanski
                        ! 4-cyclic
  CPHAS   =    20.,     ! Phase speed if IBND or JBND = 1
  LSFLG   =      0,     ! Large-scale gradient flag for variables other than
                        ! normal velocity:
                        ! 0 = zero gradient inflow and outflow
                        ! 1 = zero gradient inflow, radiative b.c. outflow
```

```
                    ! 2 = constant inflow, radiative b.c. outflow
                    ! 3 = constant inflow and outflow
 NFPT    =      0,  ! Rayleigh friction - number of points from the top
 DISTIM  =      0.,  !                  - dissipation time scale

 TIMSCL  =      0.,  ! Initial wind spin-up - time scale
 KSPIN   =      33,  !                      - below this level (velocity)
 KMSPIN  =      10,  !                      - below this level (momentum)

 IPRSPLT =       0,  ! precipitation time-split scheme - 0=off, 1=on
 IADVL   =       2,  ! Order of advection - Leapfrog - 2 or 4
 IADVF   =       2,  ! Order of advection - Forward - 2 or 6
 IPGRAD  =       1,  ! Pressure gradient scheme for topo.: 1-transform
                     !                                     2-interpolate
 FILT4   =    000.,  ! Fourth order filter coefficient (0 - off)
                     !    ( > 0  timestep at which 2 delta waves are
                     !    totally removed)
 FXLONG  =  0.0000,  ! Long filter coefficient 0=off
 FYLONG  =  0.0000,  ! Long filter coefficient 0=off

    ! Radiation parameters

 ISWRTYP =    2,   ! Shortwave radiation type 0-none, 2-Mahrer/Pielke, 1-Chen
 ILWRTYP =    1,   ! Longwave radiation type 0-none, 2-Mahrer/Pielke, 1-Chen
 RADFRQ  =  900.,  ! Frequency of radiation tendency update in seconds
 LONRAD  =    1,   ! Longitudinal variation of shortwave  (0-no, 1-yes)

    ! Cumulus parameterization parameters

 NNQPARM =   1,   1,   0,   0,            ! convective parameterization flag
                                          !  0-off, 1-on
 CONFRQ  =  900.,  ! Frequency of conv param. updates in seconds
 WCLDBS  =  .001,  ! vertical motion needed at cloud base for convection

    ! Surface layer and soil parameterization

 ISFCL   =      1,  ! surface layer/soil/veg model
                    ! 0-specified surface layer gradients
                    ! 1-soil/vegetation model

 NVGCON  =      2,  ! Vegetation type
              ! 1 -- Crop/mixed farming          2 -- Short grass
              ! 3 -- Evergreen needleleaf tree  4 -- Deciduous needleleaf tree
              ! 5 -- Deciduous broadleaf tree   6 -- Evergreen broadleaf tree
              ! 7 -- Tall grass                 8 -- Desert
              ! 9 -- Tundra                    10 -- Irrigated crop
              !11 -- Semi-desert               12 -- Ice cap/glacier
              !13 -- Bog or marsh              14 -- Inland water
              !15 -- Ocean                     16 -- Evergreen shrub
              !17 -- Deciduous shrub           18 -- Mixed woodland
 TSEASN  =  280.,    ! Average seasonal temp
 TVGOFF  =   0.,     ! Initial veg temp offset
 VWTRCON =  .000,    ! Initial veg water storage (not working)

 UBMIN   =  0.25,    ! Minimum U value to use in computing U_*
 PCTLCON =   1.0,    ! constant land percentage if for all domain
 NSLCON  =     6,    ! constant soil type if for all domain
                     !  1=sand              2=loamy sand     3=sandy loam
```

```
                    !  4=silt loam       5=loam           6=sandy clay loam
                    !  7=silty clay loam 8=clay loam      9=sandy clay
                    ! 10=silty clay     11=clay          12=peat

 ZROUGH  =  0.05,    ! constant roughness if for all domain
 ALBEDO  =   0.2,    ! constant albedo when not running soil model
 SEATMP  =  280.,    ! constant water surface temperature

 DTHCON  =  -10.,    ! constant surface layer temp gradient for no soil
 DRTCON  = .000,     ! constant surface layer moist gradient for no soil
 SOILDZ  =   0.,     ! soil model grid spacing
 SLZ     = -0.50,-0.45,-0.40,-0.35,-0.30,-0.25,-0.20,-0.15,-0.10,-0.05, 0.00,
                     ! soil grid levels
 SLMSTR  =  0.2, 0.2, 0.2, 0.2, 0.2, 0.2, 0.2, 0.2, 0.2, 0.2, 0.2,
                     ! initial soil moisture
 STGOFF  =  0.0, 0.0, 0.0, 0.0, 0.0, 0.0, 0.0, 0.0, 0.0, 0.0, 0.0,
                     ! Initial soil temperature offset from lowest
                     ! atmospheric level

    ! Eddy diffusion coefficient parameters

 IDIFFK = 1,         ! K flag:
                     !    1 - Horizontal deformation/ Vertical Mellor-Yamada
                     !    2 - Anisotropic deformation (horiz and vert differ)
                     !    3 - Isotropic deformation (horiz and vert same)
                     !    4 - Deardorff TKE (horiz and vert same)
 CSX = .20,          ! Adjustable parameter, deformation horiz. K's coefficient
 CSZ = .20,          ! Adjustable parameter, deformation vert. K's coefficient
 XKHKM = 3.,         ! Ratio of horizontal K_h to K_m for TKE or deformation
 ZKHKM = 3.,         ! Ratio of vertical K_h to K_m for TKE or deformation
 AKMIN= .2,          ! Ratio of minimum horizontal eddy viscosity coefficient
                     !    to typical value from deformation K

    ! Microphysics

 NLEVEL  =   2,              ! moisture complexity level

 ICLOUD =   0,
 IRAIN  =   0,               ! Microphysics flags
 IPRIS  =   0,               !-------------------
 ISNOW  =   0,               ! where x= R - rain
 IAGGR  =   0,               !          P - pristine crystals
 IGRAUP =   0,               !          S - snow
 IHAIL  =   0,               !          A - aggregates

 CPARM  =  0.,
 RPARM  =  0.,               !          G - graupel
 PPARM  =  0.,               !          H - hail
 SPARM  =  0.,               ! NIxCNFL = 0 - no species
 APARM  =  0.,               !           1 - diagnostic concen.
 GPARM  =  0.,               !           2 - specified mean diameter
 HPARM  =  0.,               !           3 - specified y-intercept
                             !           4 - specified concentration
                             !           5 - prognostic concen.

AMI0    =  0.0000001,        ! minimum crystal mass (gm)
CON     =   300.0 ,          ! CCN concentration (number/cc)
THOMO   =  233.0,            ! homogeneous nucleation temperature
```

```
$END

$MODEL_SOUND
      ! Sounding specification

               ! Flags for how sounding is specified

  IPSFLG=0,    ! specifies what is in PS array
               ! 0 - pressure (mb), 1 - heights (m), PS(1)=sfc press(mb)

  ITSFLG=2,    ! specifies what is in TS array
               ! 0 - temp(C), 1 - temp(K), 2 - pot. temp(K)

  IRTSFLG=3,   ! specifies what is in RTS array
               ! 0 - dew pnt.(C), 1 - dew pnt.(K), 2 - mix rat(g/kg)
               ! 3 - relative humidity on %, 4 - dew pnt depression(K)

  IUSFLG=0,    ! specifies what is in US and VS arrays
               ! 0 - u,v component(m/s), 1 - umoms-direction, vmoms-speed

  IUSRC = 0,   !  source of wind profile:
               !  0  - umoms, vmoms, valid at sounding levels (PS)
               !  -1 - usndg, vsndg, valid at model levels    (Z)


 PS=1012.00 , 1000.00 ,  977.00 ,  949.00 ,  936.00 ,  850.00 ,  848.00 ,
     797.00 ,  700.00 ,  662.00 ,  595.00 ,  579.00 ,  565.00 ,  560.00 ,
     500.00 ,  498.00 ,  461.00 ,  443.00 ,  406.00 ,  400.00 ,  387.00 ,
     383.00 ,  328.00 ,  325.00 ,  316.00 ,  309.00 ,  307.00 ,  300.00 ,
     285.00 ,  250.00 ,  200.00 ,  150.00 ,  100.00 ,   80.00 ,   10.0 ,

 TS= 288.18 ,  288.36 ,  288.88 ,  293.11 ,  294.27 ,  298.93 ,  298.92 ,
     304.48 ,  309.35 ,  310.27 ,  313.50 ,  315.02 ,  317.23 ,  317.80 ,
     318.75 ,  318.88 ,  320.88 ,  322.03 ,  326.27 ,  327.02 ,  328.41 ,
     328.73 ,  330.56 ,  331.02 ,  333.69 ,  335.55 ,  335.89 ,  336.99 ,
     340.82 ,  343.42 ,  347.35 ,  364.39 ,  379.82 ,  398.66 ,  480.00 ,

 RTS= 90.7 ,  95.5 ,  98.0 ,  96.8 ,  96.1 , 100.0 , 100.0 ,  94.1 ,  90.6 ,
      99.3 ,  94.1 ,  75.8 ,  49.3 ,  38.4 ,  55.8 ,  55.7 ,  85.1 ,  80.6 ,
      78.0 ,  71.1 ,  57.6 ,  52.3 ,  74.9 ,  74.0 ,  39.6 ,  22.7 ,  16.0 ,
      09.7 ,  02.5 ,  06.1 ,  15.8 ,  03.6 ,  02.1 ,  01.5 ,  01.5 ,


 US= -10.0 ,  -10.0 ,  -11.0 ,  -12.0 ,  -12.0 ,  -5.0 ,   5.0 ,
       6.5 ,    8.7 ,   11.0 ,   14.0 ,   16.0 ,  17.0 ,  18.0 ,
      21.9 ,   22.0 ,   24.0 ,   26.0 ,   30.0 ,  30.0 ,  32.0 ,
      33.0 ,   34.0 ,   35.0 ,   36.0 ,   37.0 ,  39.0 ,  40.6 ,
      42.0 ,   50.7 ,   46.6 ,   35.0 ,   30.0 ,  30.0 ,  30.0 ,

 VS=   2.1 ,    2.1 ,    2.5 ,    3.0 ,    3.5 ,   4.0 ,   4.0 ,
       3.5 ,    3.1 ,    3.3 ,    3.5 ,    3.7 ,   4.2 ,   4.5 ,
       6.0 ,    6.0 ,    7.0 ,    8.0 ,    9.0 ,  10.0 ,  11.0 ,
      12.0 ,   13.0 ,   14.0 ,   14.1 ,   14.5 ,  15.0 ,  15.0 ,
      14.8 ,    8.0 ,    8.0 ,    8.0 ,    8.0 ,   8.0 ,   8.0 ,

 USNDG = 0.,   ! Wind components if IUSRC= -1
 VSNDG = 0.,   !
```

```
  KMEAN1 = 0,    !  lower model level for calculation of (umean,vmean)
  KMEAN2 = 0,    !  upper model level for calculation of (umean,vmean)

  UMEAN = 0.0,   !  u-component for Galilean transformation
  VMEAN = 0.0,   !  v-component for Galilean transformation

$END

$MODEL_PRINT
            ! Specifies the fields to be printed during the simulation

  NPLT   =  11,                ! Number of fields to be printed at each time
                               !    for various cross-sections (limit of 50)
  IPLFLD = 'UP','VP','WP','THETA','TKE','TVEG','RVEG','WVEG','SLM','TG',
           'PCPT',
                               ! Field names - see table below
! PLFMT(6) = '0PF7.2',         ! Format specification if default is unacceptable

  IXSCTN = 3,3,3,3,3,3,3,3,3,3,3,
                               ! Cross-section type (1=XZ, 2=YZ, 3=XY)
  ISBVAL = 2,2,2,2,2,10,10,10,10,10,1,

                               ! Grid-point slab value for third direction

  ! The following variables can also be set in the $PRNT namelist:  IAA,
  ! IAB, JOA, JOB, NAAVG, NOAVG, PLTIT, PLCONLO, PLCONHI, and PLCONIN.

$END

C      'UP'     - UP(M/S)     'RC'    - RC(G/KG)     'PCPT' - TOTPRE
C      'VP'     - VP(M/S)     'RR'    - RR(G/KG)     'TKE'  - TKE
C      'WP'     - WP(CM/S)    'RP'    - RP(G/KG)     'HSCL' - HL(M)
C      'PP'    - PRS(MB)      'RA'    - RA(G/KG)     'VSCL' - VL(M)
C      'THP'   - THP(K)
C      'THETA'- THETA(K)      'RL'    - RL(G/KG)     'TG'   - TG (K)
C      'THVP'  - THV'(K)      'RI'    - RI(G/KG)     'SLM'  - SLM (PCT)
C      'TV'    - TV(K)        'RCOND'- RD(G/KG)      'CONPR'- CON RATE
C      'RT'    - RT(G/KG)     'CP'    - NPRIS        'CONP' - CON PCP
C      'RV'    - RV(G/KG)     'RTP'   - RT'(G/KG)    'CONH' - CON HEAT
C                                                    'CONM' - CON MOIS
C      'THIL' - Theta-il (K)    'TEMP' - temperature (K)
C      'TVP'   - Tv' (K)        'THV'  - Theta-v     (K)
C      'RELHUM'-relative humidity (%)          'SPEED'- wind speed (m/s)
C      'FTHRD'- radiative flux convergence (??)
C      'MICRO'- GASPRC
C      'Z0'    - Z0 (M)       'ZI'    - ZI (M)       'ZMAT' - ZMAT (M)
C      'USTARL'-USTARL(M/S)  'USTARW'-USTARW(M/S)  'TSTARL'-TSTARL (K)
C      'TSTARW'-TSTARW(K)    'RSTARL'-RSTARL(G/G)  'RSTARW'-RSTARW(G/G)
C      'UW'    - UW  (M*M/S*S)                     'VW'   - VW (M*M/S*S)
C      'WFZ'   - WFZ (M*M/S*S)                     'TFZ'  - TFZ (K*M/S)
C      'QFZ'   - QFZ (G*M/G*S)                     'RLONG'- RLONG
C      'RSHORT'-RSHORT


$ISAN_CONTROL
    MSTAGE  = 0,  0,  1,         ! Main switches for
```

```
                                  ! pressure, isentropic, "varfile" processing

    NATIMES = 2,                  ! Number of times on which to perform analysis

    IAHOUR  =  0, 12,  0, 12,     ! Hours to analyze
    IADATE  =  2,  2, 26, 26,     ! Dates
    IAMONTH = 11, 11, 10, 10,     ! Months
    IAYEAR  = 87, 87, 87, 87,     ! Years

                  !    NCAR archived data file names

!   IAPR    = 'ncar/Y08164',          ! Input pressure level dataset
    IAPR    = 'lfmanal',              ! Input pressure level dataset

    IARAWI  = 'ncar_data/K6557K',     ! Archived rawindsonde file name

    IASRFCE = 'ncar_data/K6527K',     ! Archived surface obs file name

                 ! File names and dispose flags

    IFNPRS = 'ip',  ! Pressure file name prefix
    IOFLGP= 0,                ! Dispose flag:  0 = no write, 1 = write

    IFNISN = 'ii',  ! Isentropic file name prefix
    IOFLGI= 0,                ! Dispose flag:  0 = no write, 1 = write

    IFNSIG = 'is',  ! Sigma-z file name prefix
    IOFLGS= 0,                ! Dispose flag:  0 = no write, 1 = write

    IFNVAR = 'iv',  ! "Variable initialization" file name prefix
    IOFLGV= 1,                ! Dispose flag:  0 = no write, 1 = write

$END

$ISAN_PRESSURE

                 !-----------------------------------
                 !   Pressure grid information:
                 !-----------------------------------
    NPRX=41,          ! number of grid points in x (lon) direction
    NPRY=38,          ! number of grid points in y (lat) direction
    NPRZ=6,           ! number of pressure levels

    PDATA= 'LFM',     ! 'NMC' or 'ECMWF' if from NCAR archives.

    WPLON =   1.0,    ! West longitude bound of pressure data access
    SPLAT =   1.0,    ! South latitude bound
                      ! Latitude and longitude bounds are north and east
                      !   if positive, south and west if negative.


   SPCNPRX = 1.0,     ! East-west grid spacing of pressure data
   SPCNPRY = 1.0,     ! North-south spacing

                      ! Pressure levels (mb) in input dataset to access
   LEVPR  = 1000,850,700,500,400,100,

 $END
```

```
 ------------------------------------------
      Isentropic and sigma-z processing
 ------------------------------------------

$ISAN_ISENTROPIC

                  !----------------------------------
                  !     Specify isentropic levels
                  !----------------------------------

   NISN     =    35,       ! number of isentropic levels
   LEVTH    =  252,255,258,261,264,267,270,273,276,279,282,285,288,291,294,
               297,300,303,306,309,312,315,318,321,324,327,330,335,340,345,
               350,355,360,380,400,

                  !----------------------------------
                  !   Analyzed grid information:
                  !----------------------------------

   NIGRIDS =  1,          ! number of RAMS grids to analyze

!  TOPSIGZ =  10000.,     ! sigma-z coordinates to about this height
   TOPSIGZ =   9000.,     ! sigma-z coordinates to about this height

   HYBBOT  = 4000.,       ! Bottom (m) of blended sigma-z/isentropic layer in
                          ! varfiles
   HYBTOP  = 6000.,       ! Top (m) of blended sigma-z/isentropic layer

   SFCINF  = 1000.,       ! Vertical influence of surface observation analysis

   SIGZWT  =    0.,       ! Weight for sigma-z data in varfile:
                          ! 0=no sigz data, 1=full weight from surface to HYBBOT

   NFEEDVAR =    1,       ! 1 = feed back nested grid varfile info, 0 = don't

                  !----------------------------------
                  !   Observation number limits:
                  !----------------------------------

   MAXSTA=150,            ! maximum number of rawindsondes (archived + special)
   MAXSFC=1000,           ! maximum number of surface observations

   IARCSND =      1,      ! Input archived soundings ? (0-no, 1-yes)
   IARCSFC =      1,      ! Input archived surface obs ?
   ISPCSND =      0,      ! Input special soundings ?
   ISPCSFC =      0,      ! Input special surface obs ?

   NONLYS  =      0,      ! Number of stations only to be used
   IDONLYS ='76458',      ! Station ID's used

   NOTSTA  =      5,      ! Number of stations to be excluded
   NOTID   ='r70398','r71109',     ! Station ID's to be excluded
            'r71115','r72220',
            'r72265',
                          !   Prefix with 'r' for rawindsonde, 's' for surface

   STASEP  =  .  .1,      ! Minimum surface station separation in degrees.
```

```
                        !    Any surface obs within this distance
                        !    of another obs will be thrown out unless it has
                        !    less missing data, in which case the other obs
                        !    will be thrown out.

   ISTAPLT =      0,     ! If ISTAPLT = 1, soundings are plotted;
   ISTAREP =      0,     ! If ISTAREP = 1, soundings are listed;
                         !    no objective analysis is done.
                         ! If ISTAREP/ISTAPLT = 0, normal processing is done

   IUPPER  =      1,     ! 1-Do upper air analysis, 0-Only do surface

   IGRIDFL =      1,     ! Grid flag = 0, if no grid point data, only obs
                         !             1, if all grid point data and obs
                         !             2, if partial grid point and obs
                         !             3, if only grid data

   GRIDWT  =   .010,
                       ! Relative weight for the gridded pressure data compared
                       !   to the observational data in the objective analysis

   GOBSEP  =    5.0,     ! Grid-observation separation (degrees)
   GOBRAD  =    5.0,     ! Grid-obs proximity radius (degrees)

   WVLNTH  =  1200.,
                         ! Used in S. Barnes objective analysis.
                         !    Wavelength in km to be retained to the RESPON
                         !    percent from the data to the upper air grids.
   SWVLNTH =  750.,
                         ! Wavelength for surface objective analysis

   RESPON  =    .9,
                         ! Percentage of amplitude to be retained.

$END

 ------------------------------------------
     Graphical processing
 ------------------------------------------

$ISAN_GRAPH

         ! Main switches for plotting

  IPLTPRS  =   0,      ! Pressure coordinate horizontal plots
  IPLTISN  =   0,      ! Isentropic coordinate horizontal plots
  IPLTSIG  =   0,      ! Sigma-z coordinate horizontal plots
  IPLTSTA  =   0,      ! Isentropic coordinate "station" plots

         !-------------------------------------
         ! Pressure plotting information
         !-------------------------------------
  ILFT1I   =   0,      ! Left boundary window
  IRGT1I   =   0,      ! Right boundary window
  IBOT1J   =   0,      ! Bottom boundary window
  ITOP1J   =   0,      ! Top boundary window
                       !    Window defaults to entire domain if one equals 0.
```

```
  NPLEV   =   3,                ! Number of pressure levels to plot
  IPLEV   = 1000,850,500,
                                ! Levels to be plotted
  NFLDU1  =   4,                ! Number of fields to be plotted
  IFLDU1  =   'SPEED','THETA','GEO','RELHUM',        ! Field names
  CONU1   = 0.,0.,0.,0.,        ! Field contour increment
  IVELU1  = 2,0,0,0,            ! Velocity vector flag

          !--------------------------------------
          ! Isentropic plotting information
          !--------------------------------------
  ILFT3I  =   0,      ! Left boundary window
  IRGT3I  =   0,      ! Right boundary window
  IBOT3J  =   0,      ! Bottom boundary window
  ITOP3J  =   0,      ! Top boundary window
                      !    Window defaults to entire domain if one equals 0.

                      ! Upper air plots:

  IUP3BEG = 279,      ! Starting isentropic level for plotting
  IUP3END = 315,      ! Ending isentropic level
  IUP3INC =   9,      ! Level increment

  NFLDU3  =   4,                ! Number of fields to be plotted
  IFLDU3  =   'SPEED','PRESS','GEO','RELHUM',        ! Field names
  CONU3   = 0.,0.,0.,0.,        ! Field contour increment
  IVELU3  = 1,0,0,0,            ! Velocity vector flag

          !--------------------------------------
          ! Surface plotting information
          !--------------------------------------
! Uses isentropic plotting window info

  NFLDS3  =   4,                ! Number of surface fields to plot
  IFLDS3  =   'U','V','TEMP','RELHUM',        ! Field names
  CONS3   = 0.,0.,0.,0.,        ! Field contour increment
  IVELS3  = 0,0,1,0,            ! Velocity vector flag

          !--------------------------------------
          ! Sigma-z plotting information
          !--------------------------------------
! Uses isentropic plotting window info

  ISZBEG = 2,       ! Starting sigma-z level for plotting
  ISZEND =15,       ! Ending sigma-z level
  ISZINC =13,       ! Level increment

  NFLDSZ  =   3,                ! Number of fields to be plotted
  IFLDSZ  =   'PRESS','THETA','RELHUM',        ! Field names
  CONSZ   = 0.,0.,0.,           ! Field contour increment
  IVELSZ  = 1,0,0,              ! Velocity vector flag

          !--------------------------------------
          ! "Station" plotting information
          !--------------------------------------
  NPLTRAW = 25,           ! Approximate number of raw rawinsonde plots per
                          !  frame. 0 turns off plotting.
```

```
  NSTIS3  =   1,          ! number of station surface plots
  ISTIS3  =  'TEMP',      ! field names

          !--------------------------------------
          ! Cross-section plotting information
          !--------------------------------------
  NCROSS3 =    1,                 ! number of cross section slabs
  ICRTYP3 =   1,0,                ! type of slab: 1=E-W, 2=N-S
  ICRA3   =   1,0,                ! left window
  ICRB3   =   41,0,               ! right window
  ICRL3   =   25,                 ! cross section location
  NCRFLD3 =   4,                  ! number of plots on each cross section
  ICRFLD3 =  'U','V','SPEED','RELHUM',      ! field names
  THCON3  =   5.,5.,5.,5.,                  ! contour interval of isentropes
  ACON3   =   0.,0.,0.,0.,                  ! contour interval of other field

$END
 !-----------------------------------
 !   Field values for graphical stage
 !-----------------------------------
 !
 !     Pressure        Isentropic    Station       Sigma-z
 !-------------------------------------------------------------------------
 !     U               U             U             U
 !     V               V             V             V
 !     TEMP            PRESS         PRESS         PRESS
 !     GEO             GEO           TEMP          THETA
 !     RELHUM          RELHUM        RELHUM        RELHUM
 !     MIXRAT          MIXRAT        MIXRAT
 !     THETA           THETA
 !     SPEED           SPEED
 !     ENERGY          ENERGY
 !     THETAE          THETAE
 !     SPRESS          SPRESS
 !
```

Table 1. Description of the numerical experiments

Experiment	Date	Vegetation	Soil Moisture	Data Assimilation
ANAL-89	5/5 - 5/17, 1989	same as Fig. 2	dry	FDDA on all prognostic variables in the interior of the domain
CNTL-89	5/5 - 5/17, 1989	same as Fig. 2	dry	FDDA on only u and v in the interior of the domain in the upper-atmosphere
SOILM-89	5/5 - 5/17, 1989	same as Fig. 2	initialized with Fig. 9	FDDA on only u and v in the interior of the domain in the upper-atmosphere
BARE-89	5/5 - 5/17, 1989	bare-soil	initialized with Fig. 9	FDDA on only u and v in the interior of the domain in the upper-atmosphere
ANAL-87	10/26 - 11/16, 1987	same as Fig. 2	dry	FDDA on all prognostic variables in the interior of the domain
CNTL-87	10/26 - 11/16, 1987	same as Fig. 2	dry	FDDA on only u and v in the interior of the domain in the upper-atmosphere
SOILM-87	10/26 - 11/16, 1987	same as Fig. 2	initialized with Fig. 10	FDDA on only u and v in the interior of the domain in the upper-atmosphere
BARE-87	10/26 - 11/16, 1987	bare-soil	initialized with Fig. 10	FDDA on only u and v in the interior of the domain in the upper-atmosphere

Table 2 Relationship between the PDI category and the initial soil moisture values

PDI category	Initial Soil Moisture
Severe wetness	95% of soil saturation
Moderate wetness	75% of soil saturation
Normal	50% of soil saturation
Moderate Drought	30% of soil saturation
Severe Drought	15% of soil saturation
Extreme Drought	10% of soil saturation

Table 3 Computation of the LASI where p_{sfc} is surface pressure, T is temperature, and T_d is dew point temperature

Low-elevation index ($p_{sfc} > 950$ mb)	Mid-elevation index (950 mb < p_{sfc} < 850 mb)	Upper-elevation index (850 mb < p_{sfc} < 500 mb)	LASI = A + B
950 mb T - 850 mb T	850 mb T - 700 mb T	700 mb T - 500 mb T	Factor A
< 4 C	< 6 C	< 17 C	1
4 to 8 C	6 to 11 C	17 to 22 C	2
> or = to 8 C	> or = to 11 C	> or = to 22 C	3
850 mb T - 850 mb T_d	850 mb T - 850 mb T_d	700 mb T - 700 mb T_d	Factor B
< 6 C	< 6 C	< 15 C	1
6 to 10 C	6 to 13 C	15 to 21 C	2
> or = to 10 C	> or = to 13 C	> or = to 21 C	3

LASI	Potential for large fire
2 or 3	very low
4	low
5	moderate
6	high

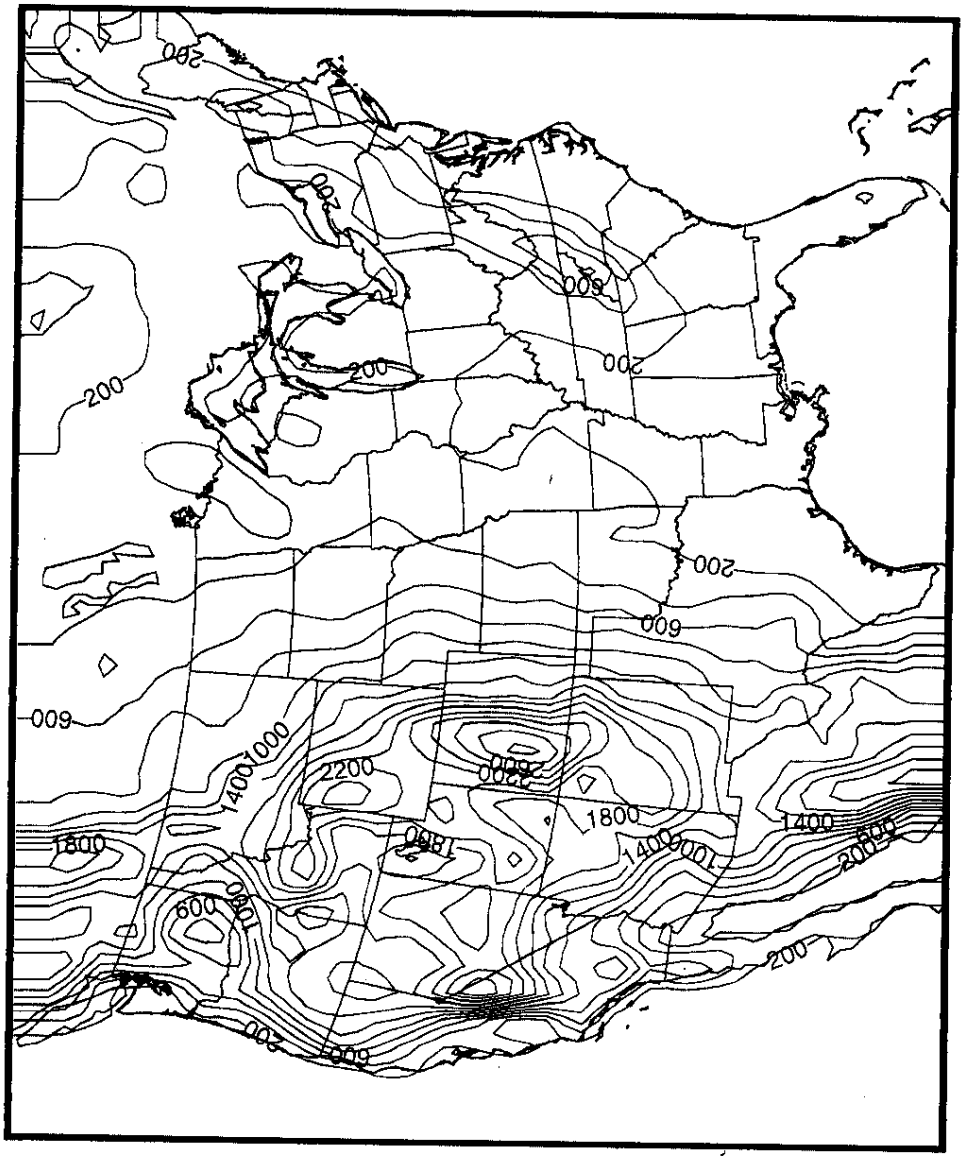

Figure 1

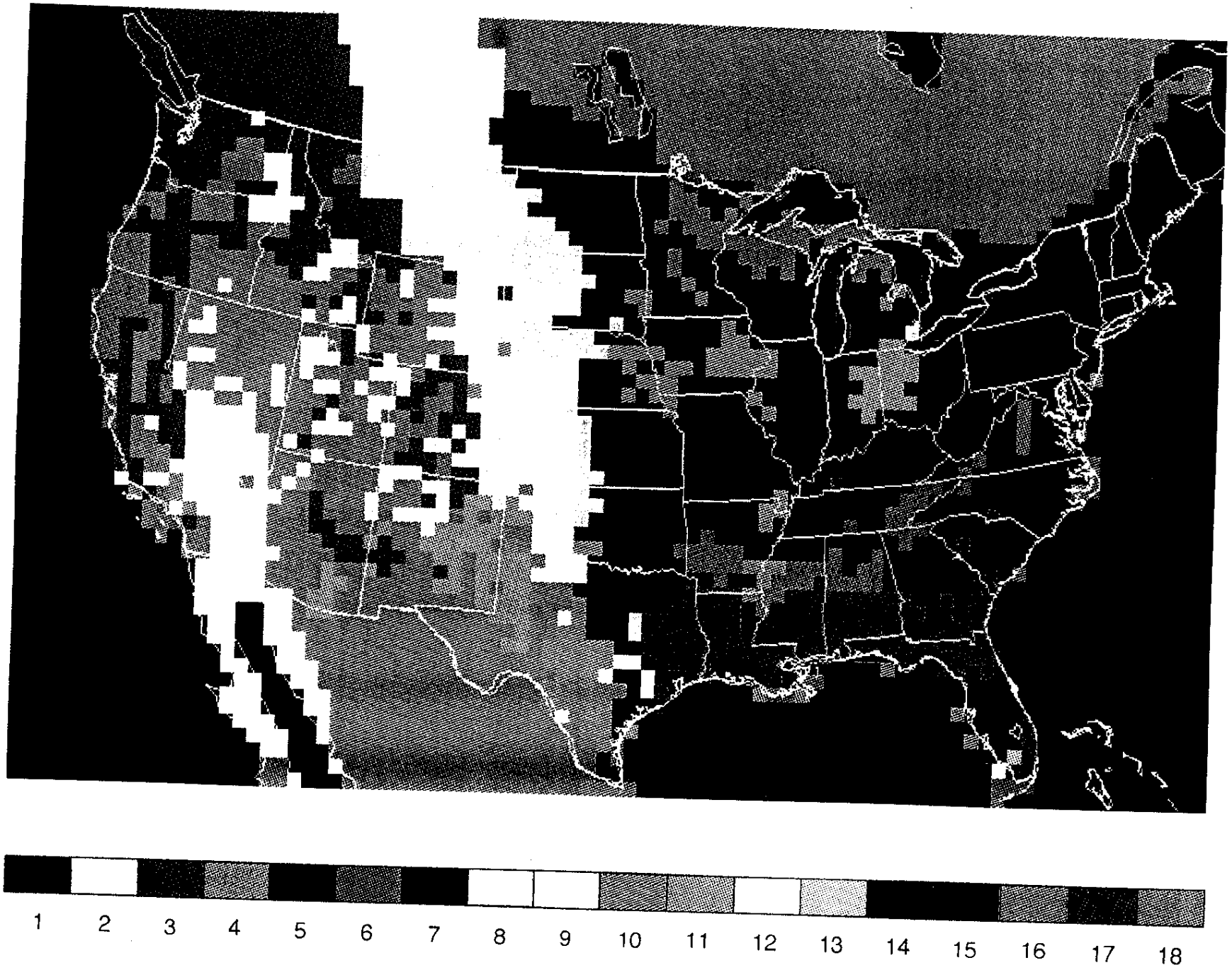

Figure 2

(a)

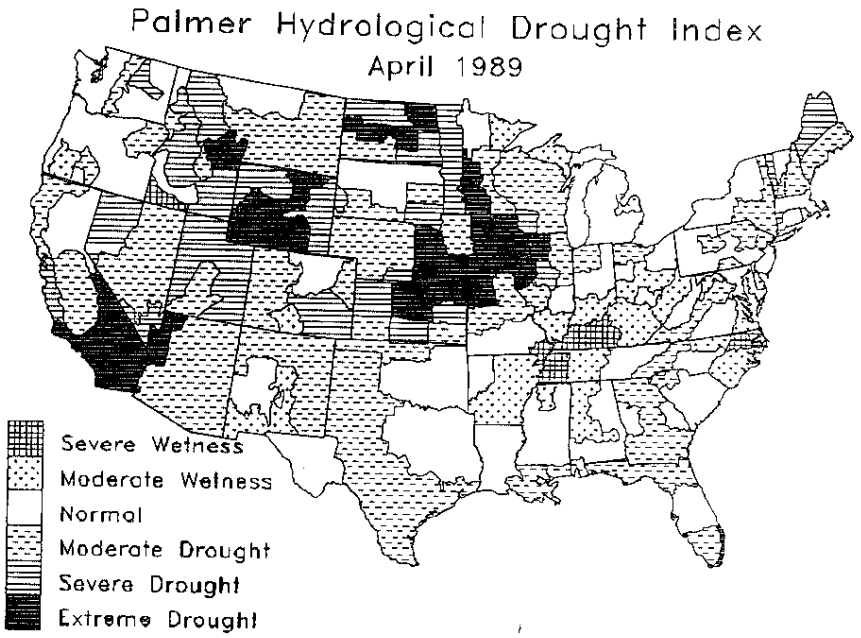
Palmer Hydrological Drought Index
April 1989
Severe Wetness
Moderate Wetness
Normal
Moderate Drought
Severe Drought
Extreme Drought

(b)

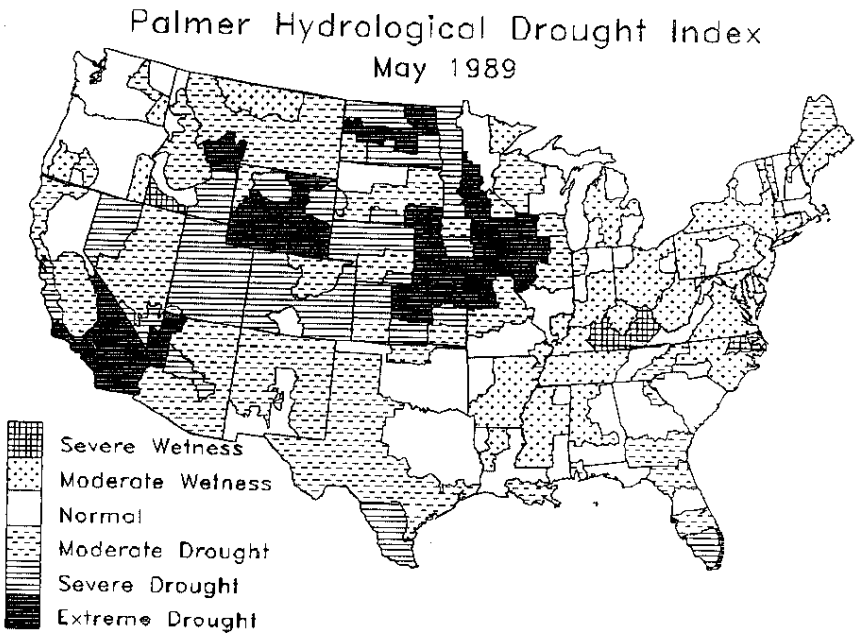
Palmer Hydrological Drought Index
May 1989
Severe Wetness
Moderate Wetness
Normal
Moderate Drought
Severe Drought
Extreme Drought

Figure 3

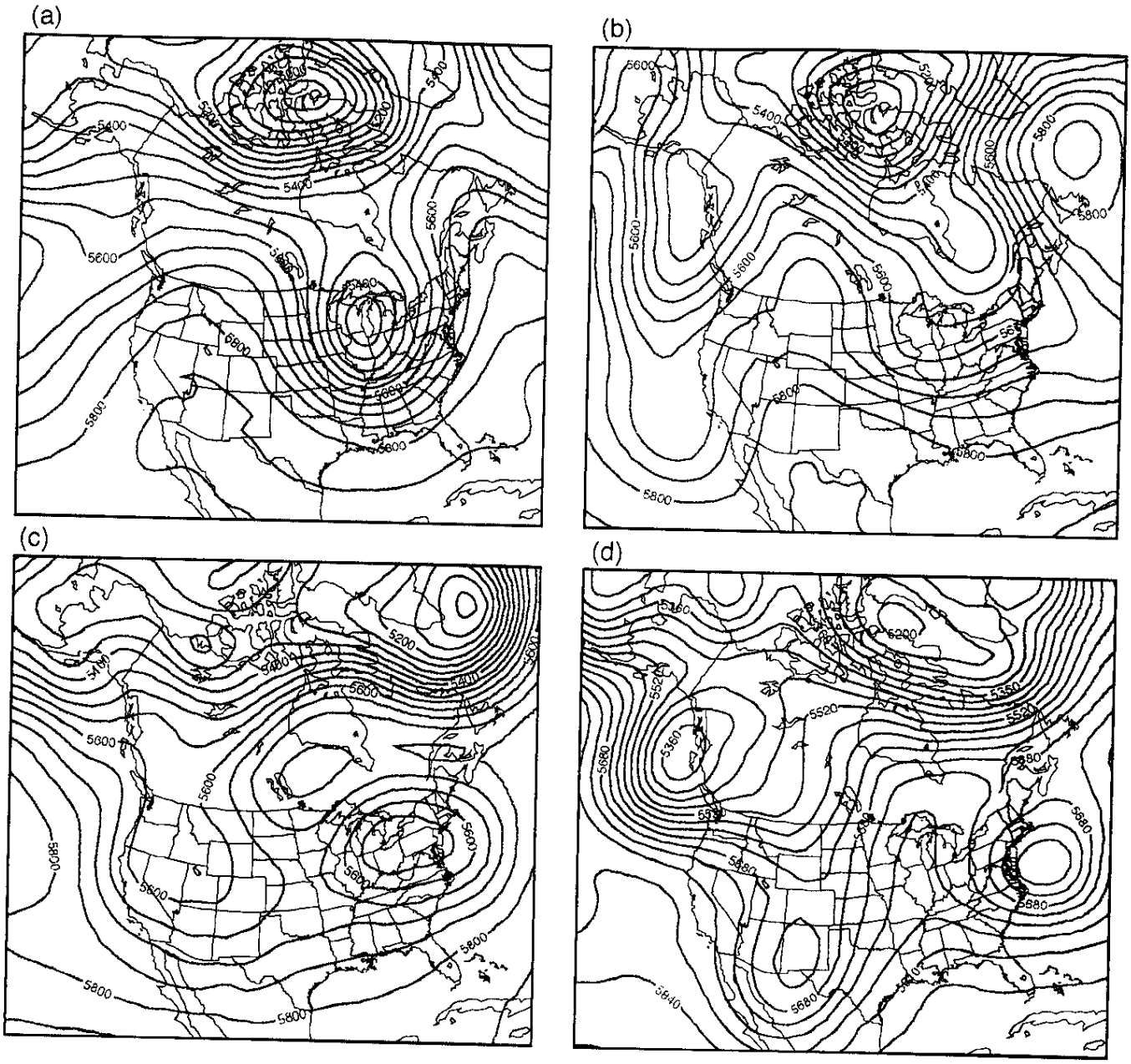

Figure 4

(a)

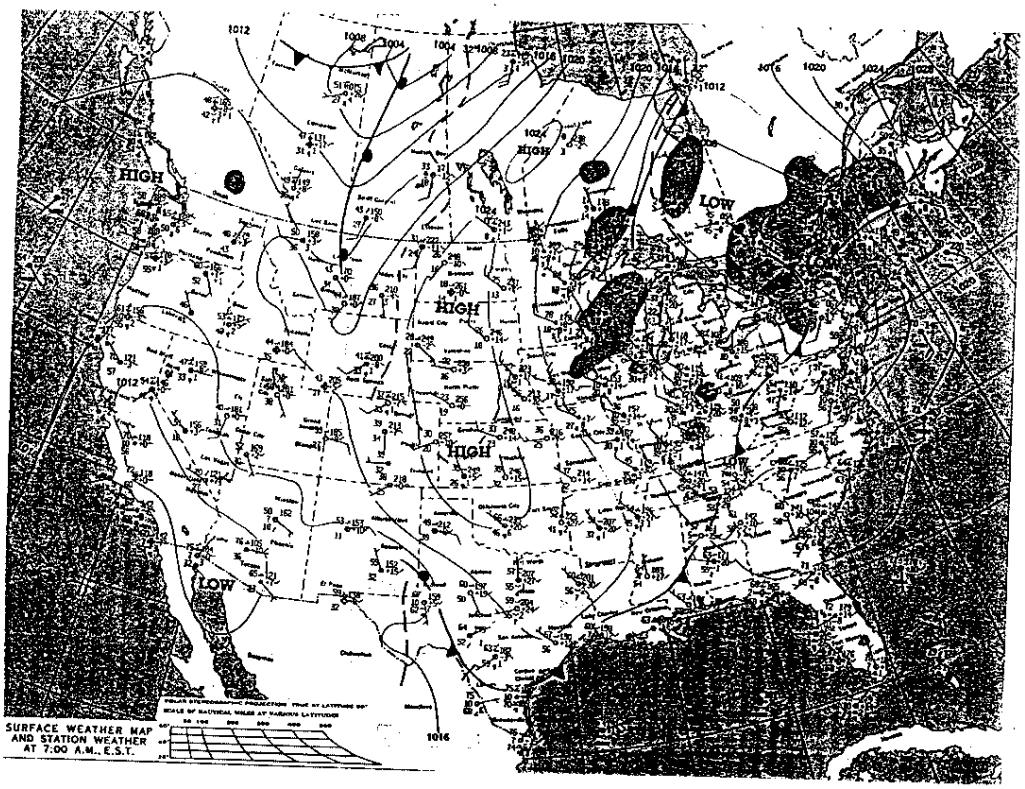
HIGH
HIGH
HIGH
LOW
LOW
SURFACE WEATHER MAP
AND STATION WEATHER
AT 7:00 A.M., E.S.T.

(b)

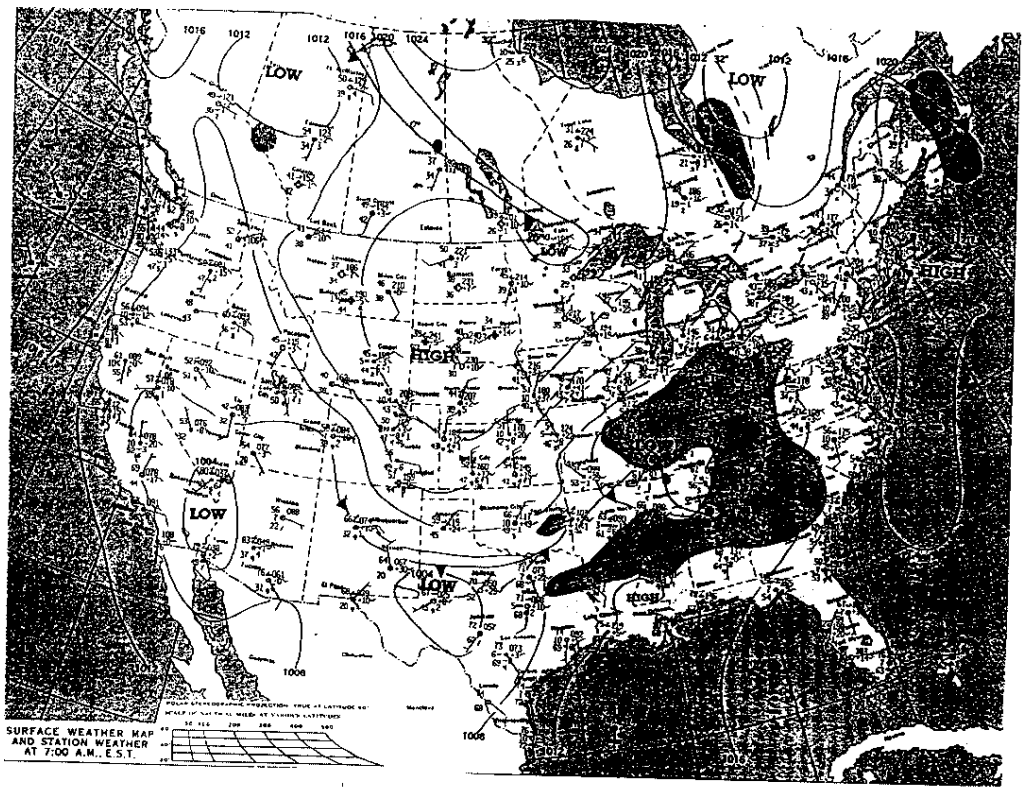
LOW
LOW
HIGH
HIGH
LOW
LOW
SURFACE WEATHER MAP
AND STATION WEATHER
AT 7:00 A.M., E.S.T.

Figure 5

(c)

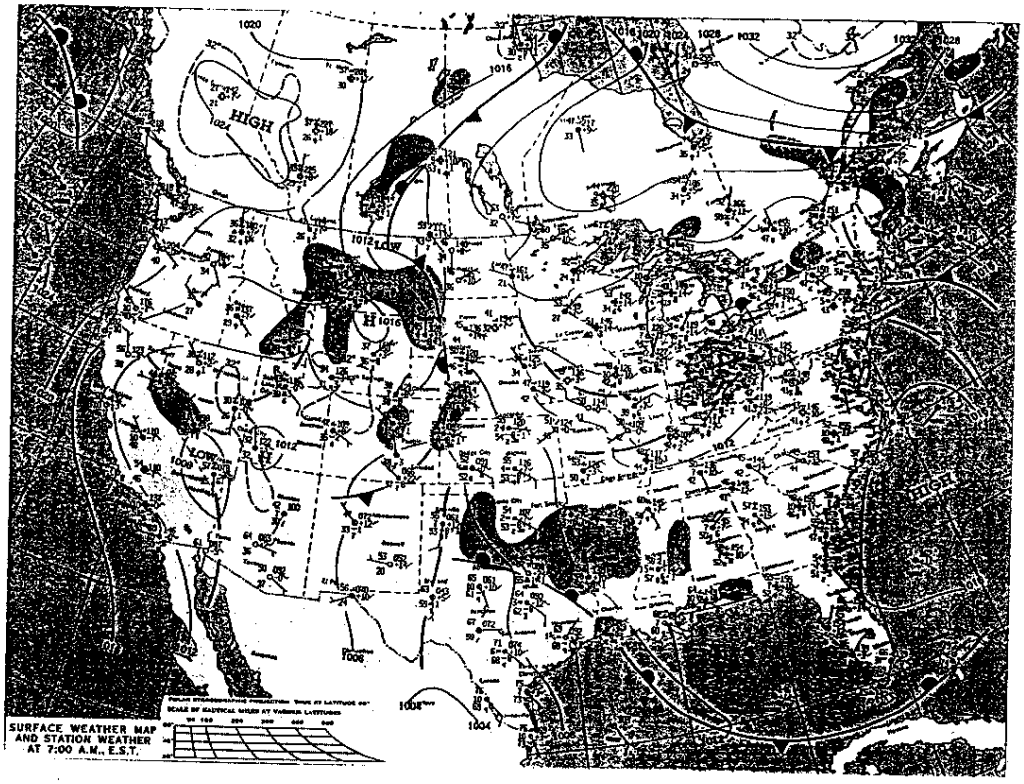

(d)

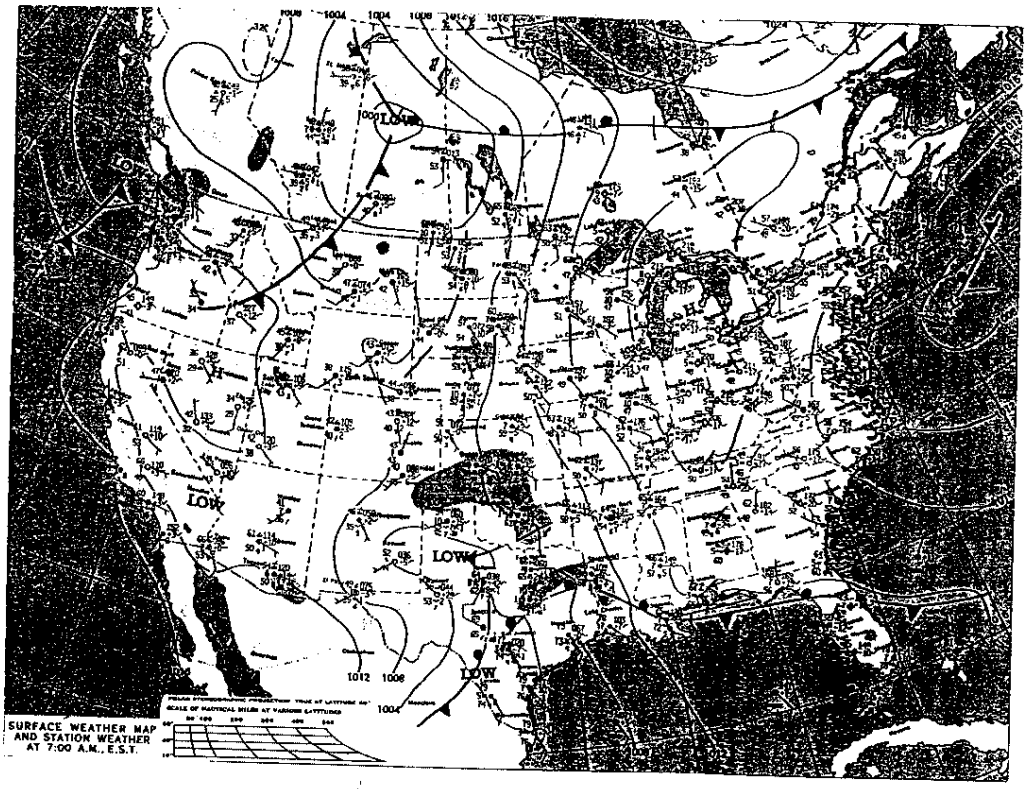

Figure 5 (continued)

(a)

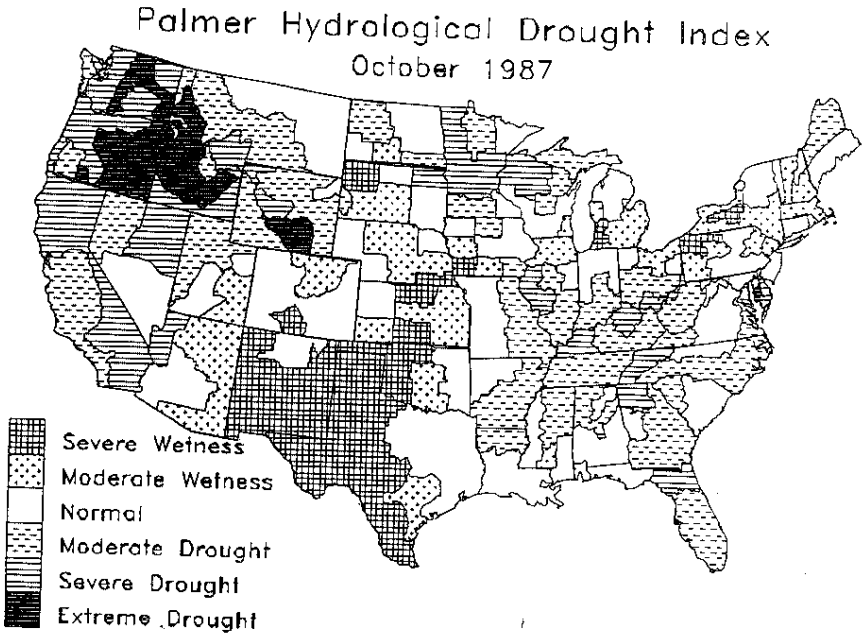
Palmer Hydrological Drought Index
October 1987
Severe Wetness
Moderate Wetness
Normal
Moderate Drought
Severe Drought
Extreme Drought

(b)

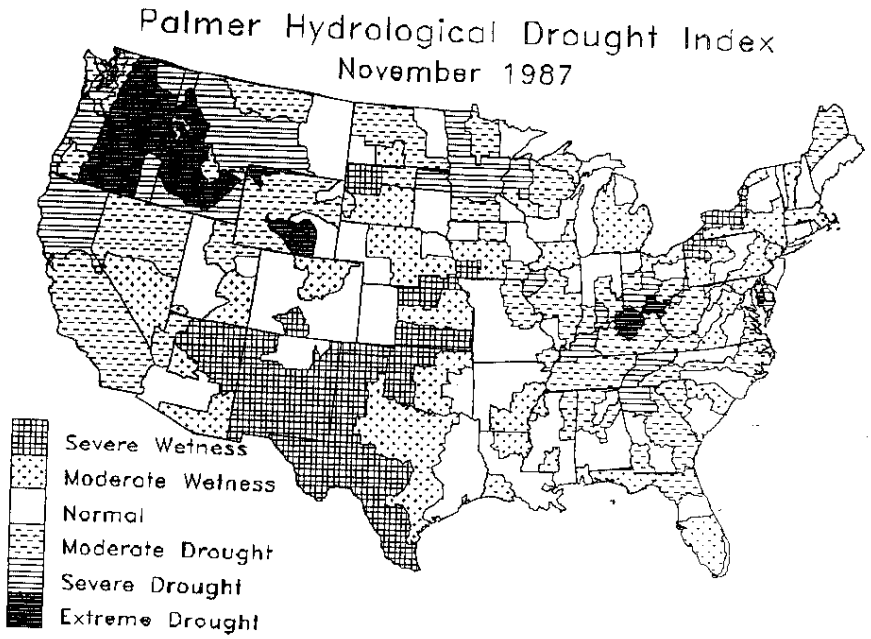
Palmer Hydrological Drought Index
November 1987
Severe Wetness
Moderate Wetness
Normal
Moderate Drought
Severe Drought
Extreme Drought

Figure 6

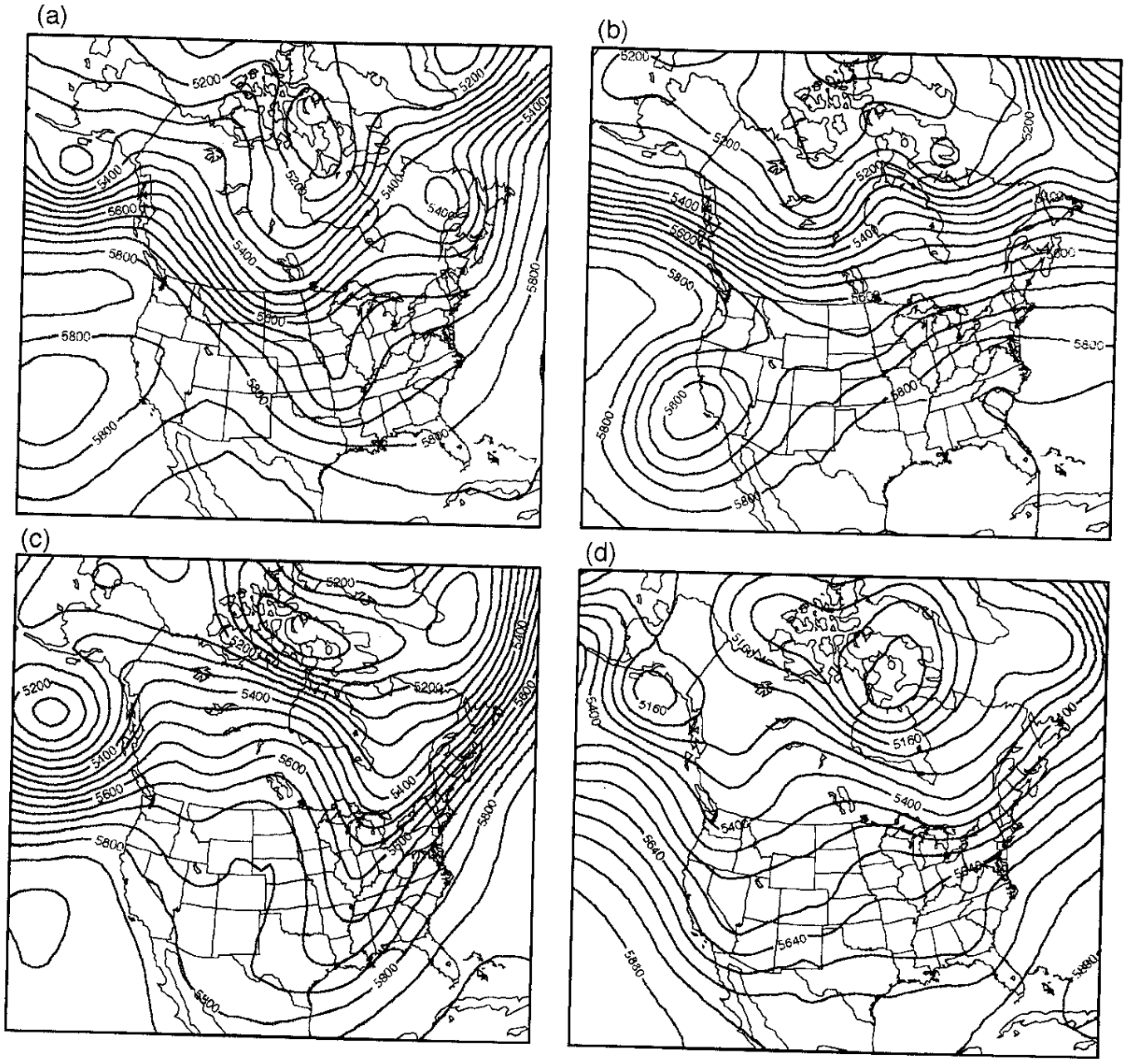

Figure 7

(a)

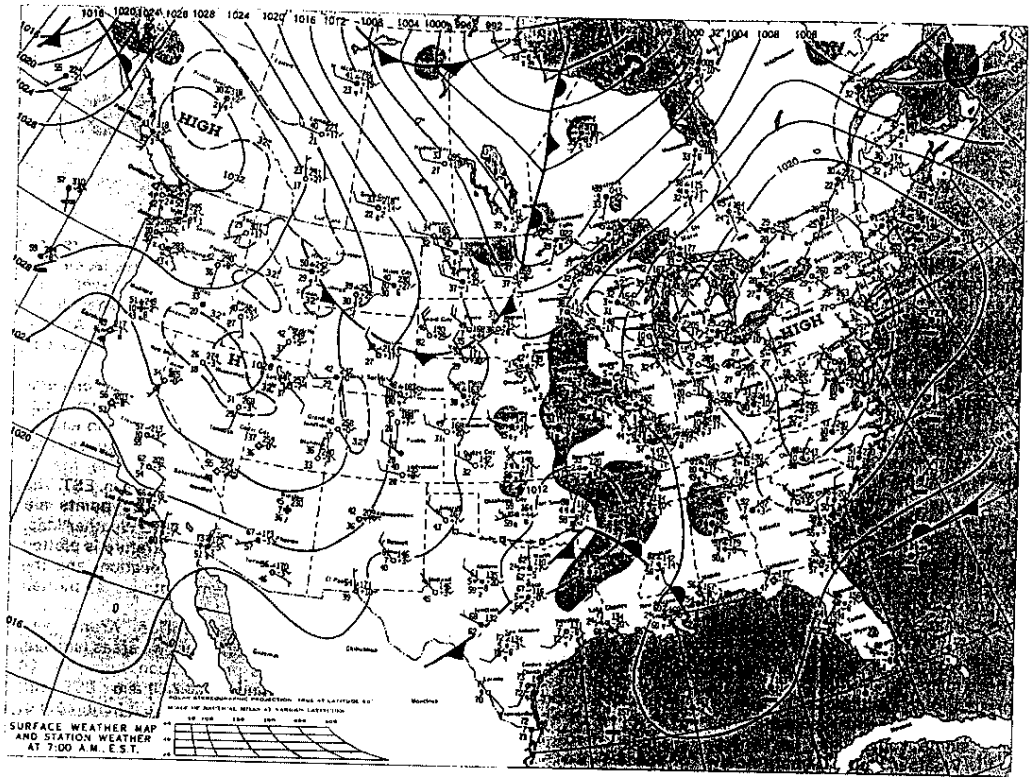
HIGH
HIGH
SURFACE WEATHER MAP
AND STATION WEATHER
AT 7:00 A.M. E.S.T.

(b)

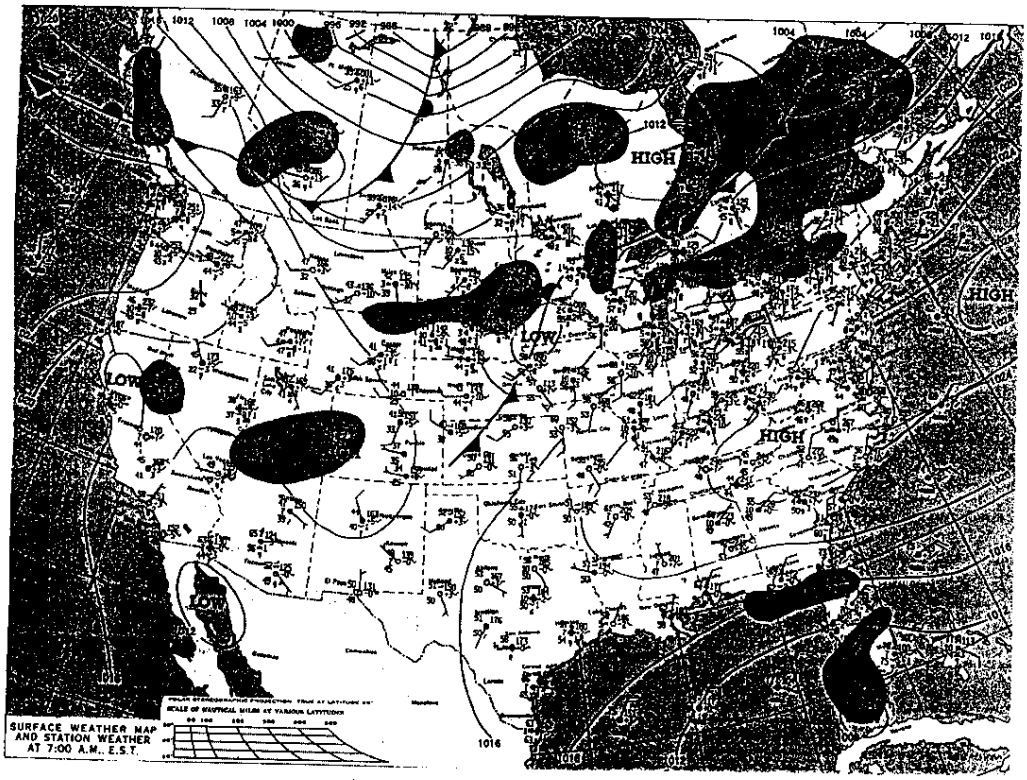
HIGH
HIGH
HIGH
LOW
LOW
LOW
SURFACE WEATHER MAP
AND STATION WEATHER
AT 7:00 A.M. E.S.T.

Figure 8

(c)

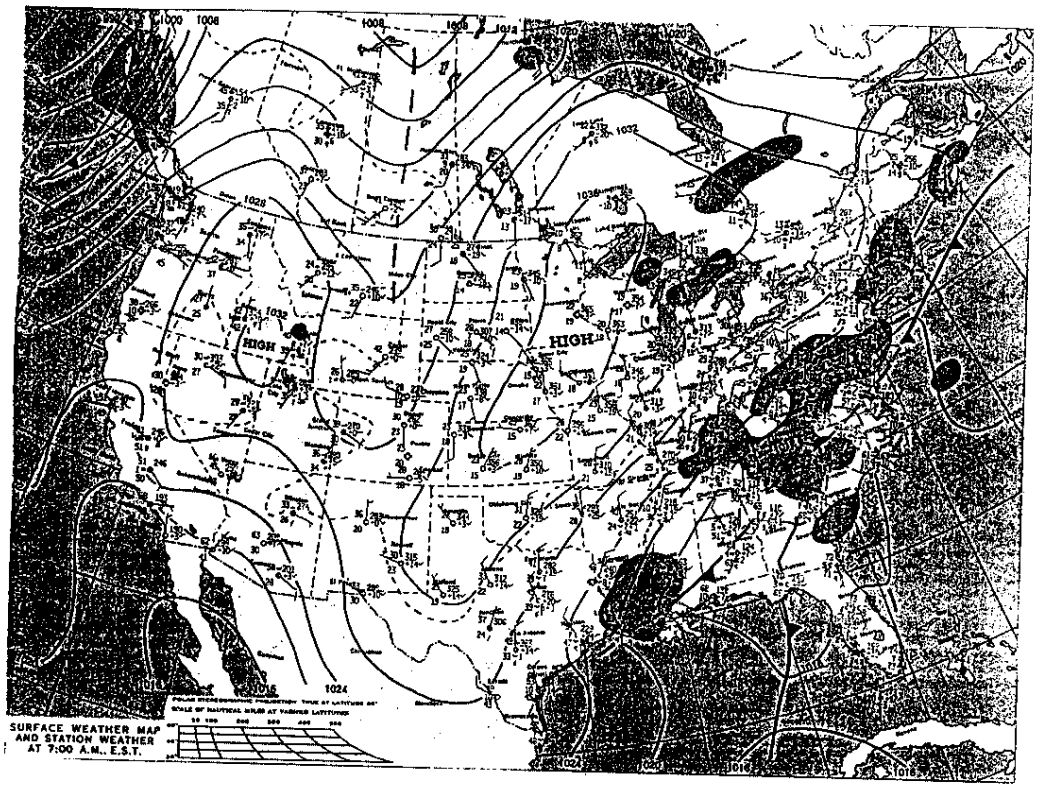

(d)

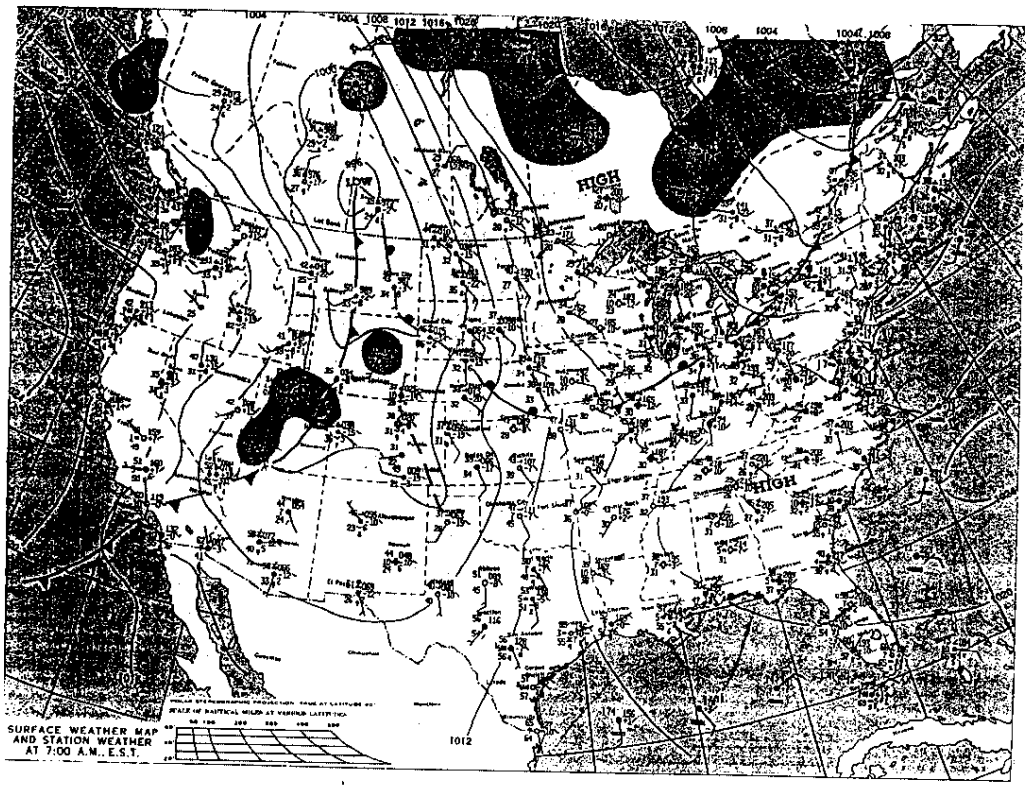

Figure 8 (continued)

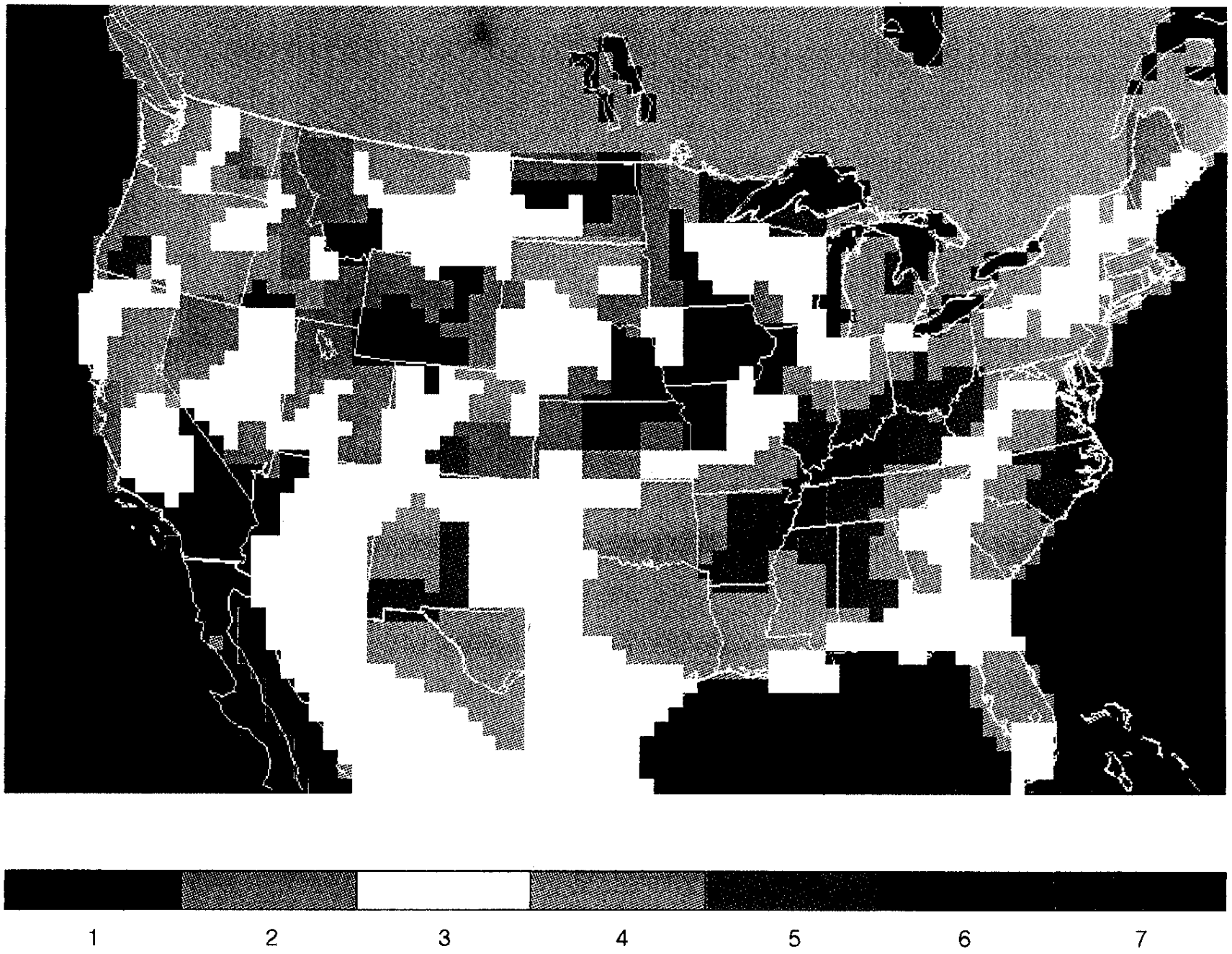

Figure 9

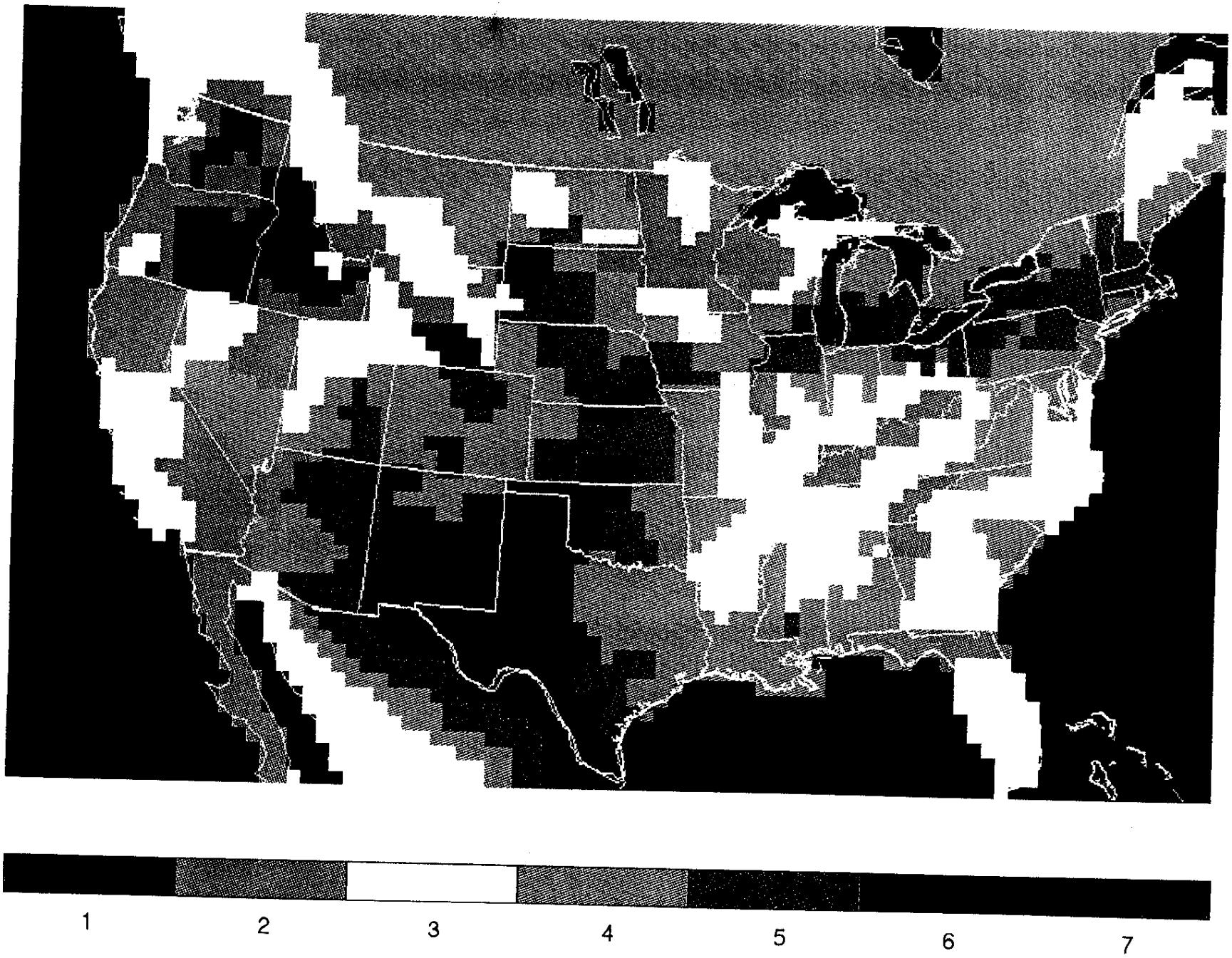

Figure 10

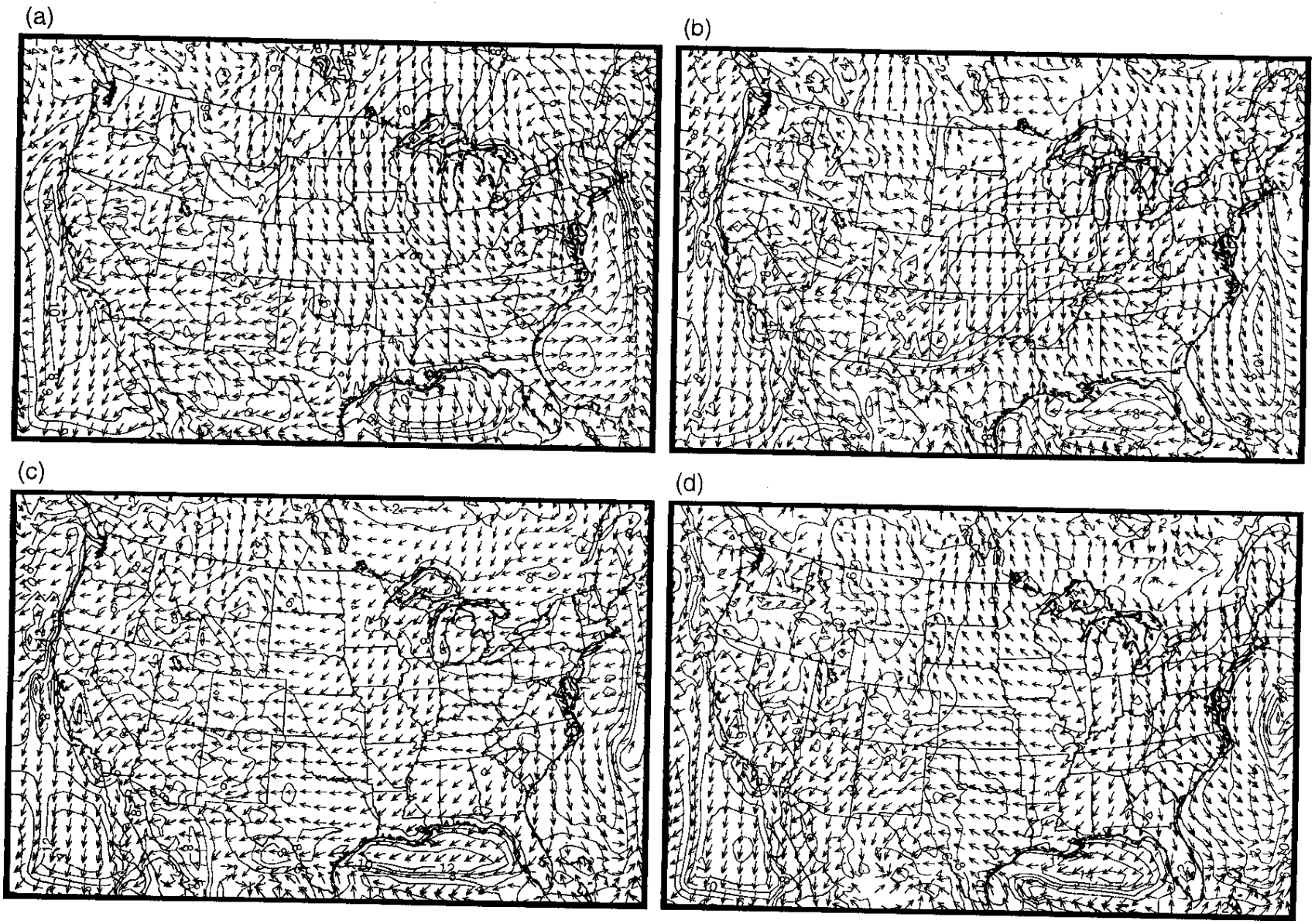

Figure 11

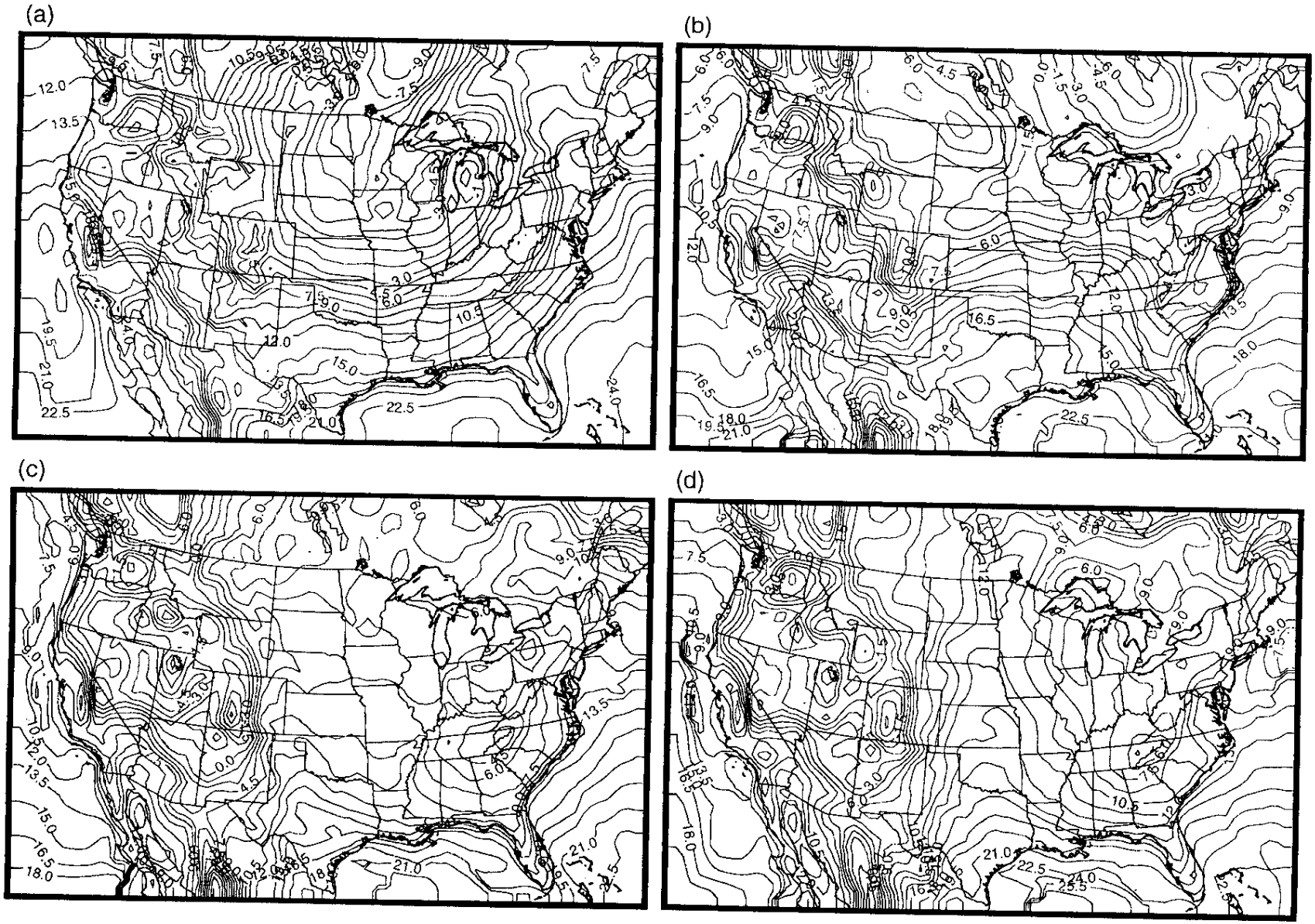

Figure 12

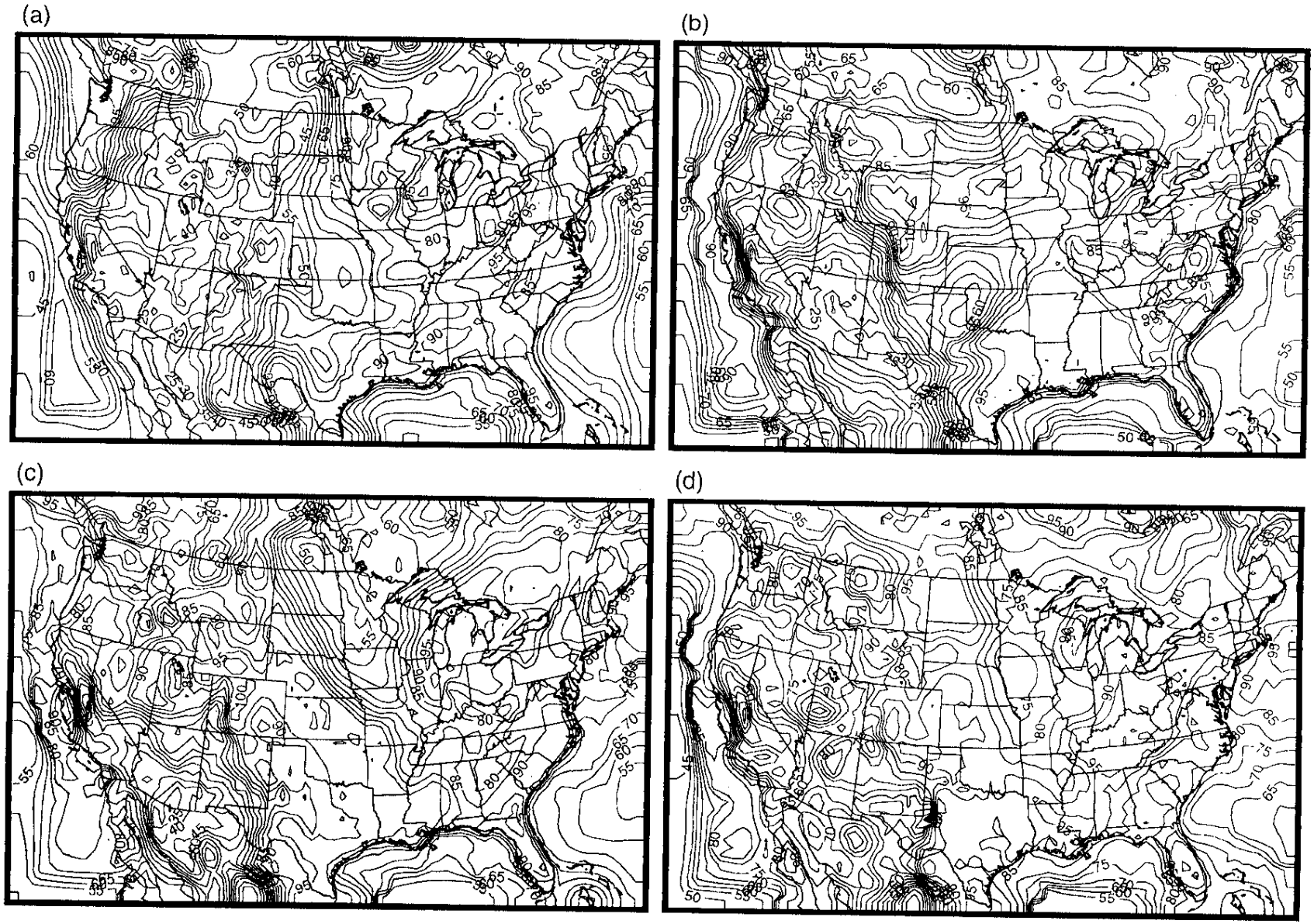

Figure 13

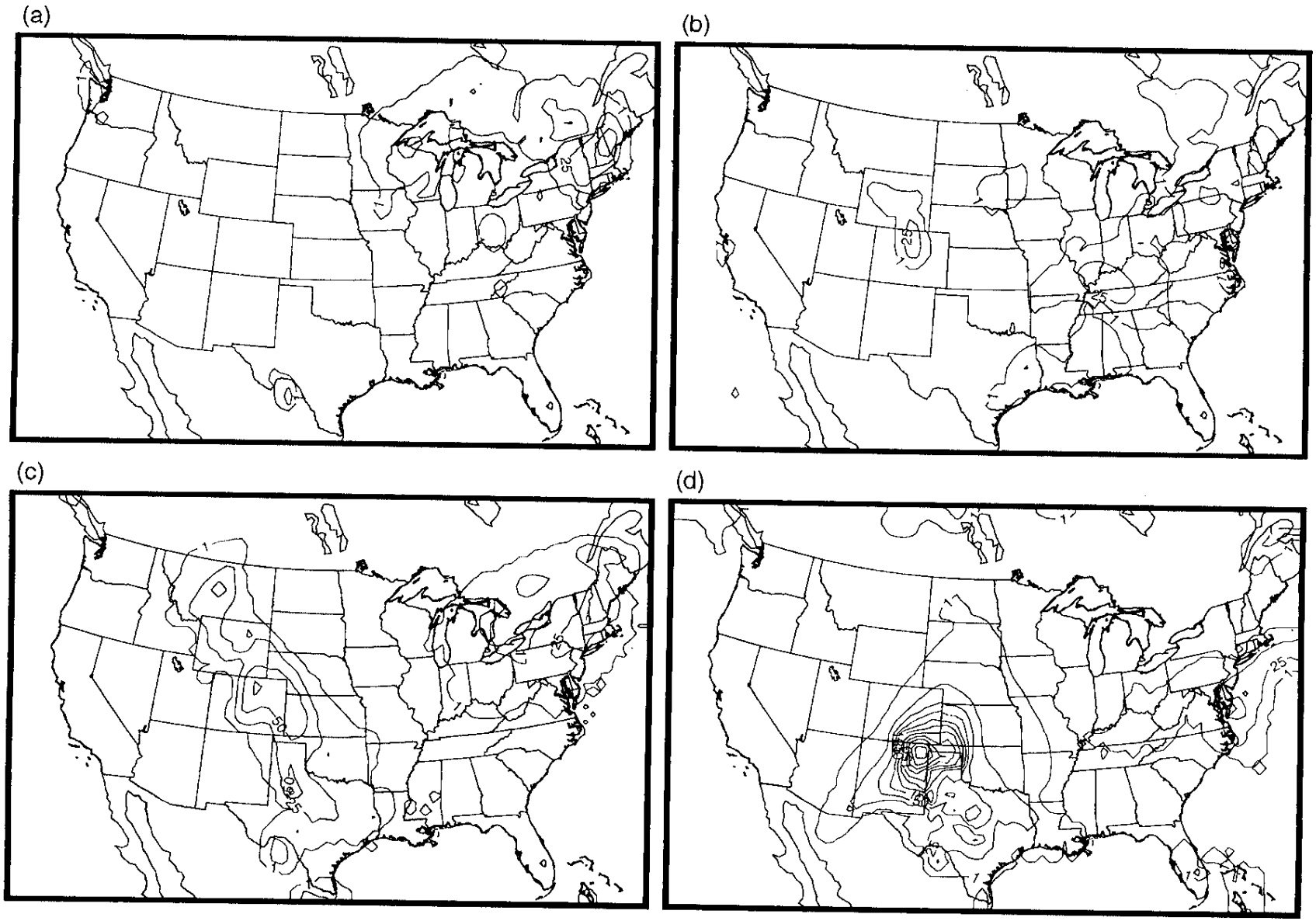

Figure 14

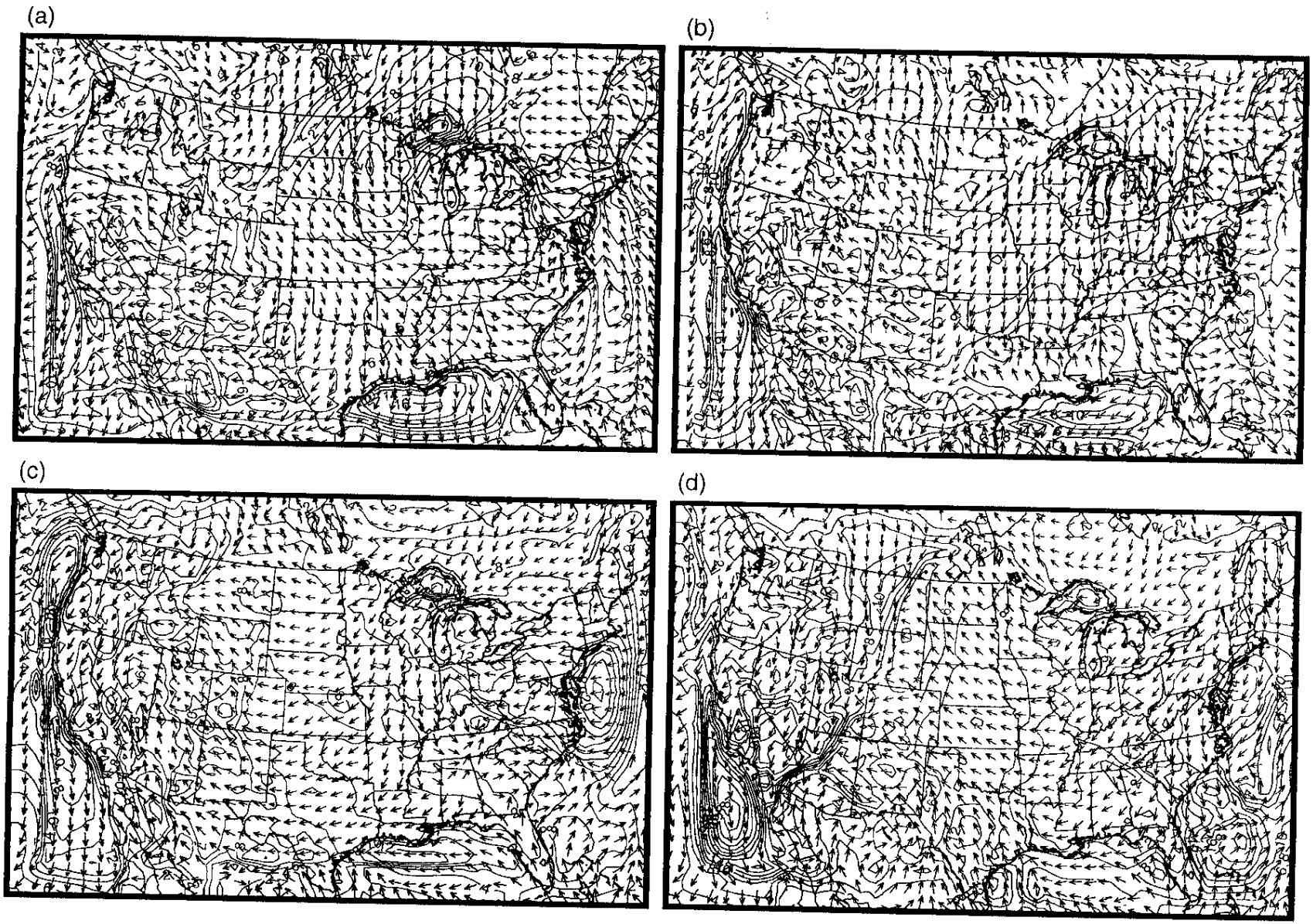

Figure 15

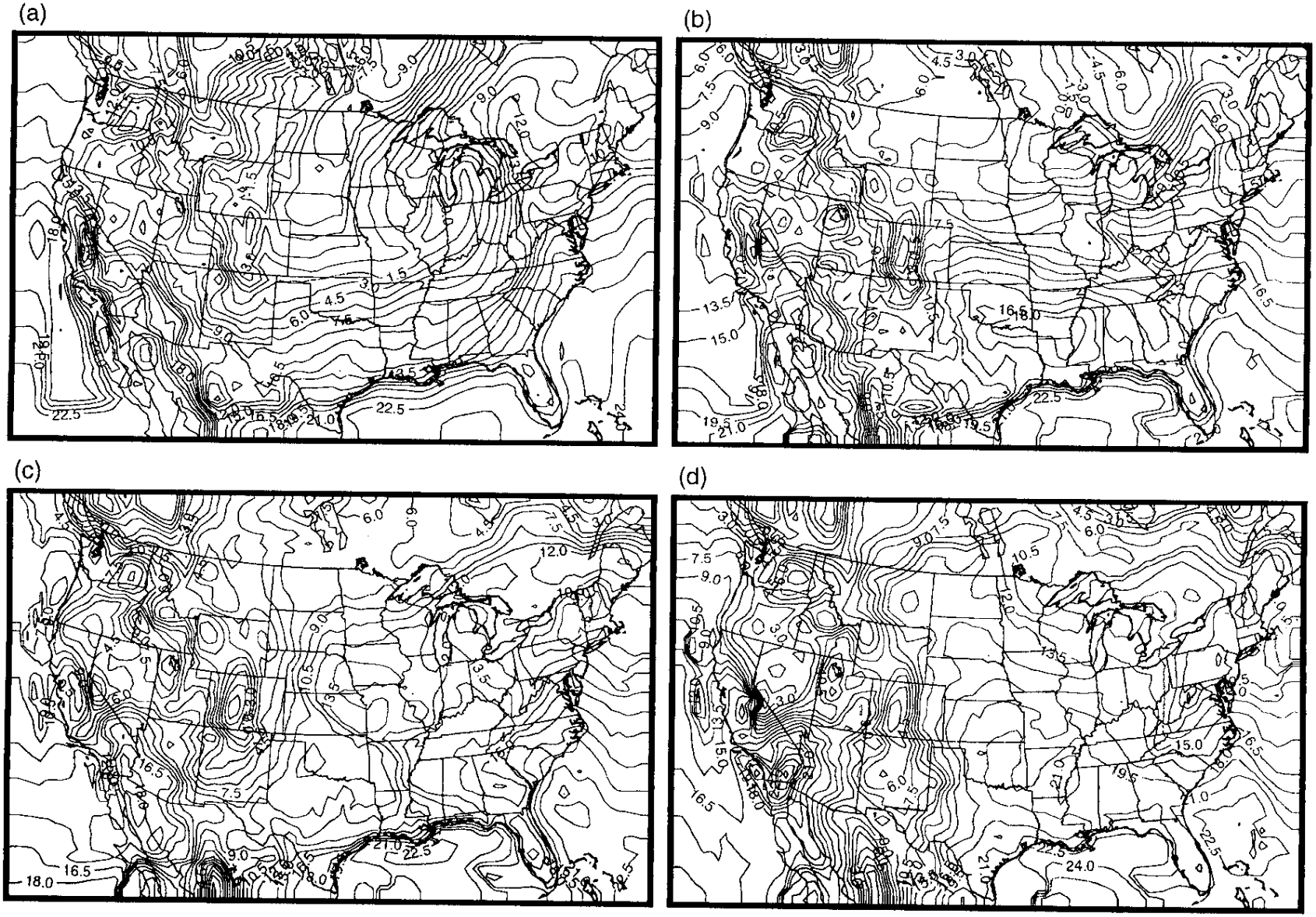

Figure 16

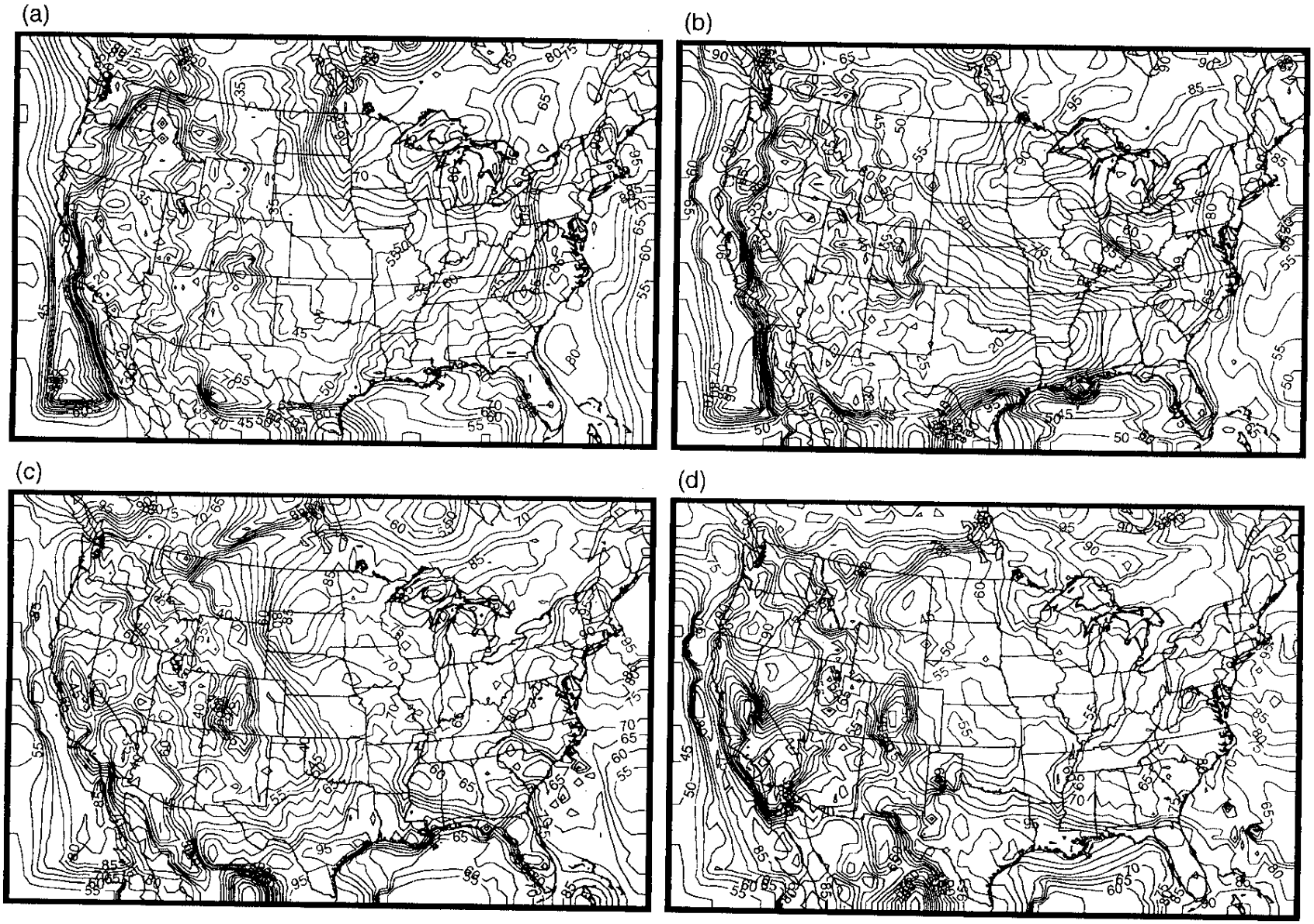

Figure 17

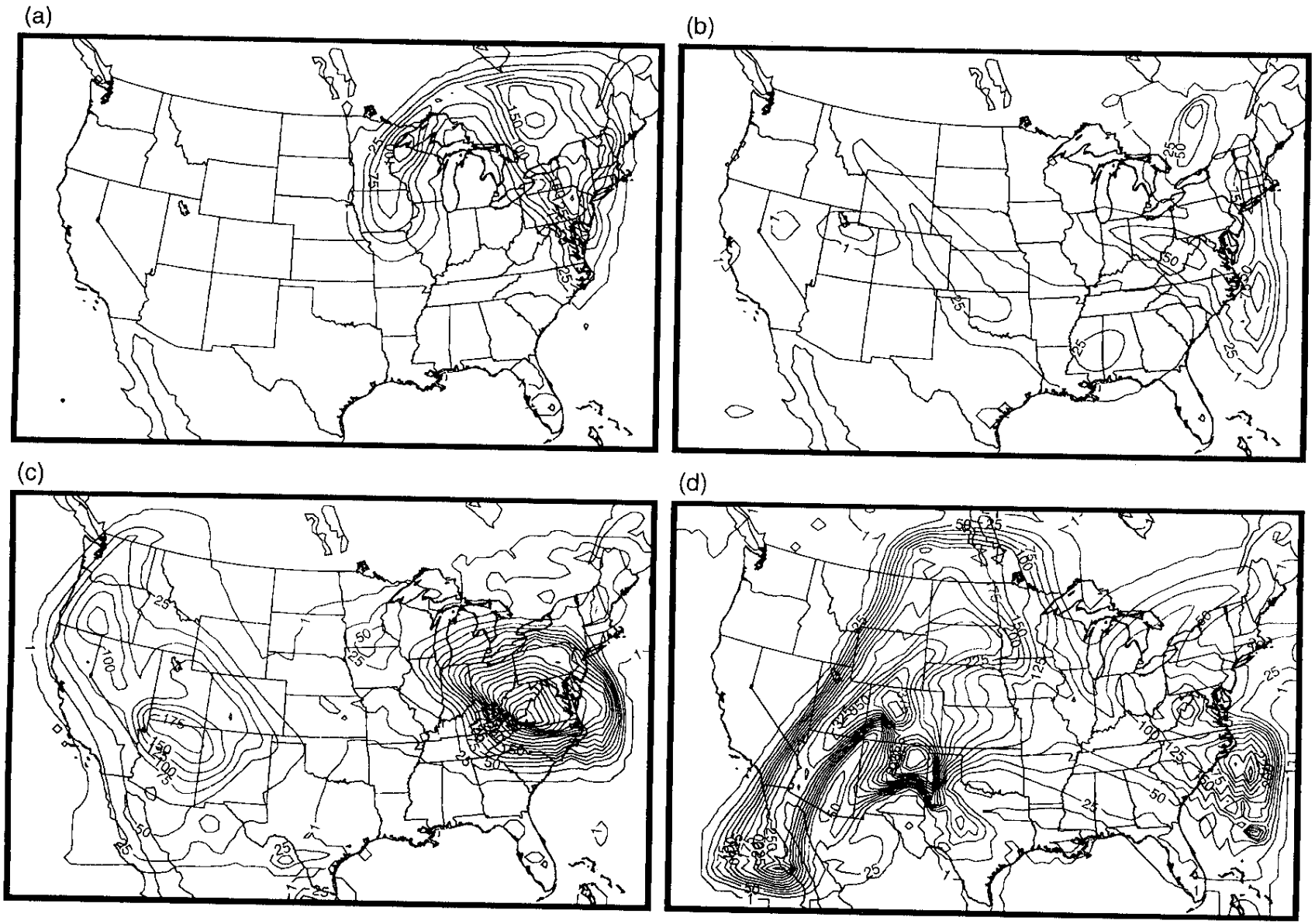

Figure 18

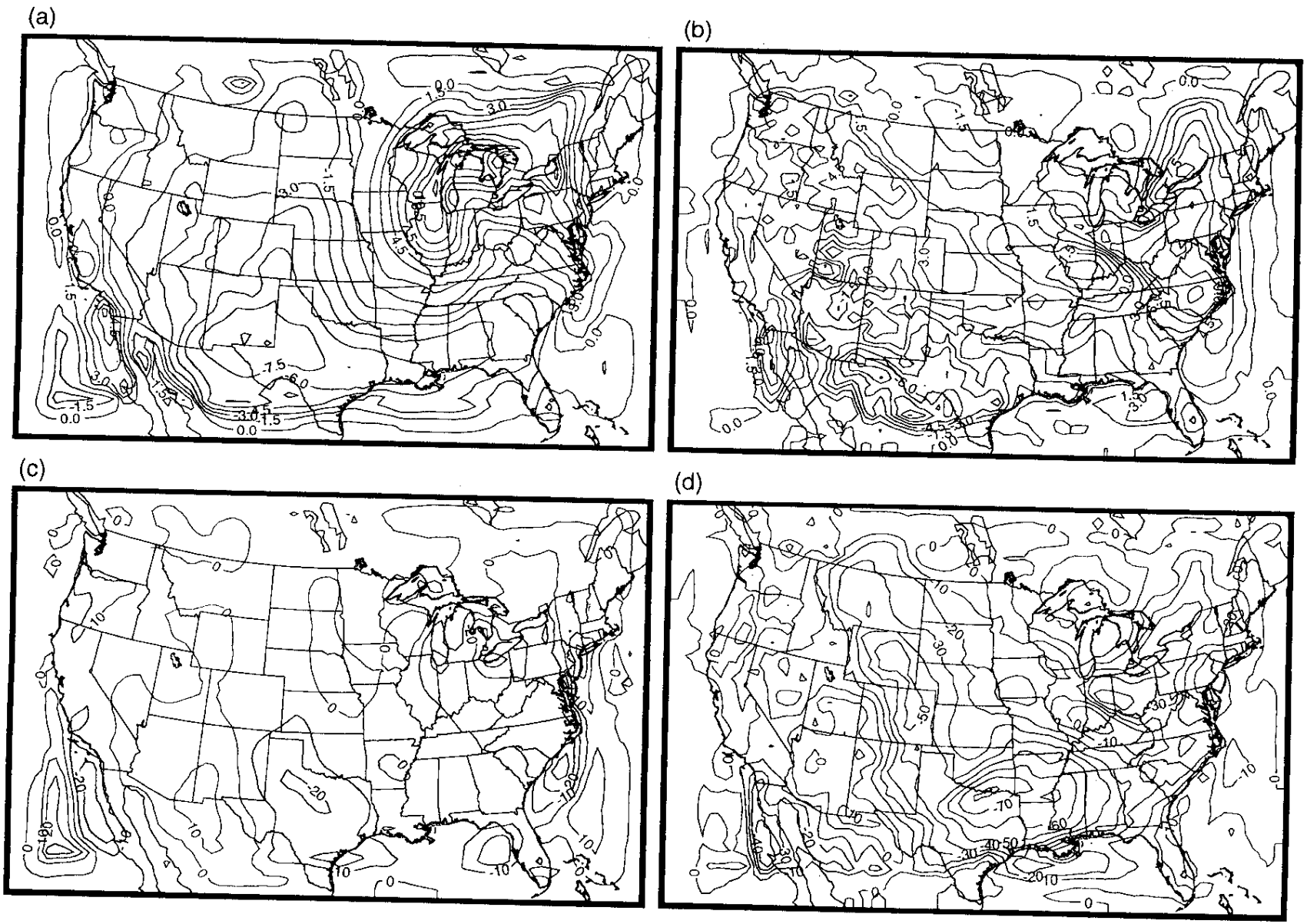

Figure 19

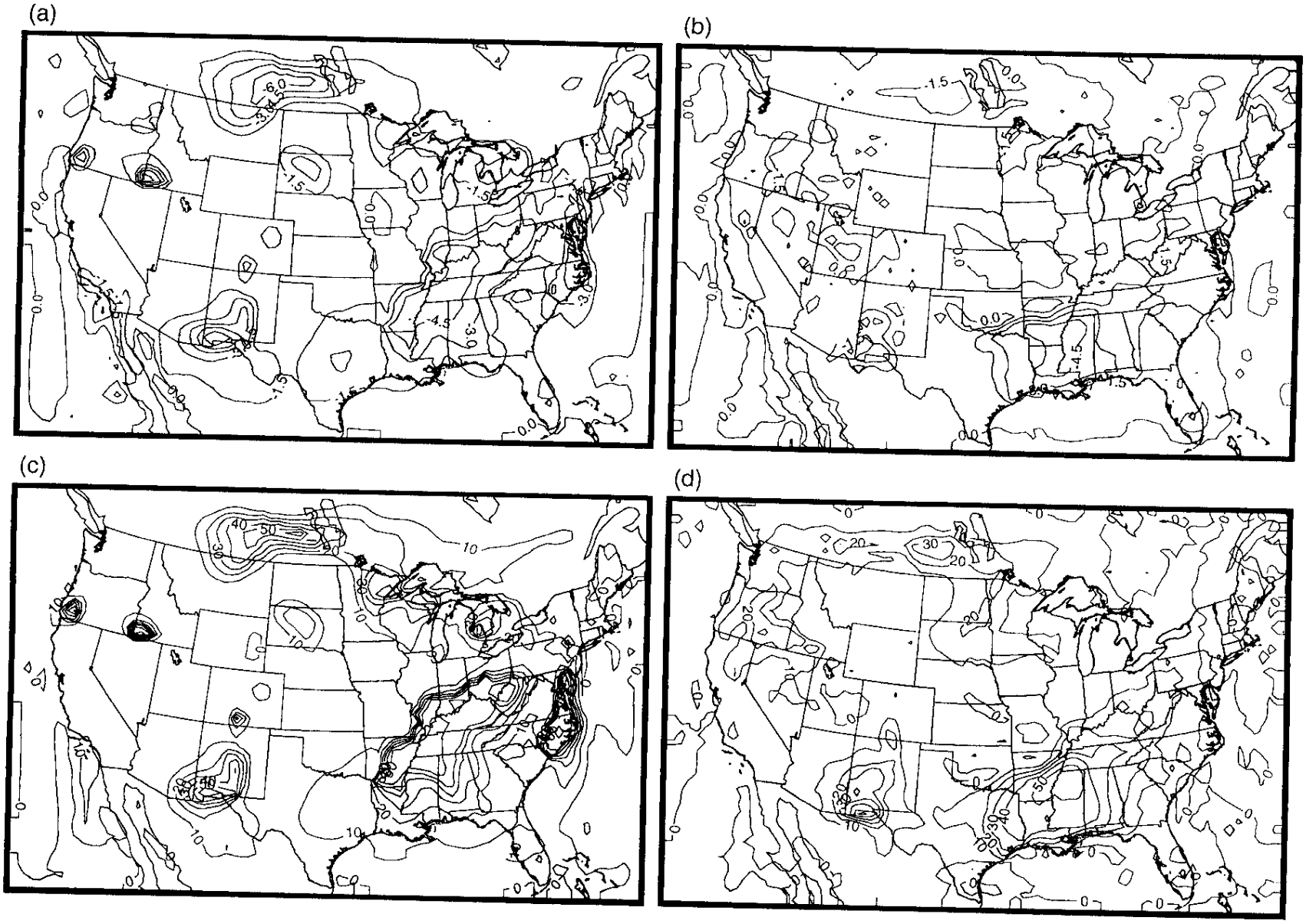

Figure 20

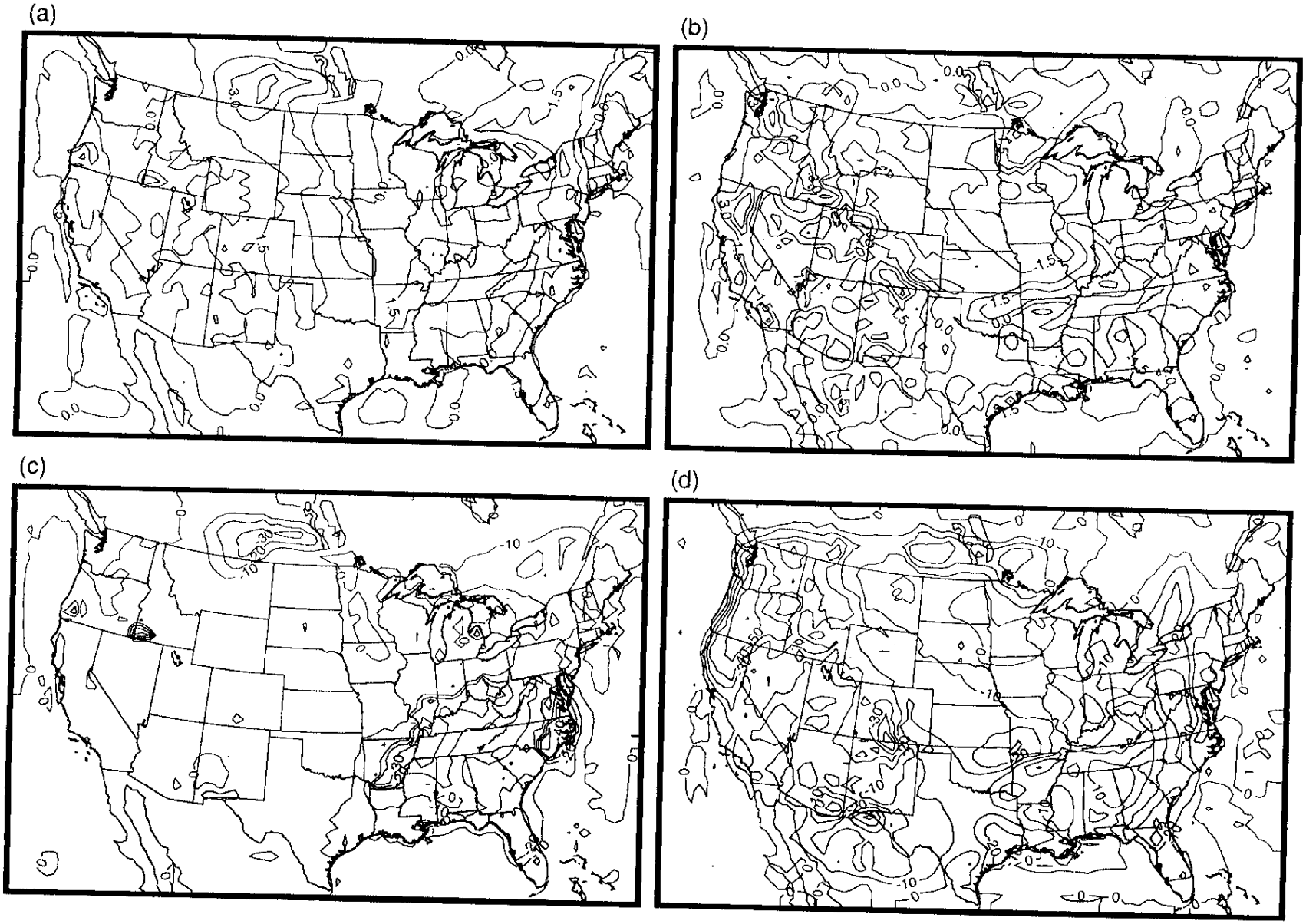

Figure 21

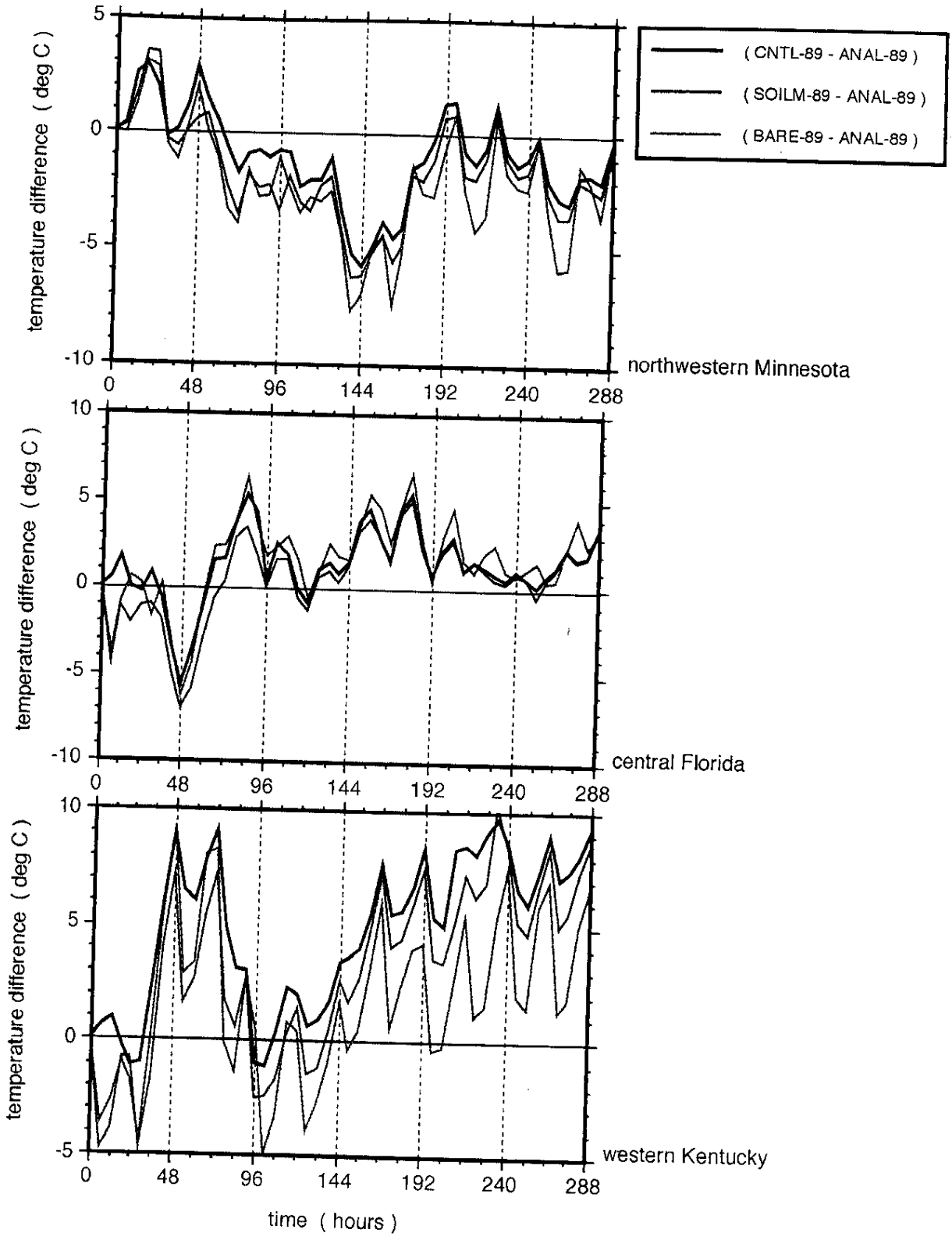
(CNTL-89 - ANAL-89)
(SOILM-89 - ANAL-89)
(BARE-89 - ANAL-89)
temperature difference (deg C)
5
0
-5
-10
0
48
96
144
192
240
288
northwestern Minnesota
10
5
0
-5
-10
central Florida
western Kentucky
time (hours)

Figure 22

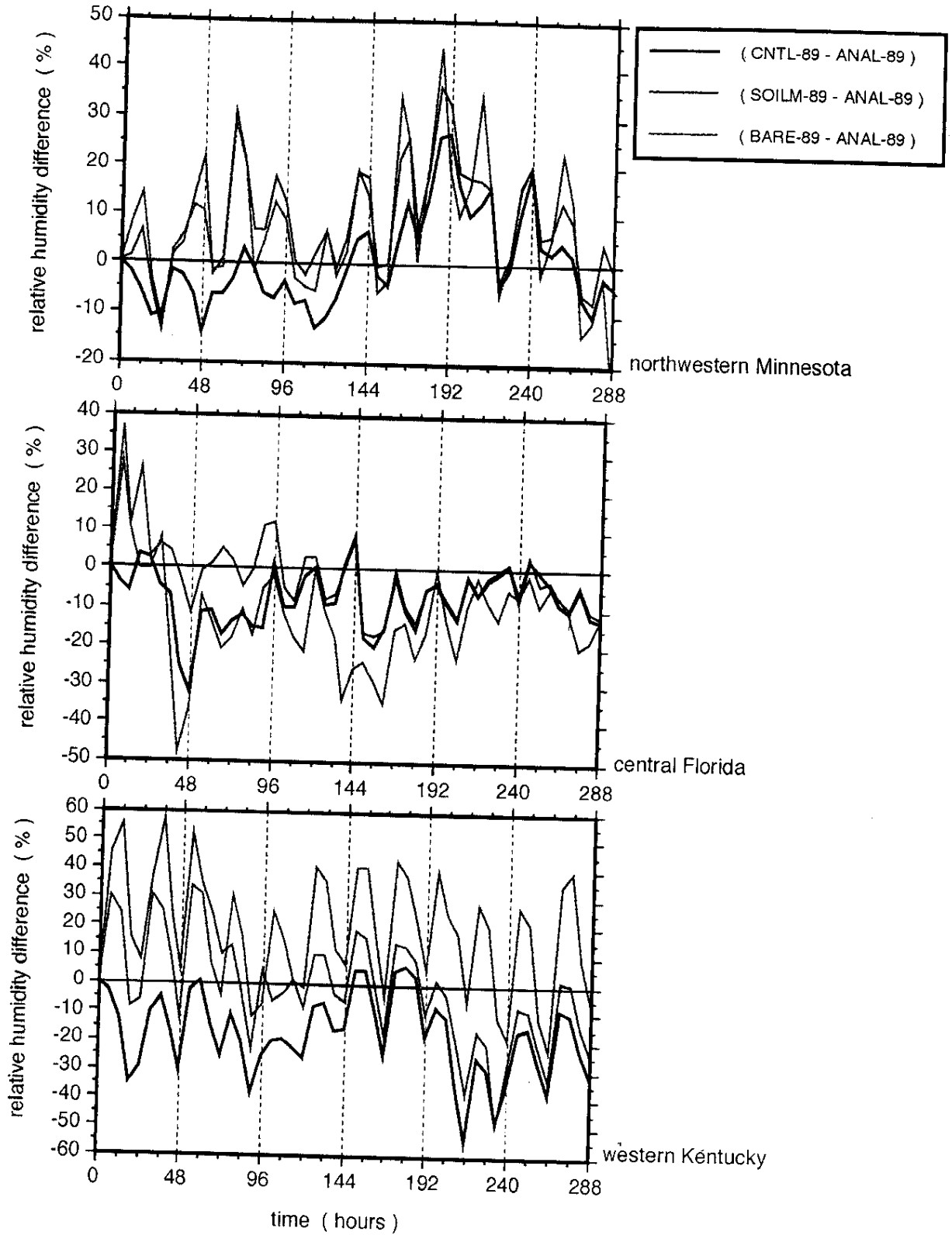
(CNTL-89 - ANAL-89)
(SOILM-89 - ANAL-89)
(BARE-89 - ANAL-89)
relative humidity difference (%)
northwestern Minnesota
central Florida
western Kentucky
time (hours)

Figure 23

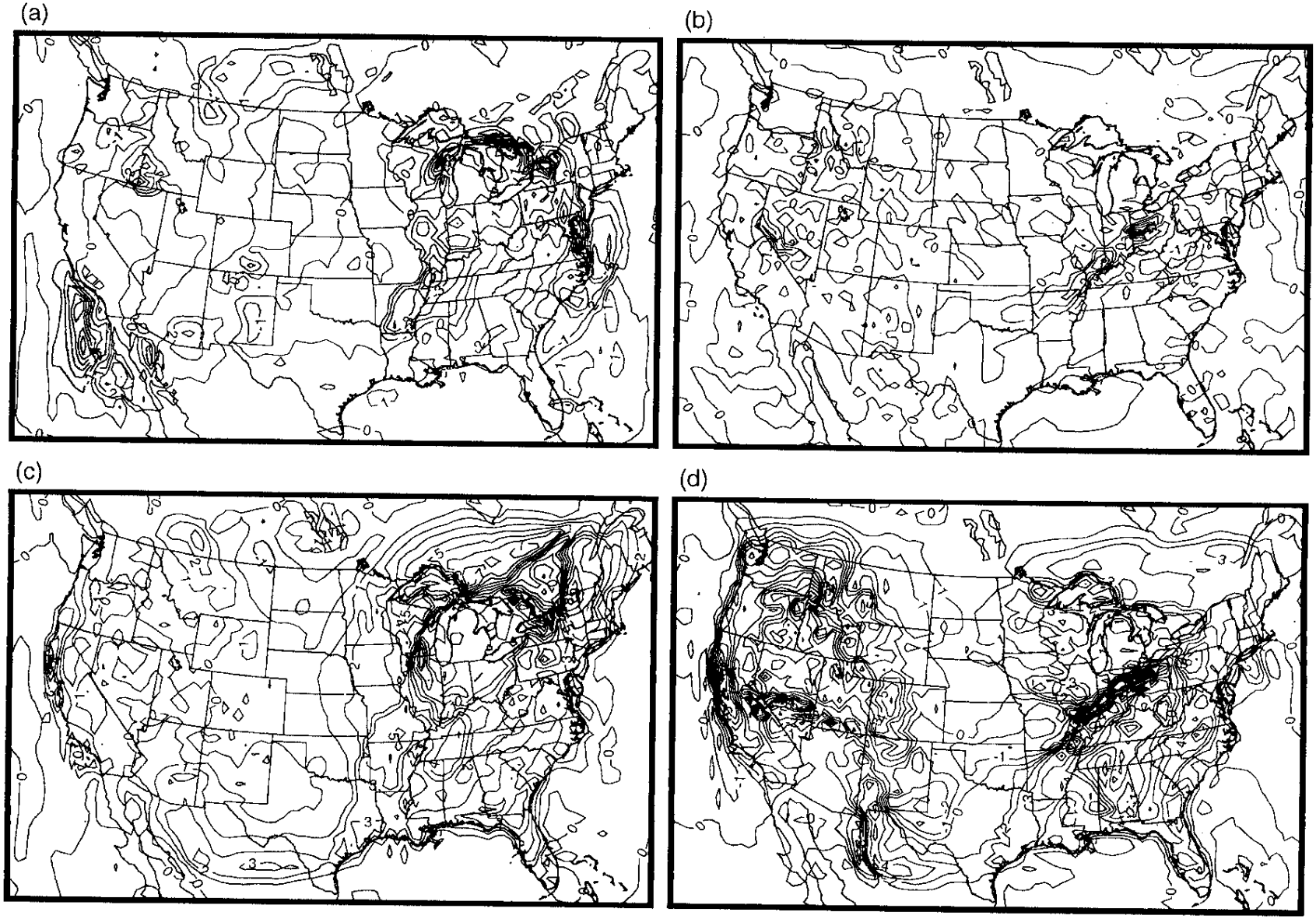

Figure 24

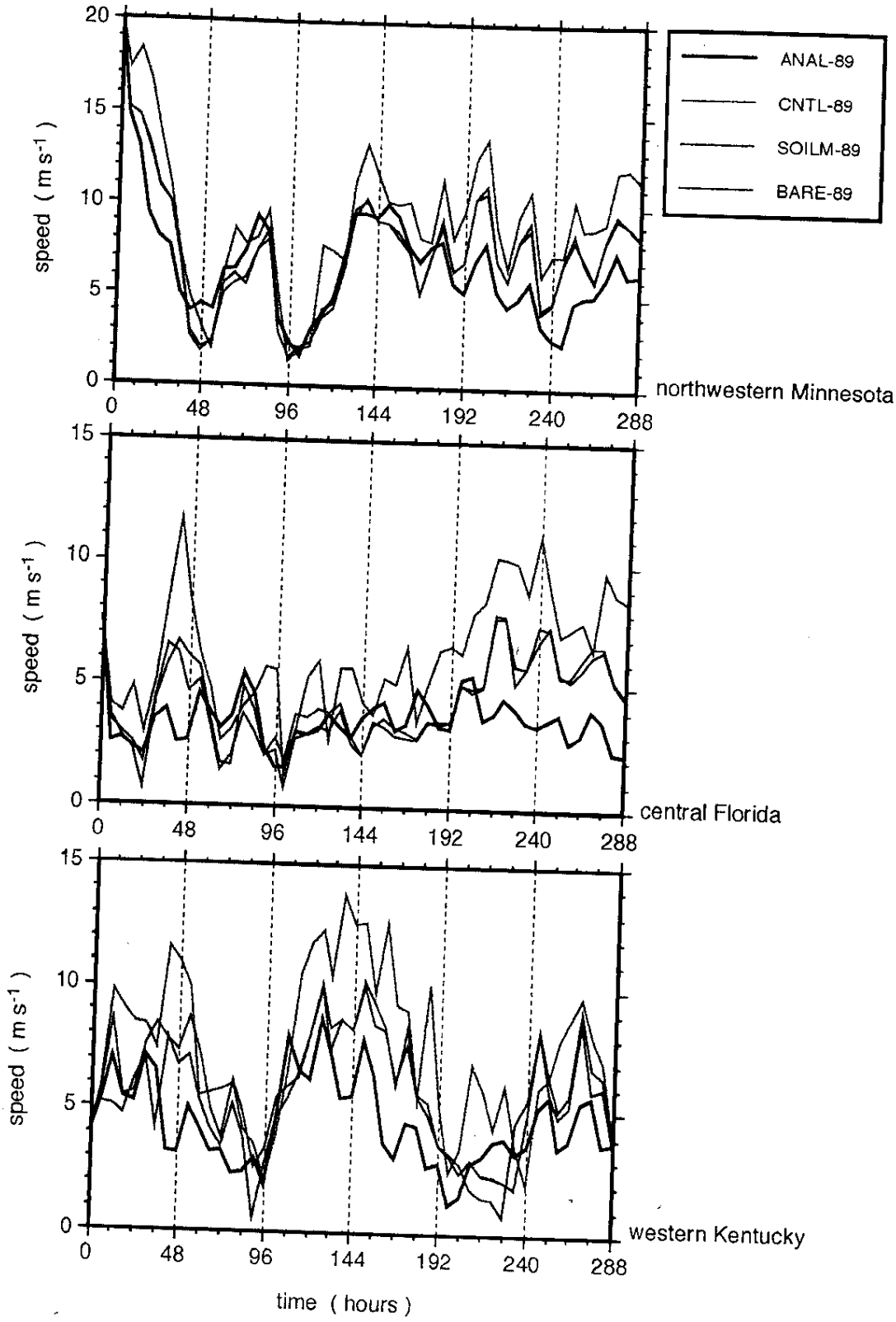
ANAL-89
CNTL-89
SOILM-89
BARE-89
speed (m s-1)
northwestern Minnesota
central Florida
western Kentucky
time (hours)
0
48
96
144
192
240
288

Figure 25

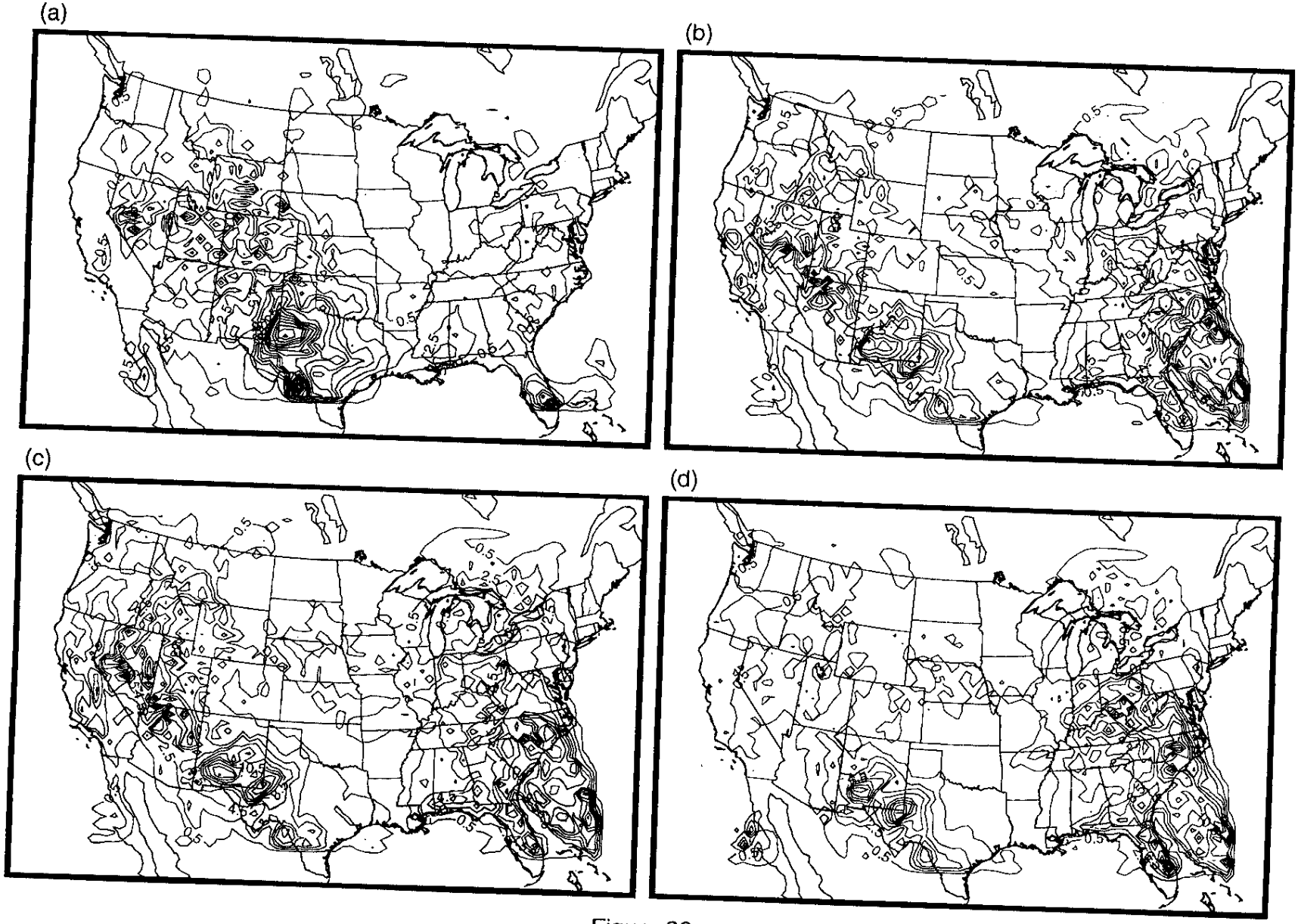

Figure 26

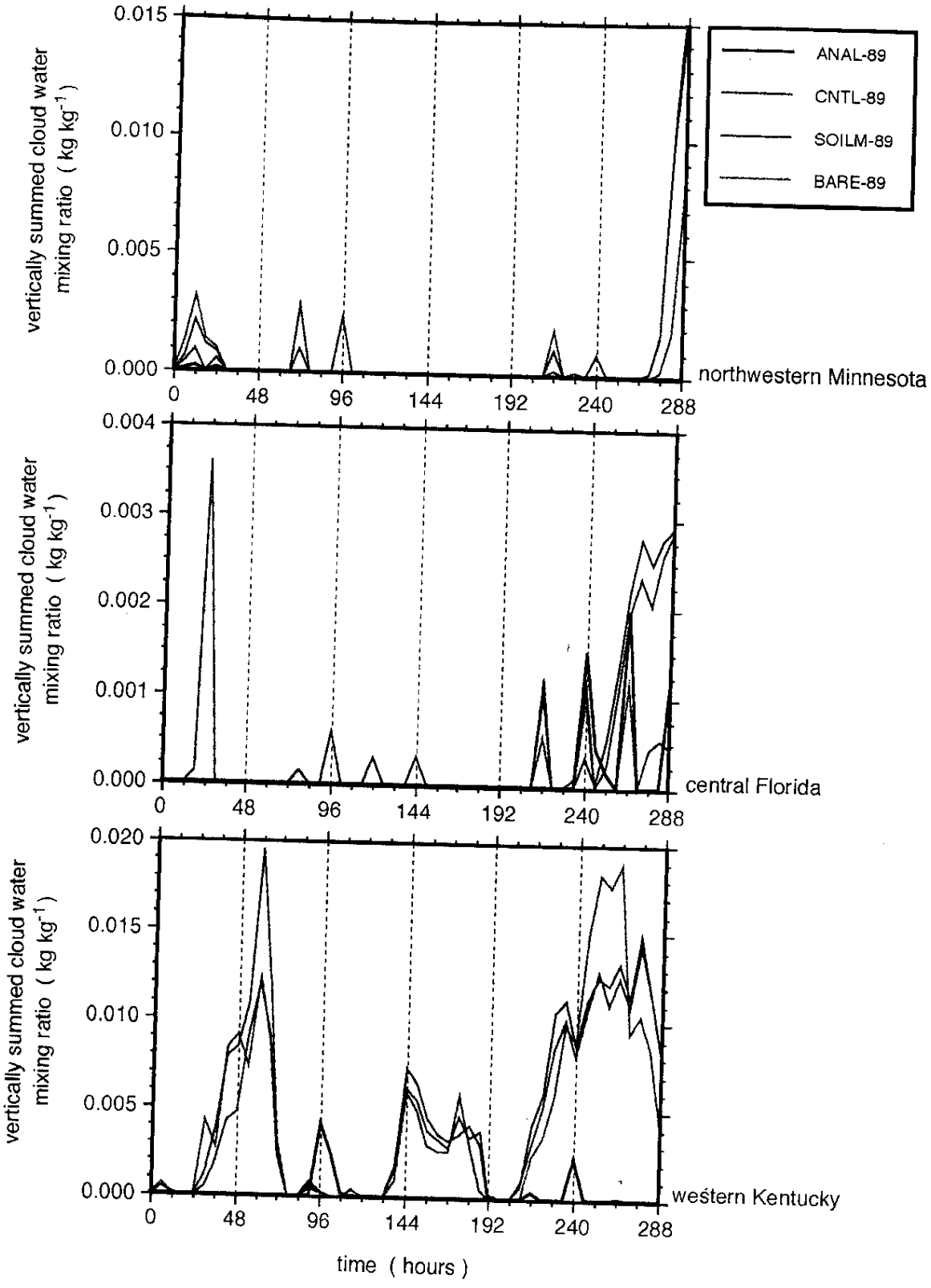
ANAL-89
CNTL-89
SOILM-89
BARE-89
vertically summed cloud water mixing ratio (kg kg-1)
0.015
0.010
0.005
0.000
0
48
96
144
192
240
288
northwestern Minnesota
0.004
0.003
0.002
0.001
0.000
central Florida
0.020
0.015
0.010
0.005
0.000
western Kentucky
time (hours)

Figure 27

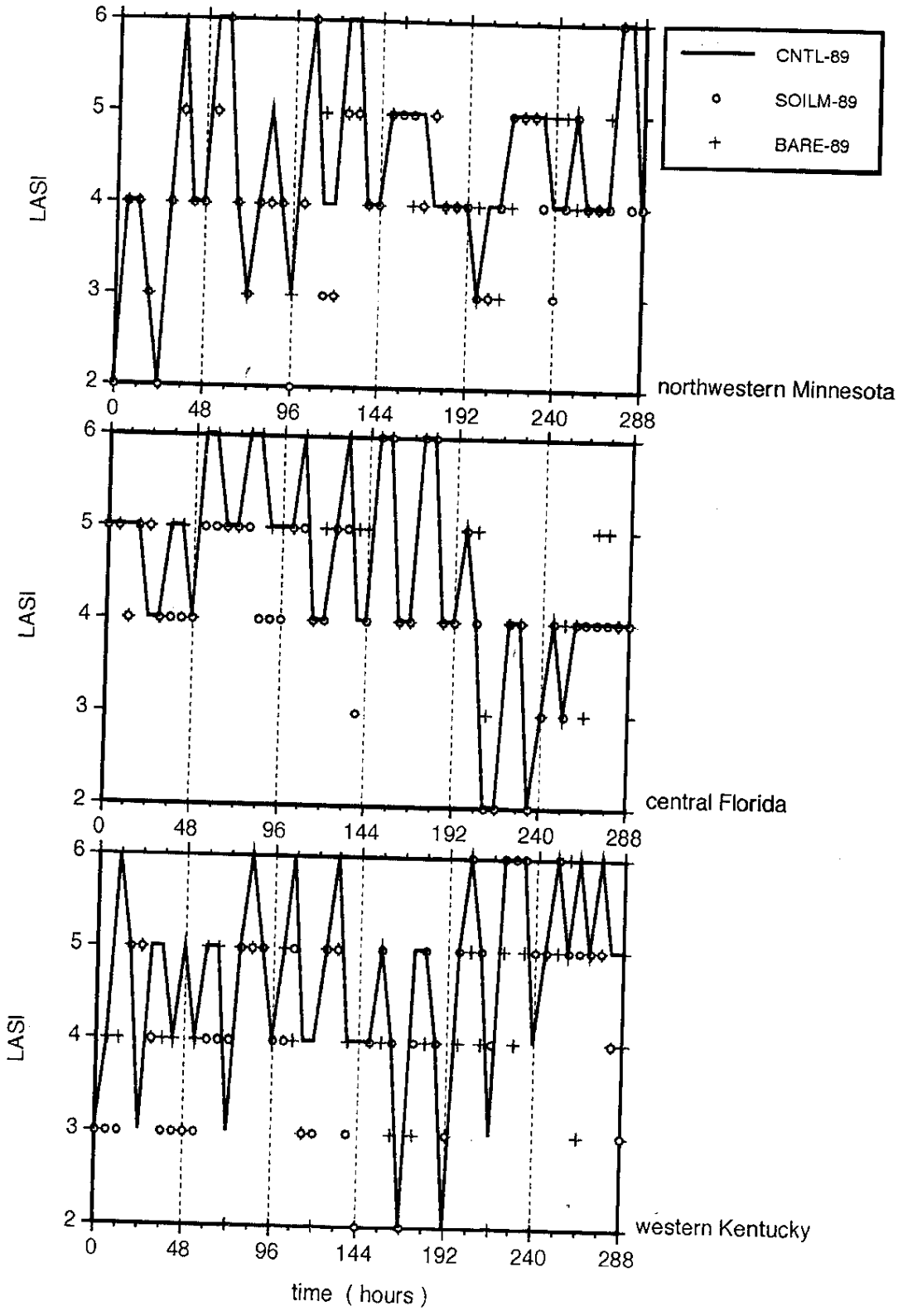
CNTL-89
SOILM-89
BARE-89
LASI
northwestern Minnesota
central Florida
western Kentucky
time (hours)
0
48
96
144
192
240
288
2
3
4
5
6

Figure 28

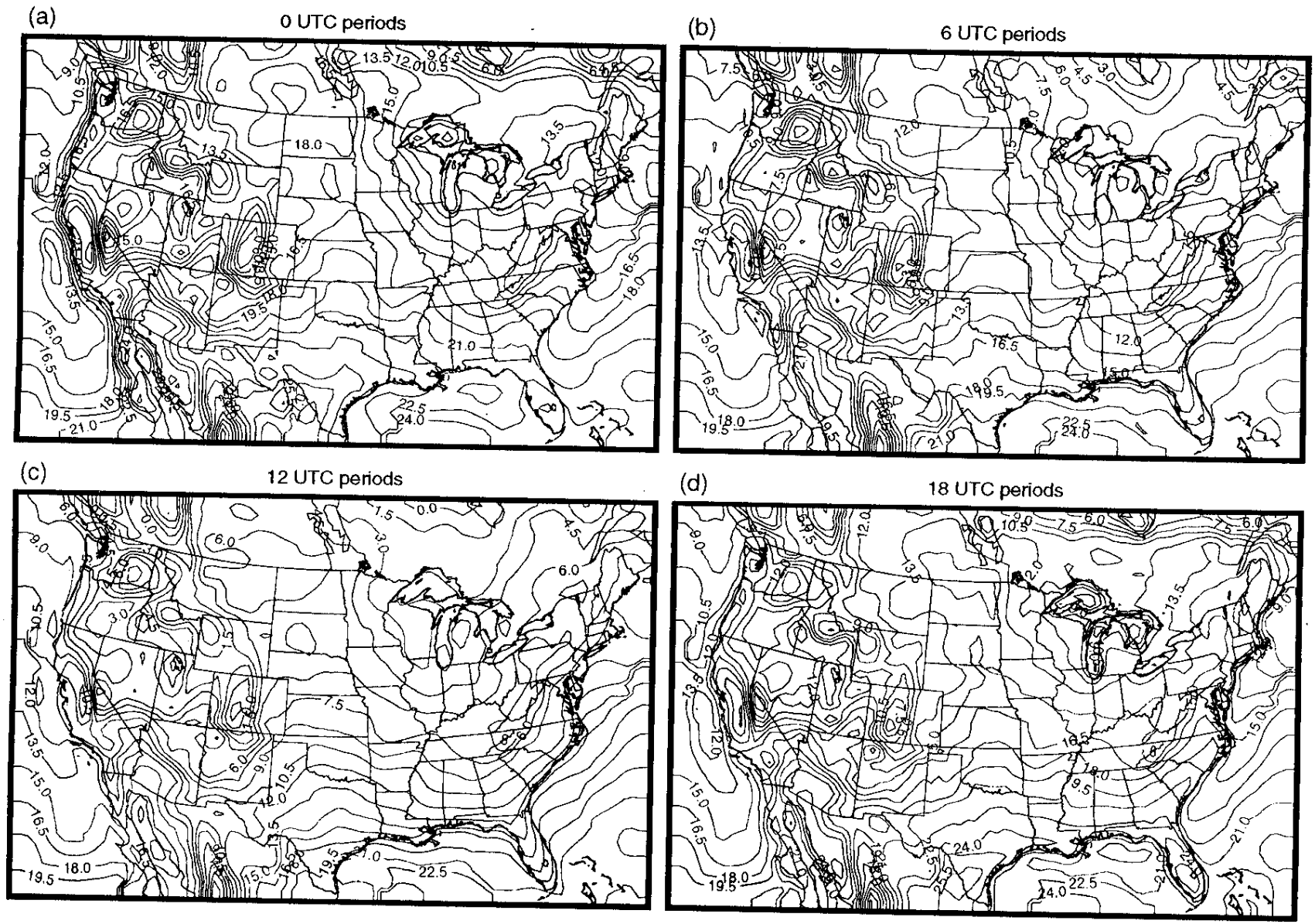
(a)
0 UTC periods
(b)
6 UTC periods
(c)
12 UTC periods
(d)
18 UTC periods

Figure 29

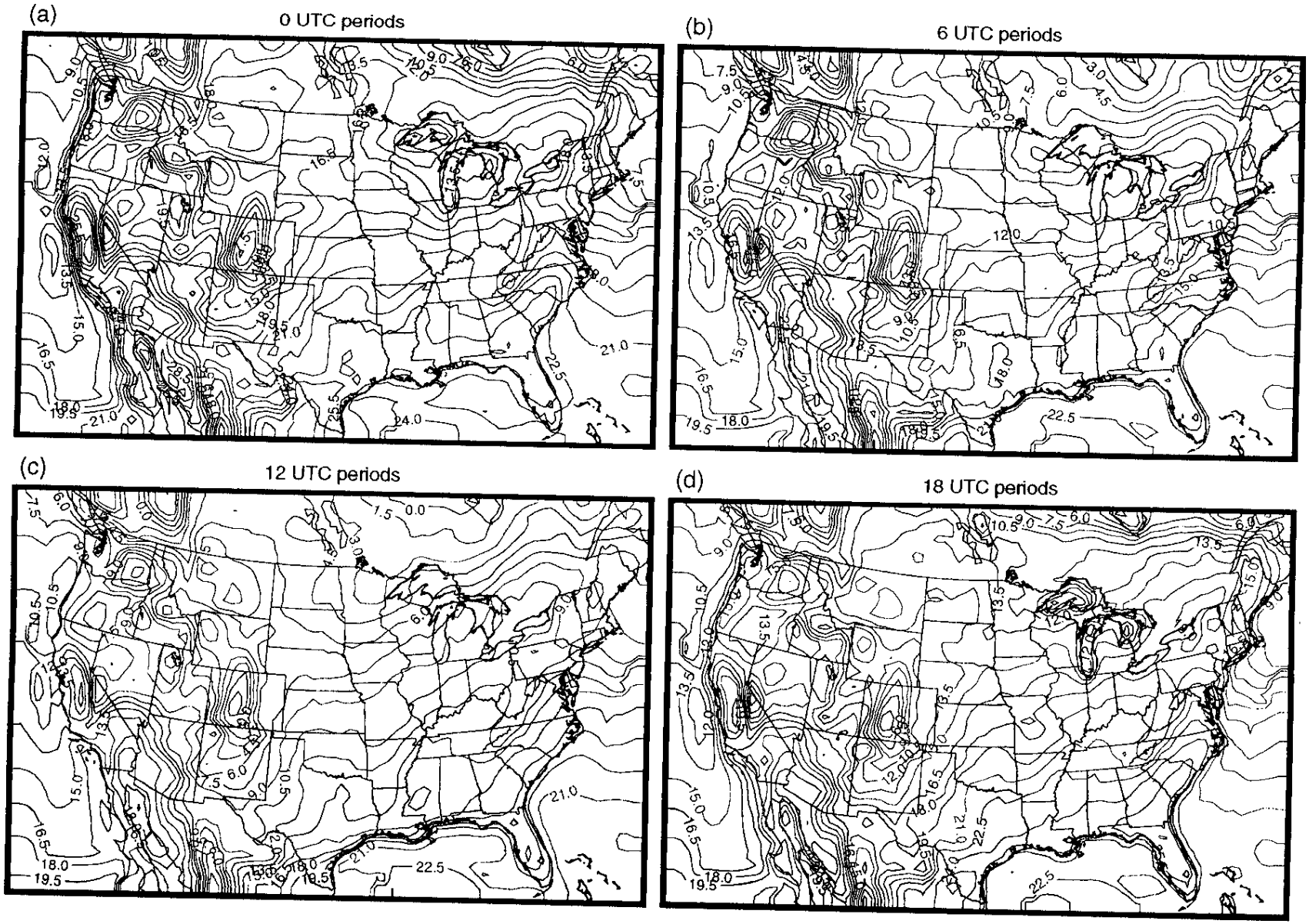
(a)
0 UTC periods
(b)
6 UTC periods
(c)
12 UTC periods
(d)
18 UTC periods

Figure 30

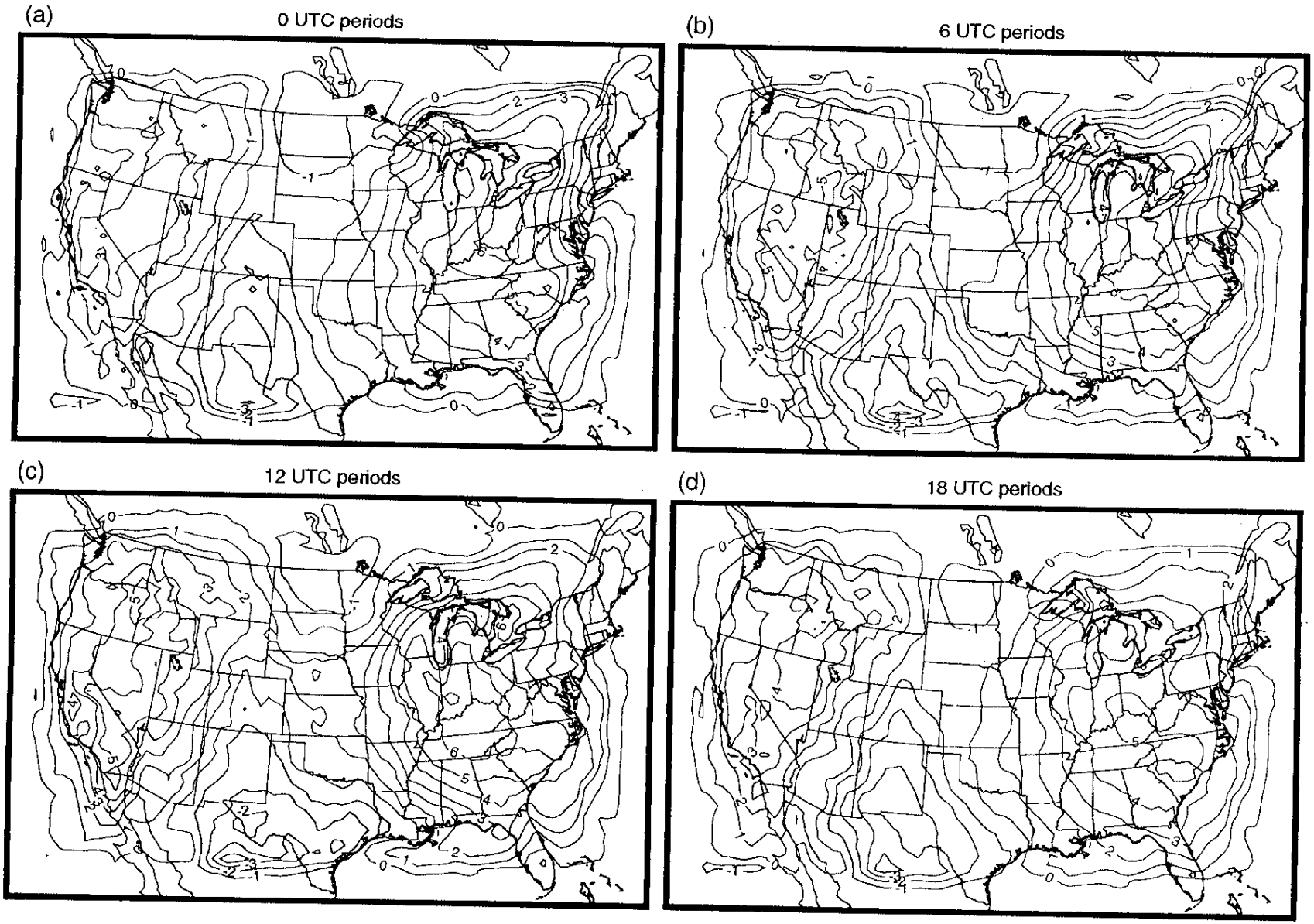
(a)
0 UTC periods
(b)
6 UTC periods
(c)
12 UTC periods
(d)
18 UTC periods

Figure 31

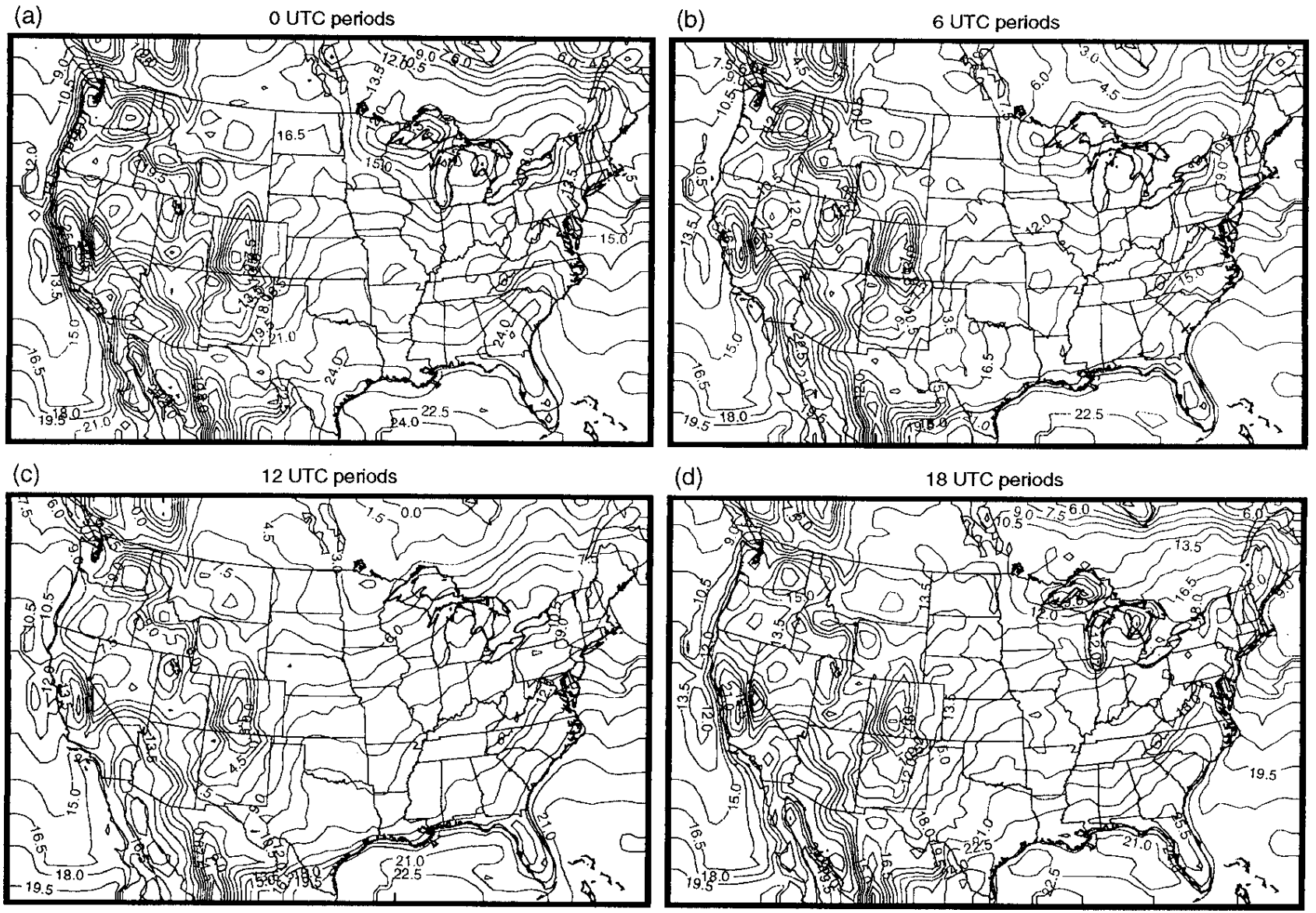
(a)
0 UTC periods
(b)
6 UTC periods
(c)
12 UTC periods
(d)
18 UTC periods

Figure 32

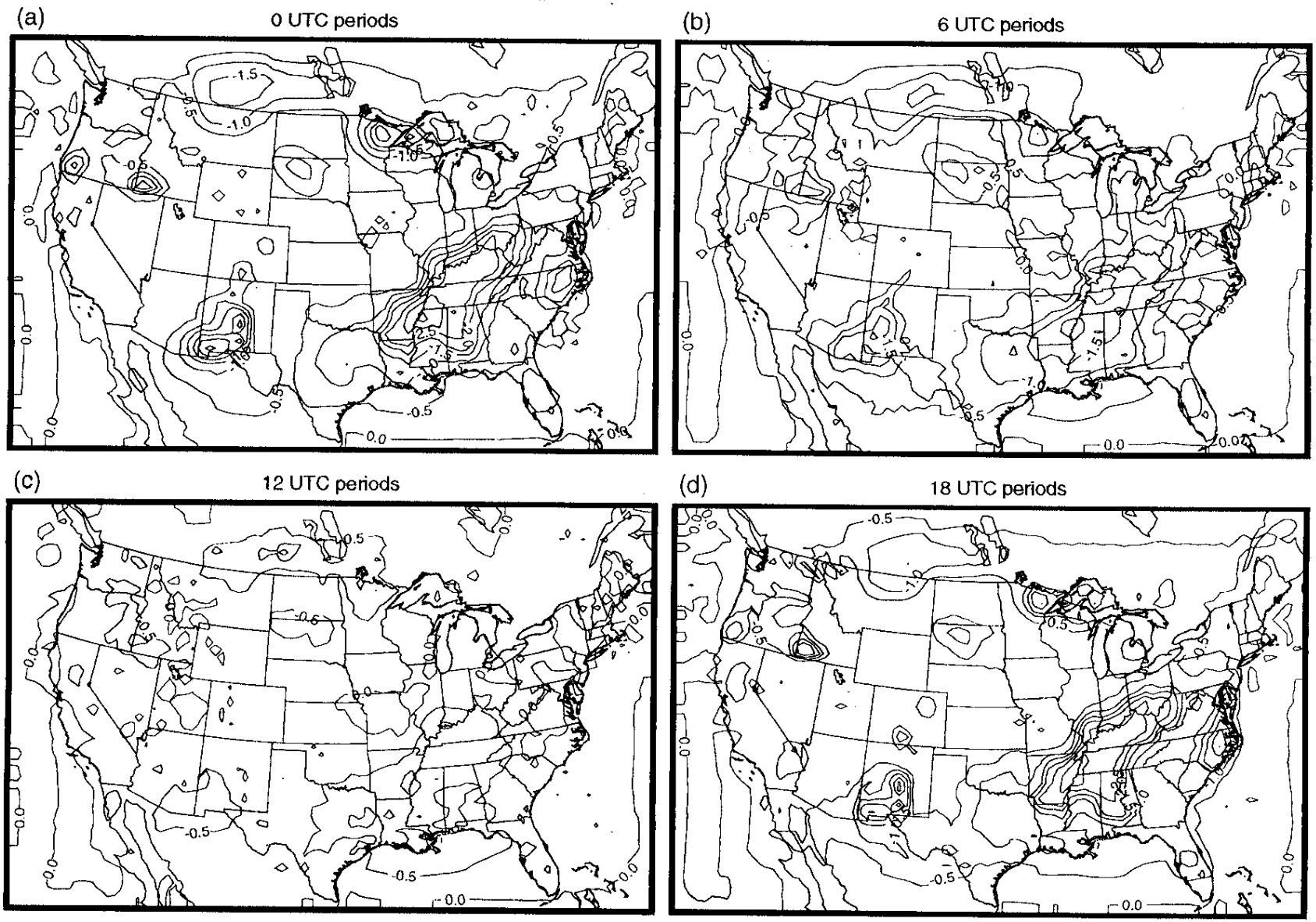
(a)
0 UTC periods
(b)
6 UTC periods
(c)
12 UTC periods
(d)
18 UTC periods

Figure 33

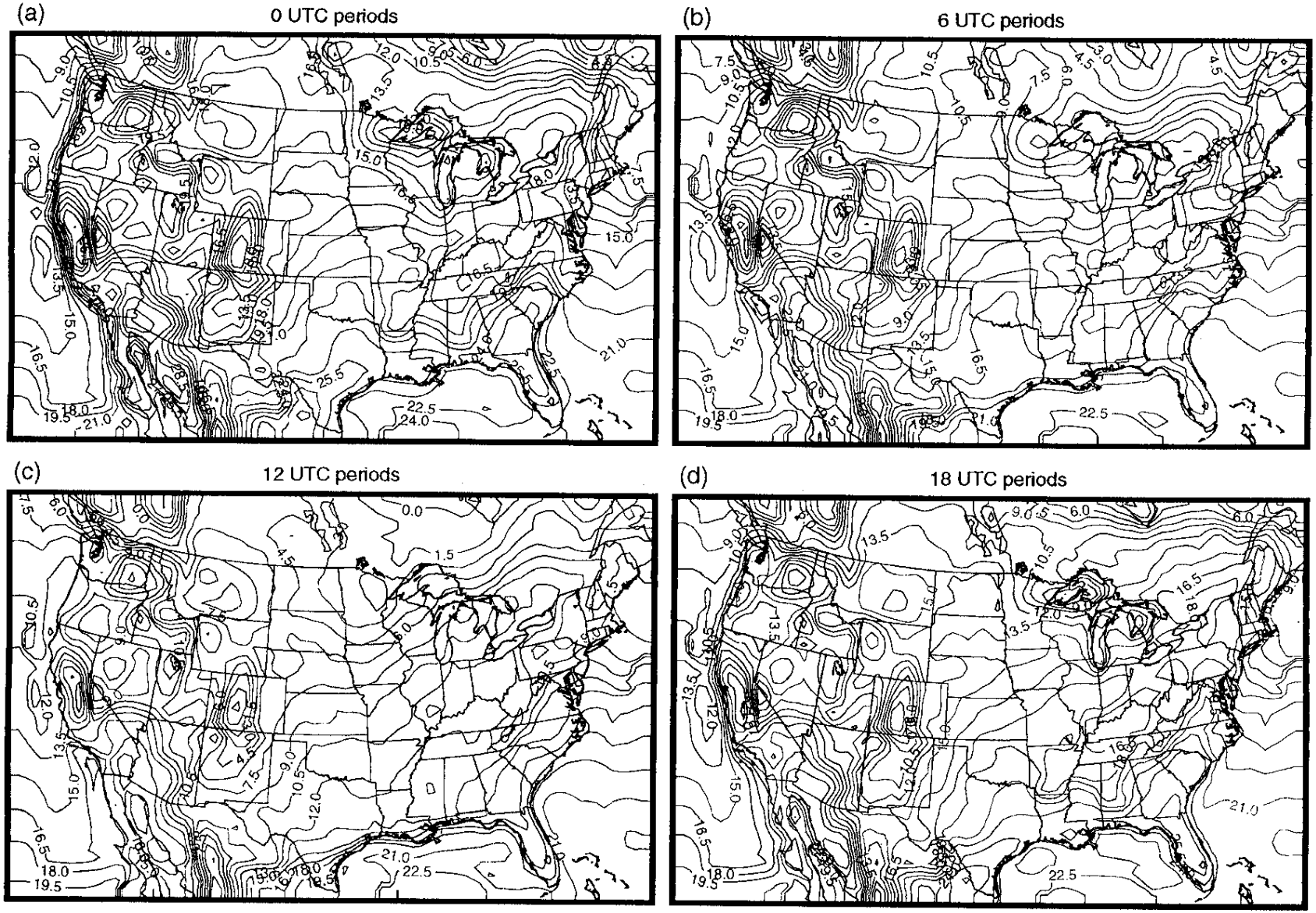
(a)
0 UTC periods
(b)
6 UTC periods
(c)
12 UTC periods
(d)
18 UTC periods

Figure 34

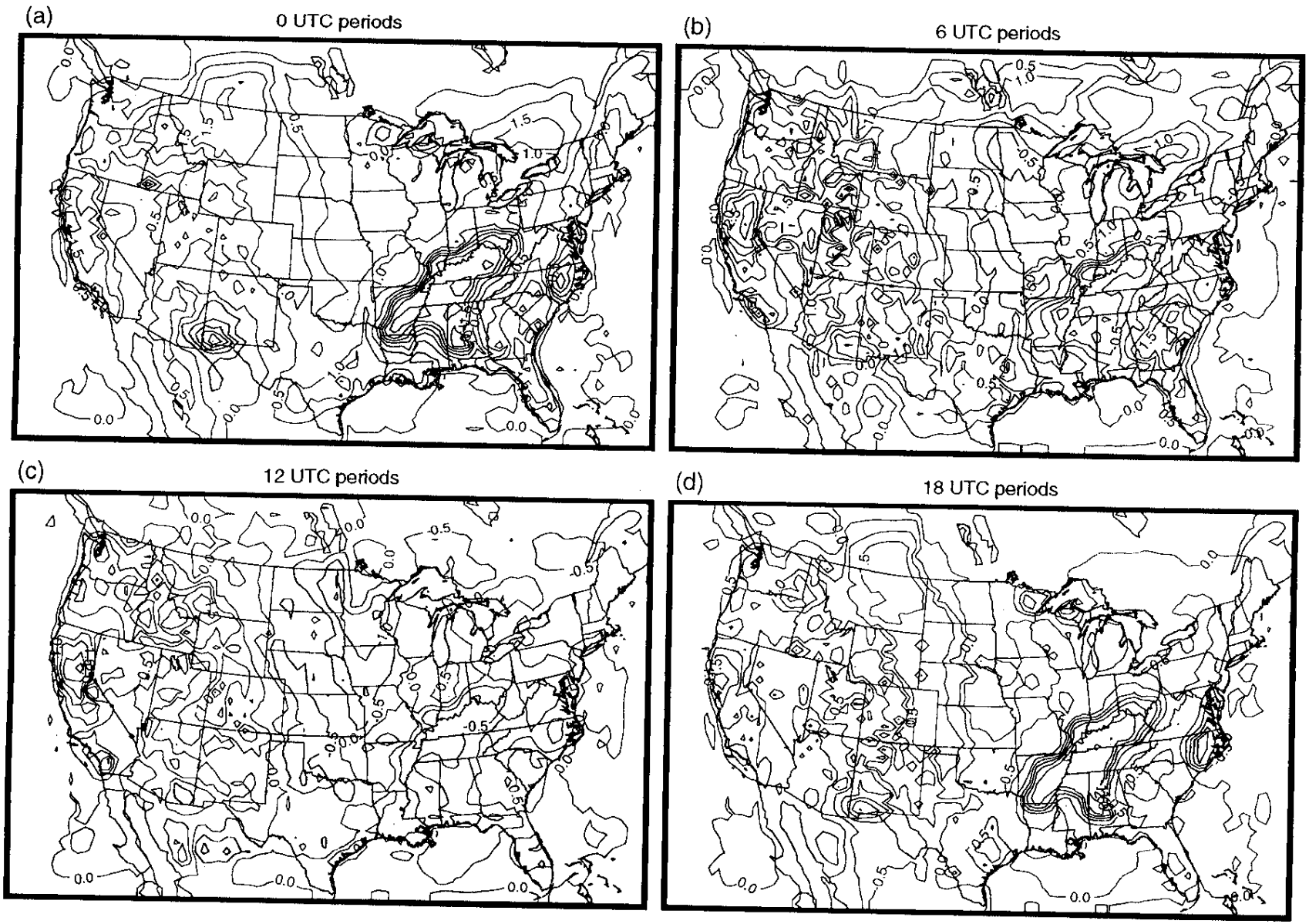
(a)
0 UTC periods
(b)
6 UTC periods
(c)
12 UTC periods
(d)
18 UTC periods

Figure 35

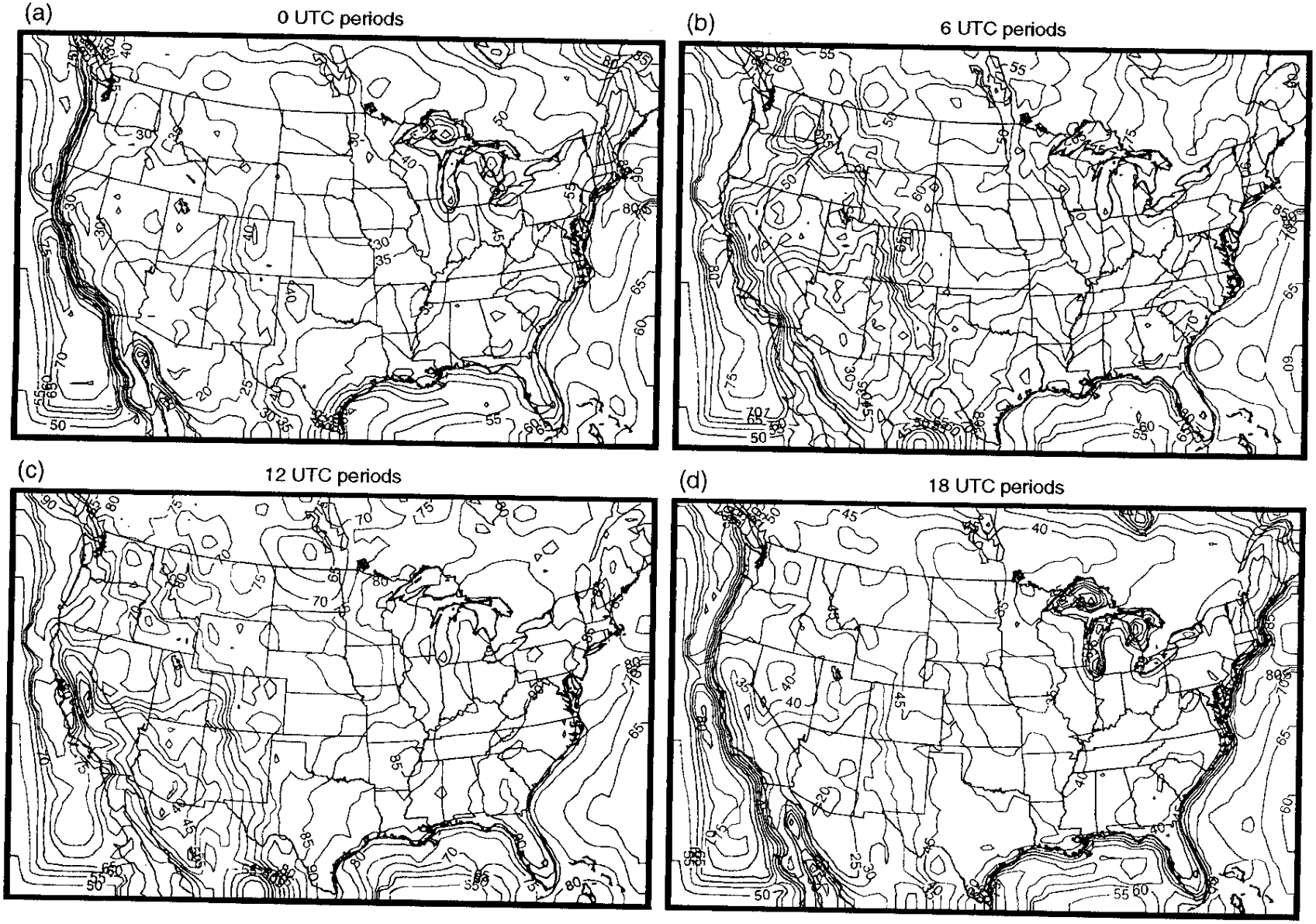
(a)
0 UTC periods
(b)
6 UTC periods
(c)
12 UTC periods
(d)
18 UTC periods

Figure 36

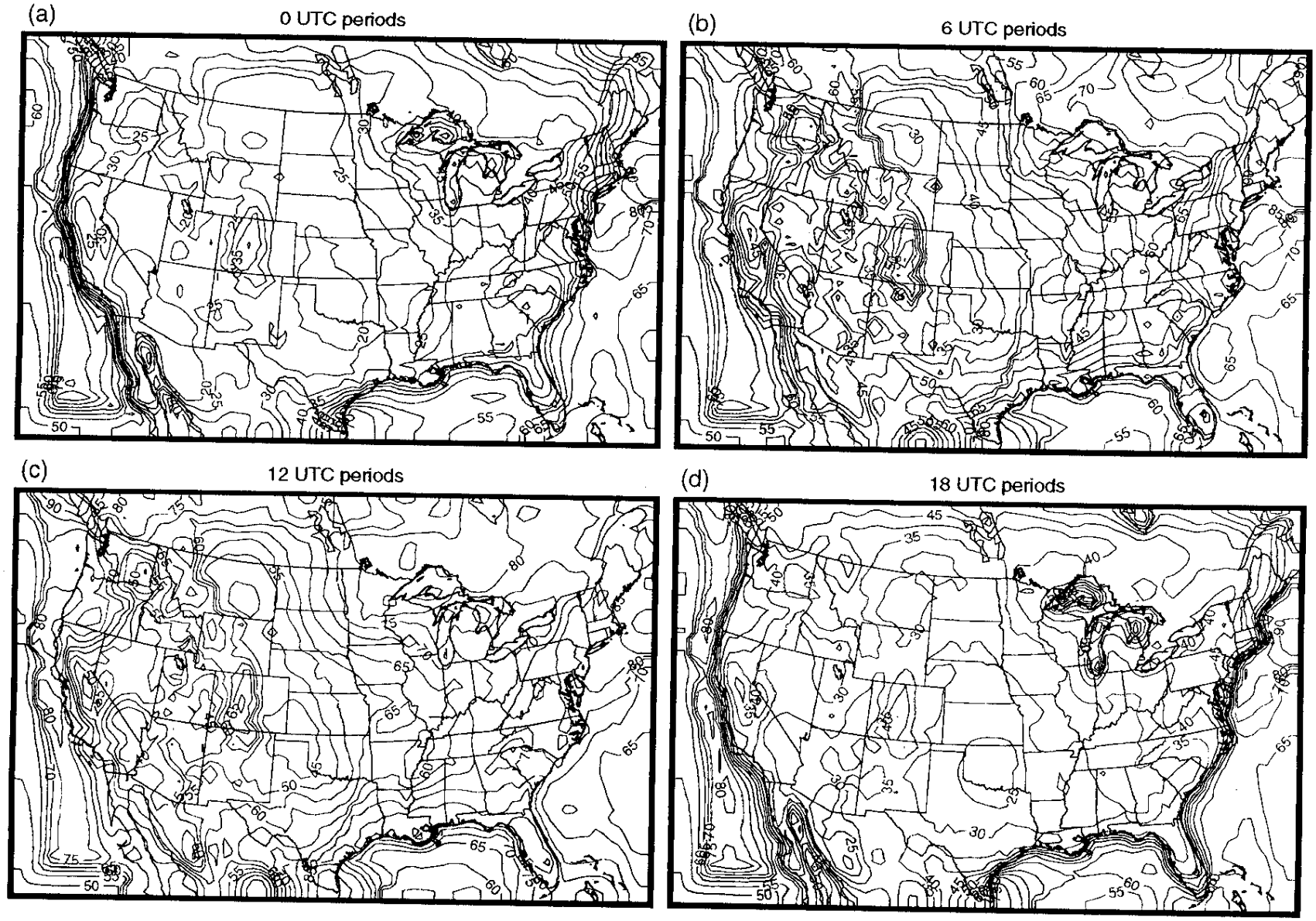
(a)
0 UTC periods
(b)
6 UTC periods
(c)
12 UTC periods
(d)
18 UTC periods

Figure 37

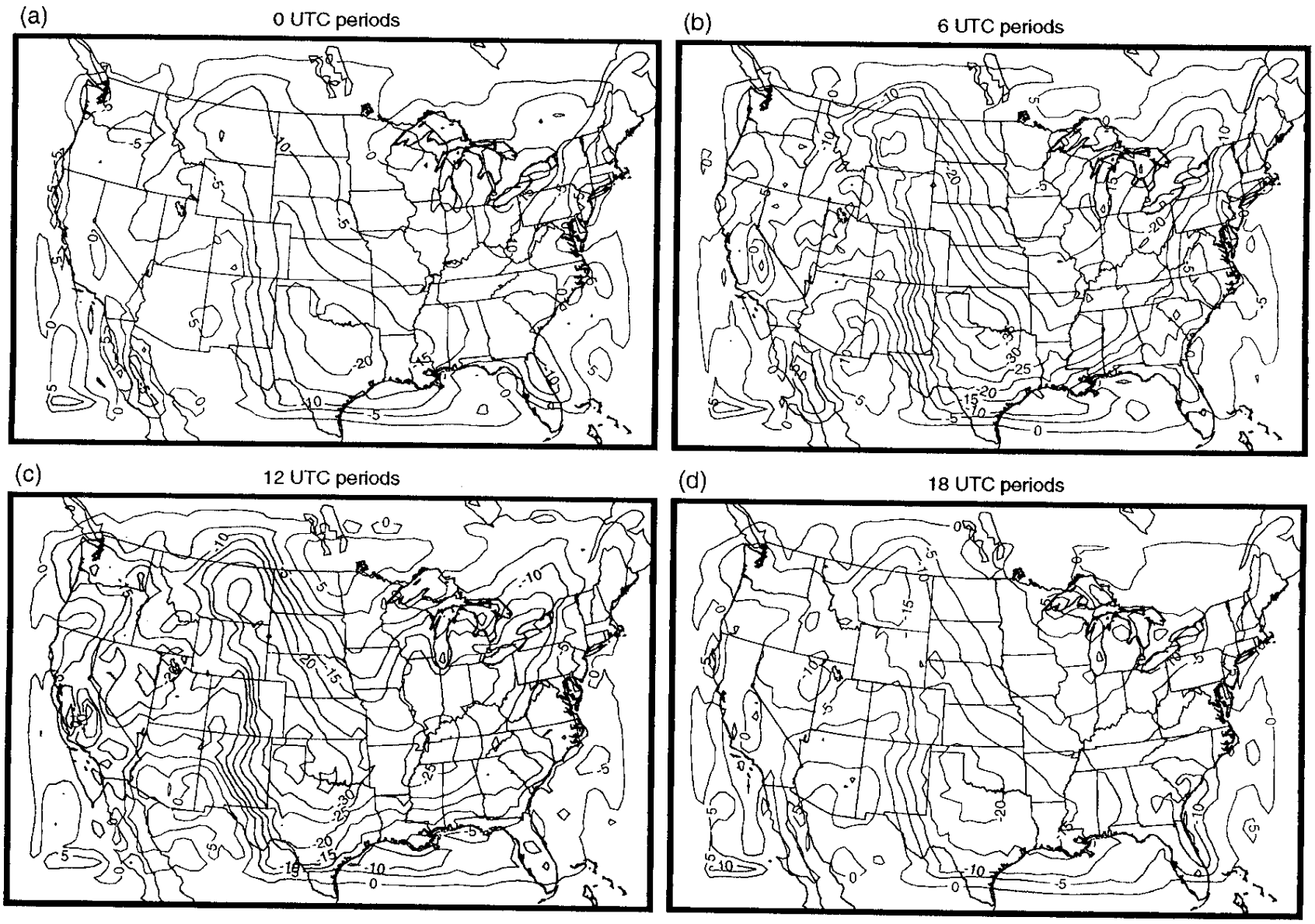
(a)
0 UTC periods
(b)
6 UTC periods
(c)
12 UTC periods
(d)
18 UTC periods

Figure 38

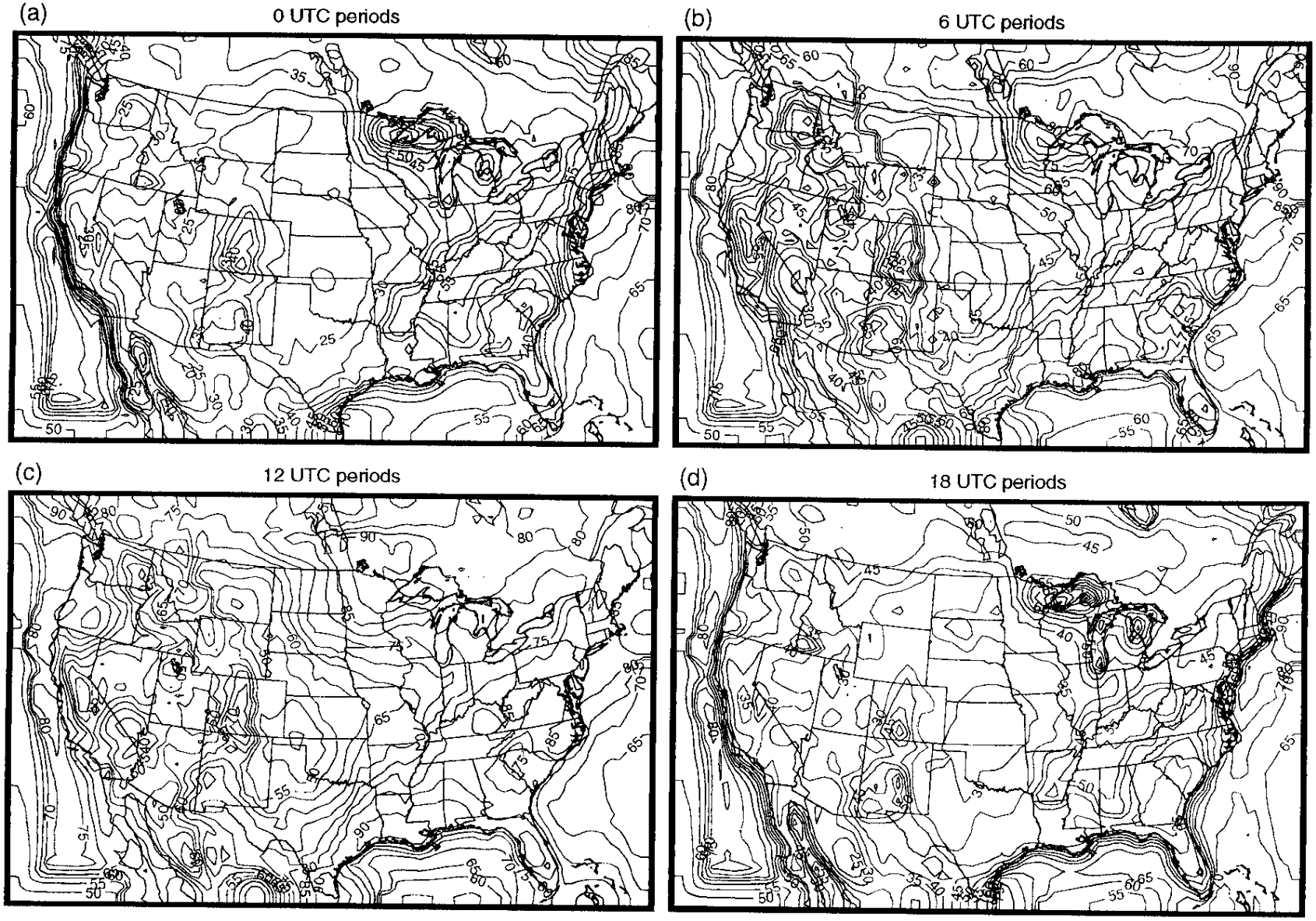
(a)
0 UTC periods
(b)
6 UTC periods
(c)
12 UTC periods
(d)
18 UTC periods

Figure 39

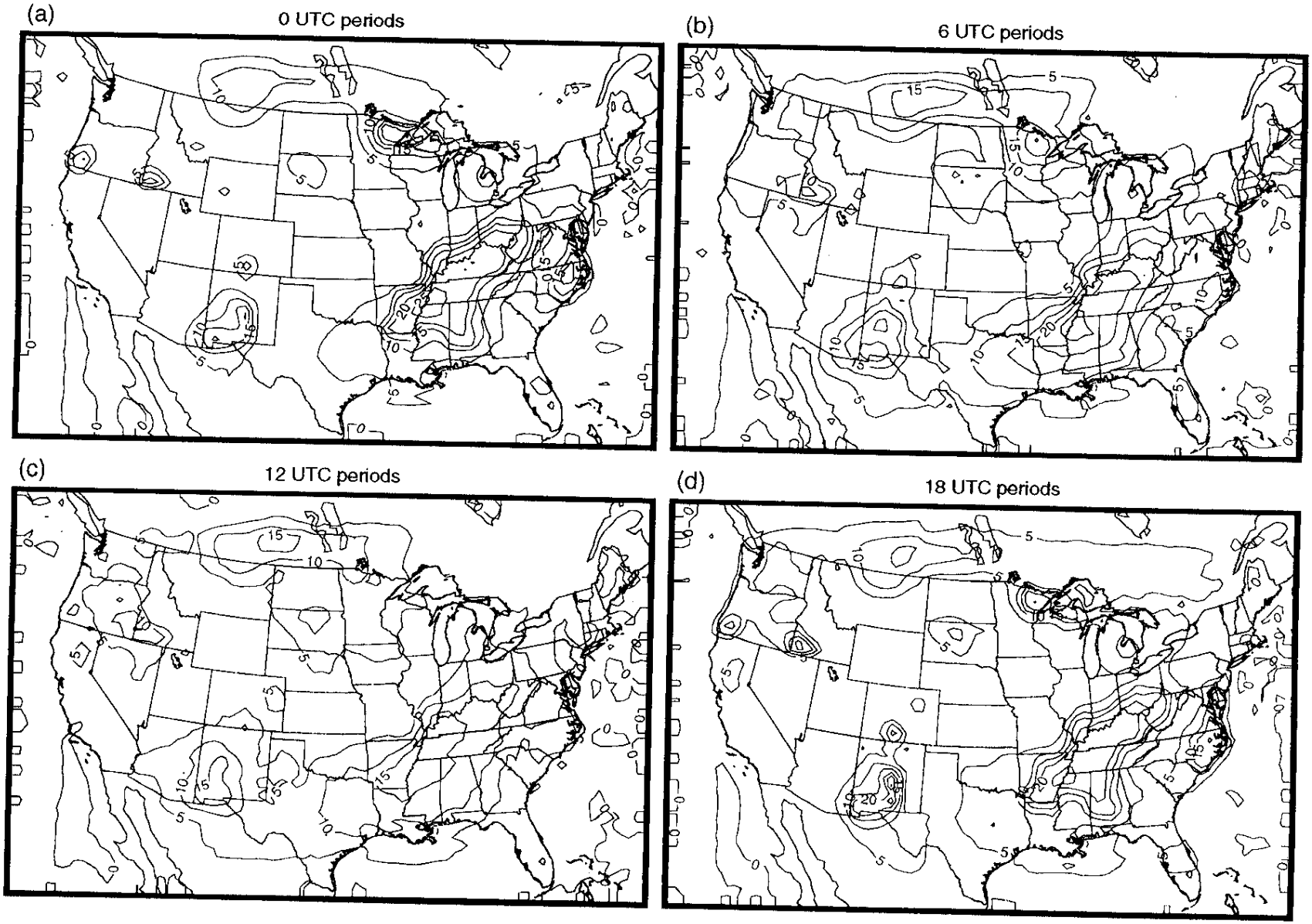
(a)
0 UTC periods
(b)
6 UTC periods
(c)
12 UTC periods
(d)
18 UTC periods

Figure 40

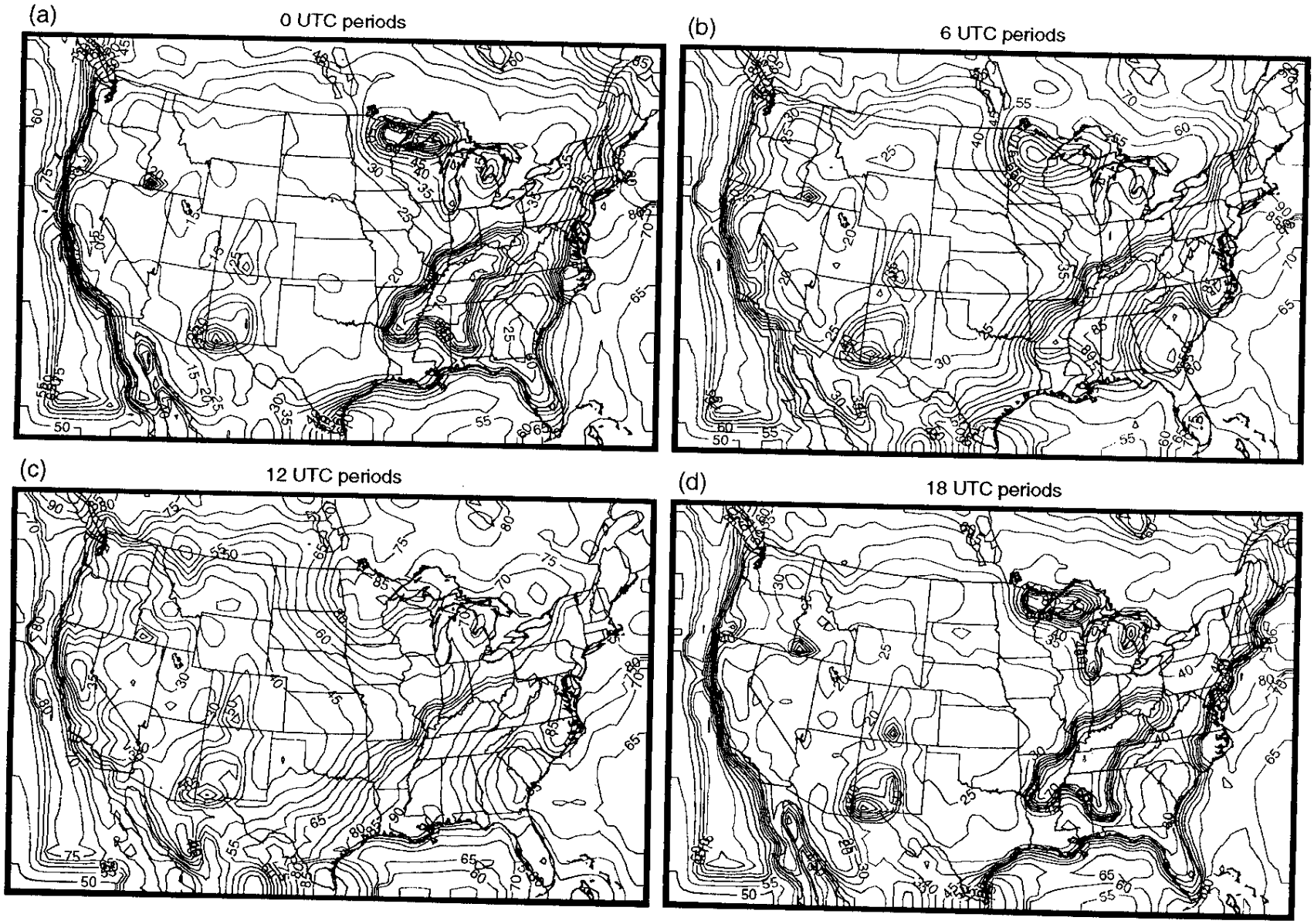
(a)
0 UTC periods
(b)
6 UTC periods
(c)
12 UTC periods
(d)
18 UTC periods

Figure 41

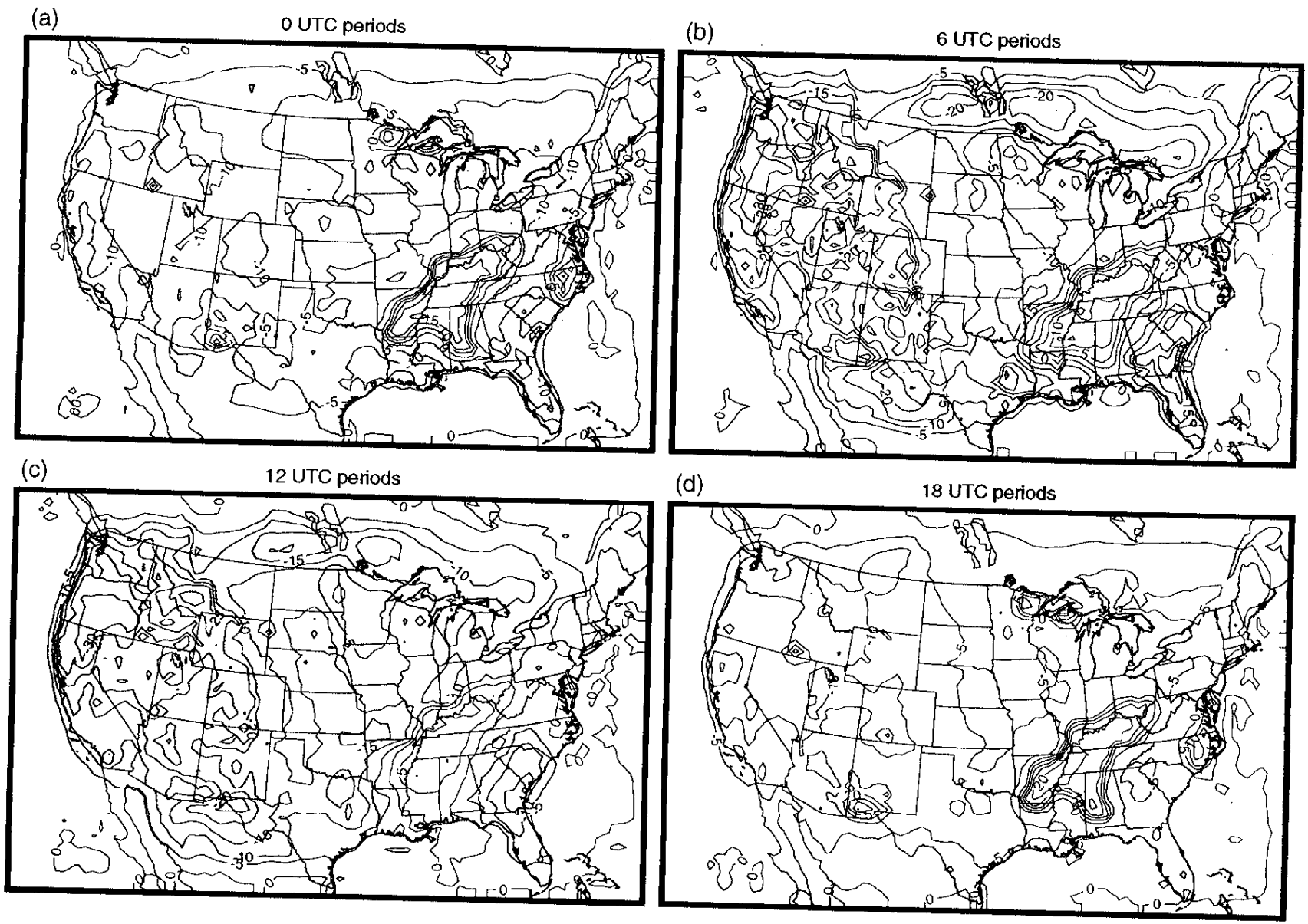
(a)
0 UTC periods
(b)
6 UTC periods
(c)
12 UTC periods
(d)
18 UTC periods

Figure 42

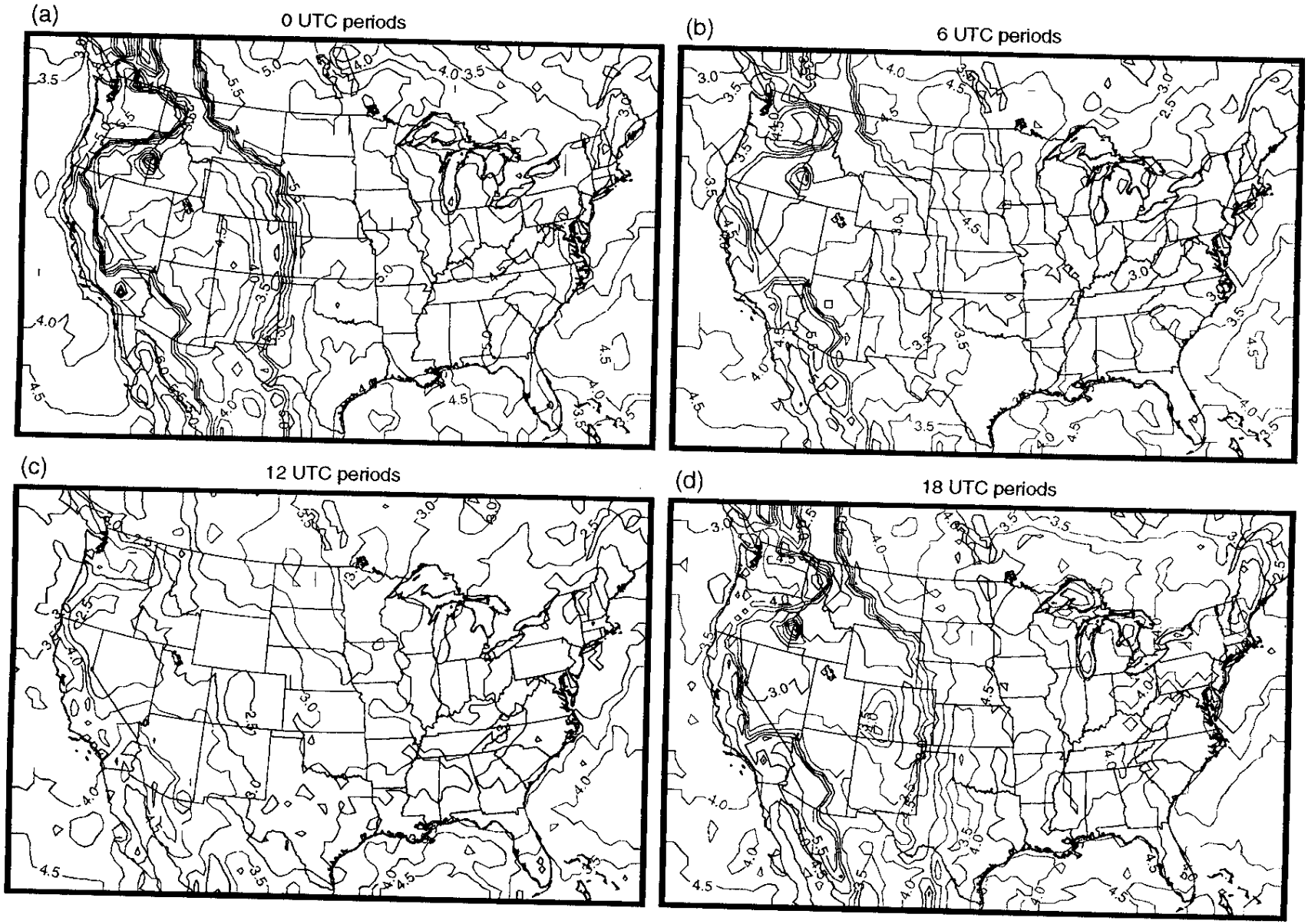
(a)
0 UTC periods
(b)
6 UTC periods
(c)
12 UTC periods
(d)
18 UTC periods

Figure 43

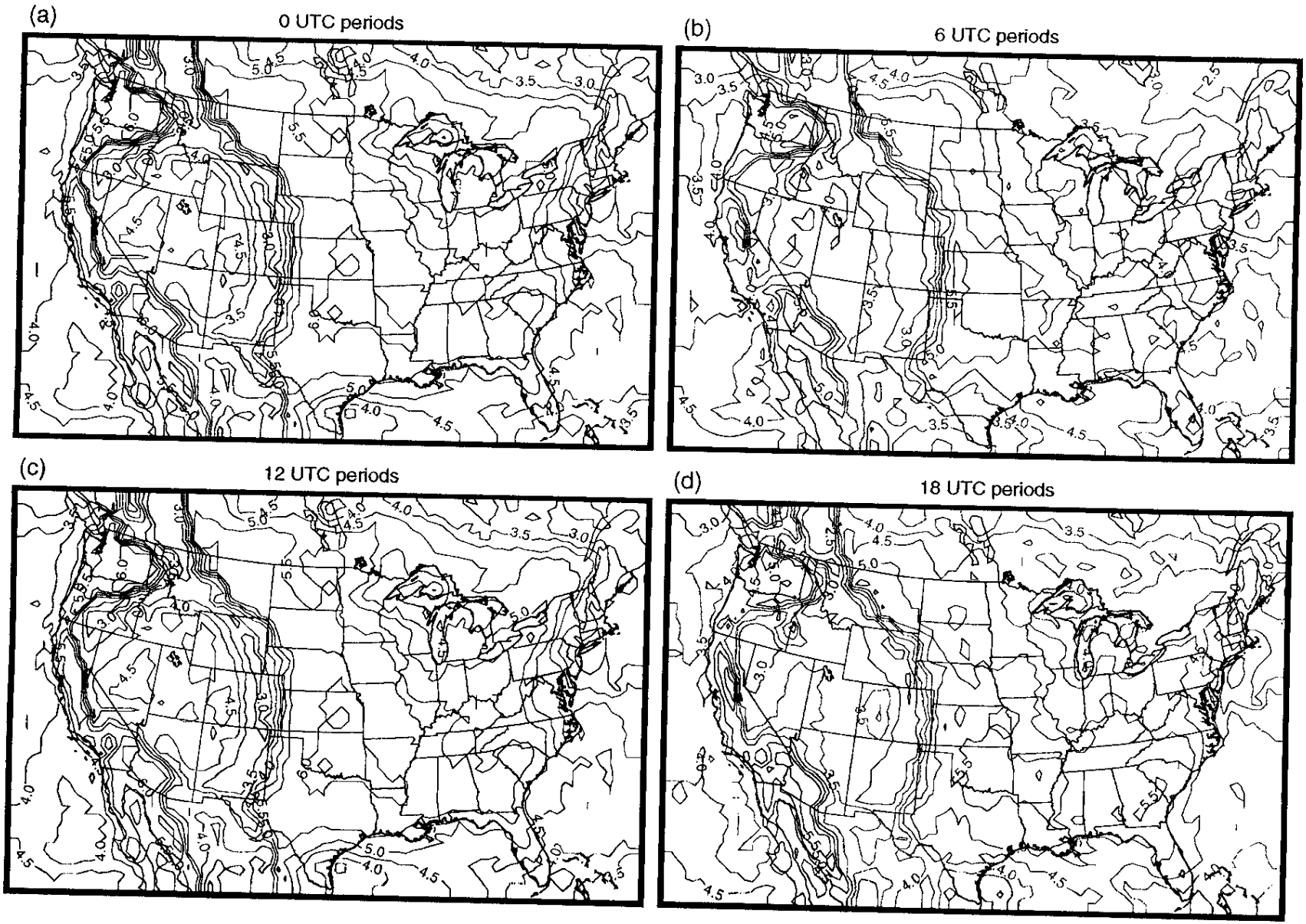
(a)
0 UTC periods
(b)
6 UTC periods
(c)
12 UTC periods
(d)
18 UTC periods

Figure 44

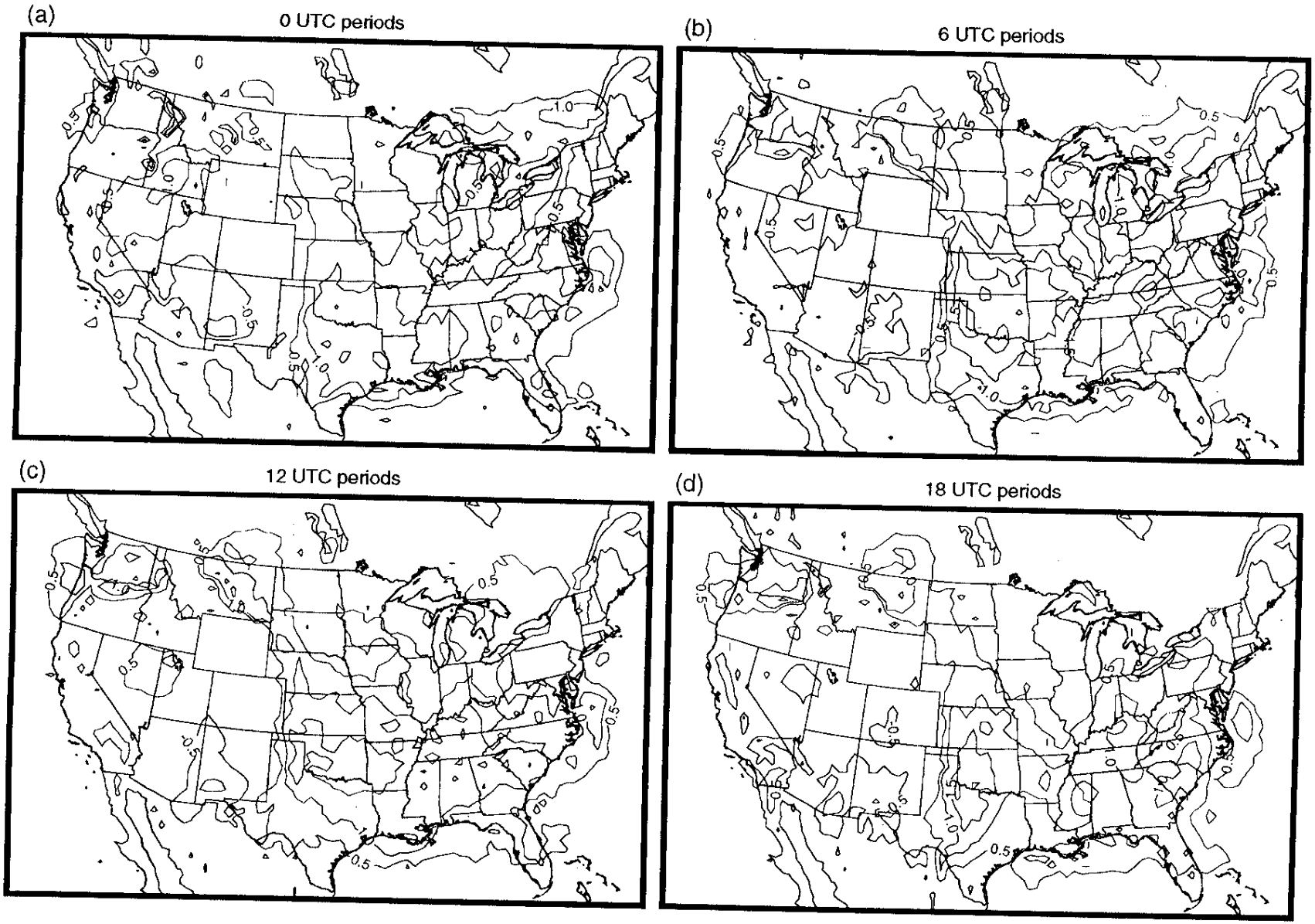
(a)
0 UTC periods
(b)
6 UTC periods
(c)
12 UTC periods
(d)
18 UTC periods

Figure 45

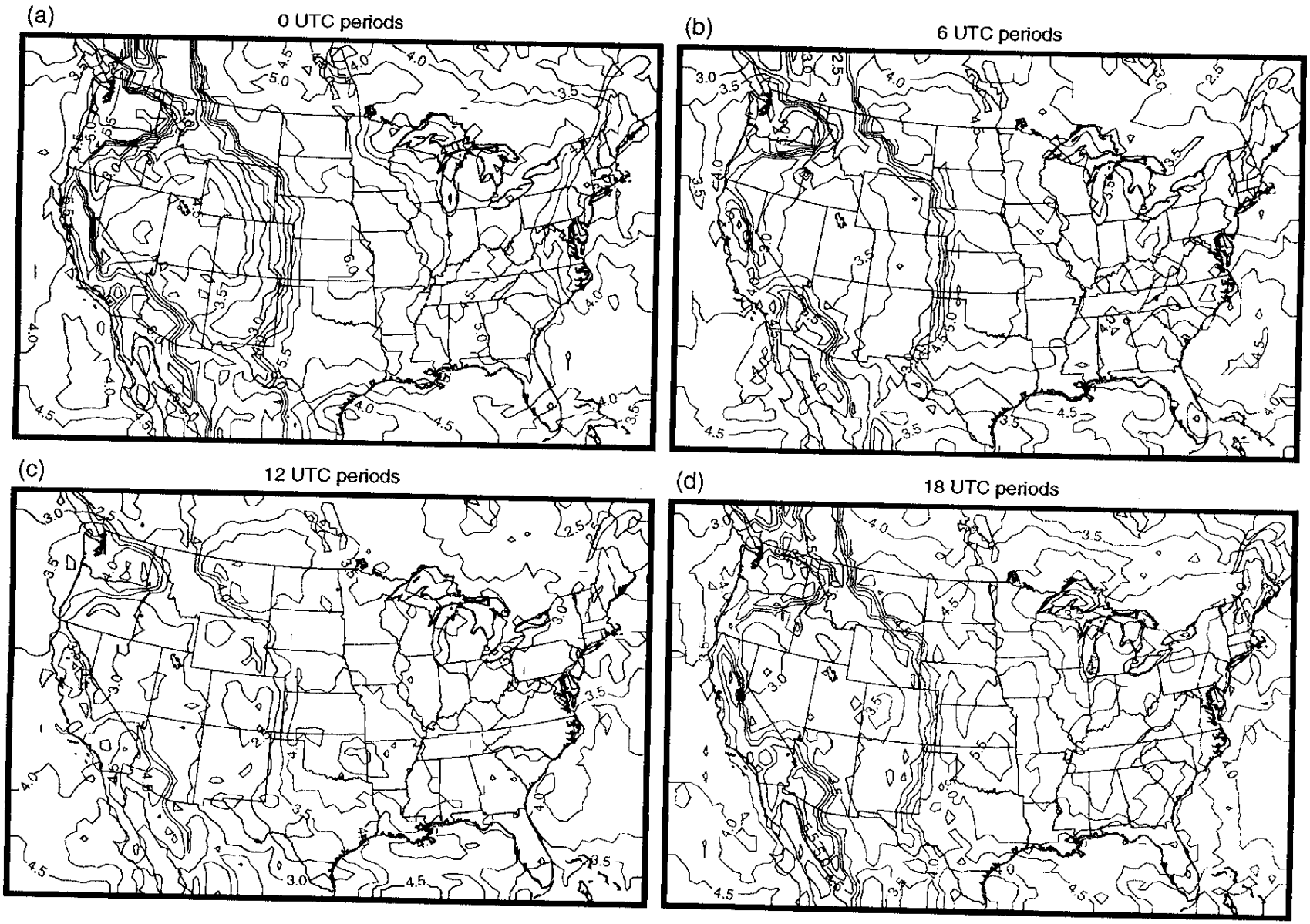
(a)
0 UTC periods
(b)
6 UTC periods
(c)
12 UTC periods
(d)
18 UTC periods

Figure 46

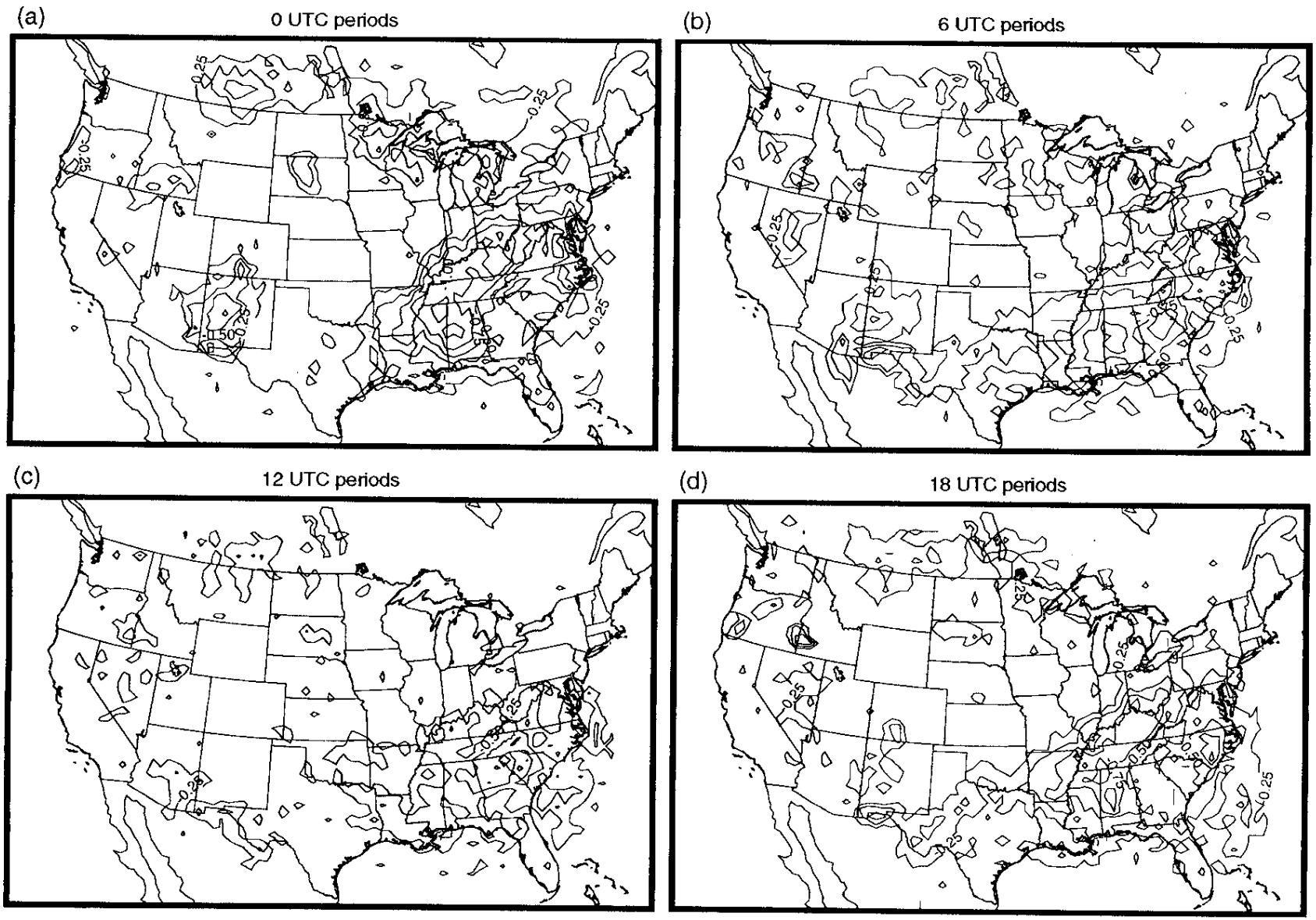
(a)
0 UTC periods
(b)
6 UTC periods
(c)
12 UTC periods
(d)
18 UTC periods

Figure 47

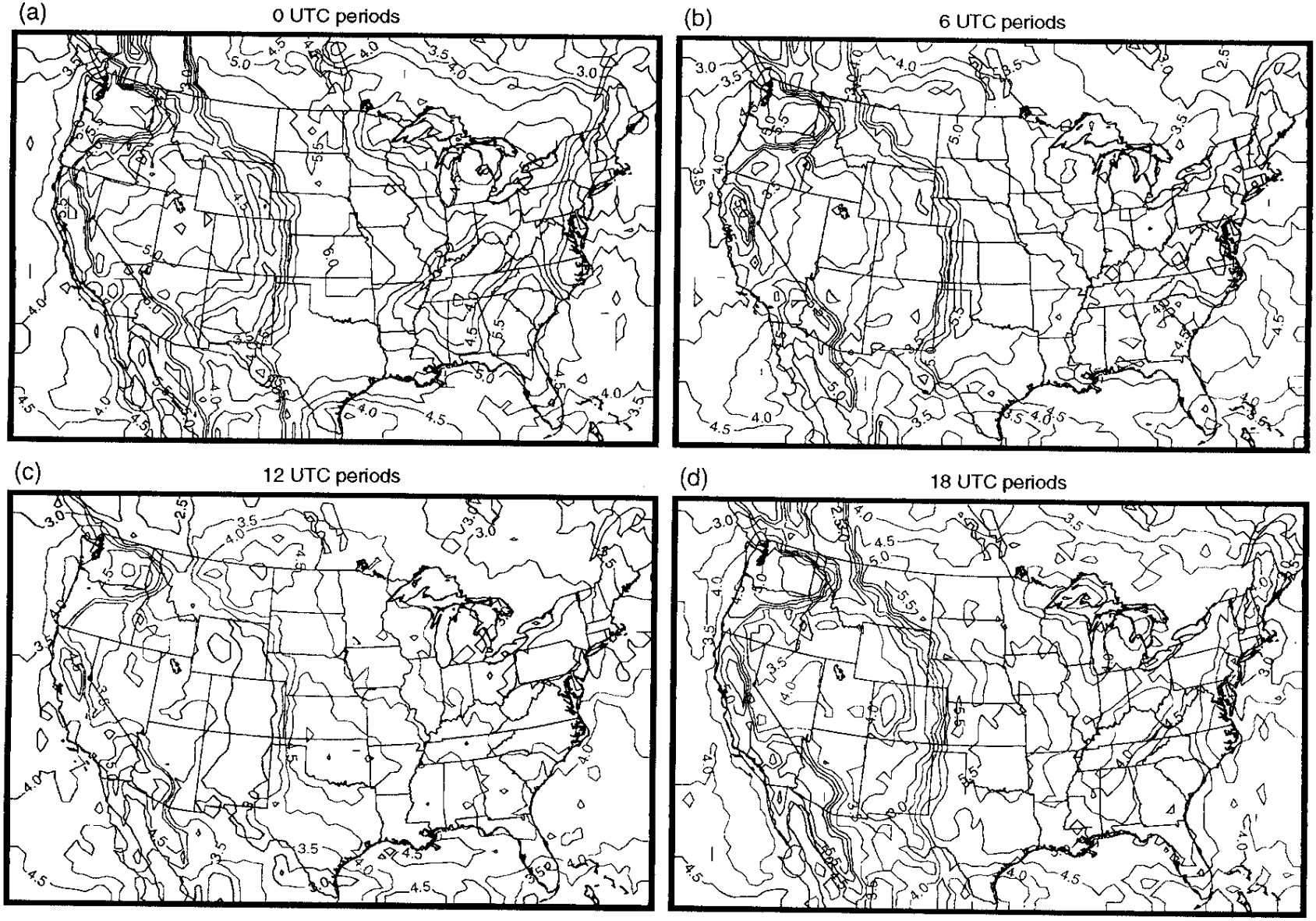
(a)
0 UTC periods
(b)
6 UTC periods
(c)
12 UTC periods
(d)
18 UTC periods

Figure 48

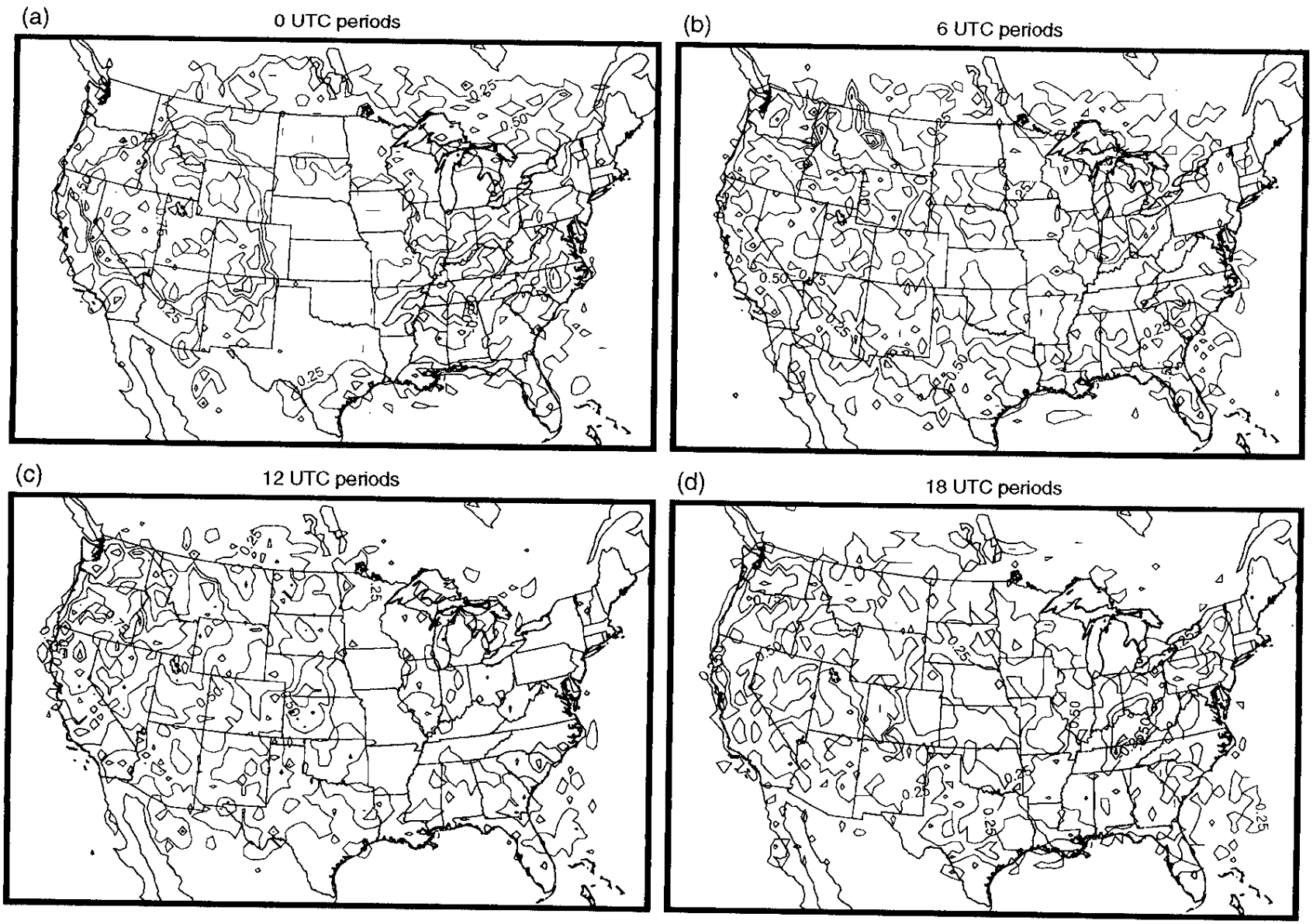
(a)
0 UTC periods
(b)
6 UTC periods
(c)
12 UTC periods
(d)
18 UTC periods

Figure 49

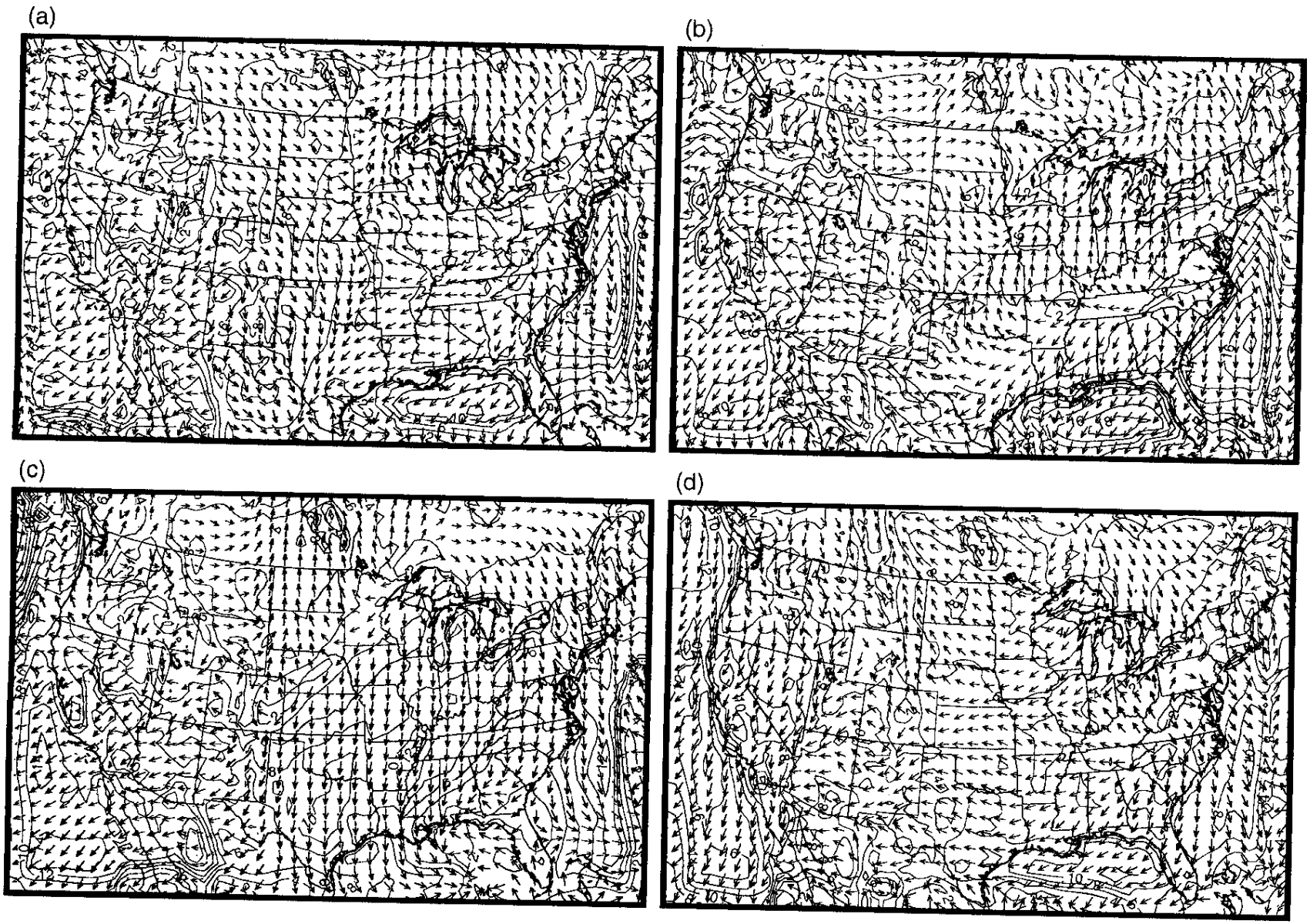

Figure 50

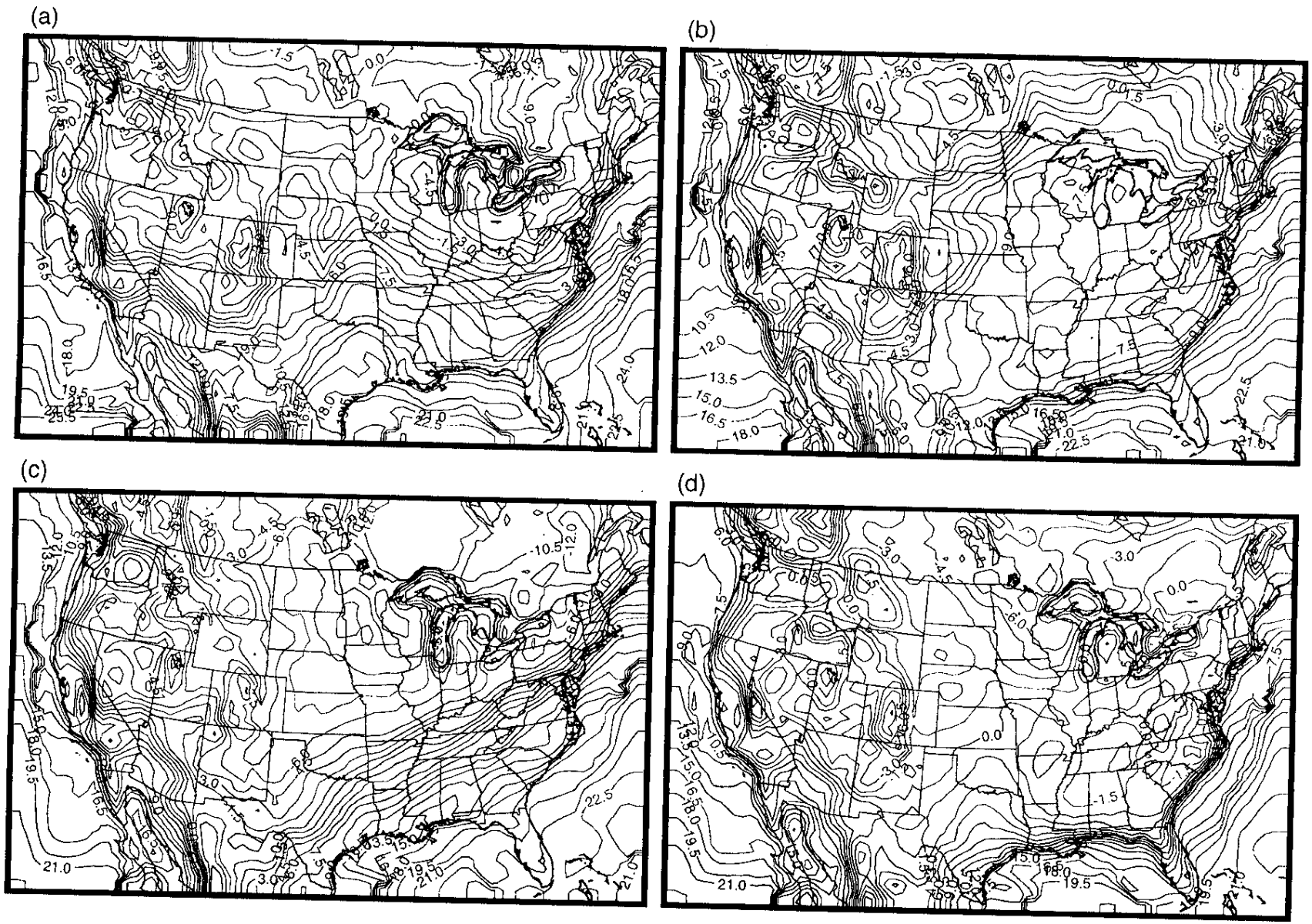

Figure 51

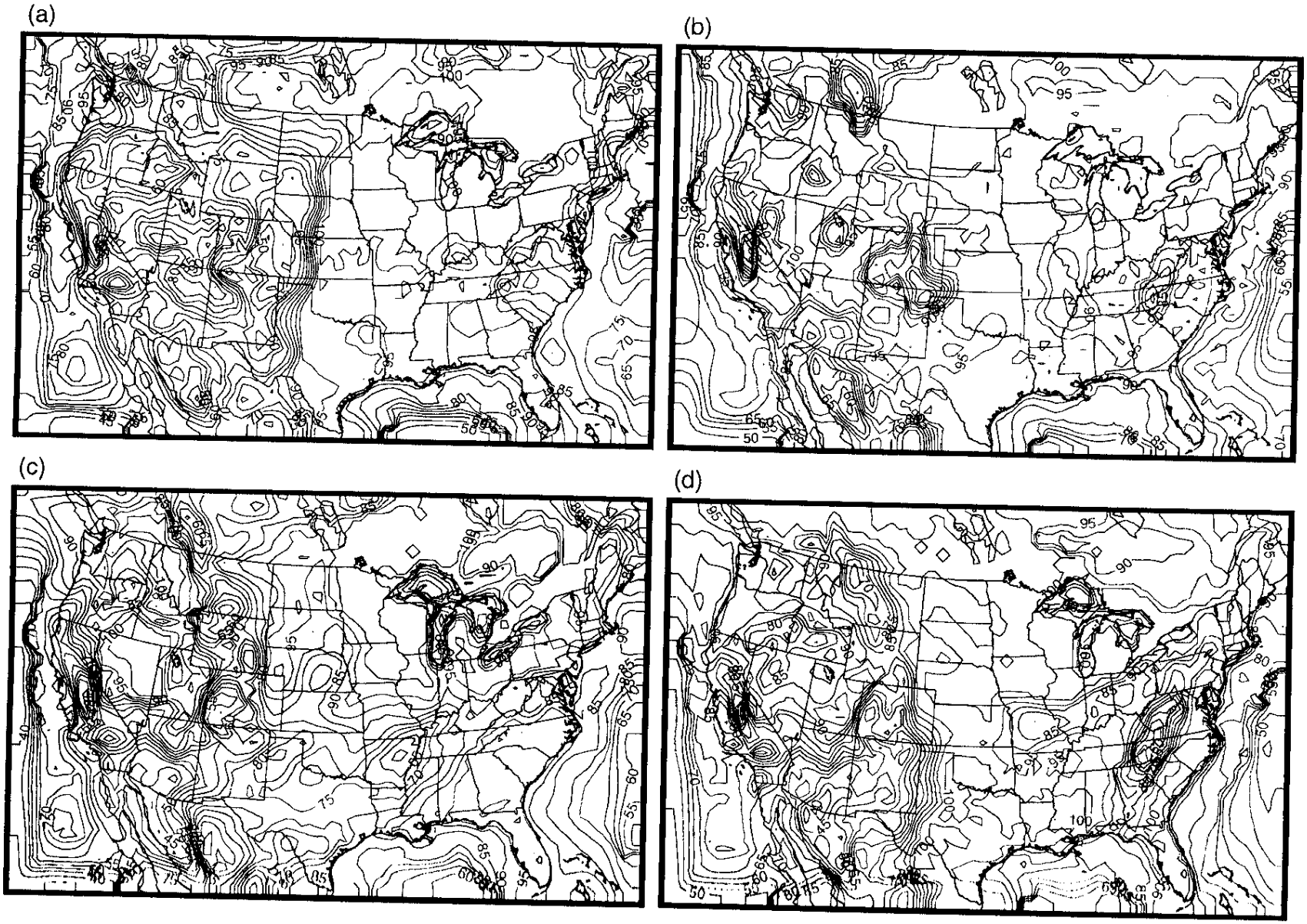

Figure 52

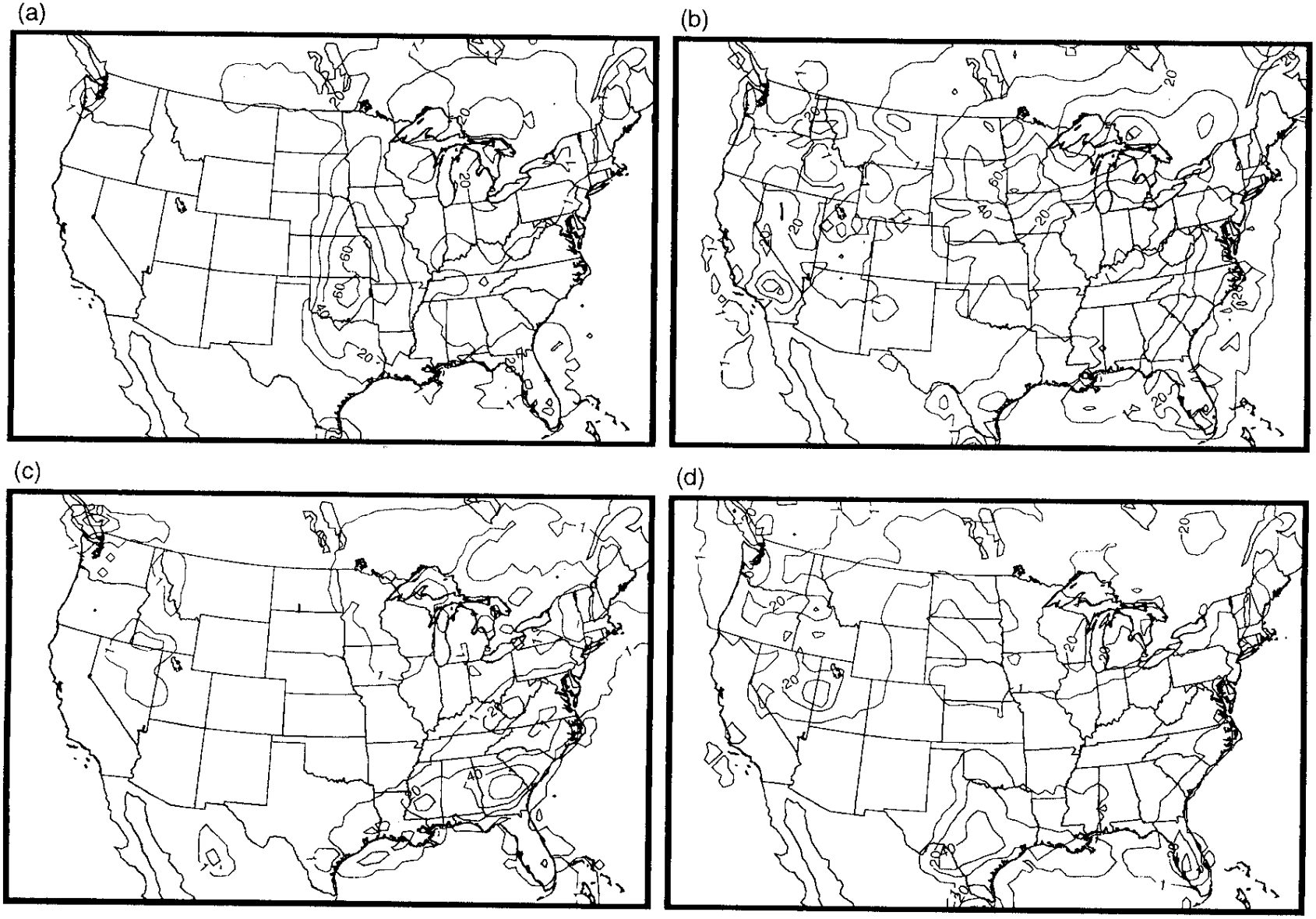

Figure 53

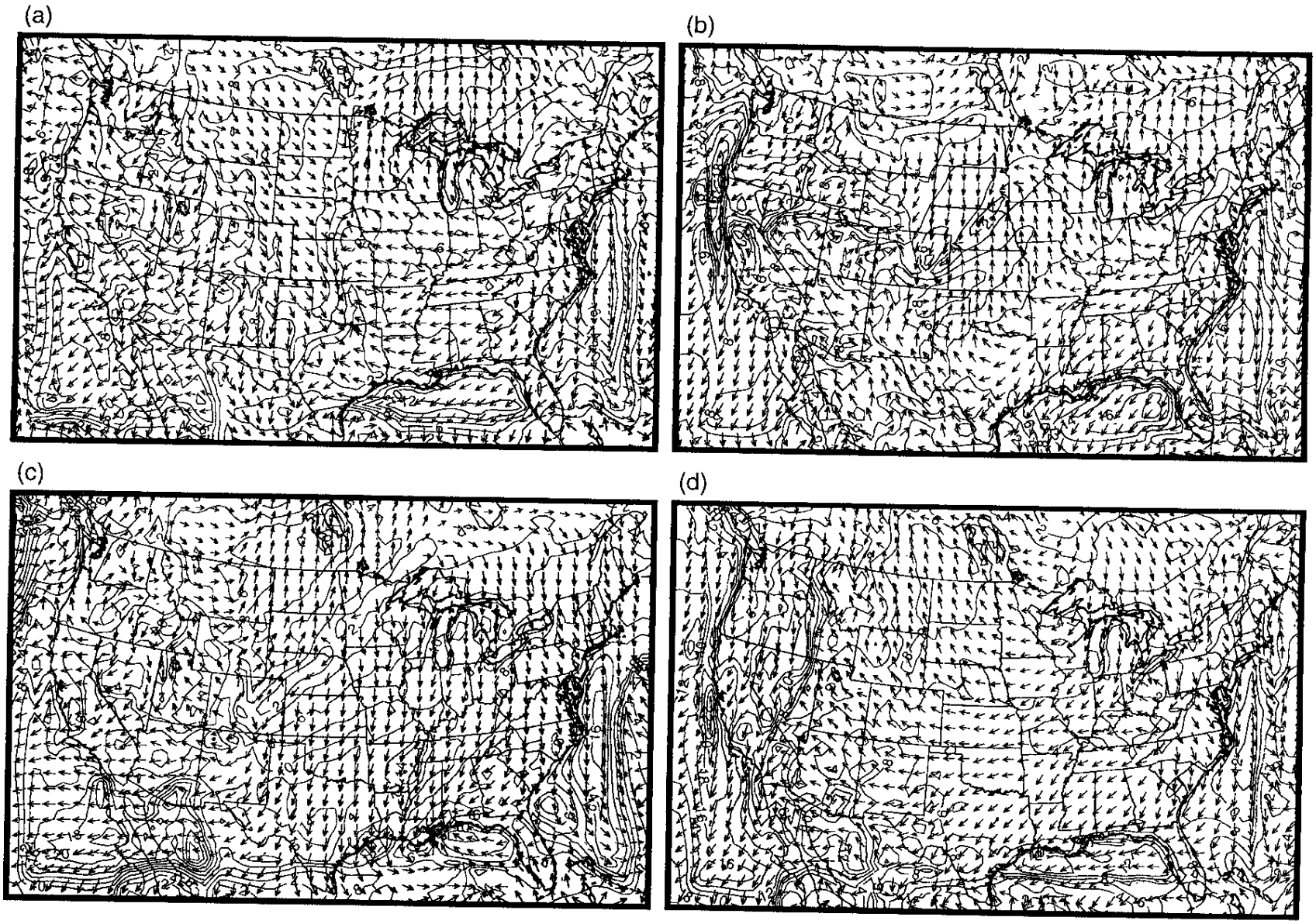

Figure 54

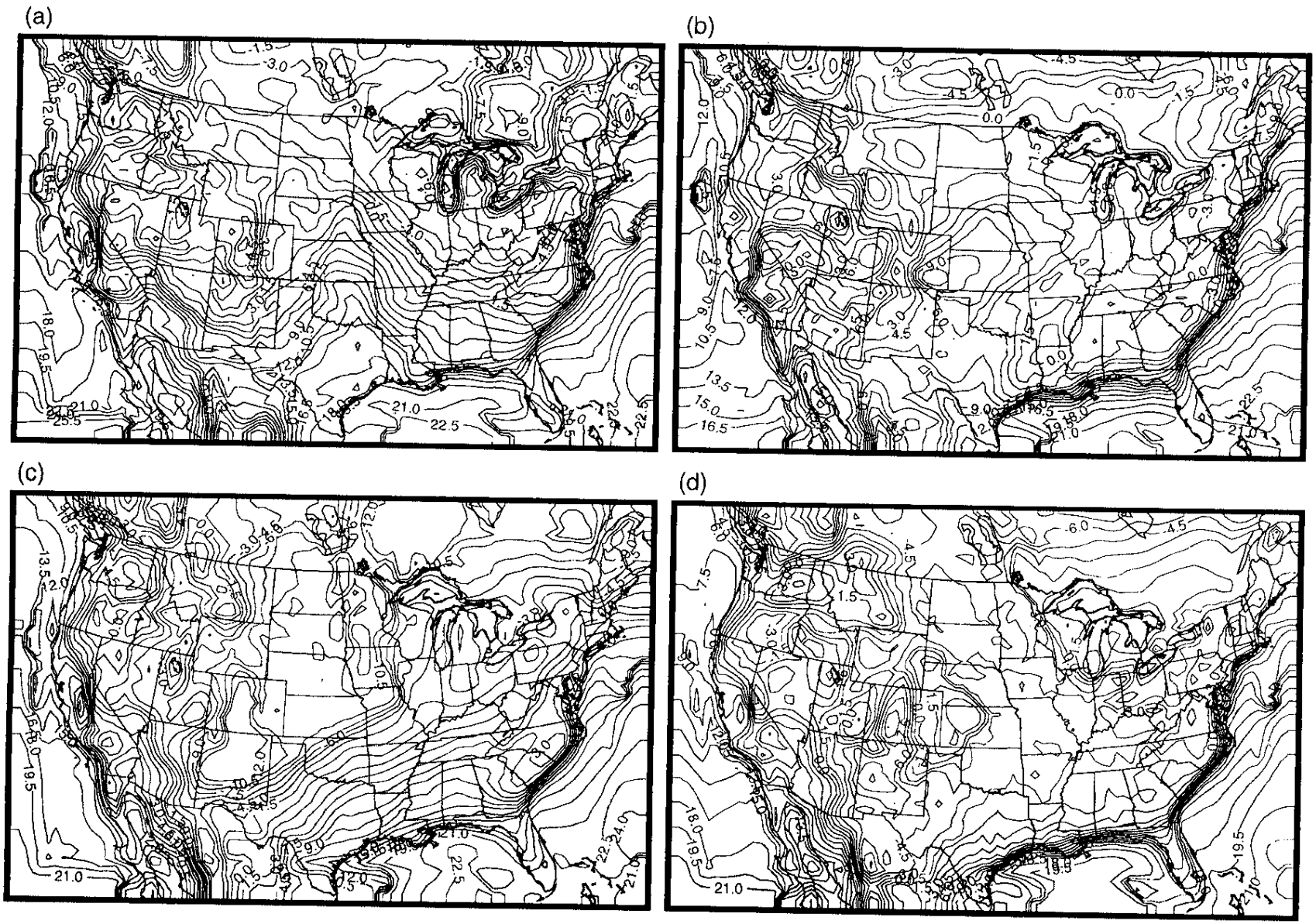

Figure 55

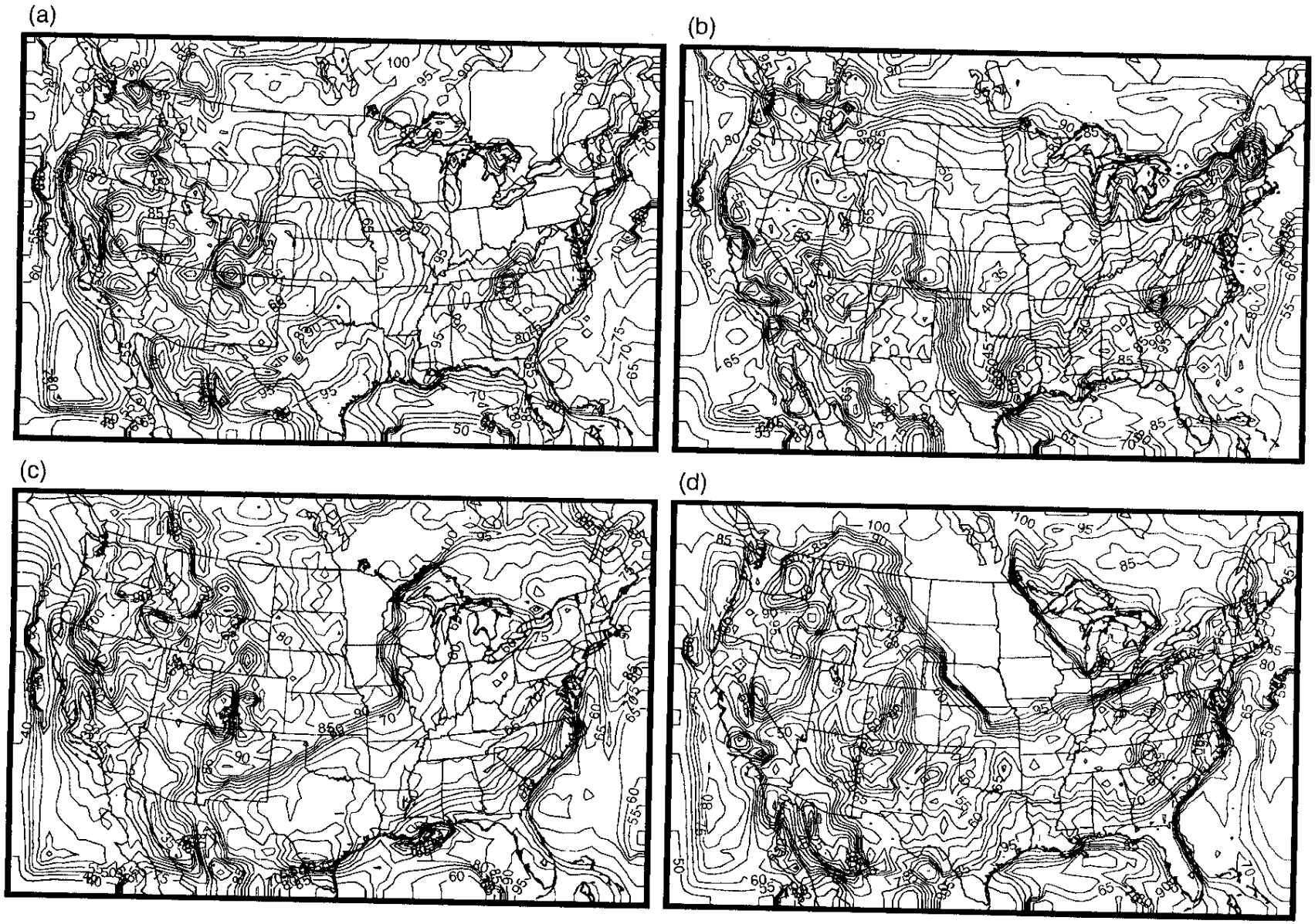

Figure 56

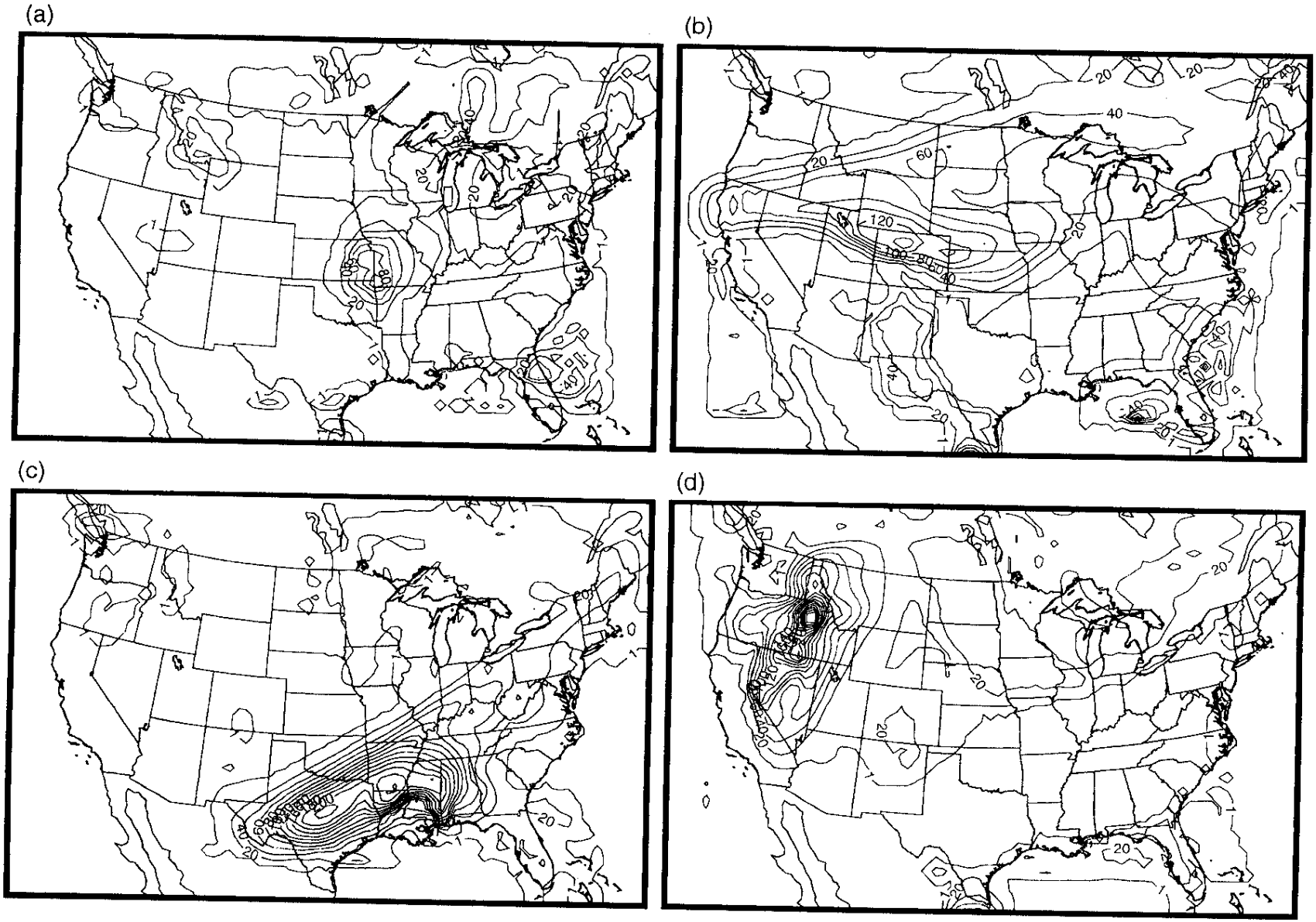

Figure 57

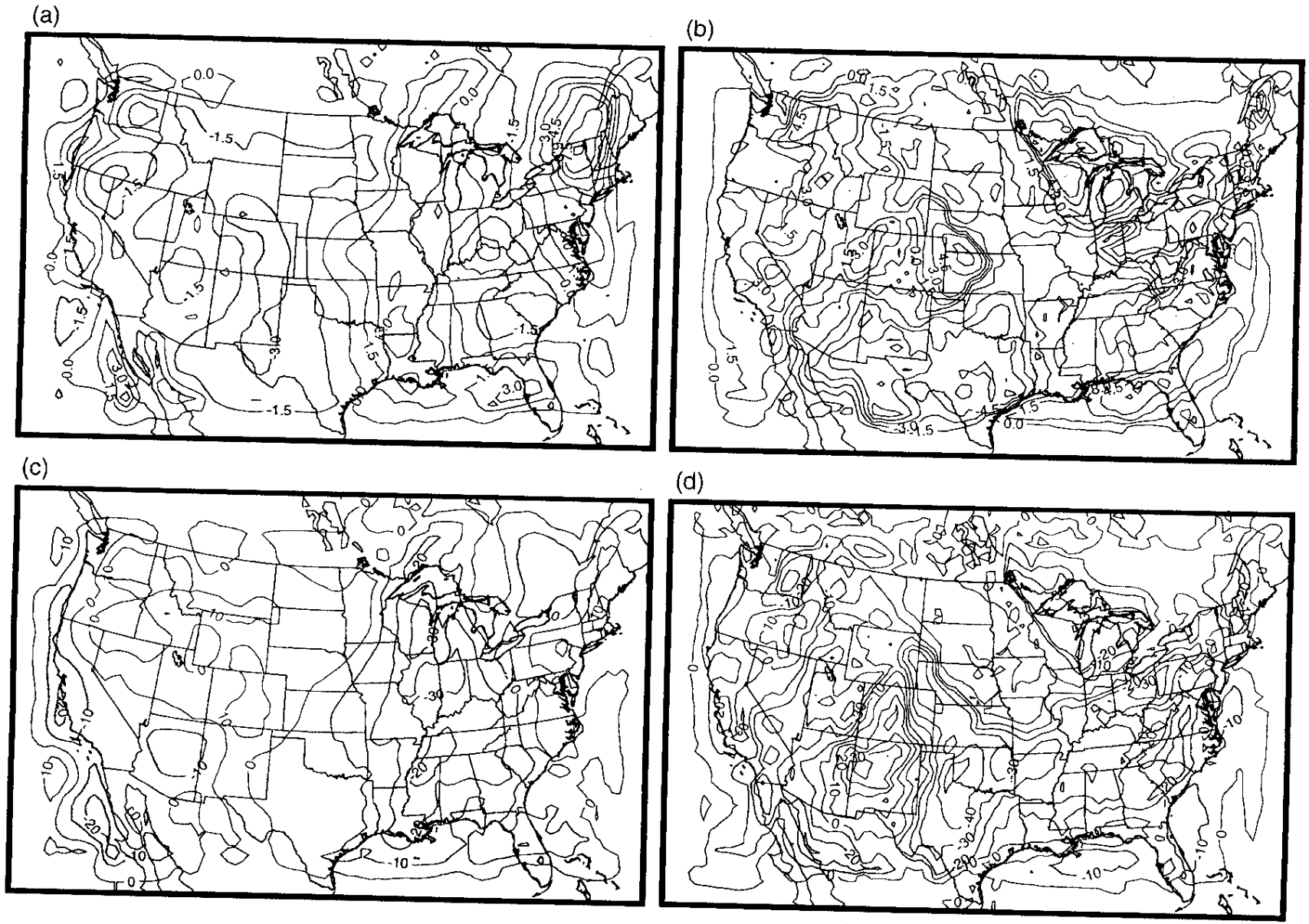

Figure 58

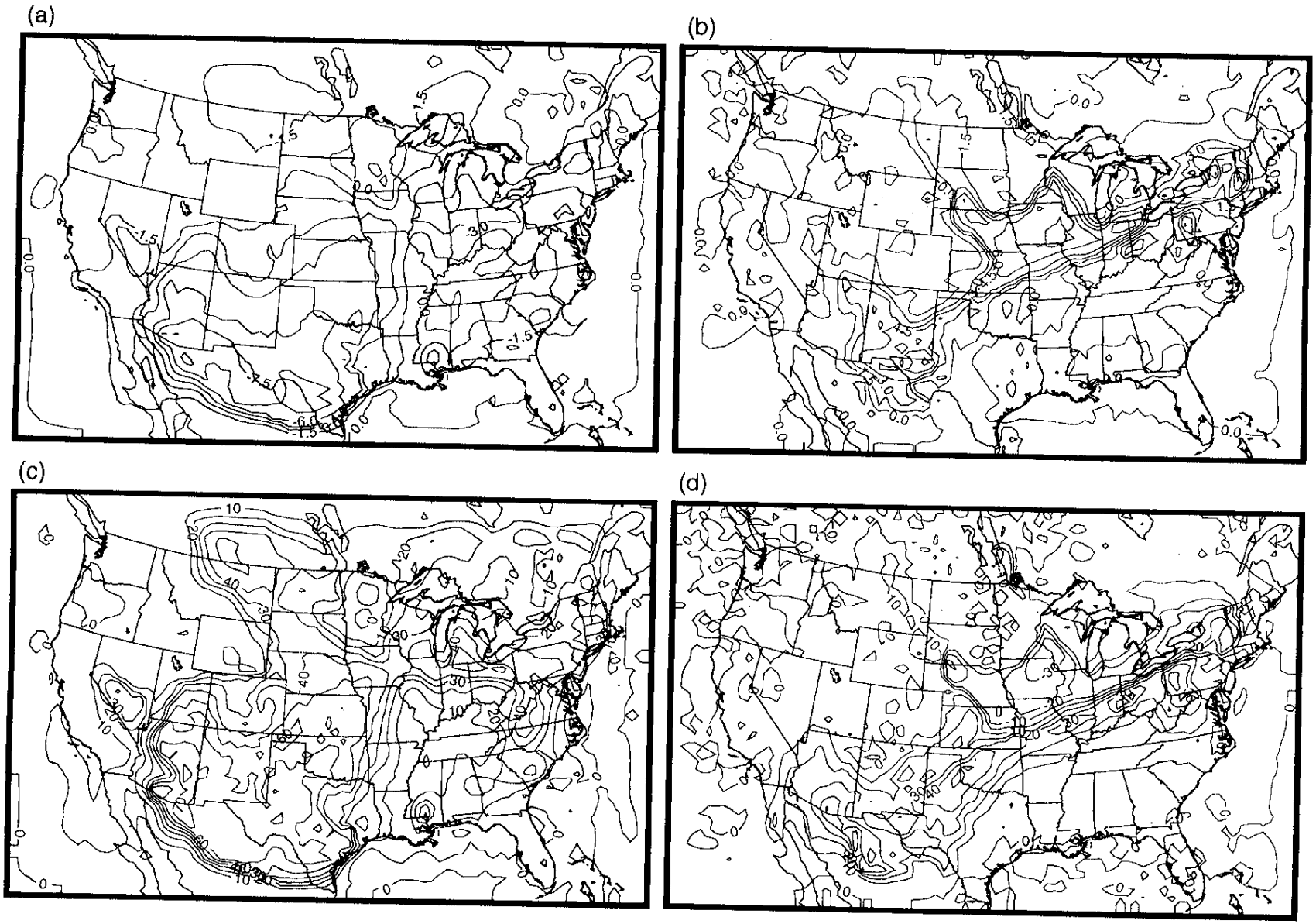

Figure 59

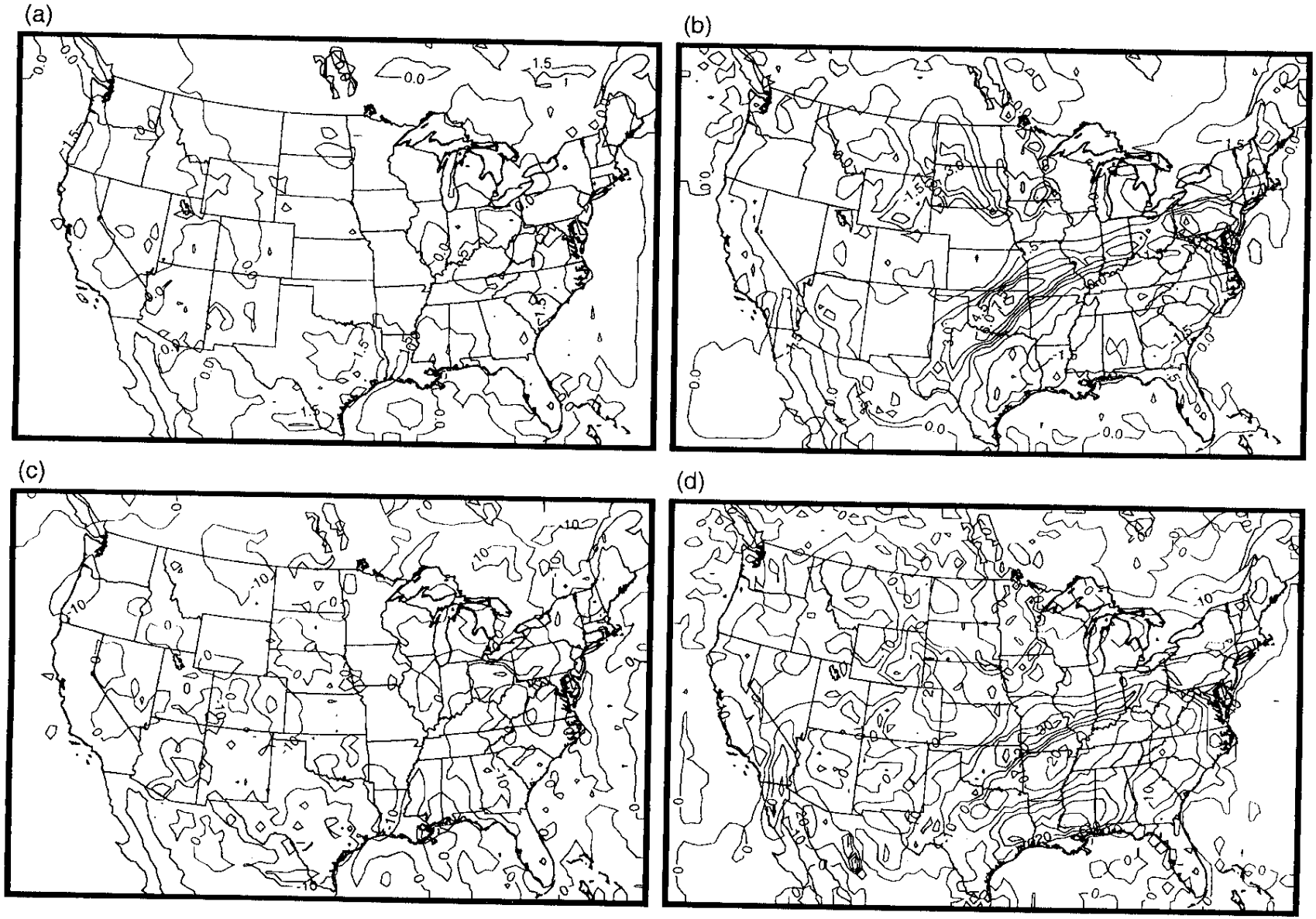

Figure 60

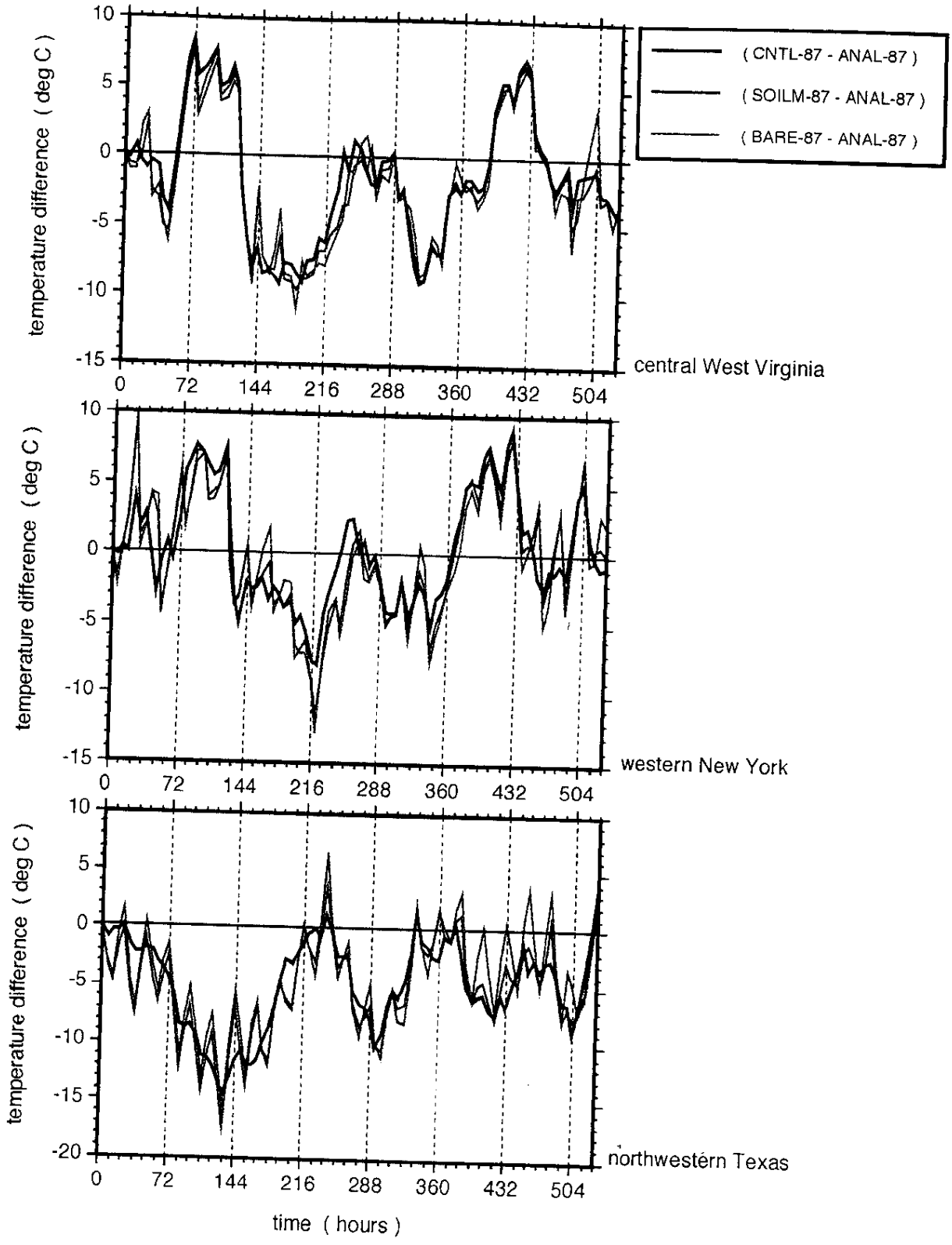
(CNTL-87 - ANAL-87)
(SOILM-87 - ANAL-87)
(BARE-87 - ANAL-87)
temperature difference (deg C)
central West Virginia
western New York
northwestern Texas
time (hours)
10
5
0
-5
-10
-15
-20
0
72
144
216
288
360
432
504

Figure 61

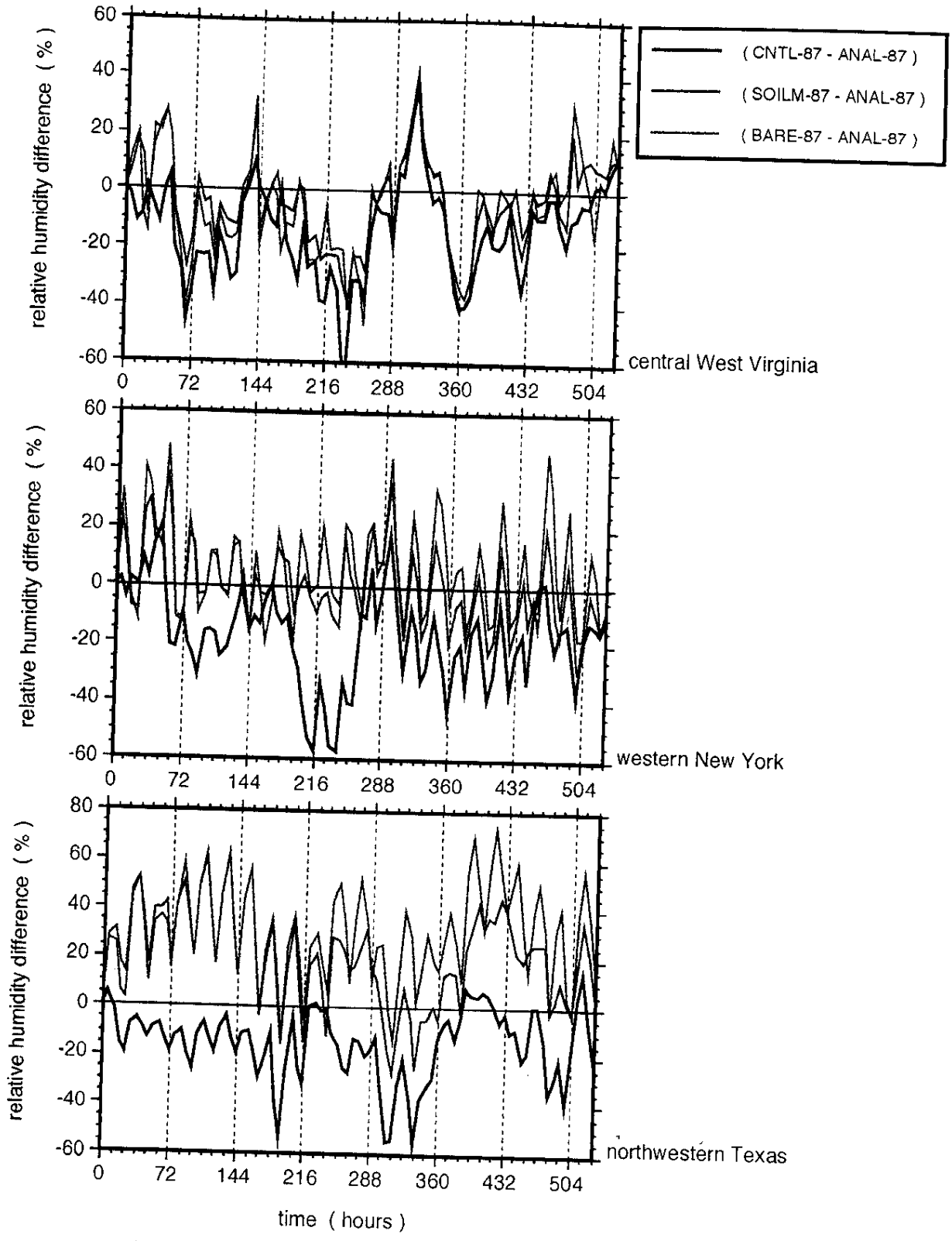
(CNTL-87 - ANAL-87)
(SOILM-87 - ANAL-87)
(BARE-87 - ANAL-87)
relative humidity difference (%)
central West Virginia
western New York
northwestern Texas
time (hours)
60
40
20
0
-20
-40
-60
80
0
72
144
216
288
360
432
504

Figure 62

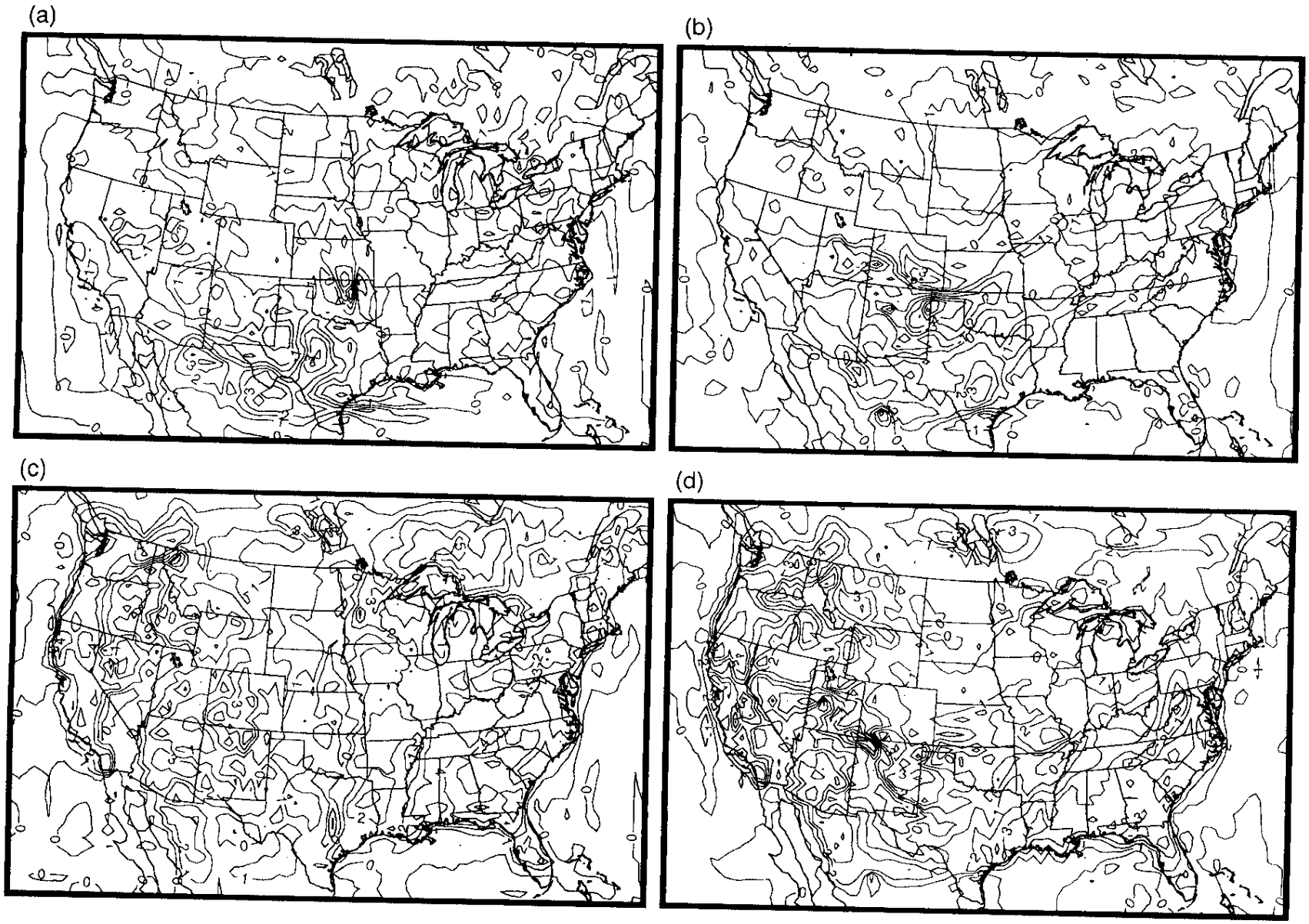

Figure 63

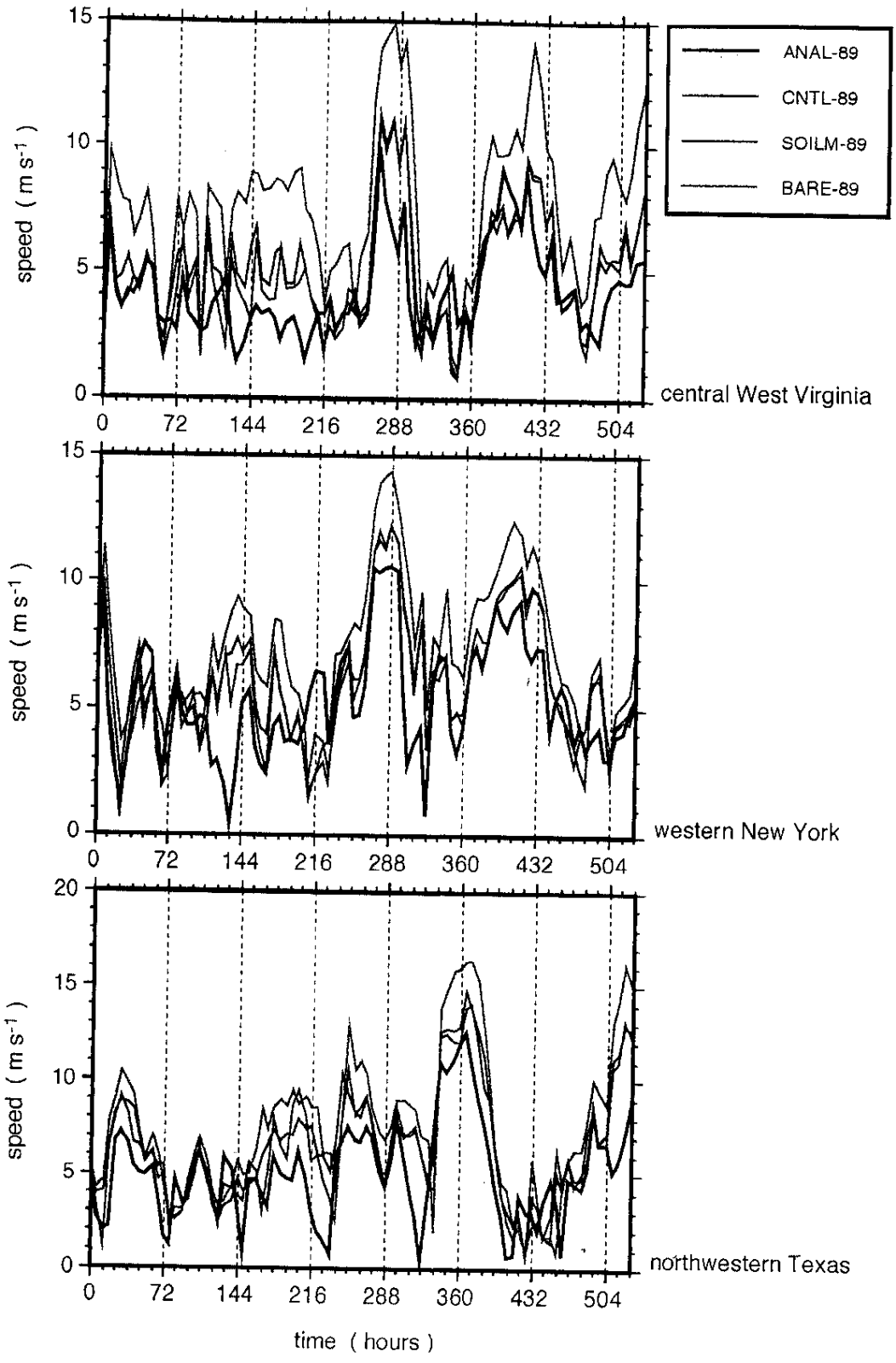
ANAL-89
CNTL-89
SOILM-89
BARE-89
speed (m s-1)
central West Virginia
western New York
northwestern Texas
time (hours)
0
72
144
216
288
360
432
504

Figure 64

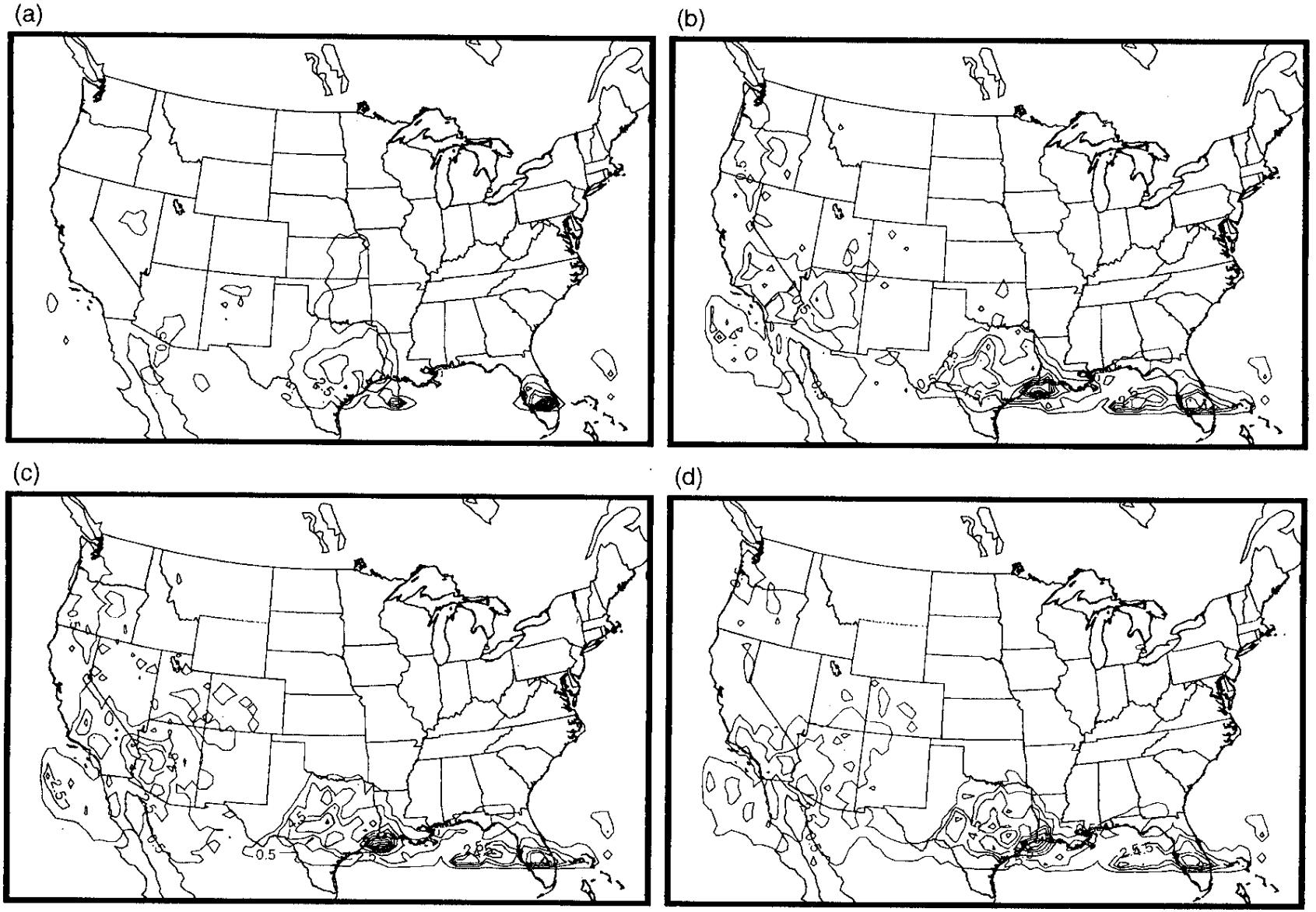

Figure 65

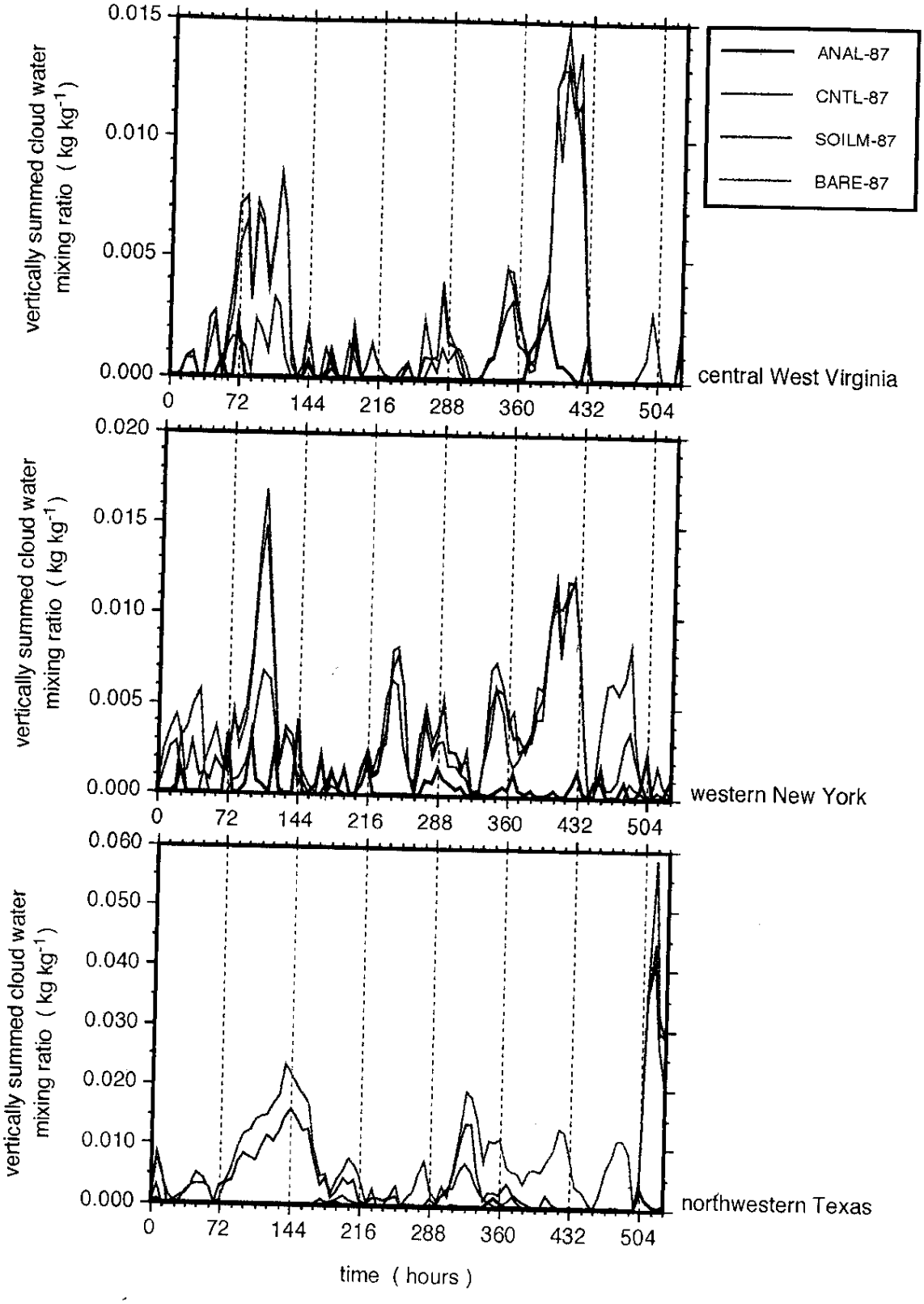
ANAL-87
CNTL-87
SOILM-87
BARE-87
vertically summed cloud water mixing ratio (kg kg-1)
0.015
0.010
0.005
0.000
0
72
144
216
288
360
432
504
central West Virginia
0.020
0.015
0.010
0.005
0.000
western New York
0.060
0.050
0.040
0.030
0.020
0.010
0.000
northwestern Texas
time (hours)

Figure 66

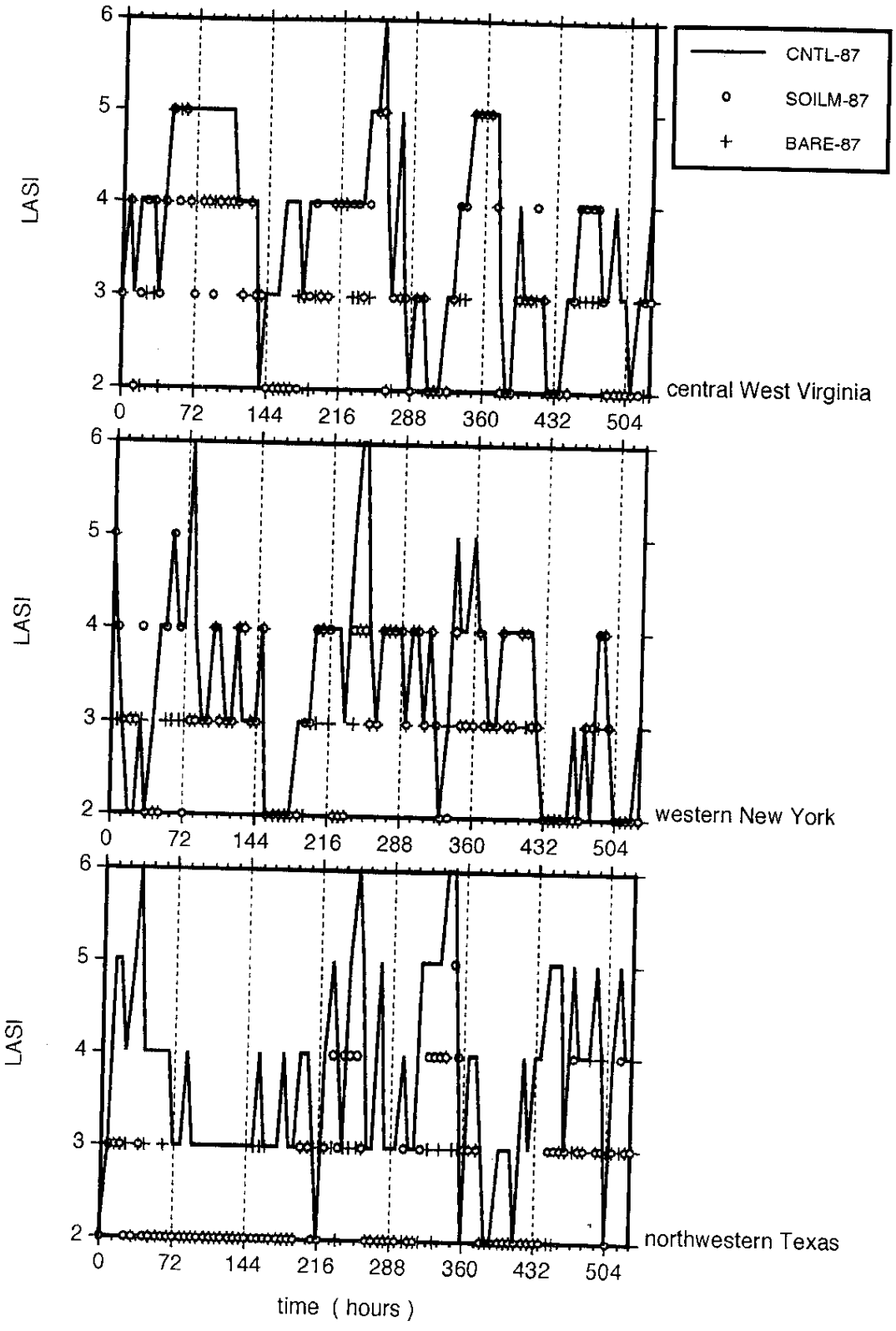
CNTL-87
SOILM-87
BARE-87
LASI
central West Virginia
western New York
northwestern Texas
time (hours)
0
72
144
216
288
360
432
504
2
3
4
5
6

Figure 67

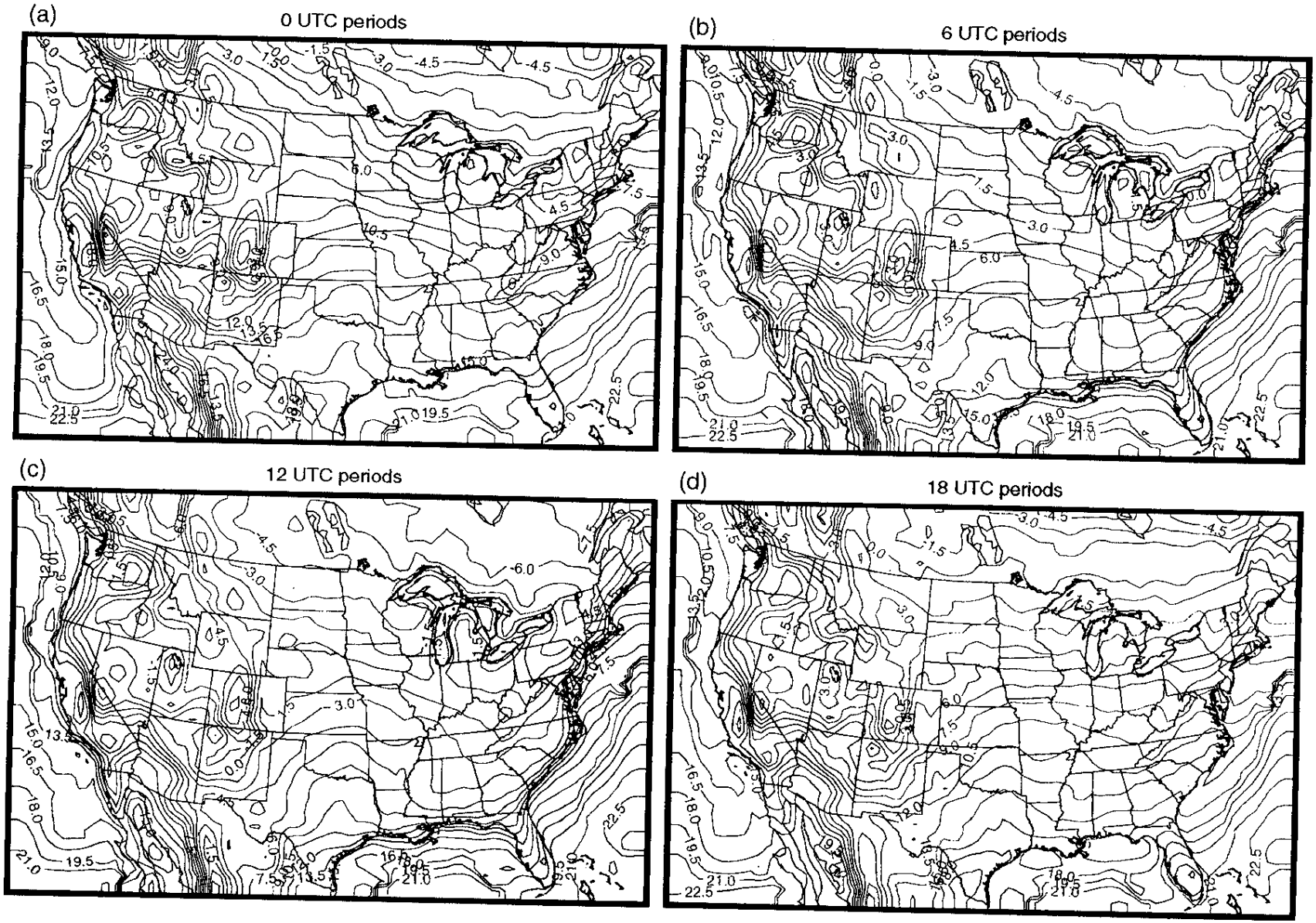
(a)
0 UTC periods
(b)
6 UTC periods
(c)
12 UTC periods
(d)
18 UTC periods

Figure 68

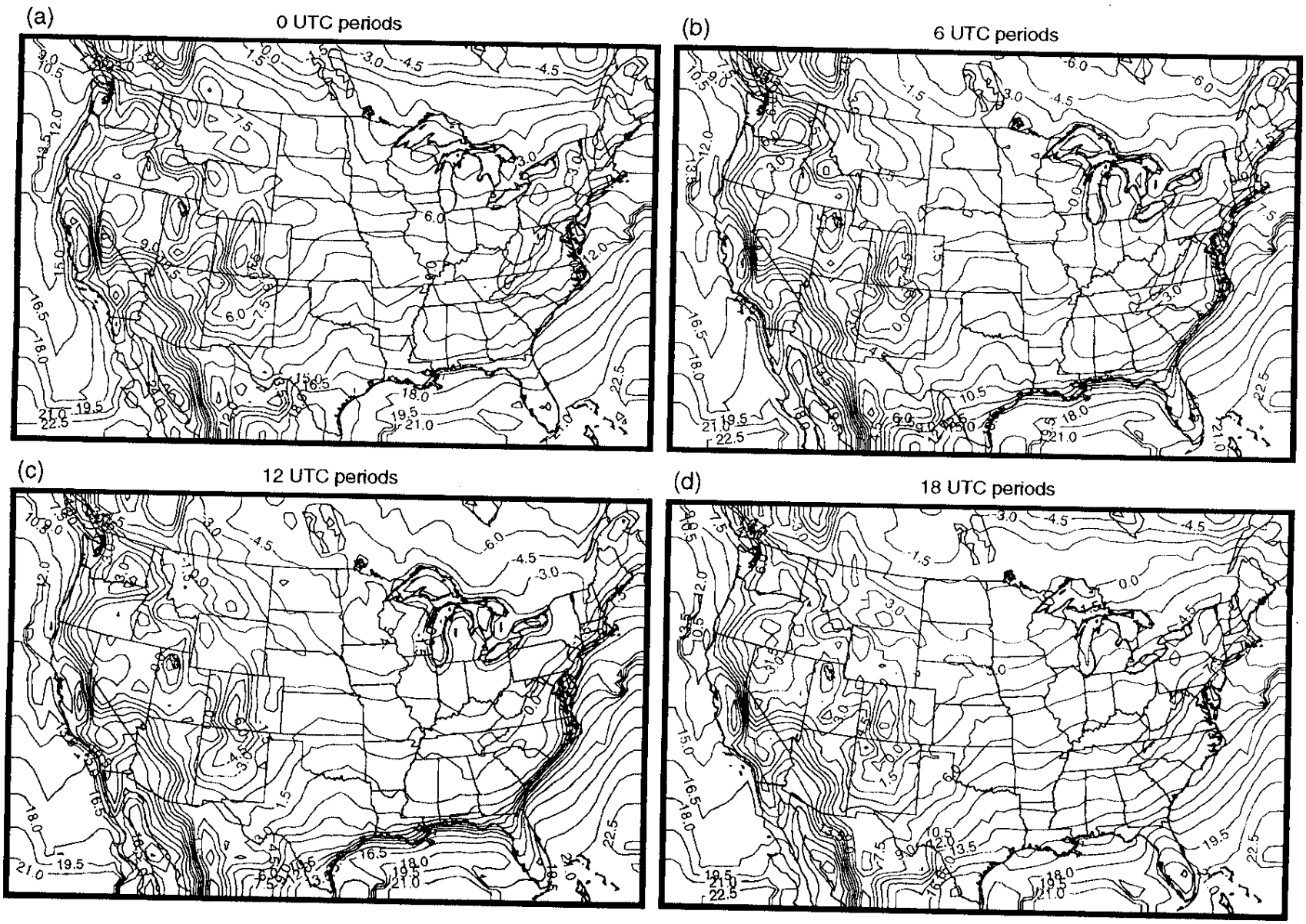
(a)
0 UTC periods
(b)
6 UTC periods
(c)
12 UTC periods
(d)
18 UTC periods

Figure 69

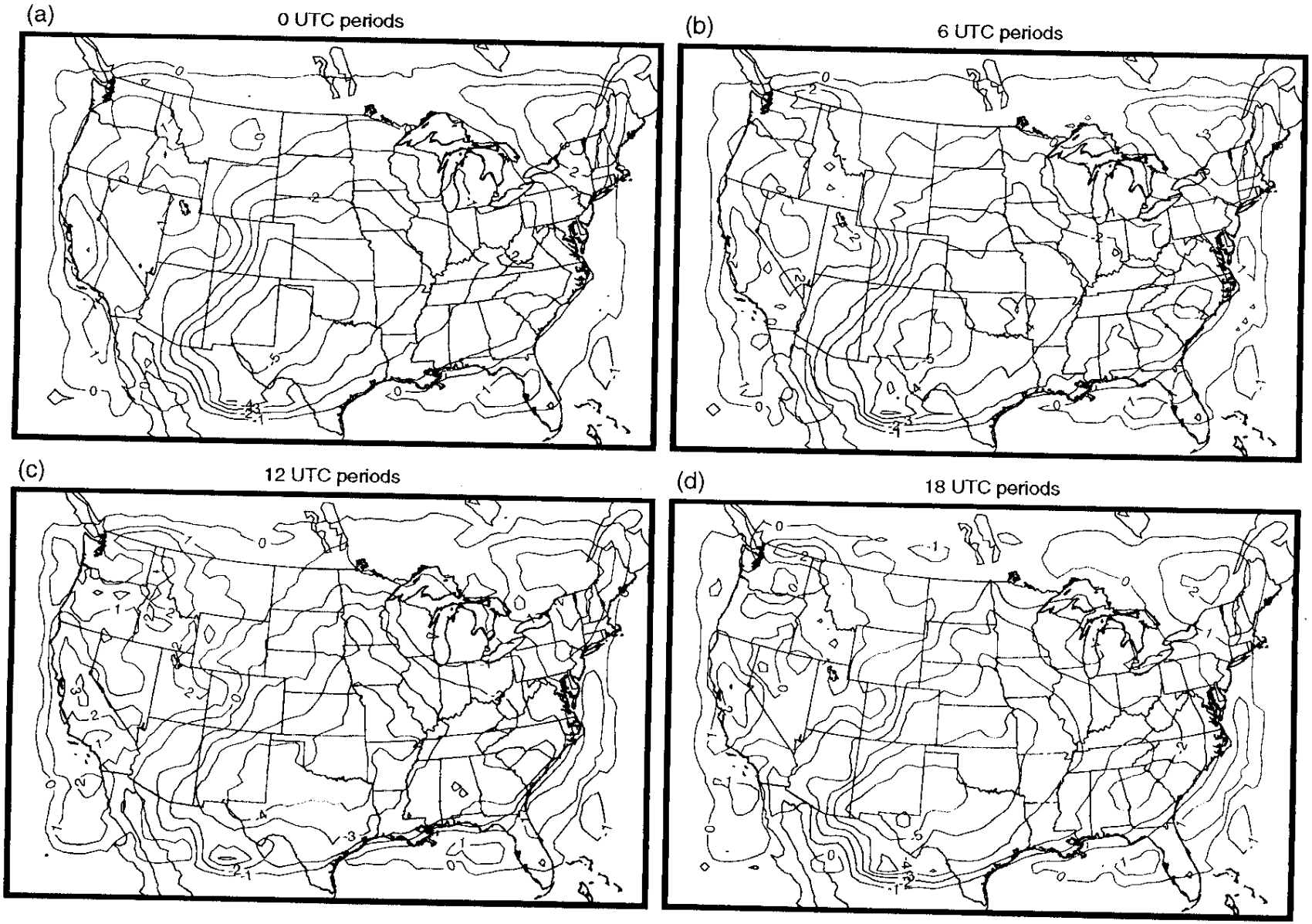
(a)
0 UTC periods
(b)
6 UTC periods
(c)
12 UTC periods
(d)
18 UTC periods

Figure 70

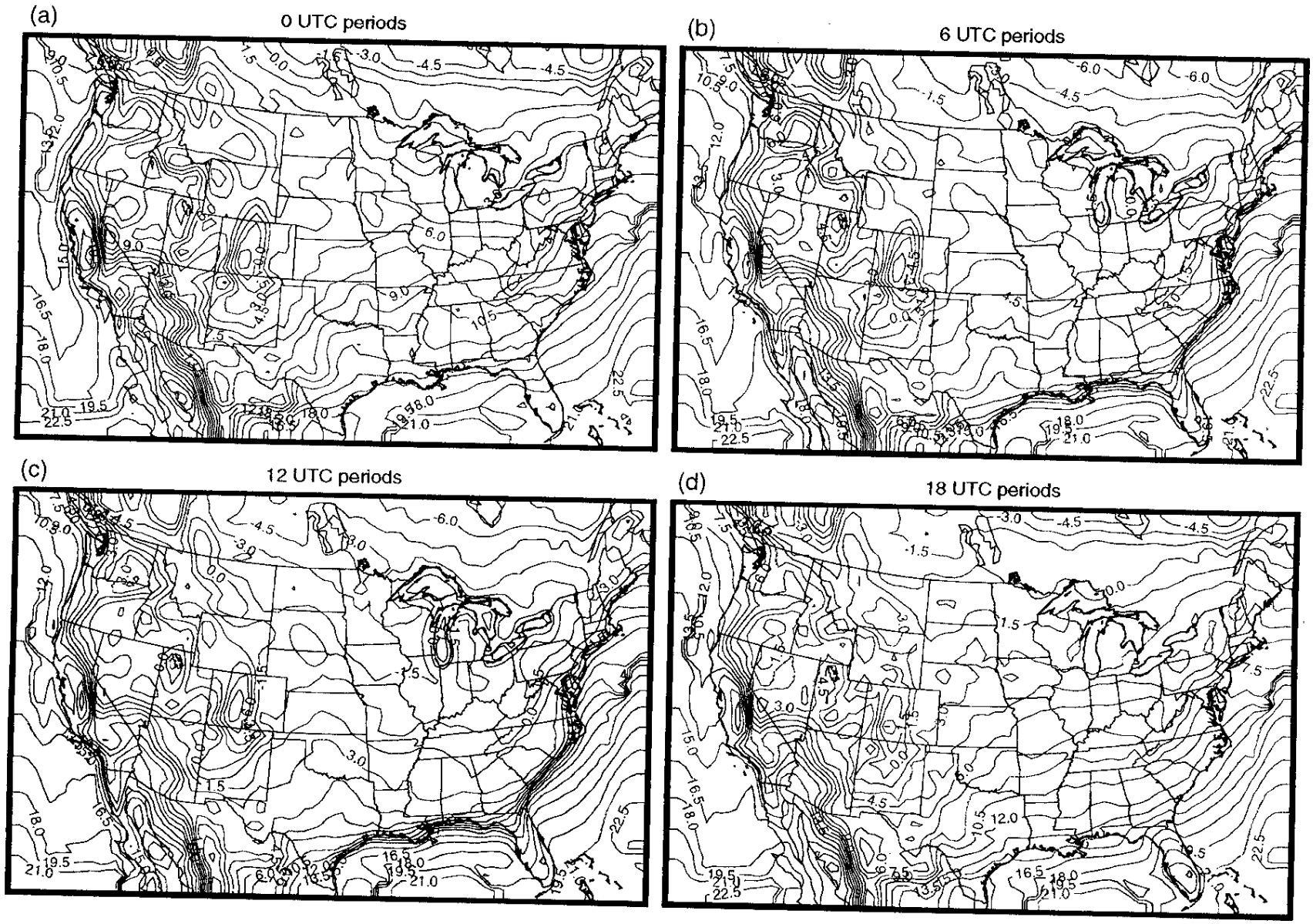
(a)
0 UTC periods
(b)
6 UTC periods
(c)
12 UTC periods
(d)
18 UTC periods

Figure 71

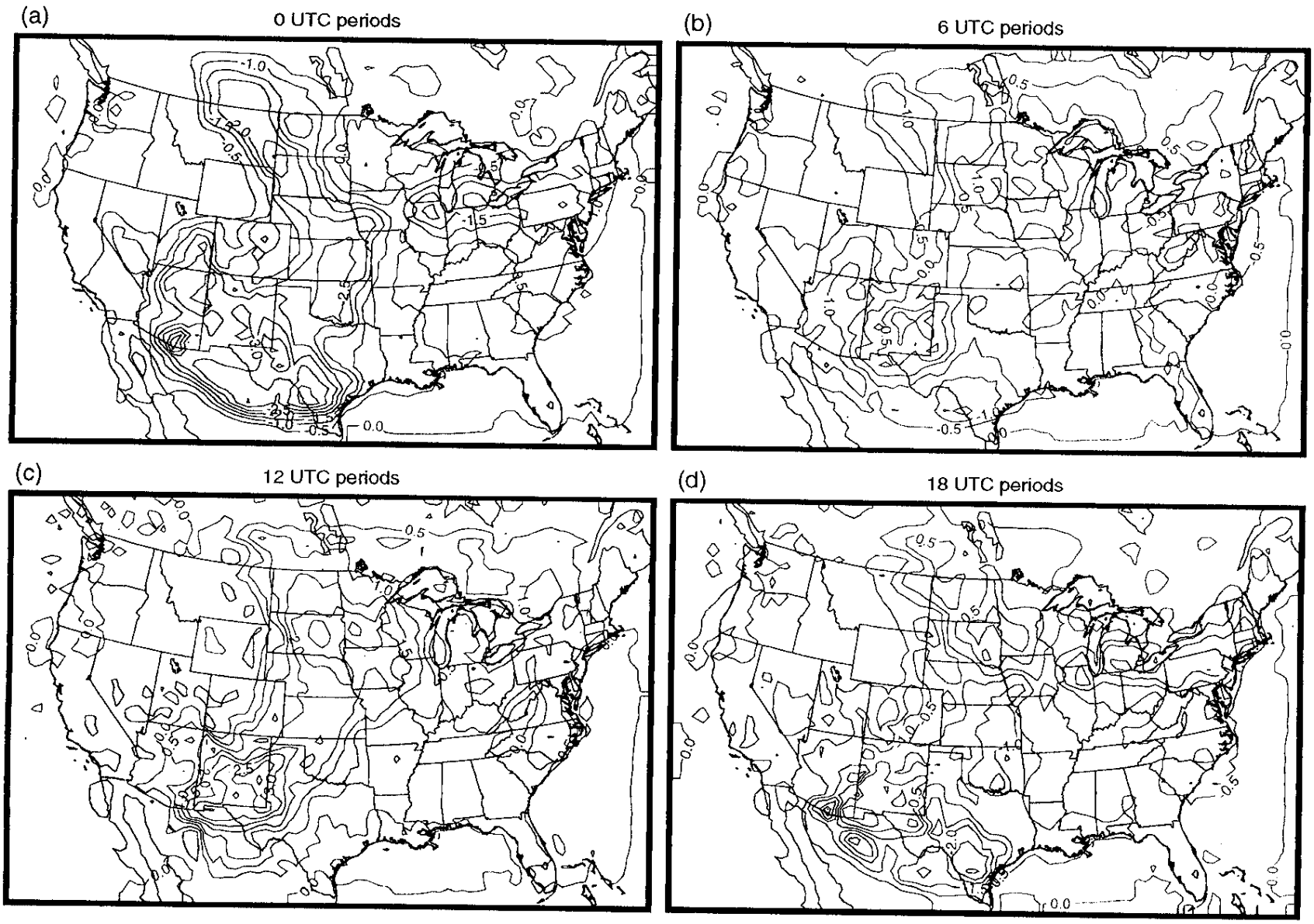
(a)
0 UTC periods
(b)
6 UTC periods
(c)
12 UTC periods
(d)
18 UTC periods

Figure 72

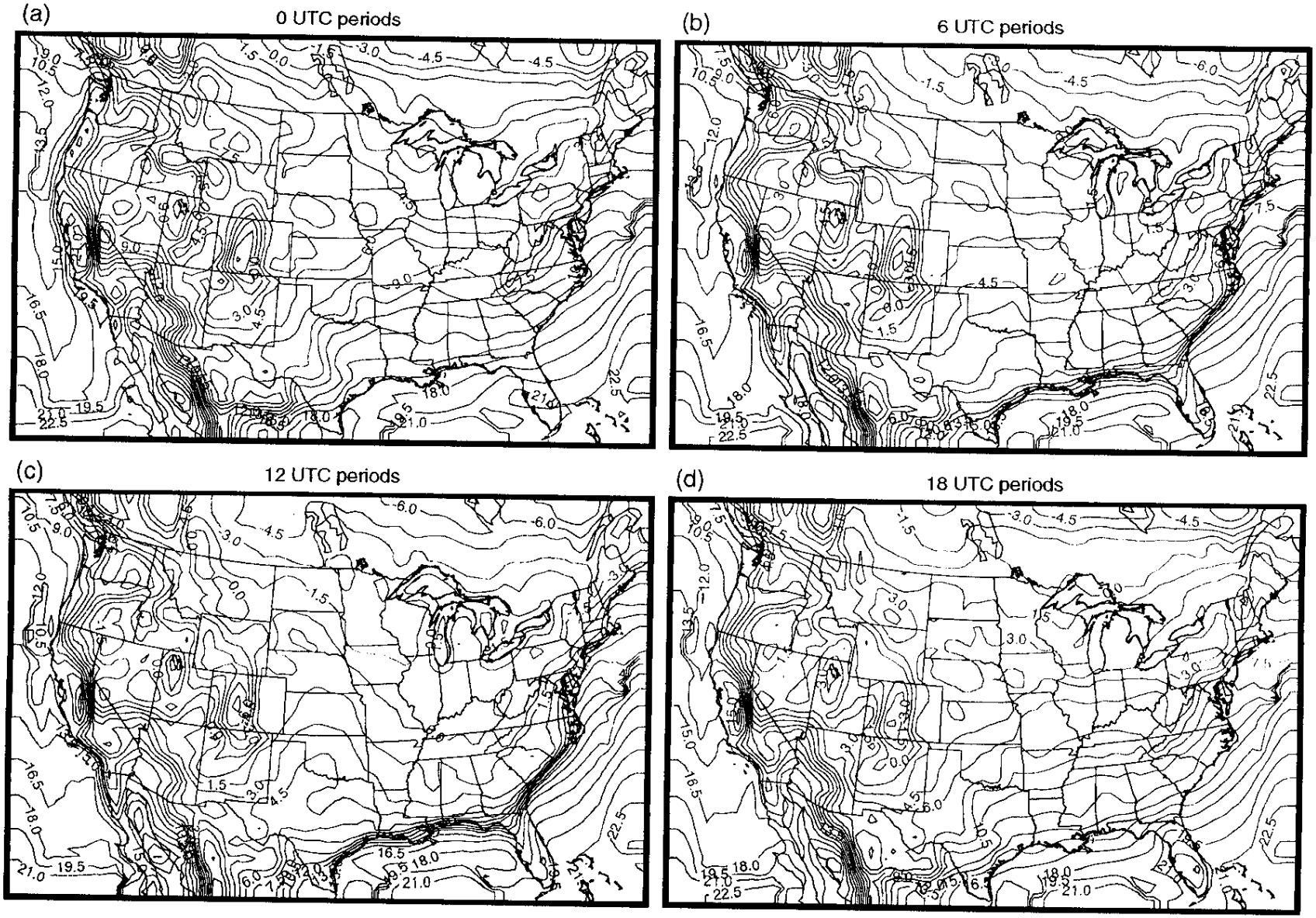
(a)
0 UTC periods
(b)
6 UTC periods
(c)
12 UTC periods
(d)
18 UTC periods

Figure 73

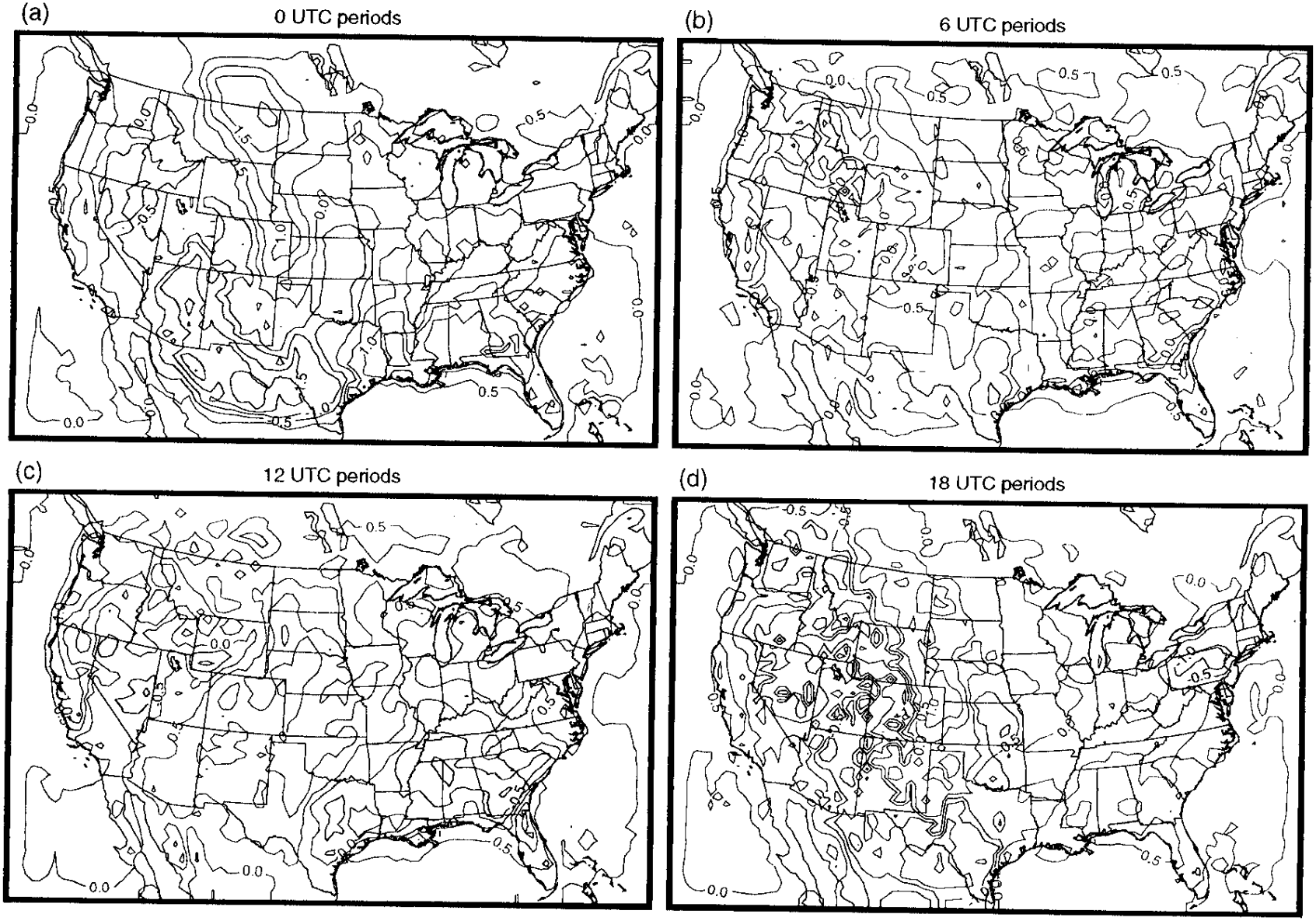
(a)
0 UTC periods
(b)
6 UTC periods
(c)
12 UTC periods
(d)
18 UTC periods

Figure 74

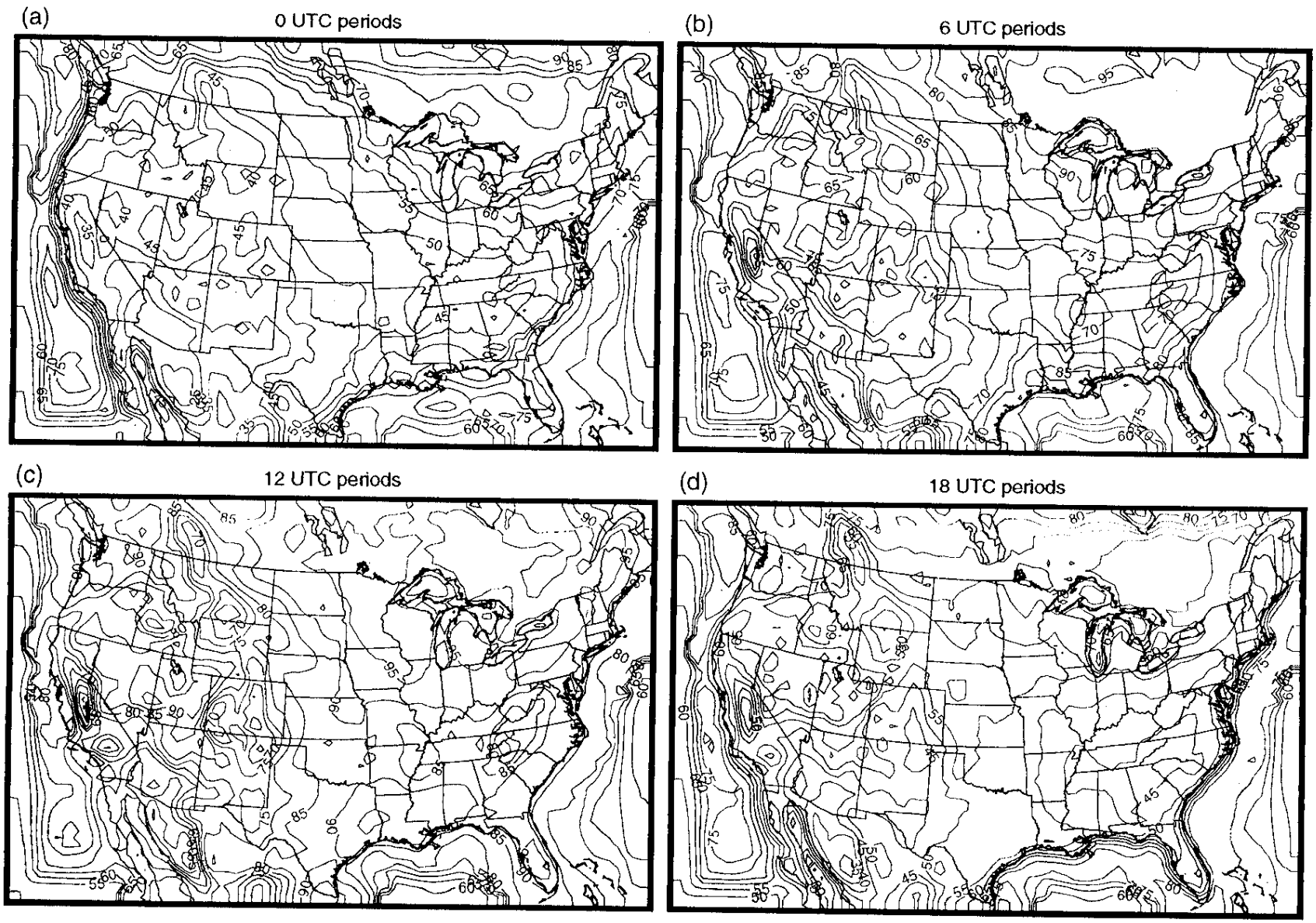
(a)
0 UTC periods
(b)
6 UTC periods
(c)
12 UTC periods
(d)
18 UTC periods

Figure 75

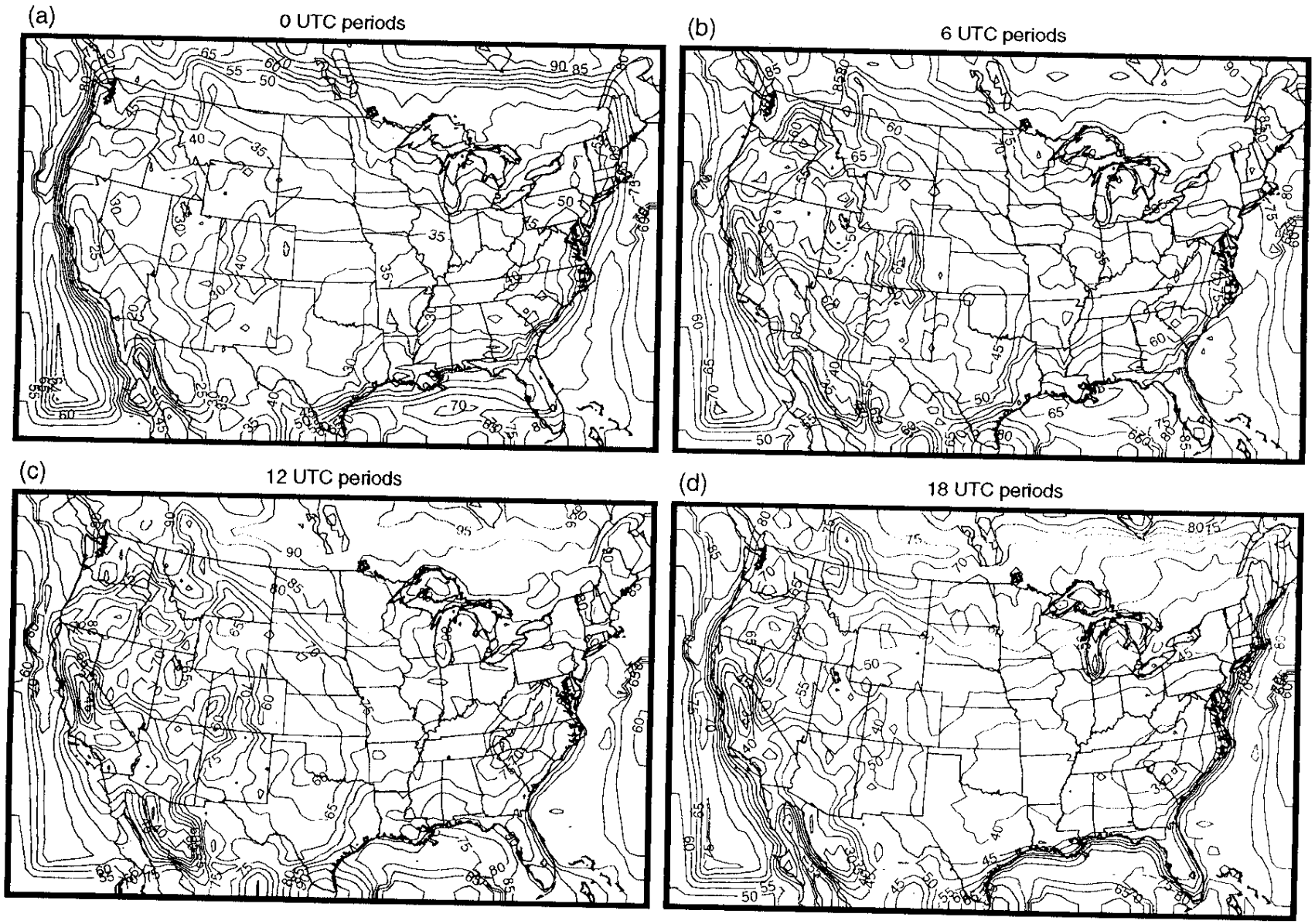
(a)
0 UTC periods
(b)
6 UTC periods
(c)
12 UTC periods
(d)
18 UTC periods

Figure 76

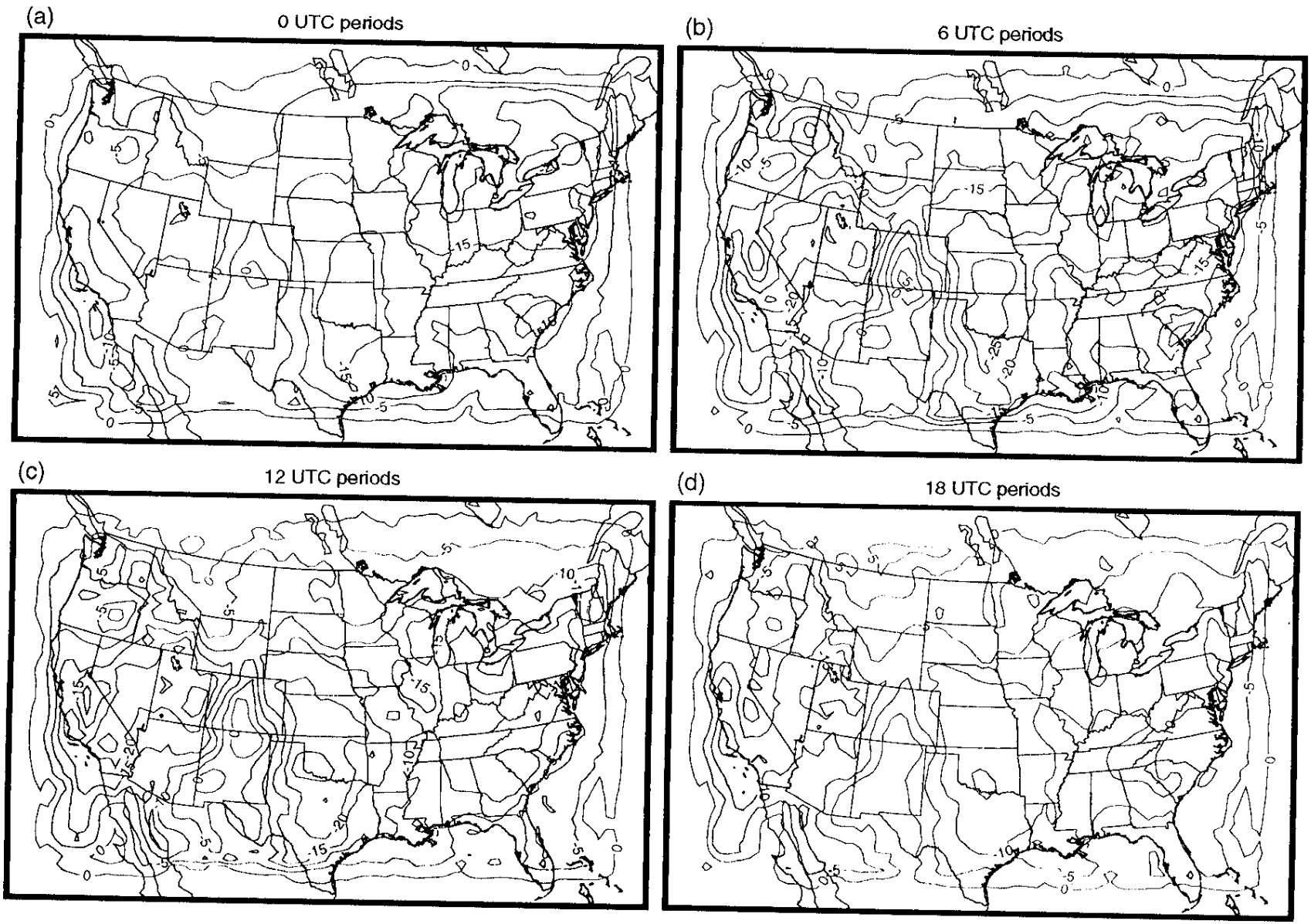
(a)
0 UTC periods
(b)
6 UTC periods
(c)
12 UTC periods
(d)
18 UTC periods

Figure 77

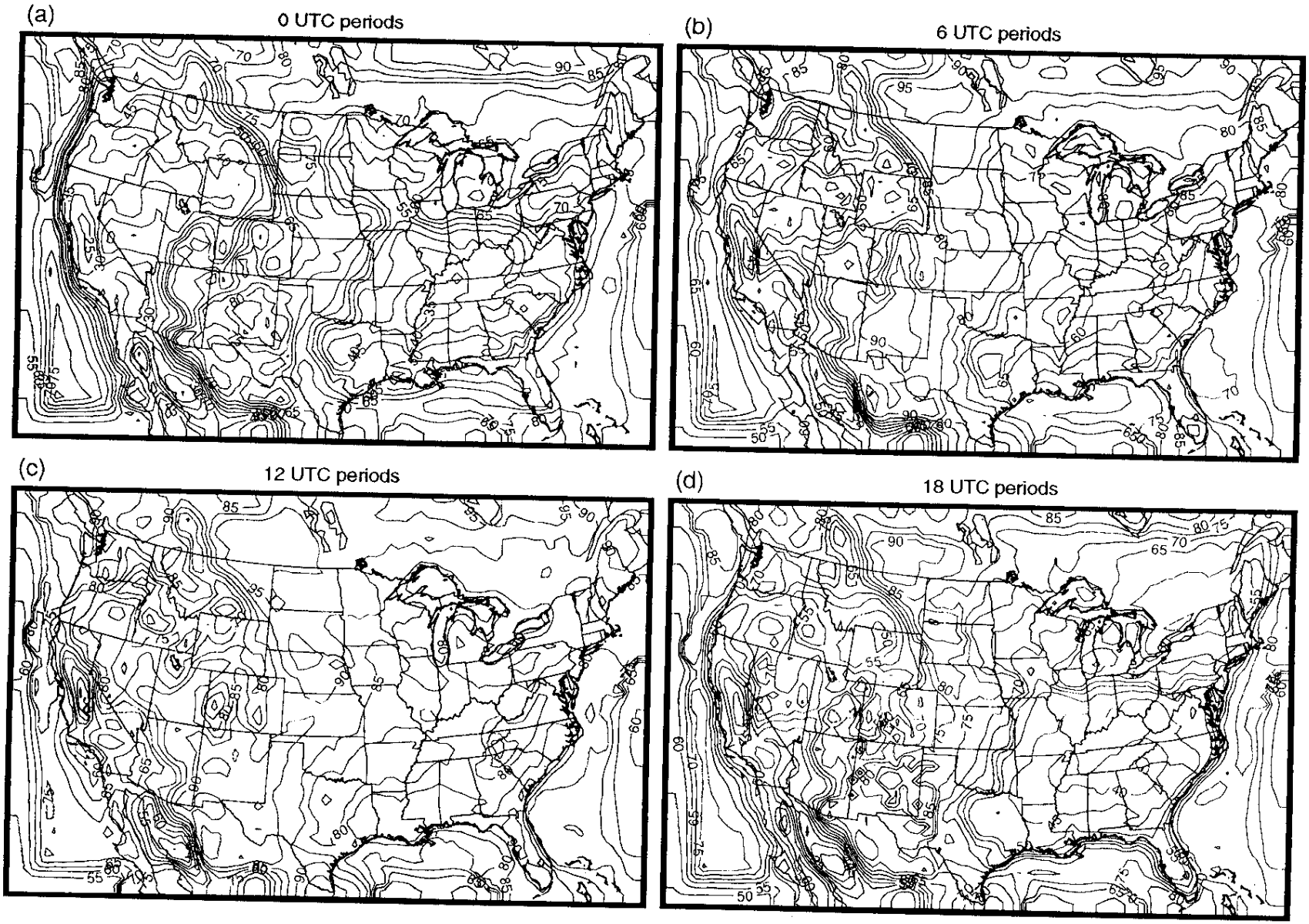
(a)
0 UTC periods
(b)
6 UTC periods
(c)
12 UTC periods
(d)
18 UTC periods

Figure 78

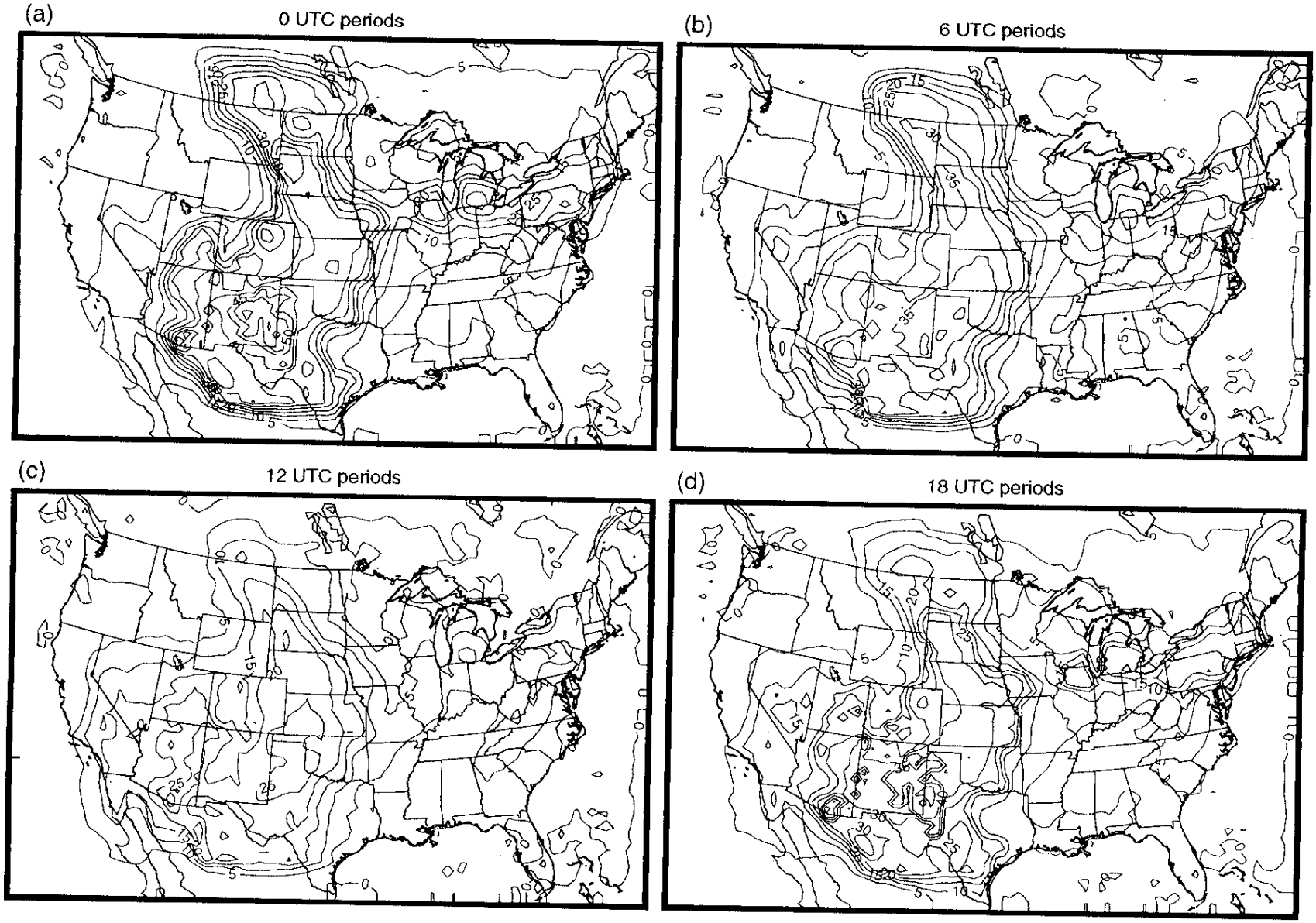
(a)
0 UTC periods
(b)
6 UTC periods
(c)
12 UTC periods
(d)
18 UTC periods

Figure 79

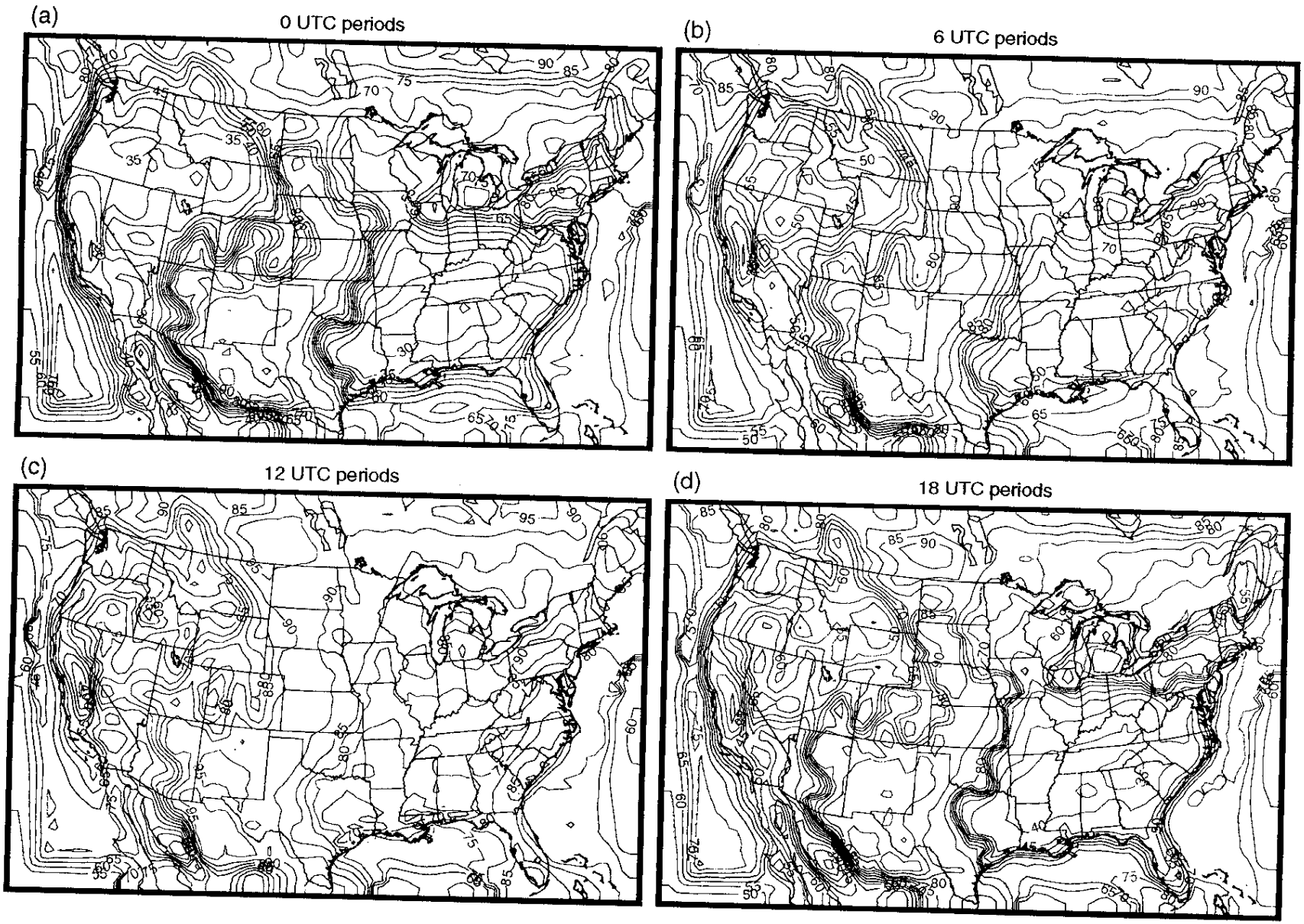
(a)
0 UTC periods
(b)
6 UTC periods
(c)
12 UTC periods
(d)
18 UTC periods

Figure 80

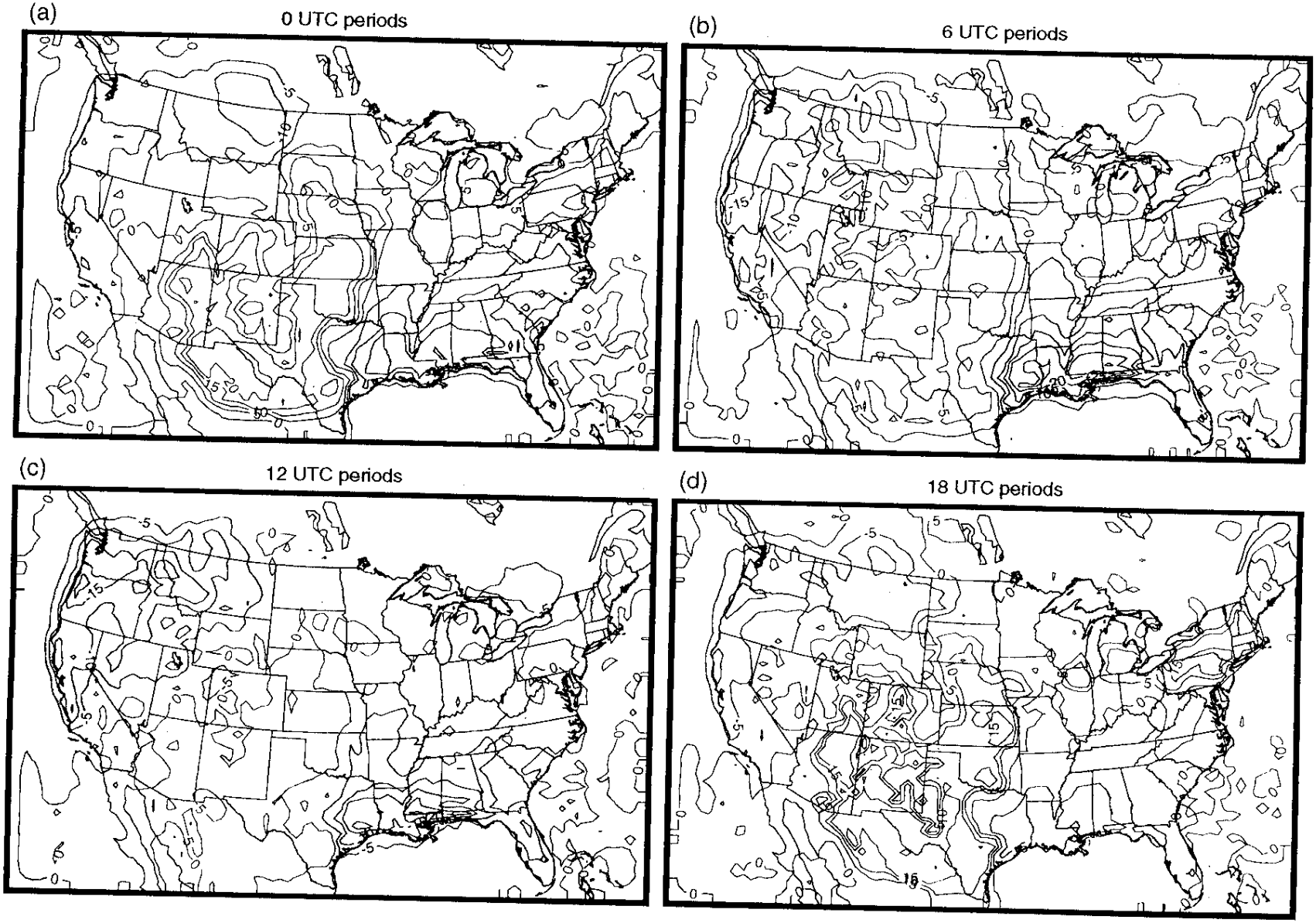
(a)
0 UTC periods
(b)
6 UTC periods
(c)
12 UTC periods
(d)
18 UTC periods

Figure 81

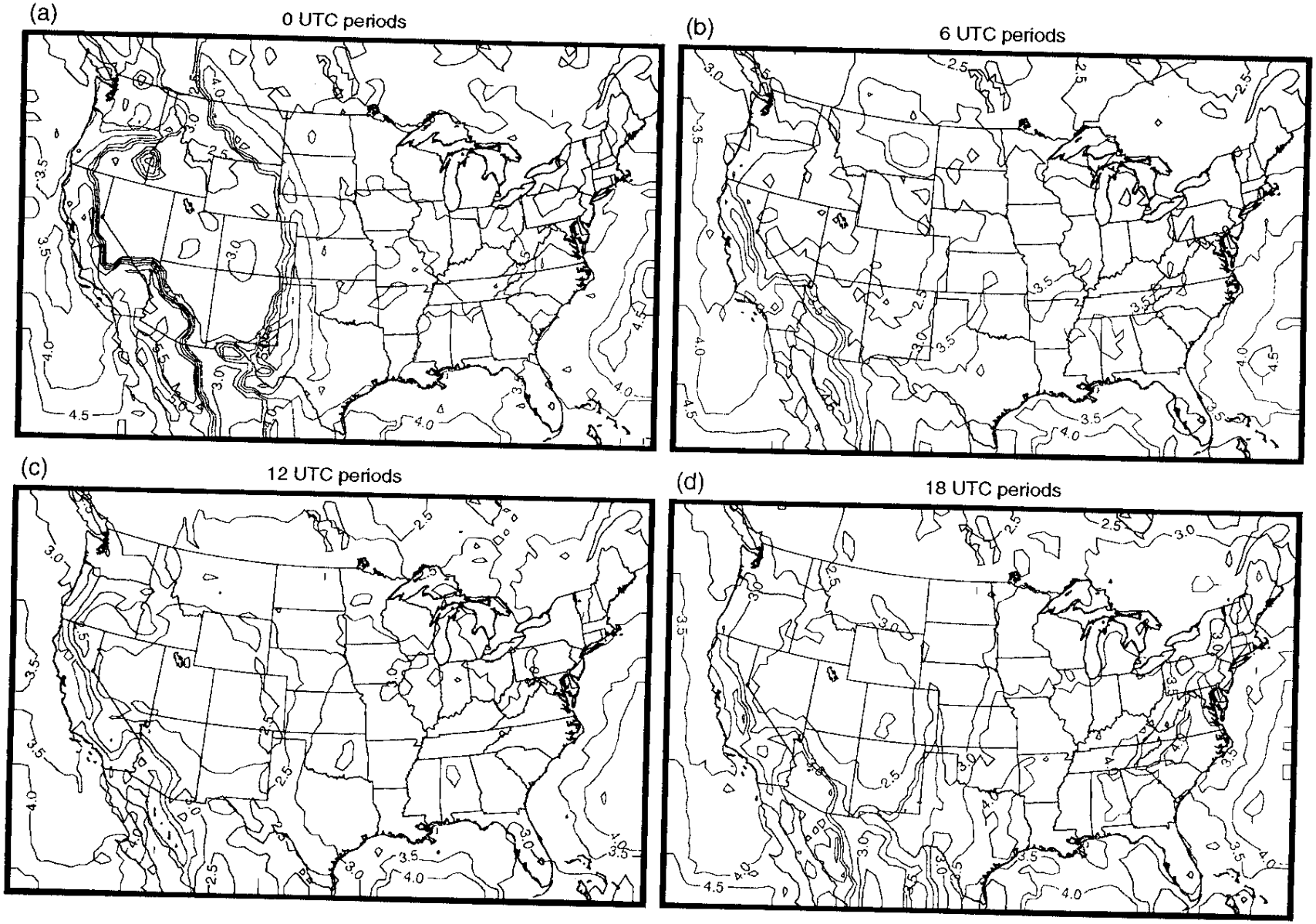
(a)
0 UTC periods
(b)
6 UTC periods
(c)
12 UTC periods
(d)
18 UTC periods

Figure 82

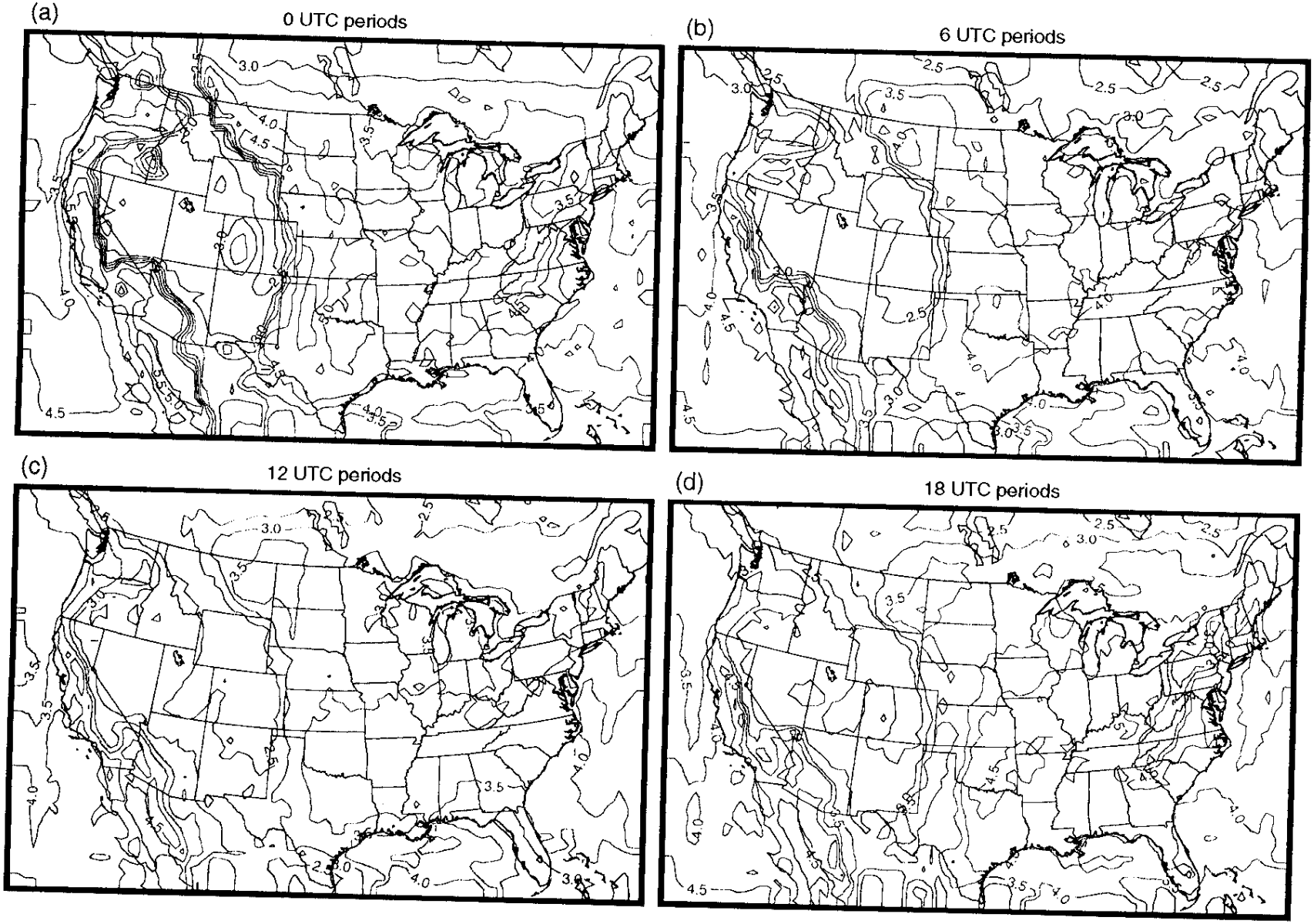
(a)
0 UTC periods
(b)
6 UTC periods
(c)
12 UTC periods
(d)
18 UTC periods

Figure 83

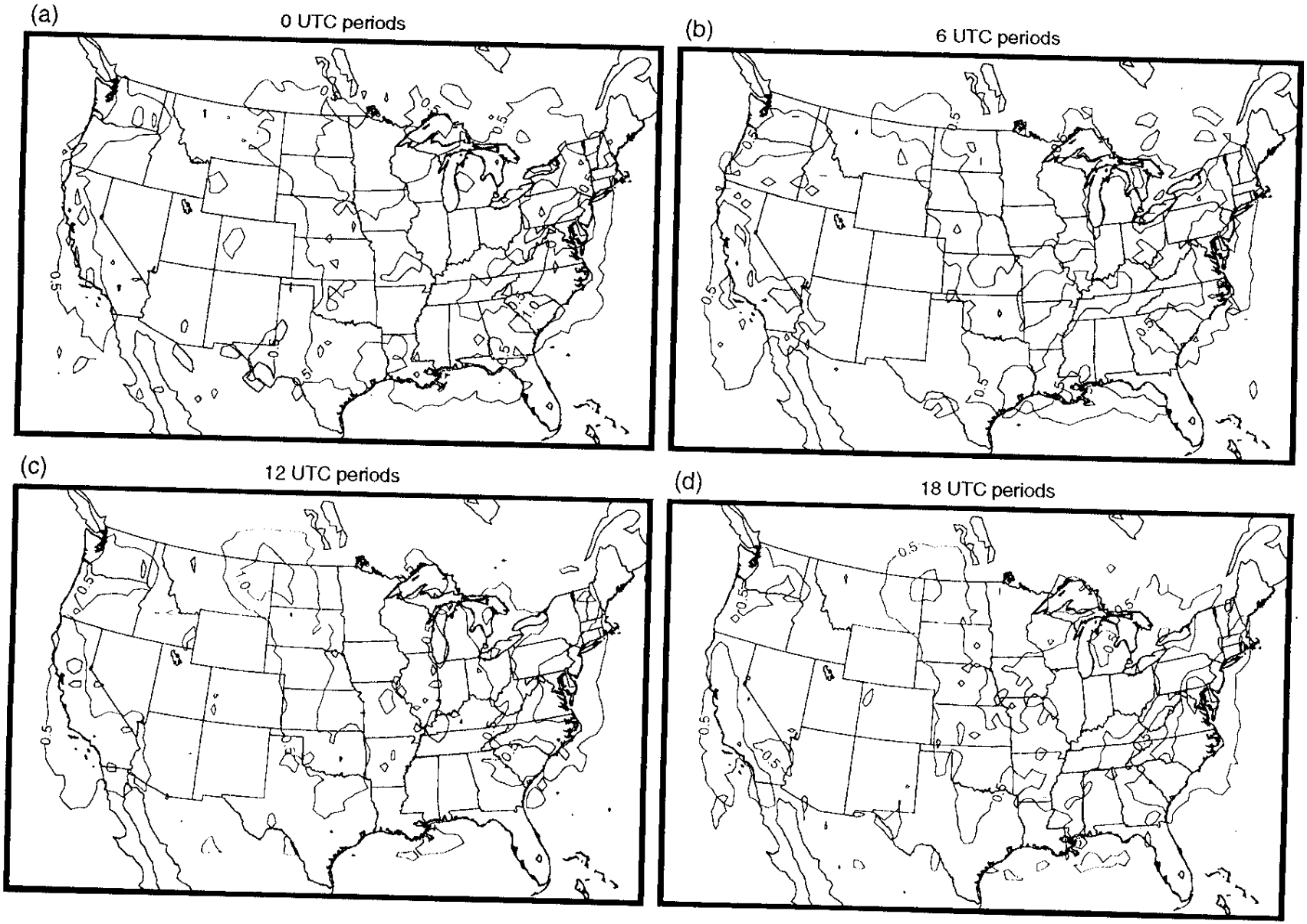
(a)
0 UTC periods
(b)
6 UTC periods
(c)
12 UTC periods
(d)
18 UTC periods

Figure 84

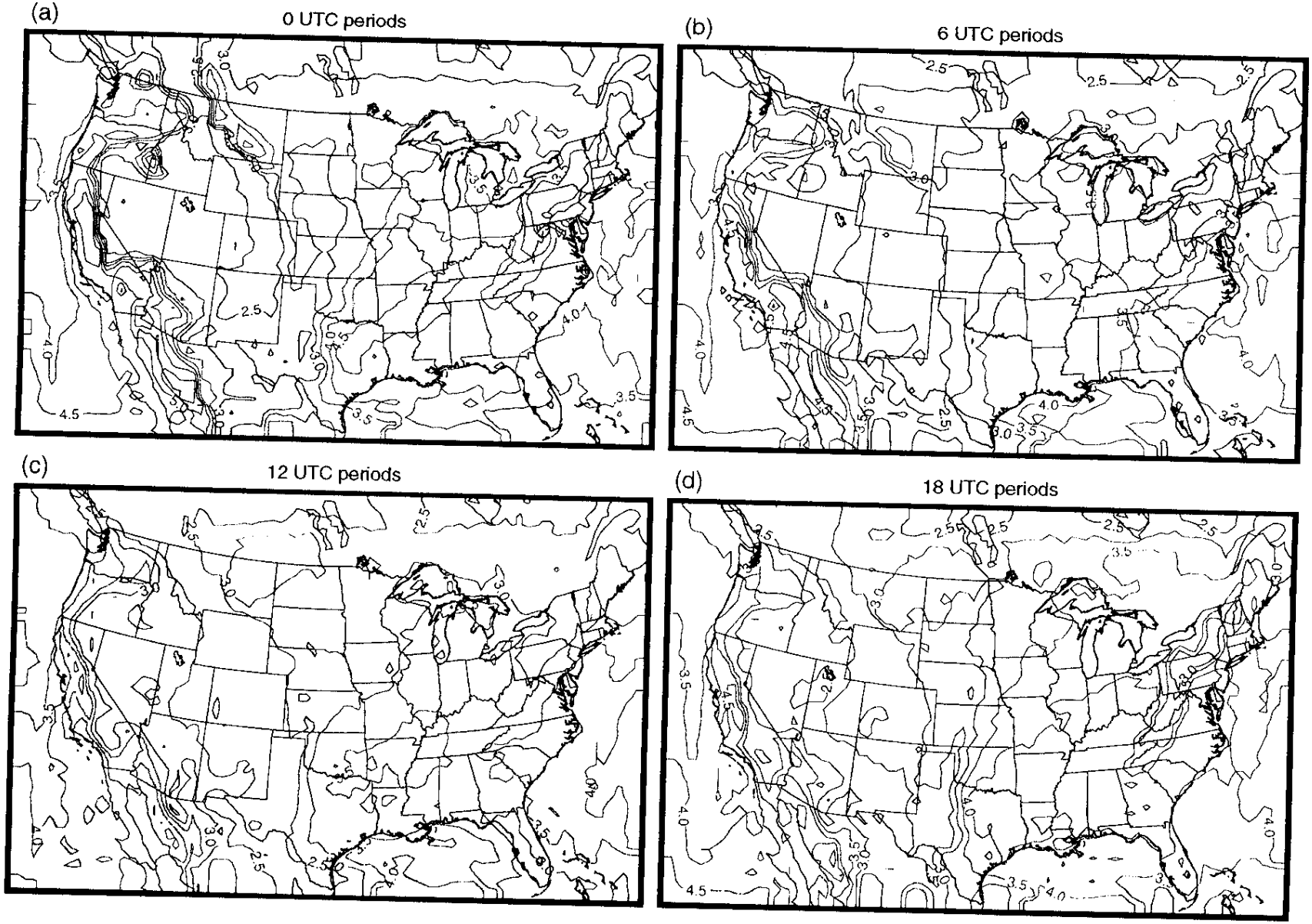
(a)
0 UTC periods
(b)
6 UTC periods
(c)
12 UTC periods
(d)
18 UTC periods

Figure 85

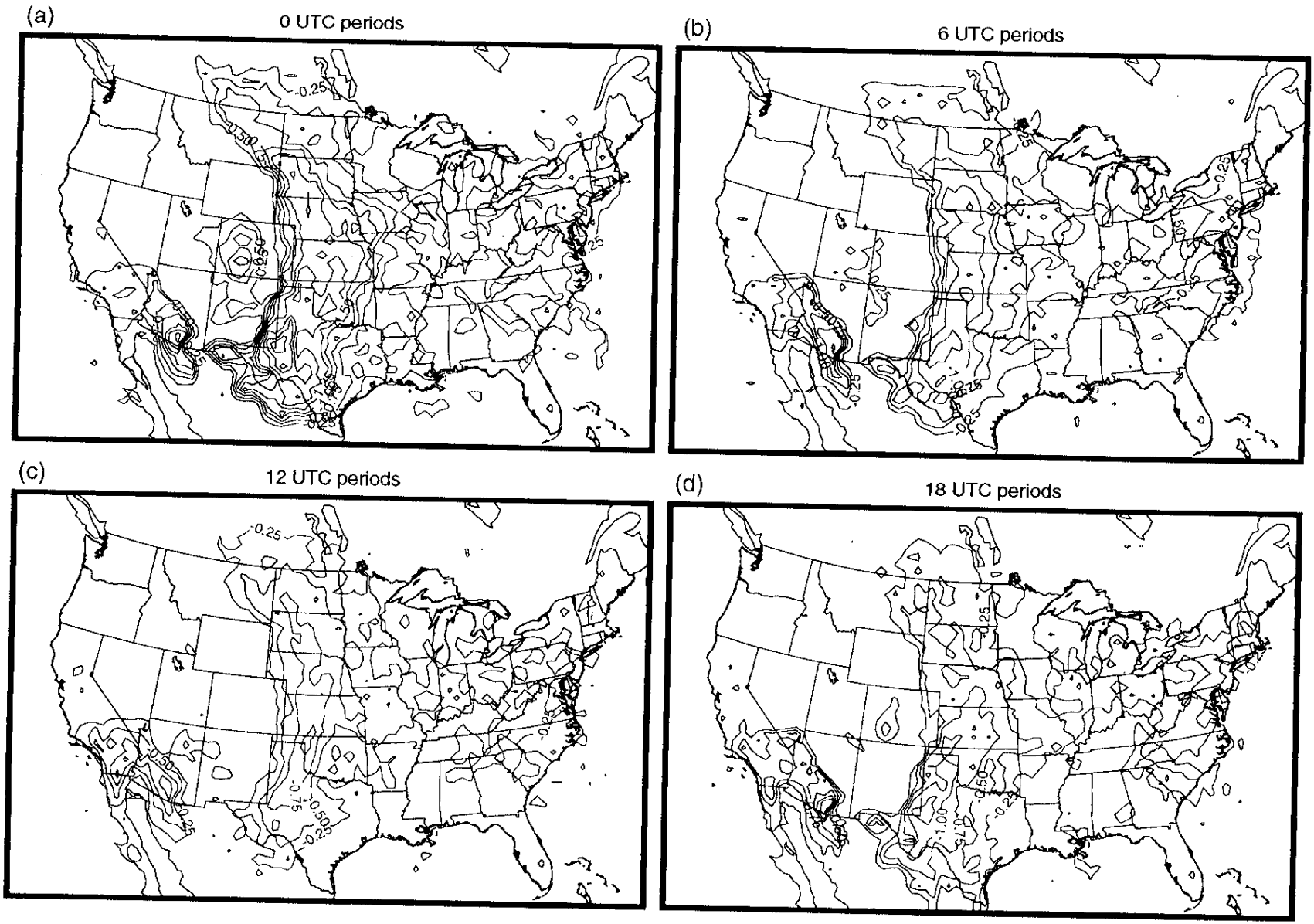
(a)
0 UTC periods
(b)
6 UTC periods
(c)
12 UTC periods
(d)
18 UTC periods

Figure 86

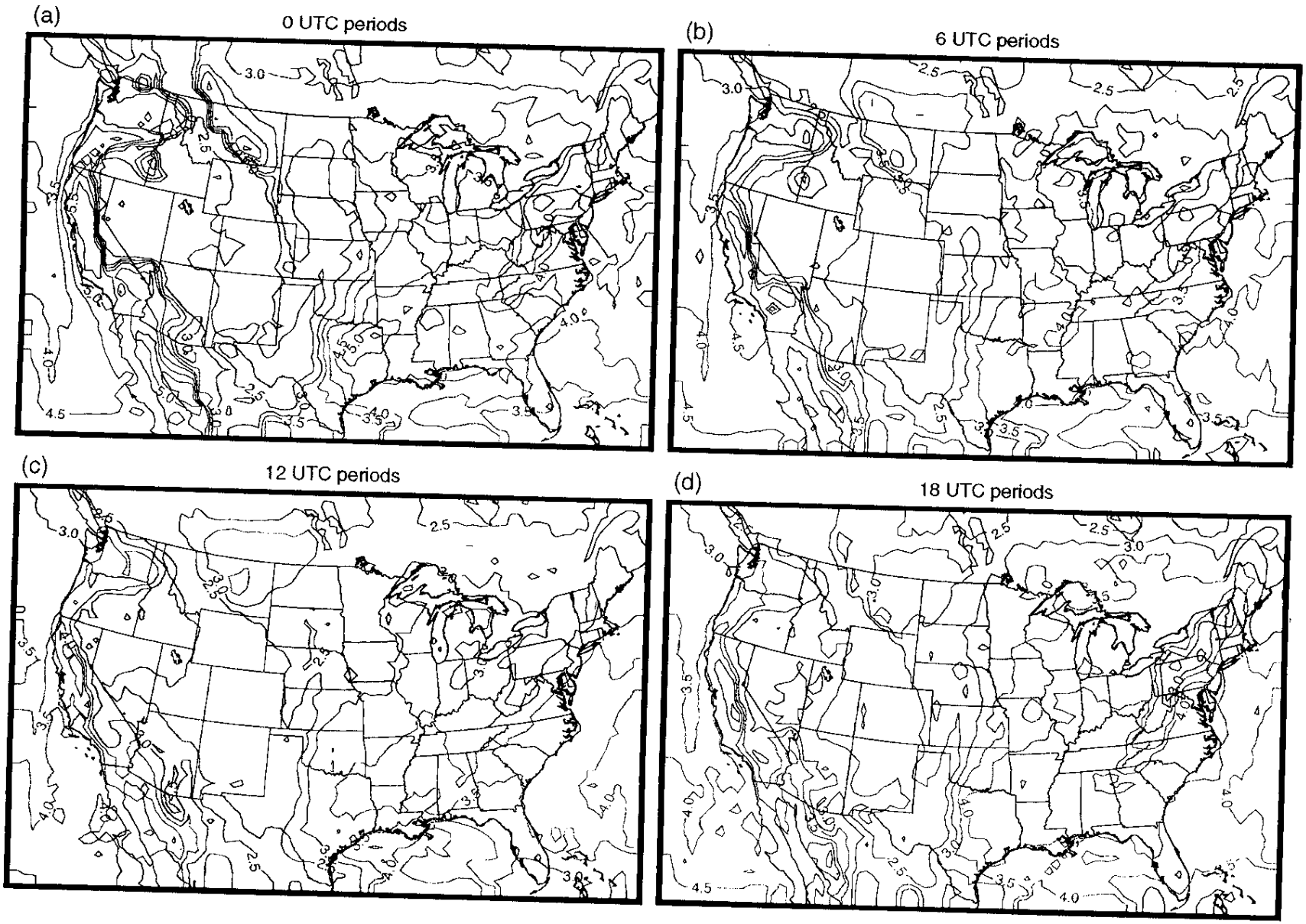
(a)
0 UTC periods
(b)
6 UTC periods
(c)
12 UTC periods
(d)
18 UTC periods

Figure 87

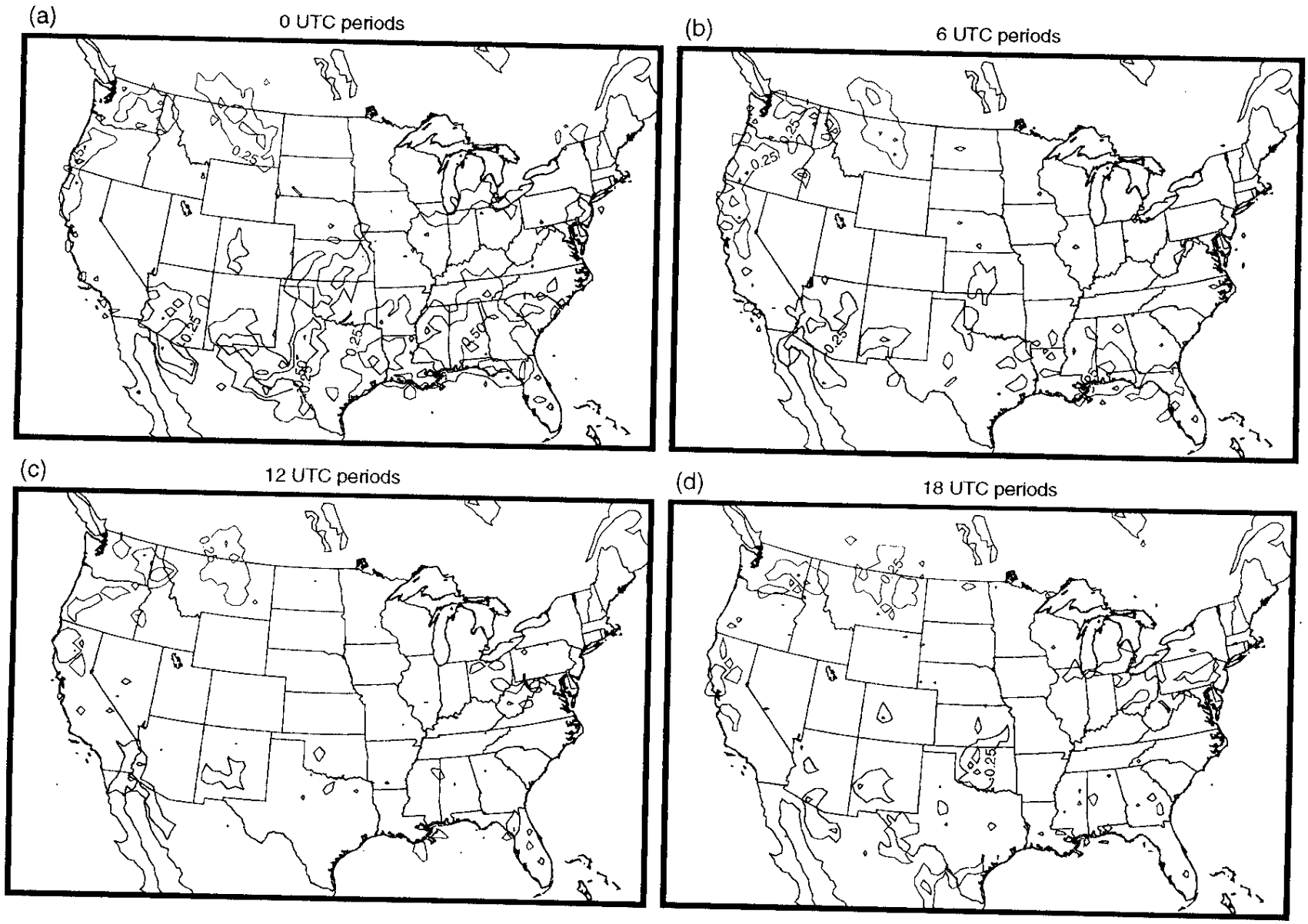
(a)
0 UTC periods
0.25
0.25
0.50
(b)
6 UTC periods
0.25
0.25
(c)
12 UTC periods
(d)
18 UTC periods
0.25

Figure 88